eman ta zabal zazu

Universidad del País Vasco

Euskal Herriko Unibertsitatea

# JATORRI NATURALEKO POLIMEROETAN OINARRITUTAKO NANOKONPOSITEEN GARAPENA

# *NATURAL ORIGIN POLYMER-BASED NANOCOMPOSITE DEVELOPMENT*

**Egilea: Uribarri Goikuria Odriozola**

**Zuzendariak: Dr. Erlantz Lizundia/ Dr. José Luis Vilas**

**PhD Thesis, Leioa, 2020**

# AURKIBIDEA

# *Eskerrak/Acknowledgment*

*Esker on atal hau idazten egoteak doktoretza tesiaren azken txanpan nagoela adierazten du eta ideia honek behar dudan motibazioa ematen dit azken bultzadarako.*

*Aitortu beharra daukat doktoretza lan hau burutzea erronka handia izan dela niretzat, une askotan uste izan baitut ez nintzela bukatzeko gai izango eta hainbat momentutan bertan beher uzteko zorian egon naizen bide korapilatsua izan da. Zenbait unetan ahalegin eta saioen ostean emaitzak ez ziren irizten eta nire buruari galdetzen nion ia jarraitzeak merezi zuen eta zergaitik arin nintzen bizitza nahasten. Hala ere, zerbait irakatsi badit prozesu honek, ikerketa arloko ezagutza teoriko eta esperimentalaz gain, nire persistentzia ahalmena ezagutzea, eta inoiz gehiegi izan ez dudan pazientzia frogan jartzea izan da.*

*Nolanahi ere, 5 urte hauen balantzea positiboa da eta alde positiboen artean Euskal Herriko Unibertsitateko eta batez ere Kimika Makromolekularreko laborategian aurkitu dudan jende aparta nabarmenduko nuke. Sentzu honetan, hasteko nire esker ona helarazi nahi nieke nire bi zuzendariei beraien laguntza eta ulerpenagaitik. Bakoitzak modu desberdin baina osagarrian zuzendu eta bultzatu nauelako espezializazio eta ikerkuntza gaitasun jabetze ibilbide honetan.*

*Bestalde, departamenduari eta fakultateari eskertu nahi nioke doktoretza tesia bertan egiteko aukera eman izanagaitik nire egorera berezia kontutan izanda, doktoretza ikasketak lanarekin bateratzen baititut, eta ondorioz ez ohizko ordutegiekin. Sentzu honetan, ezin dut Luis León ahaztu, laborategiko arduradun ohia, beren konfidantzagaitik eta oraindik topo egiten dogunean jasotzen ditudan bere animoengaitik. Ez ohizko nire ordutegien ondorioz eta ezin naizenez laborategira eta unibertsitatera egunero hurbildu, askotan komplexua egiten zitzaidan entseguen jarraipena egitea. Horregaitik, eskertu nahi nieke laborategiko eta departamenduko ikerlari eta beste ikasleei, beraien prestasunagaitk mesederen bat behar izan dudanean (Sheila, Julia, David, Alberto, Leire, Manu, Alazne…plazer bat izan da zuekin topo egin izana).*

*Era berean, SGI-ker zerbitzu orokorretako profesionalak aipatu nahi nituzke beraien efizientzia eta irisgarritasuna nabarmenduz (Aitor Larrañaga, Alex Diez, Alfredo Sarmiento…) eta Kimika Ez-organiko sailari eskerrak helarazi ekipamendu desberdinen erabilera baimendu eta erreztu eta baita Alicanteko Unibertsitatearekin bitartekari moduan egiteagaitik (Sonia Pérez, Juanma Gutierrez…). Kolaborazioen inguruan, nire esker on eta aintzatespena Pavia, Perugia eta Tuscia Unibertsitateetako kideei, beraien lanagaitik garatutako zenbait materialen entsegu biologikoen inguruan.*

*Eta azkenik, nire familia eta lagunei, nigan nik neuk baino konfidantza gehiago edukiteagaitik, eta babesagaitik nahiz eta askotan ez ulertu zertan nebilen ezorduetan unibertsitatean. Hemendik aurrera, lasaiago ibiliko naizezenez, denbora gehiago eukiko dut beraientzako, gutxienez hurrengo erronkan abiatu arte…Eta noski Goku, jakin barik gure ibilaldiak oso lagungarriak izan direlako burua argitzeko nahasmen uneetan.*

*ESKERRIK ASKO DANORI!!*

“Saiatzen ez denak ez du zekula irabazten. Benetako arrakasta huts egin ondoren jaikitzea da” (Anonimoa).

“El primer paso al éxito es negarte a ser un cautivo de tu entorno” (Mark Caine).

“Many of life´s failures are people who did not realice how close they were to success when the gave up” (Thomas A. Edison).

“Conserva en tu memoria durante el resto de tus días las cosas buenas que surgieron de las dificultades. Ellas serán una prueba más de tu capacidad y te infundirán confianza ante cualquier obstáculo” (Paulo Coelho).

# 1

# Sarrera

## 1.1. Tesiaren helburua eta antolaketa

Gaur egun oraindik aurkitu ditzakegun material plastiko gehienak petrolio jatorriko polimerotan oinarrituta daude, jatorri naturaleko polimeroen inguruan gero eta gehiago ikertzen ari dan arren. Bestalde, bizitzen ari garen krisialki klimatikoak ezinbesteko egiten du produktu jasangarri eta berriztagarrien erabilera eta sorrera bultzatzea eta gastu energetikoa gutxitzea.

Testu inguru honetan, tesi honen helburua zelulosa nanokristaletan (ZNK) oinarritutako nanokonposite berrien garapena eta karakterizazioa da, material honen inguruan jakintza berria sortzeko helburuarekin. Hain zuzen ere, zelulosa nanokristalak, baliabide naturaletatik ateratako zelulosalen deribatuak baitira. Zehazki, neurri nanometrikoa duten biopolimeroak dira, eta dimentsio txiki honetan zelulosaren propietate bereziei beste batzuk gehitzen zaizkio. Beraz, bionanomaterial polimeriko bat dela ezan dezakegu.

Zelulosa nanokristalak forma desberdinak izateko fabrikatu daitezke, hauen arten filmak eta estaldurak, gelak, edo aerogelak aurkitu daitezke. Bestalde, funtzionalizazio eta hibridazio aukera ugari eskaintzen dituzte, besteak beste, material inorganikoen (metalekin) edo organikoekin (beste polimero batzuekin, adibidez). Hibridazio aukera hauek berriz propietate modifikazio desberdinen aukera dakarte eta honekin erabilera posibilitate berriak ingurumen, energia edo biomedikuntza moduko eremuetan.

Lan honetan, filme eta aerogel egiturako zelulosa nanokristaletan oinarritutako nanokonpositeak garatu eta aztertu egin dira. Kasu bietan, lehenbizi zelulosa hutsez osatutako laginak sintetizatu dira eta ondoren, nanopartikula metaliko desberdinen adizio edo generazio bitartez, filme eta aerogel hibridoak garatu dira. Horrela, aditibazio edo errefortzu metaliko desberdinen eragina analizatua eta parekatua izan da, zenbait propietate aldatzeko orduan.

Azkenik, aplikazioetara begira, nanokonpositeen integritatea ziurtatzeko eta hobetzeko, bigarren aerogel hibrido mota bat garatu da. Aerogel mota hau beste polisakarido batekin (sodio alginatoa) gurutzatuz lortu da eta erresistentzia mekanikoa moduko propietateak frogatuak izan dira. Bukatzeko, garatutako biopolimero-metal porodun sistemen errekerimendu-betetzea eta kustomizazio-aukeren analisia jaso da, gas inguruan, ingurumen eta energia aplikazioei begira.

Memoria hau ondorengo atal eta edukien arabera antolatua izan da:

1. Sarrera atal honetan, lanaren helburuak eta dokumentuaren edukina azaltzeko eta honekin, lan esperimentalaren eta emaitzen laburpena jasotzeko. Azkenik, dokumentuan zehar agertuko diren sinbolo, sigla eta laburdura nagusiak zerrendatu dira, ingelesez eta alfabetikoki.

2. Bigarren atalean, testuingurua eta ikerketa eremuko aurrekari teorikoak azaltzen dira eta sarrera orokorraz gain, sekzio hau 3 ataletan banatzen da:

    - Lehenik, biopolimeroen deskribapena eta sailkapena egiten da, bestalde nanoteknologia eta nanopartikula motak eta lortzeko metodoak azalduko dira eta azkenik nanokonposite polimerikoen onarri teorikoak jasotzen dira.

    - Jarraian, nanozelulosaren deribatuen inguruan zakonduko da eta honekin batera zelulosa nanokristaleten (ZNK) oinarritutako nanokonpositeen eta material hauen ezaugarri eta aplikazioak azalduko dira

    - Azkenik, lanean zehar erabilitako metodo eta karakterizazio teknika desberdinen oinarri teorikoak jaso dira.

3. Hirugarren atalean, lortutako emaitza experimentalak azaldu eta eztabaidatzen dira garatutako nanokonposite mota desberdinen eta aztertutako propietateen arabera:
    - Partikula metalikoekin funtzionalizatutako zelulosa nanokristal filmak: karakterizazioa eta propietate termikoen analisia.
    - Partikula metalikoekin funtzionalizatutako zelulosa nanokristal filmak: karakterizaioa, bakterio-aurkako propietateak eta deskonposizio azterketa.
    - Partikula metalikodun zelulosa nanokristaletan oinarritutako aerogel hibridoak: karakterizazioa eta propietate desberdinen azterketa.
    - Metalak eusten dituzten porodun sistema hibridioen errekerimendu aurretiko analisia eta adaptazio aukerak gas ingurunean, energia eta ingurumen aplikazioei begira
4. Laugarren atalean, lanaren ondorioak laburbiltzen dira eta bestalde, garatutako materialen inguruko joeren eta etorkizunerako aplikazio eta garapen aukeren analisia egiten da.
5. Bukatzeko, ikerkuntza eta garapen lan honekin lotutakoe emaitzak, kontribuzio zientifikoak, adierazten dira.

Azkenik, aurreratu nahi dut memoria bi hizkuntzetan idatzita dagoela, zehazki, sarrera eta oinarri teorikoen atalak euskeraz idatzi dira eta emaitza esperimentalak, eztabaida eta ondorioak ingelesez. Honen arrazoia praktikotasuna eta aurretik prestatutako materialak (publikazioak) itzuli barik aprobetxatu ahal izatea izan da.

## 1.2. Laburpena/Abstract

Lan honetan nanoegituratutako zelulosaren deribatuak, zelulosa nanokristalak (ZNKak) aztertzen dira nanokonposite polimeriko berriak garatzeko oinarrizko material moduan. Zelulosa nanokristalak jatorri naturaleko polimerotan oinarritzen dira eta interes handia erakarri dute, beraien biodegradakortasun, toxikotasun-eza eta eskuragarritasunaz gain, erakusten duten dentsitate baxu, gainazal espezifiko altu eta funtzionalizazio ahalmen zabalagaitik.

Hain zuzen ere, zelulosa nanokristalak oinarrizko material moduan filma, gel edo aerogel moduko nanokonpositeak osatzen aurkitu daitezke jomuga erabilera eta aplikazioaren arabera, nahiz eta oraindik hainbat ezaugarriren hobekuntza beharrezkoa den. Helburu horrekin, nanopartikula mota, forma, tamaina eta kontzentrazio desberdinen dispertsio bitarteko zelulosa nanokristalen funtzionalizazioa, aproximazio ernagarria da material eta gailu aktibo eta multifuntzionalak diseinatu eta sintetisatzeko orduan.

Sentzu horretan, ikerketa honetan zelulosa nanokristaletan oinarritutako filmak eta aerogelak garatu dira surfaktante gabeko eta ur inguruan garatutako prozesu simple eta eskalagarrien bitartez. Ondoren, zelulosa nanokristalak nanopartikula metalikoen (NPM) dispertsioaren bitartez funtzionalizatu dira, ZNK/NPM konposite hibridoak lortuz eta propietate desberdinen aldaketak aztertuz.

Garatutako filmen kasuan, alde batetik ZNKak bost nanopartikula metaliko desberdinekin kargatu dira, burdin oxidoa ($Fe_2O_3$), aluminio oxidoa ($Al_2O_3$), silizio dioxidoa ($SiO_2$), titanio dioxidoa ($TiO_2$) eta zink oxidoa (ZnO) eta egonkortasun termikoaren azterkerta eta konparaketa egin zaie teoria desberdinak erabiliz. Beste alde batetik, zilar oxidoa ($Ag_2O$), silizio dioxidoa ($SiO_2$) eta titanio dioxidoa ($TiO_2$) barneratu dira ZNK matrizera eta lortutako filmen ikerketa detailatua burutu da.

Ondoren, propietate desberdinetan duten eragina analizatu da: propietate optikoak, mikrobioen aurkako aktibitatea eta konpost kondizioetan erakusten duten deskonposaketa ahalmena.

Aerogelei dagokienez, ZNKak prozesuan bertan lortutako kobre eta paladio oxido nanopartikulen hibridatu dira eta karakterizazio zakona egiteaz gain, gainazal ezaugarriak, bustikortasuna eta egonkortasun termikoa moduko propietateak aztertu dira.

Azkenik eta aplikaziora begira, erresistentzia mekanikoa sustatzeko helburuarekin, bigarren aerogel hibrido mota bat garatu da sodio alginato biopolimeroarekin katioi metalikoek eragindako gurutzaketa lortuz. Porodun sistema hibrido hauen potentziala eta errekerimenduen aurretiko analisia jaso da ,gas ingurunean erabiltzeko, energia edo ingurumen arloko aplikazioetan.

Garatutako nanokonpositeak eta sortutako ezagutzak bide berriak zabaltzen dituzte, ZNKn oinarritutako nanokonpositeak aplikazio desberdin eta berritzaileetan erabiltzeko orduan hainbat arloetan, hauen artean ingurumen, energia, biomedikuntza, enbalatze industria edo sentsorika eremuak nabarmendu daitezke.

*In this work, a nanostructured cellulose derivate, cellulose nanocrystal (CNC) has been studied as base material for new polymeric nanocomposite development. Cellulose nanocrystals are natural origin nanoparticles that have attracted a great interest due to their biodegradability, no toxicity and disponibility besides their low density, high specific surface area and numerous functionalization possibilities.*

*Cellulose nanocrystals can be considered as base material for the fabrication of film, gel or aerogel like nanocomposites depending on the target use and desired applicability but there are still some properties that need to be improved. For this purpose, the dispersion of nanoparticles having different size, shape, and composition-dependent properties is an exciting approach to design and synthesize multifunctional and active materials and devices.*

*In this sense, in this work CNC-based films and aerogels have been developed by surfactantless, simple and scalable processes. Moreover, CNC have been functionalised using dispersed metal nanoparticles (MNP) and obtaining CNC/MNP hybrid composites which properties modifications have been analysed.*

*In the case of CNC-based films, on the one hand CNC has been loaded with five different metal nanoparticles, iron oxide ($Fe_2O_3$), aluminium oxide ($Al_2O_3$), silicon dioxide ($SiO_2$), titanium dioxide ($TiO_2$) and zinc oxide (ZnO) and thermal stability analysis and comparison has been done using different theories. On the other hand, CNC-based films containing zinc oxide (ZnO), titanium dioxide ($TiO_2$), and silver oxide ($Ag_2O$) have been obtained and studied in detail. Furthermore, different properties as optical properties, antimicrobial activity and disintegrability in composting conditions have been analysed.*

*Regarding aerogels, CNC hybridized with in situ created copper and palladium oxide nanoparticles have been deeply characterised and surface properties, wettability and*

*thermal stability have been studied. Besides, looking to achieving the enough mechanical resistance for final applications tests, a second hybrid aerogel kind have been developed by sodium alginate biopolymer crosslinking promoted by metallic cations. Finally, developed metal supporting bio-based porous systems preliminary requirements analysis has been included, looking forward to gaseous medium application, in environmental and/or energy applications.*

*Developed nanocomposites and generated knowledge can contribute to open new pathways for the application of CNC-based nanocomposites in novel and innovative applications in different fields such as environment, energy, bio-health, envelope industry or sensor production.*

## 1.3. Glossary

| | |
|---|---|
| ALG | alginate |
| $\theta$ | apparent contact angle |
| ATR | atenued transmittance reflectance |
| BC | bacterial cellulose |
| BET | Brunauer-Emmett-Teller |
| CNC | cellulose nanocrystal |
| CNF | cellulose nanofibril |
| DMA | dynamic mechanical analysis |
| DSC | differential scanning calorimetry |
| E | Young modulus |
| $E_a$ | activation energy |
| ΔEw | hydration free energy |
| EDX | energy-dispersive X-ray spectroscopy |
| EISA | evaporation induced self-assembly |
| FTIR | Fourier transform infrared spectroscopy |
| FWHM | Full width at half maximum |
| MCC | microcrystalline cellulose |
| PI | polydispersity index |
| Mw | average molecular weight in weight |
| MCC | microcrystalline cellulose |
| MNP | metal nanoparticles |
| NFC | nanofibrillated cellulose |
| OFW | Ozawa-Flynn-Wall |
| SEM | scanning electron microscopy |

| | |
|---|---|
| SFE | surface free energy |
| TEM | transmission electron microscopy |
| TGA | thermo gravimetric analysis |
| $U_E$ | electrophoretic mobility |
| WCA | water contact angle |
| V̆ | Poisson´s Ratio |
| XPS | X-ray photoelectron spectroscopy |
| XRD | X-ray diffraction spectroscopy |
| $\gamma_{LV}$ | liquid–air interfacial tension |
| $\gamma_L$ | liquid surface tension |
| $\gamma_S$ | solid surface tension |
| $\gamma_{SV}$ | solid–air interfacial tension |
| $\gamma_{SL}$ | solid–liquid interfacial tension |
| Z | Z-potential |

# 2

# Aurrekariak eta oinarri teorikoak

## 2.1. Sarrera

Atal honetan, lanean zehar erabilitako eta sintetizatutako materialen inguruko deskribapena egiten da, materialen hauen aurrekariak aipatzen dira eta polimeroetan oinarritutako nanokonpositeen alde teorikoak azaltzen dira.

Lehenik, 2.2 atalean, biopolimeroen deskribapena, sailkapena eta klasifikazioa egiten da, garatutako materialak biopolimeroetan oinarrituta baitaude. Ondoren, nanoteknologia eta nanopartikulei buruz jarduten da, nanopartikulak sailkatuz eta lortzeko metodo eta aplikazio nabarmenenak aipatuz. Azkenik, material nanokonposatuak definitzen dira, eta material hauen eboluzioa eta aplikazioak. Konpositeen artean polimeroetan oinarritutako nanokonposatuak nabarmentzen dira.

Bestalde, 2.3 atalean zelulosa nanokristaletan oinarritutako nanokonpositeetan zakontzen da. Zentzu horretan, nanozelulosaren xehetasunak eta deribatuak azaltzen dira, hauen artean zelulosa nanokristalak. Honekin lotuta, zelulosa nanokristalekin lortu daitezkeen egitura desberdinak deskribatzen dira eta zelulosa nanokristaletan oinarritutako nanokonpositeen aplikazio eremuak ere azaltzen dira.

Azkenik, 2.4 atalean, ikerketan zehar erabilitako karakterizazio tekniken eta metodoen oinarri teorikoak erakusten dira. Gehienak, polimeroak eta konpositeak karakterizatzeko arrunki erabiltzen diren teknikak dira.

## 2.2. Biopolimeroak eta nanokonposite polimerikoak

### 2.2.1. Biopolimeroak eta polimero biodegradagarriak

Polimeroak lotura kobalente bitartez lotutako molekulen kate luzez osatutako material organikoak dira. Organikoak direnez, polimeroak osatzen dituzten elementuak karbonoa, hidrogenoa, oxigenoa eta beste elementu ez metalikoak izaten dira. Polimero kate luze hauetan, unitate basiko bera errepikatzen da, monomero moduan ezagututakoa, eta honek ematen dio bere ezaugarria materialari. Lagin polimeriko batek, luzera desberdineko kateak izaten ditu eta hauek elkargurutzatuta egon daitezke lotura kobalente bitartez edo hidrogeno-zubi edo Van der Waals moduko lotura ahulagoen bitartez. Polimeroen kateen luzera polimerizazio graduak ematen du eta honek eragina dauka polimeroaren pisu molekularrean [1].

Polimeroak, estrukturaren arabera, lineal edo adarkatuak izan daitezke eta sare tridimentsionalak ere sor ditzakete. Polimeroak sintetizatzeko erreakzioak polimerizazio moduan ezagutzen dira, eta erreakzio mota desberdinak bi talde orokorretan sailka daitezke: polikondentsazioa edo etapa-polimerizazioa eta poliadizioa edo kate-polimerizazio [2]. Bestalde, polimeroak kristalinoak, amorfoak edo erdibide bat izan daitezke (erdikristalinoak) eta orokorrean ez dira ez beroaren ez elektrizitatearen eroale onak. Karga mekaniko aplikazio bitartez kate molekularrak bata bestearen gainean irrist egiteko gaitasuna daukate, indartsuki gurutzatuta ez badaude, edo loturen inguruan biratzeko ahalmena izan dezakete. Ahalmen hauei esker, polimeroak material deformagarri eta harikor bilakatzen dira. Hala ere, zeramika edo metalekin parekatu ezkero, polimero gehienek modulu elastiko, zailtasun eta trantsizio temperatura baxuak izaten dituzte. Bestalde, errez fabrikatzen dira, kasu batzuetan merkeak dira baina mekanizatzeko orduan ez dira material onak.

Polimeroak baliabide naturaletatik atera daitezke (kimika berdea), bai zuzenean edo naturak eragindako molekula txikien polimerizazioaren bitartez [3,4] ,edo petrolioaren deribatuetatik sintetizatu daitezke (polimero sintetikoak). Gaur egun, polimero sintetikoak dira erabilienak, plastikoen osagai nagusiak eta aplikazio eremu askotan aurki daitezke nahiz eta polimero naturalen inguruko merkatua eta ikerkuntza hazten dauden [5].

Hain zuzen ere, plastikoen erabilera oso arrakastatsua izan da, bereziki enbalatzeko material bezala. Baina enbalatzeko plastiko gehienek bizi-ziklo oso laburra dute, eta, ondorioz, ezabatze-bolumen handia eta ezabatze-denbora luzea. Mundu mailan urtero 300 milioi tona inguru sortzen dira eta kopuru horrek etengabeko gorakada izan du azkenengo 15 urteetan. Kopuru horren % 30ak bizi-ziklo laburra dauka, eta soilik % 9 birziklatzen da: % 12 inguru erraustu egiten da, eta % 79 hondakindegietara edo ingurumenera eta, bereziki, itsasora iristen da, 100 urte baino gehiagoko desagerpen-denborekin . Lehen aipatu bezala, plastikoak material polimerikoetan oinarrituta daude eta polimero erabilienak petroliotik eratortzen direnez, baliabide fosil eta ez-berriztagarri horren menpe daude. Hain zuzen ere, munduan ateratzen den petrolio guztitik % 5 plastiko-industriara bideratzen da. Bestalde, mineral fosil honen prezioa ez da batere egonkorra, eta, aurreikuspenen arabera, egungo kontsumo-erritmoan 50 urte barru agortu egingo litzateke [6].

Jasangarritasun faktoreek bioplastiko eta berez biopolimeroen igoera eragin dute, eta mundu-mailan ingurumen- eta politika-arloko eskakizunak material jasangarrien inguruko ikerkuntza ari dira bultzatzen, petroliotik eratorritako ohizko plastikoak ordezkatzeko helburuarekin. Hain zuzen ere, petroliotik eratorritako polimeroak arazo larriak eragiten ari dira ingurumenean birziklatzeko orduan erakusten duten konplexutasunaren ondorioz, ez baitira biodegradagarriak ezta konpostagarriak ere.

Biopolimero bat jatorri natural edo biologikoa duen material polimeriko bat da eta orokorrean, honen ezaugarriak biodegradakortasuna, berriztagarritasuna eta ugaritasuna dira, beste propietate berezien artean [7-8]. Biopolimeroak lortzeko baliabide naturalen adibide ezagun moduan, artoa, soja, azukre-kana edo egurra aipatu daitezke, berriztagarriak dira, prezio egonkorrak dituzte, eta, oro har, biosfera osoan zehar eskuratu daitezke. Arrazoi horiengatik, baliabide interesgarriak dira materialak garatzeko eta petrolioaren transformazioan oinarritutako materialak ordezkatzeko aukera bezala.

Testuinguru honetan, baliabide natural edo biologikoetatik sintetizatutako polimeroak gailentzen dira polimero biodegradagarriak lortzeko, baita kontsumo energetikoa murrizteko asmoarekin. Tamalez, gaur egun material horiek lortzeko eta produzitzeko teknikak ez dira oraindik industrialki lehiakorrak, ohizko prozesu petrokimikoekin parekatzen baditugu [9]. Lehiakortasun industrialera hurbiltzen den prozesu bat papergintzan da, baliabide berriztagarrietan oinarritutako produktuak eskala industrialean arrakastarekin garatu ditzakeen sektore bakarretakoa baita. Horren harira, papera produzitzeko teknikak plataforma bideragarritzat har daitezke polimero biodegradagarriekin produktu berriak garatzeko orduan.

Horrela, biopolimeroak eta biopolimero biodegradagarriak garapen betean daude, plastiko arruntek ingurumenarentzat suposatzen duten arazoa eragozteko helburuarekin [10]. Modu horretan, polimero naturaletan oinarritutako alternatibak garatu dira azken urteetan, polimero konbentzionalen propietateak eta funtzionalitateak mantentzeko nahian. Polimero natural horiek hainbat arlotan erabiltzen dira: enbalatze-industrian eta etxeko enbalatzeetan, plastikozko poltsetan, sukaldaritzan, medikuntzan, nekazaritza-produktuetan edo barazki ekoizpenean [5-7].

Polimero biodegradagarriei erabilera-denboran propietateak mantentzea eskatzen zaie, eta, epea bukatu ondoren, estruktura kimikoa aldatuz, ingurumenarekiko

bateragarriak diren osagaietan deskonposatzea. Gehienetan, biodegradazioz deskonposatzen dira; hain zuzen ere eragile biologikoek (entzimek, bakterioek edo mikroorganismoek) eragiten duten degradazio prozesu kimiko bitartez. Produktu baten degradazioa, ingurumenaren eraginpean, mikroorganismoen inplikazioaren bidez gertatzen denean; prozesuaren ondorioz, pisu molekularra txikitzen da eta polimeroa puska organiko sinpletan degradatzen da.

Jatorri naturala duten polimero biodegradagarriak, hiru kategoriatan sailka daitezke [8,11] (ikusi **1. irudia**):

1) *Zuzenean biomasatik lortzen diren polimeroak*

Kategoria honen adibide desberdinak daude; almidoia, kitina, kitosanoa, zelulosa eta gisako polisakaridoak, kolagenoa, keratina edo zeta moduko proteinak, edo latex-etik (Hevea Brasiliensis-etik) ateratzen den kautxu naturala [12,13,14].

Almidoia aplikazio handieneko termoplastiko biodegradagarria da; honen izaera hidrofiliko handiari, kostu baxuari eta ugaritasunari esker, gehigarri biodegradagarri gisa erabili daiteke, edo, plastiko tradizionaletan, ordezkatze-material moduan. Konposatu horrek polimero sintetikoen kateen degradazioa edo frakmentazioa bizkortzen ditu, eta mikrobio-akzioak, bere aldetik, almidoia kontsumitzen du, polimeroan poroak sortaraziz eta materialaren desegitea eraginez [15].

Bestalde, zelulosa dugu biomasatik lortu daitekeen material interesgarri eta oparoenetarikoa. Nahiz eta badiren 150 urte inguru zelulosa erabiltzen denetik, gaur egun bere garrantsia eta interesa areagotu egin da ingurumen eta jasangarritasunaren behar berrien ondorioz, beste arrazoi batzuen artean. Hain zuzen ere, zelulosa polisakarido berriztagarri, biobateragarri eta merkea da ,ingurumenean hainbat iturri naturaletik lortu ahal dena. Zelulosa lortzeko iturriak oso anitzak dira, landare eta arbolen zelula hormetatik, ezagunenetarikoak kotoia

edo egurra izanik, baita fruitu, zereal edo landareen nekazal hondakinetatakik eta alga edo bakterioetatik atera daiteke [16]. Biopolimero hau β-glukosa unitateez osatuta dago eta zelulosa eta honen deribatuen (zelulosa mikrokristalinoa, zelulosa fibrak edo zelulosa nanokristalak) erauzte eta lorpena burutzeko zenbait prozesu mekaniko eta kimiko beharrezkoak dira, aurrerago azalduko den bezala.

Zelulosaz gain, material organiko ohizkoenetarikoa kitina da; itsas krustazeoetatik eta intsektuetatik atera daitekeen polimero naturala delarik. Beste adibide bat lignina da, material ugaria hau ere; landareen eta zenbait zelularen hormetatik ateratzen den kate aromatiko konplexuz (ez-hidrokarbonatuak) osatutako polimeroa da [17].

Talde honen barruan alginatoa ere kokatu dezakegu, nahiz eta biopolimero hau bakterioek ere produzitu dezaketen. Alginatoa alga marroietatik (Macrocystis pyrifera, Sargassum siliquosum) atera daitekeen polisakarido linear eta hidrofilikoa dugu, konkretuki (1→4)-β-D azido manuroniko (M) eta (1→4)-α-L azido glukuroniko (G) unitatez osatutako sodio alginato azido gatza da [9]. Aipatutako azido hauek homopolimero (MM edo GG blokeak) edo heteropolimero (MG edo GM bloqueak) sekuentziez osatu daitezke eta hain zuzen ere M/G ratio, masa molekularrarekin (Mw) batera parametro garrantsitsua da polimeroaren portaera ulertzeko. M eta G izenpetutako unitate honeek hidroxilo eta karboxilo talde lateralak dituzte eta talde hauek toki erreaktiboak dira zenbait modifikazioetarako. Bereziki ezaguna da alginatoak $Ca^{+2}$ edo $Ba^{+2}$ moduko katioi bibalenteen bitartez gurutzateko duen ahalmena. Honen ondorioz, bere itxuragaitik arrautza kutxa moduko gel egitura egonkor eta tridimentsionala hartu dezake. Alginatoa polimero biobateragarri, biodegradakor eta merkea da, hainbat aplikaziotan erabiltzen dena, besteak beste biomedikuntza, farmazia, elikagaigintza, ehungintza edo fabrikazio gehigarrian [18,19].

2) *Baliabide naturaletatik ateratako monomeroen sintesi kimiko bidez produzitutako polimeroak*

Mota honen adibide aipagarriena poliazido laktikoa da (PLA) da . Azido 2-hidroxi-propioniko edo azido laktiko monomeroaren polimerizazio kontrolatutik sintetizatzen den polimeroa. Monomeroa, bestalde, artoak, gariak edo azukretan aberats diren beste produktu batzuek gordetzen duten karbohidrato sinpleen fermentazio bidez sintetiza daiteke. PLA azken urteotan poliestireno (PS) edo polietilentereftalatoa (PET) moduko ohizko plastikoen alternatiba aparta bilakatzen ari da. Polimero horren ezaugarri nabarmenenak atxikitako biodegradagarritasun-ahalmena, erresistentzia mekaniko handia eta prozesatzeko erraztasuna dira [20,21].

Talde honen barnean, landare olioetatik (oliba edo kastore olioa) ateratako triglizeridoak ere poliuretanoa bezalako polimero iturri bezala erabiltzen dira eta abian daude azido sukzinikoen eta gatz azidoen deribatuen inguruko ikerketak [22].

*3) Bakterioen edo mikroorganismoen bidez lortutako polimeroak*

Polimero horien artean polihidroxialkanatoak (PHAk) edo nanozelulosa bakterianoa nabarmendu daitezke. PHAk jatorri mikrobianoa duen eta pseudomona aeruginosaren bitartez lortutako poliester lineala da. Polimero horrek polipropilenoaren (PP) antzeko propietateak ditu, eta puzte eta moldaketaren bitartez lortzen da. Polimero honen desabantaila nagusia garestitasuna da [23,24]. Bigarren adibidea, nanozelulosa bakterianoa, interes handia erakartzen ari da; eta bakterioek eragindako biosintesiaren bidez produzitzen den polimeroa da, aurrerago azalduko den bezala [25].

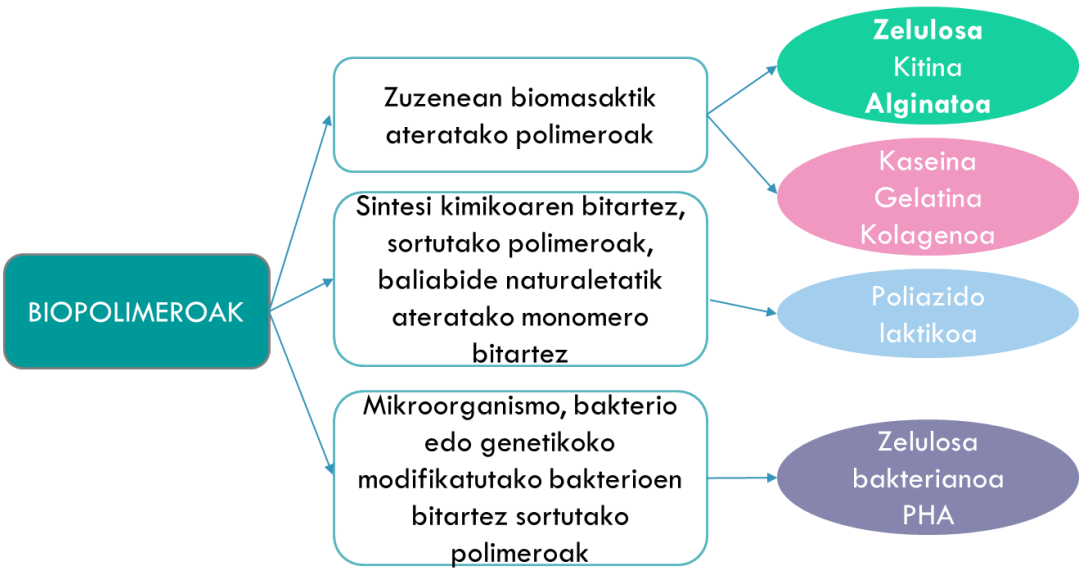


**1. irudia** Biopolimeroen sailkapen orokorra eta adibideak [7,10].

**1. irudian** sailkatutako polimeroak biopolimeroak dira, jatorri naturala dutelako eta biodegradagarriak dira. Hala era, badira jatorri sintetikoa izan arren biodegradagarriak diren polimeroak; horien artean polikaprolaktona moduko poliesterrak aurkitu daitezke.

Atal honetan aipatutako biopolimeroak ugariak dira naturan, polimero sintetikoetan gehitzeko aproposak dira, eta orokorrean, prezio baxuez gain, biodegradagarriak dira eta biobateragarritasun-propietate apartak dituzte. Horien artean, zelulosari atzematen zaio etorkizun oparoenetariakoa.

Bereziki fabrikazioan hobekuntzak lortu ahala, gero eta nabarmenago agertuko da material hori baliabide berriztagarriez guztiz edo partzialki osatutako eguneroko produktuetan [26].

## 2.2.2. Nanopartikula metalikoak

Nanoteknologia edo nanozientziak hazkunde handia izan du 80. hamarkadatik hona eta teknologia garrantsitzuenetarikotzat jotzen da ekonomiaren hazkundea eta garapena bultzatzeko . Nanometro bateko eskala azpitik, mekanika kuantikoaren

arauek, eta 100 nmtatik gora mekanika kuantiko klasikoak diktatzen dituzte materialen propietate fisiko eta kimikoak. Baina 1 eta 100 nm artean, hibridazioa gertatzen da eta gertaera interesgarriak ematen dira, propietate mekaniko, optiko edo magnetikoak, bestea beste, modu nahiko desberdinean jokatuz .Nanozientziak, materialen arloan, nanoegiturak edo egitura nanometrikoak ikertu, diseinatu, garatu eta maneiatzen ditu. Aditu gehienak bat datoz material bat nanometrikoa izan dadin bere hiru dimentsioetatik gutzienez bat 100 nm baino txikiagoa izan behar dela [27]. Egitura nanometrikoak garatzeak materialen oinarrizko propietateak (termiko, optiko, elektriko, mekaniko, etab.) kontrolatzea eta aldatzea ahalbidetzen du konposizio kimiko berdinarekin. Egitura nanometrikoak konposizio eta dimentsioaren arabera (1, 2 edo 3) sailkatu daitezke. Bestalde, konposizioa kontutan izan ezkero nanomaterial mota desberdinak bereiztu daitezke [28, 29]:

- *Nanopartikula metalikoak*: nanopartikula inorganikoak dira eta talde honetan metal eta oxido metalikoetan oinarritutako nanopartikulak nabarmentetzen dira [30,31]. Lanean zehar hainbat mota erabili eta sintetizatu dira (ZnO, $TiO_2$, $Ag_2O$, Pd, CuO, $Fe_2O_3$) eta aukera ugari daude.
- *Nanopartikula polimerikoak*: nanozelulosa eta honen deribatuak (ZNK, ZNZ, ZNB), proteina eta beste polimero natural edo sintetikoz osatutako nanopartikula organikoak dira eta nanozuntz, nanohagazka, nanoesfera edo nanokapsula egituran aurkitu ditzekegu [33].
- *Karbonozko edo karbonoan oinarritutako nanopartikulak*: karbonoz konposatutako nanopartikulak dira eta talde honetan fullerenoak, grafenoak, karbono nanohodiak edo karbono nanozuntzak aurkitzen dira, besteak beste [32].
- *Nanopartikula zeramikoak eta mineralak*: material inorganiko ez metalikoak dira, zeramikoetatik ateratzen direnak, fusio temperatura handiak eta

erresistentzia mekanikoa oso handiak dauzkate eta mineraletan nabarmenenak nanobuztinak (*nanoclay* gisa ezagunak) dira [34].

- *Nanopartikula erdieroaleak*: edo *quantum dot*-ak (QD) material eroale eta ez-eroaleen arteko propietateak dituzte eta oso interesgarriak dira optika edo elektronikan erabilzeko. Talde honetan ezagunak dira kadmioan oinarritutatoak (Cd/Se, adibidez) [35]. Nahiz eta nanopartikula hauek metalikoak diren, berritasunagaitik bereiztea komeni da.
- *Lipidoetan oinarritutako nanopartikulak*: molekula organiko bioaktiboak daramatzatzen partikula esferikoak dira eta hainbat aplikazio biomedikoetarako interes handia daukate [36].

Nanopartikula metalikoei dagokienez, lortzeko bide desberdinak daude [37], *Top down* metodoak non tamaina handiko metalaren satiketatik nanopartikula metalikoak lortzen diren eta *Bottom up* metodoak non atomo eta molekula metalikoetatik nanopartikulak nukleatu eta hazi egiten dira (**2. irudia**).

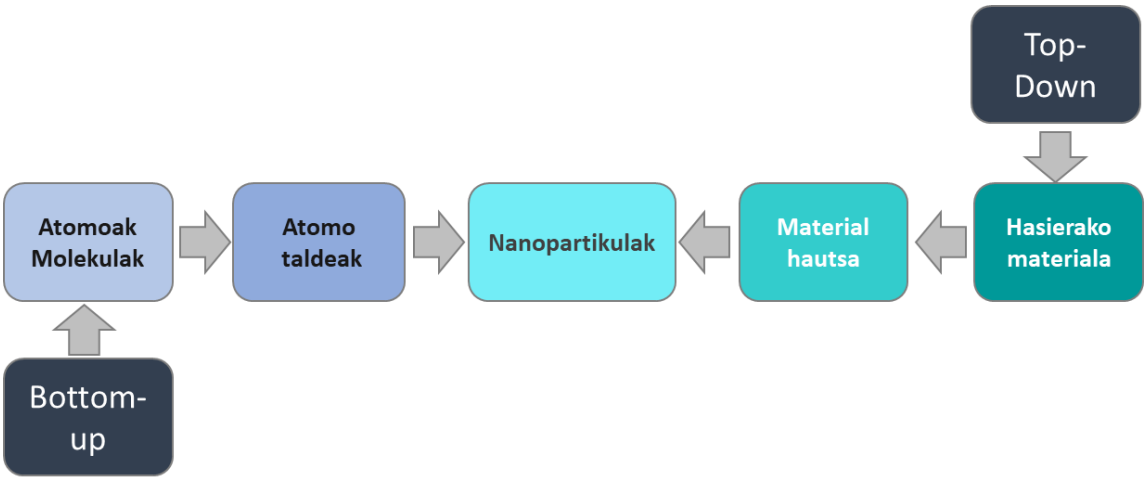


**2. irudia** Nanopartikulak lortzeko modu orokorren ilustrazioa [28,38].

I. **Behetik gorako edo *bottom up* metodoak***:* Modu honetan, aitzindari bat erabiltzen da atomoak lortzeko eta atomoen agregazio bitartez nanopartikulak lortzeko.

   - Nanopartikula metalikoen kasuan modu honetako metodo erabilienak **egoera likidoan ematen diren teknikak** dira eta hauen hartean ***Erredukzio Kimiko*** teknika eta ***Sol-Gel*** teknika dira erabilienak beraien sinpletasunagaitik.

     - ***Erredukzio Kimiko*** metodoan, gatz ioniko bat inguru egokian erreduzitu egiten da. Erreakzioa gauzatzeko hiru eragile kontutan hartu behar dira, agente erreduzitzailea, agente egonkortzailea eta inguru baldintzak (temperatura eta pHa). Batzuetan agente erreduzitzaileak egokonkortzaile bezala ere jokatu dezake. Erredukzio erreakzio desberdinak lortu daitezke erreduzitzailearen indarraren arabera eta erreakzioaren baldintzak aldatuz eta nanopartikulen morfologia eta tamaina kontrolatu daitezke. Orokorrean, erreduzitzaile indartsuek nukleazio fasearen abiadura handitzen dute eta honek nanopartikula tamaina txikiagoa dakar. Erreduzitzaile erabilienak sodio borohidruroa ($NaBH_4$), glukosa ($C_6H_{12}O_6$), etilenglikola ($C_2H_6O_2$) , etanola ($C_2H_5OH$) eta hidrazina ($N_2H_4$) dira [39]
     - ***Sol-Gel*** teknika buztian gauzatzen den sintesi kimikoa da, non Sol fasea likido batean etendako soluzio koloidala da eta Gel fasea disolbatzaile baten murgildutako makromolekula bat. Erreakzioa gauzatzeko metal aintzindari moduan diharduen soluzio kimikoa gel fase barnean dispertsatzen da irabiatze magnetiko edo ultrasoinuen bitartez [40].

- Bestalde, egoera likidoan ***Hydrothermal*** edo ***Solvothermal*** metodoak ere aurki daitezke, presio eta temperatura altuetan ematen diren metodoak, edo baita ***aproximazio organometalikoa*** [41,42,43].

- Likido egoeran ez ezik, badaude **solido edo gas egoeran ematen diren bottom up metodoak**. Hauen artean, ***lurrun deposizio kimikoa*** (*chemical vapor deposition* CVD, ingelesez) eta ***lurrun deposizio fisikoa*** (*physical vapor deposition* PVD, ingelesez), oso erabiliak dira estaldura edo *coating* metaliko edo zeramiko oso finak lortzeko. Teknika hauetan erreakzio kimiko eta fisikoen eraginez presio eta temperatura kontrolatutako erreaktore batean, materialen atomoz osatuako geruza finak lortzen dira, atomo metalikoak material euskarriaren gainean depositatuz [44]. Gas egoeran ematen diren metodoei dagokienez, ***Spray pirolisi***, ***Laser pirolisi*** eta ***Flame pirolisi*** teknika berritzaile eta etorkizun handikoak aipatu daitezke [45].
- Bestalde, nola nanoteknologia eta nanopartikulen arloan ikerketa geldiezina dan, teknika eta tekniken konbinazioa berriak etengabe ari dira nanopartikulak lortzeko metodo berriak ematen. Honen adibide izan daitezke sintesi berdea edo sintesi biologiko izenpean garatu diren hainbat *bottom up* metodo. ***Sintesi berde metodoen bitartez*** nanopartikulak lortzeko mikroorganismoak, onddoak, algak eta landareak bezalako izaki bizidunak erabiltzen dira [46]. Teknika berri hauek interes handia piztu dute merkeagoak direlako, jasangarriagoak, ez baitute erreaktibo kimikoen beharrik , gauzatzeko behar diren temperatura eta kontsumo energetikoak baxuak dira eta eskalatzeko errezagoak dira. Nanopartikula metalikoak lortzerako orduan, sorrera biologikoko metodoak bi kategoriatan sailkatzen dira: ***bioerredukzioa*** metal ioiak mikroorganismoen entzimen bitartez erreduzitzen direnean eta ***bioadsortzioa*** non metal katioiek organismoen

zelula horma eta peptidoekin elkar eragiten duten nanopartikula egonkorrak sortzeko.

II. **Goitik beherako edo *top-down metodoak***: Nanopartikulak modu honen bitartez lortzeko, hasierako materialak kanpokaldetik indar edo alterazio bat jasotzen du eta horrek erreakzioa eragiten du materialean. Alterazio hori eragiteko eta nanopartikulak lortzeko metodo desberdinak daude: indar mekanikoa eta materialaren deskonposizioa, deskonposizio termikoa, laser erradiazio edo argi izpi bitarteko deskonposizio fotokimikoa, plasma edo ultrasoinuen bitarteko deskonposizio sonokimikoa, besteak beste [47,48]. Nahiz eta modu kimikoan nanopartikulak lortu, erradiazio ultramorea edo ultrasoinuak erabili daitezke, nanopartikulen oxidazio egoera aldatzeko edo nanopartikulen tamaina homogeneizatzeko, teknika desberdinak konbinatuz.

Metodo bakoitzak bere xehetasunak ditu eta batzuk hobeagoak dira nanopartikulen tamaina kontrolatzeko eta neurri edo morfologia (borobila, hexagonala, adartua eta abar) interesgarrienak lortzeko. Hain zuzen ere, metodo fisiko eta kimikoen artean, modu kimikoek abaintailak dituzte nanopartikulen erreproduzibilitatea eta tamaina kontrolatzerako orduan.

Gaur egun, nanopartikula metalikoak hainbat aplikaziotan erabiltzen dira, ingurumen arloko aplikazioetan, erreakzio desberdinen katalizatzaile moduan, optika eta elektronikan, energia bilketan, erregai zelda eta baterien elektrodoetan, sentsorikan, optika, biomedikuntza, farmakoen horniketan, plasmonikan eta abar [37].

Aipatutako aplikazioetarako, nanopartikulak gehienetan beste material batean eutsita eta dispertsatuta joaten dira (lan honen kasuan nanozelulosa matrizeetan) eta aipatu bezala, hainbat nanopartikula aukera daude (karbonozkoak, mineralak, metalikoak eta abar) ezaugarri desberdinekin, aplikazioaren berezitasunaren arabera.

Nanopartikula metalikoei dagokienez, eta nanopartikulak metalikoak jasatzen dituzten nanokonpositeak edo sistema moldakorrak lortzeko orduan, nanopartikula metaliko aukerak ere zabalak dira. Hauen artean, ezagunenak metal nanopartikulak (zilarra Ag, urrea Au, kobrea Cu, burdina Fe, platinoa Pt, eta abar) metal sulfuro nanopartikulak, metal oxido nanopartikulak eta dopatutako metal-metal nanopartikulak. edo interes handiko konposatu metal-organikoak (ingelesez *Metal-Organic-Framewoks*-MOF) eta hauen artean, kobre (Cu), zink (Zn) edo manganesoan (Mn) oinarritutakoak [49]. Azken hamarkadan material polimerikoak eta, batez ere, biopolimeroak eta jatorri naturaleko nanomaterialak oso ikertuak izaten ari dira bai nanopartikulen euskarri bezala baita nanokonposite hibrido berritzaileak lortzeko helburuarekin, lan honetan detailatuko den bezala [50].

Azkenik, aipatu beharra dago, dimentsio txikiko nanomaterialek, propietate bereziez gain, kaltea ere eragin dezaketela bizudun handietan. Hain zuren ere 50 eta 70 nm arteko nanomaterialek zelulak zeharkatu ditzakete eta 30 nm dituztenak burmuniera heldu daitezke. Hala ere, oraindik nanomaterialen eta nanopartikuen erabileraren inguruko toxikotasun eta segurtasunaren inguruan informazio gutzi dago eta proiektuak, gidak eta arautegia garatzen ari dira [51,52,53].

### 2.2.3. Konpositeak eta nanokonpositeak

Material konposatuak edo konpositeak XX. mendearen erdialdean agertu ziren teknologia eta ingenieritza arloko etorkizun handiko material bezala. Orokorrean, konpositeak propietate desberdinak dituzten bi edo material gehiagoz osatuta daude, non osagaiak interfaze bitartez bereizi daitezke [54]. Gehienetan, konpositeetan fase eten bat fase jarrai baten barruan aurkitu daiteke, fase eten hau (errefotzu moduan ezagututakoa) fase jarraia baino gogorragoa eta indartsuago izanik. Errefortzu material horiek modu kontrolatuan gehitu daitezke matrizean, materialaren propietate

fisikoak modulatzeko, ohikoenak modulu elastikoa, egonkortasun termikoa edo hausturen propagazioa izan daitezke, baina konpositeek flexibilitate handita ematen dute materialen konbinaketa aukera zabalei esker. Bestalde, konpositeak osagai desberdinen banakako propietateak erakutsi ditzake edo osagaiek efektu sinergikoa eragin dezakete, konpositeari osagai indibidualek ez duten ezaugarri berriak sortuz.

Konpositeak, errefortzu eta matrizearen jatorriaren arabera sailkatu daitezke (**3. irudia**), horrela matrizeari dagokionez, metalikoak, zeramikoak edo polimerikoak aurkitu daitezke. Matrize polimerikoei dagokienez, polimero sintetikoak edo biopolimeroak izateaz gain, elastomeriko, termoegonkor eta termoplastiko bezela ere sailkatu daitezke. Bestalde, ohizko errefortzu materialak zuntzak, partikulak edo laminak izaten dira, errefortzu motak eragin handia duelarik konpositean. Errefortzu mota bakoitzean material desberdinak izendatu daitezke eta errefortzuaren eta orientazioaren arabera materialak anisotropikoak edo isotropikoak aurkitu daitezke [55].

Konpositeek zenbait abantail dituzte material metaliko edo zeramiko soilekin parekatuta, adibidez korrosio eza, haustura edo neke erresistentzia handia edo pisu arina. Hala ere, prezio altua edo makinabilitate txarra moduko eragozpenak ere badituzte.

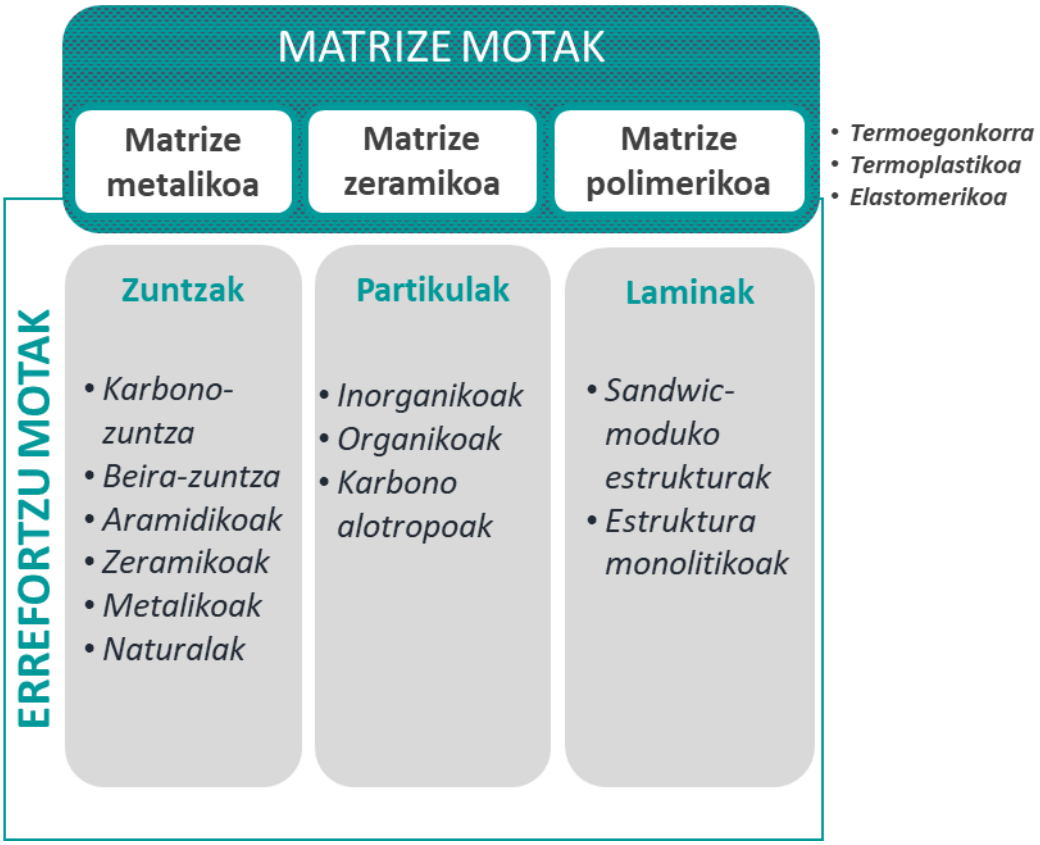


**3. irudia** Konpositeak lortzeko aukerak osagaien arabera [55].

Konpositeen artean biokonposite eta nanokonpositeek interes handia piztu dute azken urteotan. Biokonpositeak laborategian sintetizatu daitezkeen fibra naturaleko (lihoa, kalamua, sisala) konpositeak izan daitezke (matrizea polimero sintetikoa edo biopolimeroa izanik) baina giza gorputzean eta naturan ere aurkitu ditzakegu, hezurrak edo tendoiak dira biokonposite anisotropikoen adibideak [56].

Bestalde, eta aipatu bezala, material konposatu bat nanokonposite moduan izendatzeko, gutzienez materiala osatzen duen fase bat 100 nm baino txikiagoa izan behar da [27].

Azken hamarkadan, nanokonposite polimerikoak oso sakonki garatuak eta ikertuak izaten ari dira. Konposite horiek, matrize polimerikoa daukate eta gutzienez dimentsio bat 100 nm baino txikiagokoa duten nanomaterialak dauzkate dispertsaturik (**4.**

**irudia**). Errefortzu nanomaterialak propietateren baten hobekuntza dakarkio materialari [57].

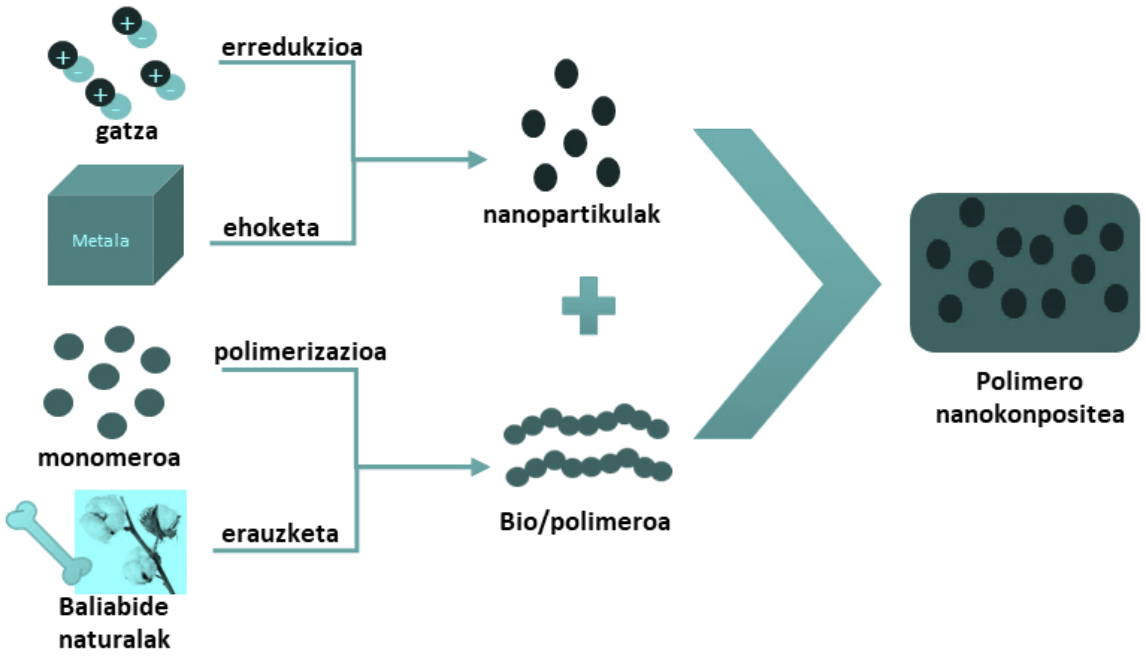


**4. irudia** Nanokonposite polimerikoen osagaiak [59].

Nahiz eta nanokonpositeak gero eta ospe gehiago duten, jadanik 1860an lortu zen lehen fabrikatutako nanokonpositea eta, konkretuki, ikatz beltzez erreforzatutako hagun bat izan zen. Orduan ikertzaileek baieztatu zuten, kautxoan dispertsatutako ikatz beltz nanopartikulek kautxu bulkanizatuaren propietate mekanikoak hobetzen zituztela. Aurrerago, XX. mendearen hasieran, silizio kea eta prezipitatutako kaltzio karbonatoa moduko beste nanoerrefortzu batzuk hasi ziren erabiltzen.

1950ean, National Lead Company-k lehen nanobuztin konpositea patentatu zuen, konposite honetan nanobuztinak erabiltzen ziren elastomeroak indartzeko. Baina produktuak ez zuen komertzializazio handirik izan eta Toyota enpresak 1988an nanobuztin-poliamida patentatu zuenean, hasi zen onartzen silikato kapa molekularren kontribuzioa materialaren propietate makroskopikoetan.

Garapenarekin jarraituz, Toyotak aurretik patentatutako konpositearen aplikazio komertziala atera zuen, hain zuzen ere % 95 poliamida eta % 5 nanobuztindun

konpositez fabrikatutako banaketa uhal bat izan zen. Polimero geruzen artean kokatutako nanobuztinek, trakzio erresintentzia eta distortsio termikoak hobetzen zituzten. Hortik aurrera, 2001an Toyotak material hau dimentsio handiagoko osagaietarako erabili zuen (karrozeria eta kolpe-leungailuak) eta bere aldetik General Motors-ek, 2002an nanobuztindun konpositeak GM Safari edo Chevrolet bezalako modeloetako edergarri eta beste osagai batzuetan barneratzen hasi zen [57,58].

Gaur egun, nanokonpositeak hainbat aplikaziotan aurkitu daitezke, hezurren osatze denbora hobetzen, propietate antibakteriano egozle moduan, sugarraren atzeratzaile edo ehun zuntzak iragazgaizten edo zuntz moduko matrizeei korrosioaren aurkako ezaugarriak ematen haize-sorgailu edo turbina aeronautikoetan. Bestalde, nanokonpositeak automozioan erabilera berriak dituzte, erresistentzia-pisu ikusgarriak ekarriz, baita eraikuntzan eta ingurumen erremediazio edo energia metaketa moduko aplikazioetan [60].

Nanokoponsite berriak garatzeko orduan joera eta etorkizun handiko aukerak ikusten ari dira karbonoan oinarritutako nanokonpositeen inguruan eta baita nanoegituratako material berriztagarrien inguruan. Zentzu honetan, karbono alotropo (karbono nanotutuak, grafenoa edo fullerenoak) edo nanoegituratutako biopolimeroen deribatuak (CNC eta CNF moduko zelulosaren deribatuetan) aukera interesgarriak dira bai propietate berrien aldetik eta baita aplikazio aukera zabal eta berritzaileengaitik, aurrerago azalduko den moduan. Hain zuzen ere, karbonozko nanokonpositeak lortzeko bide bat nanozelulosan oinarritutako nanokonpositeen karbonizazioa da, pirolisi kontrolatu bitartez [61].

## 2.3. Zelulosan nanokristaletan oinarritutako nanokonpositeak

Zelulosa material interesgarria da dituen ezaugarri apartengaitik eta naturan aurkitu daitekeen polimero natural oparoena da. Zelulosa hainbat landareetan aurkitu daiteke (kotoia, linoa, etab.); baina zereal, fruitu, itsasbelar edo onddo batzuen fillamentuetatik ere atera daiteke . Bestalde, ezin daiteke elikagai bezala erabili, eta, horren ondorioz, ez dago, almidoiarekin gertatzen den bezala, etikaren inguruko arazorik, eta hori ere abantaila bat da. Beraz, zelulosa, landare zelulen hormek osatzen dituzten mikrozuntzek osagai nagusia eta egitura hierarkikoa duen matrizea da, baina ez da bakarrik aurkitzen eta lignina, peptina eta hemizelulosa moduko osagaiez inguraturik dago. Zelulosak erakusten dituen propietate nabarmenenak honako hauek dira [62]:

- Propietate mekaniko paregabeak: zurruntasun eta modulu elastiko altuak, nahiz eta zelulosaren jatorriaren arabera aldakorra izan. Propietate horiek nanozuntz elementaletan oinarrituta dauden zuntz naturalen egitura hierarkikoaren ondorio dira.
- Izaera hidrofilikoa.
- Uretan ez-disolbagarria.
- Berriztagarritasuna.
- Toxikotasunik baxua (LD50 orl rat : >5000 mg/kg, LC50 ihl rat : >5800 4h mg/m³, LD50 drm rbt : >2000 mg/kg)
- Biodegradagarritasuna: degradazio entzimatikoaren bidez zelulosa zelobiosa bihurtzen da, eta honen degradazioaren bitartez, glukosa eta energia lortzen dira.

Egitura kimikoari dagokionez, β-D-glukosa (glukopiranosa) 1-4 loturen bitartez osatutako zelobiosa-unitateen errepikapenaren bitartez osatutako polimero bat da

zelulosa (**5. irudia**). Lerro-formako kateak sortzen dira eta kate horiek elkarren arteko hidrogeno-zubien bitartez elkarri eragiten diote, eta zuntzak eta sareak osatzen dira. Loturen eta sareen orientazioa aldakorra izan daiteke zelulosaren alomorfo desberdinak aurkituz, hain zuzen ere 6 polimorfo ezagutzen dira (I, II, $III_I$, $III_{II}$, $IV_I$, $IV_{II}$). Hala ere zelulosa natiboan $I_\alpha$ eta $I_\beta$ aurkitzen dira, eta jatorriaren arabera bata edo bestea nabarmenduko da. Beste polimorfoak zelulosa jasatzen dituen tratamendu desberdinen ondorioa dira [69].

Nahiz eta zelulosa natiboaren polimerizazio-gradua esperimentalki kalkulatzea konplexua den, 10.000tik gertu dagoela esan daiteke, eta hori 3,2 x $10^6$ g/mol inguruko pisu molekularra da. Zelulosa-mikrozuntzek zurruntasunarekiko, ez-disolbagarritasunarekiko eta eraso entzimatikoekiko erresistentzia-ezaugarriak agertzen dituzte, alde kristalinoak dituzte, eta alde ez-ordenatu eta amorfoak, propietate mekaniko txarragoak dituztenak. Zelulosaren aplikazioen artean nabarmenena eta ezagunena papergintza da; hala ere, ehungintzako eta elikagaigintzako eta kosmetika-industrietako osagaia ere bada [63].

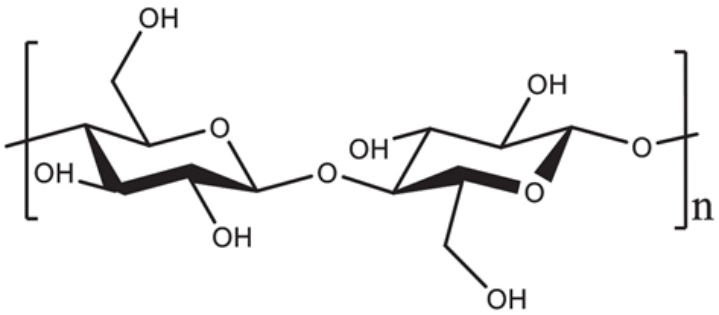


**5. irudia** Zelulosaren egitura kimikoa.

### 2.3.1. Nanozelulosa eta nanozelulosaren deribatuak

Aurreko atalean aipatu den bezala, zelulosa material interesgarria da eta aski ezaguna; hala ere, ikerketa arloan, nanomaterialak ari dira interes handia eragiten. Zelulosari dagokionez, zelulosaren nanoestrukturak dira interes handia sortzen ari direnak, haien ezaugarri berezien ondorioz.

Eskala nanometrikoko materialen inguruan piztu den interesa, neurri txiki horretan agertzen dituzten propietate fisiko-kimikoen ondorioa da. Horrela, atomo eta molekulen eskalako materialak sakonki aztertzen eta garatzen ari dira horien ezaugarri berezien eta propietateen suspertzean duten eraginagatik. Adibidez, nanoeskalako materialek gainazal espezifiko altua dute (itxura-erlazio handiaren ondorioz) eta ezaugarri horrek eragin garrantzitsua dauka propietateetan. Testuinguru honetan, nanozelulosa da naturalki lor daitekeen nanomaterial interesgarrienetariko bat, besteak beste, haren multifuntzionaltasun-aukerengatik [64].

Bestalde, nanozelulosak baditu ezohiko propietate batzuk beste material batzuetatik bereizten dutenak:

- Morfologia bereziak (ikusi **6. irudia**).
- Neurri nanometrikoak, aldakorrak nanozelulosa-motaren arabera.
- Azalera espezifiko handia: 10 $m^2/g$ eta 1.000 $m^2/g$ artekoa.
- Berezko berritze eta biodegradagarritasuna.
- Dentsitate baxua: 1,4 $g/cm^3$ eta 1,6 $g/cm^3$ artekoa
- Gardentasun optikoa: % 80 inguruko transmitantzia.
- Zurruntasun eta tentsio-erresistentzia handiak.

- Malgutasun-modulu axial handia (Young modulua): 110-220 GPa, kristalinitatearen arabera
- Egonkortasun termikoa ≈ 200 ºC eta espantsio termikoaren koefiziente txikia: 3 ppm/ºC eta 22 ppm/ºC artekoa.
- Azal-erreaktibotasun kimikoa, egokitze-aukera ugariek kontrolatutako interakzioen bitartez (beste polimeroekin, nanopartikulekin, molekula txikiekin edo material biologikoekin).
- Kristalinitate altua (batez ere zelulosa nanokristalen kasuan).
- Kristal likidoaren portaera, zenbait egoeratan
- Hesi-propietateak, gasen aurkako irazgaiztasuna.
- Biobateragarritasuna eta toxikotasunik eza.

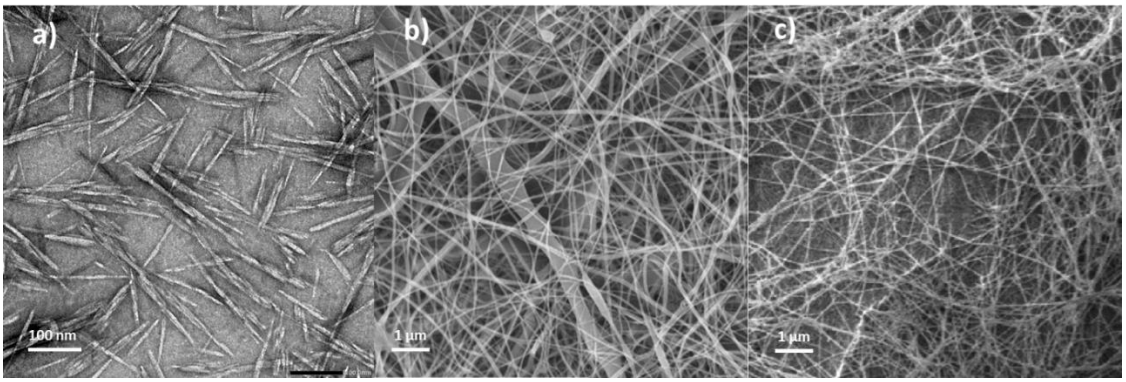


**6. irudia** Nanozelulosaren deribatuak (a) Zelulosa nanokristalak ZNK (b) Zelulosa nanozuntzak ZNZ (c) Nanozelulosa bakterianoa NZB [65,66,67].

Esan bezala, nanozelulosa baliabide natural desberdinetatik lor daiteke. Ezagunenak landareak dira, baina ez bakarrak; izan ere, egitura eta mota desberdinetan lor daiteke nanozelulosa, teknika edo prozesu desberdinak erabiliz [68]:

1. biosintesi bidez: bakterioak moduko mikroorganismoek zelulosa purua sor dezakete mintz zitoplasmatikoan dauden zelulosa entzimen bitartez, zelulosa

zelulen kanpoan lortzen da. Bakterioen artean, Gluconacetobacter xylinus bakterioa da ikertuenetatik emankorrena [90].

2. landareen desintegrazioaren bidez: prozesu mekanikoak eta aurre-tratamenduak erabiliz zuntzak eta nanozuntzak lortzen dira landareen zelulen hormetatik; ondoren, hidrolisi kimikoa eraginez, alde amorfoak desegiten eta alde kristalinoak mantentzen dira (ikusi **7. irudia**).

Aipatutako sintesi- moduek 3 hurrengo ataletan azalduko diren nanozelulosa mota desberdinetara daramate.

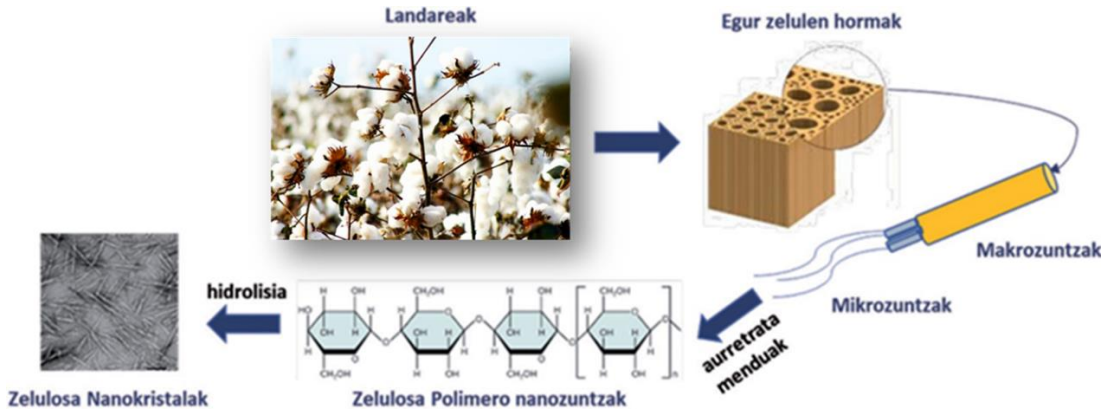


**7. irudia Zelulosa-nanokristalen lorpen prozesua** [69].

### *2.3.1.1. Zelulosa-nanokristalak edo ZNKak*

Zelulosa-nanokristalak (ZNKak), zelulosa nanokristalino izenez ere ezagunak, egur-pulpetan edo kotoi landareetan aurkitu daitekeen zelulosa naturaletik ateratzen daitezke. Behin prozesu mekanikoen eta aurretratamenduen bidez zelulosa mikrokristalinoa lortuta, hidrolisi azido moduko prozesu kimiko bitartez zelulosa-nanokristalak lortzen dira. Nanokristal horiek, hidrolisi-prozesuan ohikoa den azido sulfurikoaren eraginez, sulfato taldeekin negatiboki kargatuta geratzen dira, eta horrek eragin handia du material honen erreaktibotasunean. Honako hauek dira, orokorrean, zelulosa-nanokristalen ezaugarri nabarmenenak [64, 70]:

- Sintesi-metodoa: prozesu kimikoa (hidrolisi-azidoa), alde amorfoak desegiteko eta alde kristalinoak mantendu eta nanokristalak lortzeko (ikusi **7. irudia**).
- Morfologia-egitura: hagatxo moduko nanopartikulak; hagatxo bakoitza kristal zurrun bakar bat bezalakoa da.
- Partikulen neurriak: 5 nm eta 50 nm arteko zehar-sekzioa eta 50 nm eta 500 nm arteko luzera.
- Kristalinitatea: % 88 ingurukoa.
- Transmitantzia optikoa eta kristal likido portaera zenbait egoeratan
- Dentsitate baxua: 1,5 g/cm$^3$ eta 1,6 g/cm$^3$ artekoa.
- Gainazal handia 10 m$^2$/g eta 100 m$^2$/g artekoa.
- Zurruntasun eta erresistentzia mekaniko nabarmena, Young Modulu axial handiekin (130 GPa inguru).
- Ur koloide egonkorra osatzeko eta ura biltzeko ahalmen handia eta kristal likido portaera.
- Gainazala-aldaketa kimiko erraza, erreaktibitatea.

Propietate berezi hauei esker ZNKa material egoki bihurtzen da polimero matrizeak indartzeko, barneratzen diren polimero horien propietate mekaniko, termiko eta optikoak edo hesi-propietateak hobetzeko.Hala ere, zelulosa nanokristalen propietateak oso baldintzatuta daude erauzte eta isolamendu tratamenduekin, baita zelulosa lortzeko autatutako iturri naturalarekin (landare, itsasbelar, fruitu edo zereal mota) eta hauen ezaugarriekin [71]. Nahiz eta egitura kimikoa berdina izan, purutasun, polimerizazio maila edo kristaltasun maila desberdina bada, honek eragin handia dauka propietateetan . Orokorrean,

erauzketa prozesu mekanikoa indartsua da eta ondorengo pausua berriz, azido indartsuekin gauzatzen den hidrolisi erreakzio da.

Hidrolisiaren helburua lotura glikosidikoak apurtzea da, alde amorfoak galdu eta alde kristalinoak (zelulosa I polimorfismoa) mantentzeko, materiala txikitzen delarik. Hidrolisirako azido sulfurikoa da azidorik erabiliena, eta zelulosa azido soluzio baten (%wt 64), temperatura (45 ºC) eta denbora jakin batean (30-45 min) urperatzen da etengabe irabiatuz. Behin hidrolisia burututa, erreakzioa eten egiten da eta azido hondarrak urarekin eta sodio hidroxidoarekin garbitzen eta neutralizatzen dira, ala ere zelulosa nanokristalaren gainazala sulfato ester taldeekin ($-OSO_3^-$) geratzen da Z-potentzial balore negatiboetara helduz [72]. Negatiboki kargatutako gainazala abantaila bat da ZNKak ura bezalako zenbait disolbatzaile polarretan dispertsatzeko orduan baina, desabantaila moduan egonkortasun termikoa txikiagotzen dute, ez kargatutako zelulosarekin parekatuta.

Nahiz eta azido sulfurikoa den azido erabiliena ZNKak lortzeko, azido klorhidrikoa, bromidrikoa, fosforikoa edo nitrikoa ere erabili izan ohi dira. Bestalde, beste hidrolisi modu edo tratamendu modu batzuk berriki agertu direnak, hauen artean likido ioniko bitarteko hidrolisia (1-butil-3-metilimidazolium kloruro bitartez) edo hidrolisi entzimatikoa (endoglukanasa entzimek eragindakoa) [73, 74]. Nanozelulosarekin erabilitzen den tratamendu ezaguna TEMPO-oxidazioa da, prozesu honen bitartez ZNKaren gainazalko hidroxilo taldeak karboxilo (-COOH) taldeetan transformatzen dira 2,2,6,6-tetrametilpiperidina-1-oxilo (TEMPO) erreaktiboa erabiliz. Erreakzio hau oso erabilia da ZNZen lorpen prozesuan aurretratamendu moduan gainazal kargaren eragina indargabetzeko eta delaminazioa hobetzeko [75].

Aipatu bezala, zelulosa eta zelulosaren deribatuak diren zelulosa nanokristalak ezaugarri interesgarriak dituzte baina zenbait desabantaila ere badituzte bere egitura kimikoaren ondorioz. Desabantaila hauen artean solubilitate txarra, ur absortzio gaitasun handia edo termoplastizitate falta nabarmendu daitezke. Hala ere, egitura kimikoak eta konkretuki OH taldeez jositako gainazalak, hiru OH talde anhidroglukosa unitateko, aukera asko ematen ditu gainazala eraldaketa bitartez propietateak modifikatzeko [76]

Orokorrean, gainazala lotura kobalentea sendoekin modifikatu daiteke edo interakzio ez kobalente ahulagoen bitartez (indar elektrostatikoak edo Van der Waals indarrak). Bestalde, erreakzionatzen edo interakzionatzen duten talde funtzional, molekula, makromolekula edo erreaktiboen arabera zelulosa nanokristalen gaianazala eraldatzeko aukera erabilienak hurrengo hauek dira (**8. irudia**):

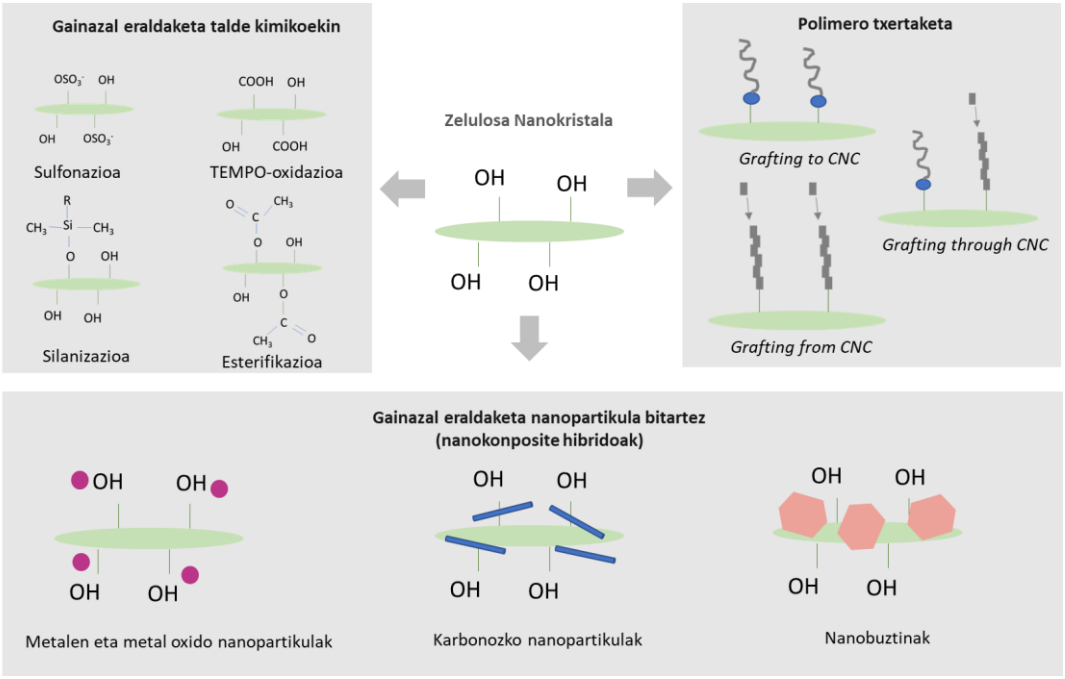


**8. irudia** Zelulosa nanokristalen gainazal eraldaketa aukerak (elaborazio propioa) [77].

- **Talde kimikoen bidezko gainazal eraldaketa**: Teknika honetan erreakzio kimikoen bitartez ZNKren gainazaleko OHak beste talde funtzional edo talde erreaktibo, sinple edo konplexuagoengaitik, ordezkatzen dira. OH taldeak ordezkatzeak gainazal egitura kimikoa eraldatzen du eta honek eragin handia dauka propietateetan, besteak beste hidrofilia moduko propietateetan. Nahiz eta aukera zabalak dauden, sulfonazioa, azetilazioa, esterifikazioa, sililazioa, kationizazioa, aminazioa, edo tempo oxidazioa dira funtzionalizazio aukera ezagunenak [78].

- **Polimero txertaketa edo *polymer grafting-a:*** teknika honekin lotura kobalente bitartez, zelulosa nanokristalari beste polimero bat (edo gehiago) lotzen zaizkio talde funtzionalen bitartez edo polimerizazioa ZNKan bertan eraginez. Polimero txertaketa propietate berriak dituen ZNK funtzionala prestatzeko modu sofistikatu bat da eta aukerak eta teknikak anitzak dira konplexutasun desberdinekin [79]. Txertatzen diren polimeroak natural edo sintetikoak izan daitezke eta baita hidrofobia edo hidrofilia ezaugarri garrantsitzua bat da aukeraketa egiteko orduan. Hala ere, orokorren txertaketa burutzeko hiru modu daude:

  - ***Polymer grafting to CNCs*** teknikaren kasuan, beste polimero bat ZNKrekin lotzen da gainazaleko -OH taldeez baliatuz. Teknikaren abantaila txertatzen den polimeroa karakterizatu daitekela da eta emaitza ondo kontrolatu daitekela. Poli(2-metil-2-oxazolina) PEOX, poli (etilenglicol) PEG edo poli(isobutil vinil eter) PIBuVE txertaketa amino taldeez funtzionalizatutako zelulosara dira teknika honen adibide batzuk. Gehienetan, txertatzen den polimeroa polimerizazio ioniko edo polimerizazio kationiko bitartez lortua izan da, zelulosa estrukturara akoplatu aurretik [80].

- ***Polymer grafting from CNCs*** deritzon bidea erabili ezkero, monomero bat ZNK gainazalean lotzen da eta hortik aurrera polimerizazioa gertatzen da. Teknika desberdinak erabili daitezke [81]:

  - *Ring Opening Polimerization* (ROP) teknika, non laktona, ε-kaprolaktona, eta karbonato edo eter zizliko moduko monomeroak erabiltzen diren ZNKan polimeroak sortzeko eta ZNK-g-esterrak sintetizatzeko, besteak beste [82].

  - *Surface-Initiated Free Radical Polymerization* (SI-FRP) teknika, teknika hau erabiliena da eta zelulosa nanokristaletan binilo polimeroak sortzeko hasarazle bat erabiltzen da. hidrogeno abstrakzioa kasu askotan. Honen adibidea, azio akrilikoarekin CNC-g-PAA polimerizazioa da non poli(azido akriliko) PAA kateek ur erretentzio propietate apartak ematen dizkioten zelulosa nanokristal gelari.

  - *Surface-Initiated Controlled Radical Polymerization* (SI-CRP). Polimeroak hazteko teknika hau oso efektiboa da polimeroren arkitektura, konposizio, pisu molekular edo dentsitatearen kontrola behar direnean. Teknika honetan, adibidez, kobre bitarteko SI-CRPak talde funtzional askorengan dauka tolerantzia eta ZNK kate polimeriko barietate handi batekin txertatu daiteke.

- ***Polymer grafting through,*** aurreko metodo bien erdibidean dagoen teknika da. Metodo honek bi pauso nagusi ditu: lehenik makromonomeroak, hau da, hazten ari den kateak gainazaleko toki aproposean erreakzionatzen du beharrezkoa den hasarazle eta temperatura aplikatuz, eta ondoren erantsitako molekula hazten

jarritzen da monomero gehiago gehituz. Teknikaren abantaila, edozein polimerizazio teknika ezagunekin erabili daitekela da, polimerizazioa bera izanda kontrol hobea ematen duena txertatutako kateengan. Polimerizazio teknika hau ez da oso erabilia izan material zelulosikoetan, zelulosaren deribatuen makromonomeroen erabilgarritasun urria dela eta [83].

- ***Nanopartikula bitarteko funtzionalizazioa*:** partikula organikoak edo inorganikoak erabiltzen dira ZNK errefortzu bezala eta lortutako materialak nanokonposite hibrido moduan ezagutu daitezke, errefortzuak inorganikoak direnean. Orokorrean, hiru nanopartikula mota dira erabilienak:

  - ***Nanopartikula metalikoak**:* talde honetan metal eta metal oxido nanopartikulak aurkitzen dira. Aukera zabala dago ,nanokonpositearen aplikazio eta propietate beharren arabera ($TiO_2$, $Fe_2O_3$, Au, Cu, Ag, Pt eta abar). Zentzu honetan, nanopartikula metaliko bitarteko gainazal eraldakatek mota askotako propietate eta ezaugarriak eman ditzake gainazal funtzionalizazio bitartez, propietate elektrikoak, magnetikoak optikoak, katalitikoak, antibakterianoak, hidrofoboak, bestek beste [65].

  - ***Karbonozko nanopartikulak*:** Talde honetan karbono nanohodiak edo karbonozko nanozuntzak moduko karbono alotropoak nabarmendu daitezke. Nanoegitura interesgarriak dira, adibidez, propietate mekanikoak hobetzeko edo konduktibitate elektrikoa lortzeko [84].

  - ***Nanopartikula mineralak***: talde honetan montmorillonita ($M_x(Al_4–_xMg_x)Si_8O_{20}(OH)_4$).edo saponita ($M_xMg_6(Si_8–_xAl_x)Si_8O_{20}(OH)_4$) bezalako nanogeruza egiturako silikatoak edo nanobuztinak nabarmentzen dira [85]. Buztin nanopartikulek interes handia dute polimeroen

egonkortasun termiko, estabilitate dimentsional, propietate mekaniko eta hezi propietateak hobetzerako orduan.

Lan honetan, zelulosa nanokristalak funtzionalizatzeko nanopartikula metalikoen aukera aztertu da eta baita katioi metaliko bitarteko beste polimero baten elkargurutzaketa. Zentzu honetan, nanokonposite hibridoen inguruan (polimeroa eta errefortzu metalikoak) gaur egun dagoen erronkarik handienetakoa nanoerrefortzuak matrizeen ondo dispertsatzea da [86].

### *2.3.1.2. Zelulosa-nanozuntzak (ZNZ) edo nanofibrilatutako zelulosa (NFZ)*

Zelulosa-nanozuntzak (ZNZak) edo zelulosa nanofibrilatua lortzeko lehen pausoa zuntzak egurraren pulpatik, kotoi-landaretik, paper birziklatutik edo gisako materialetatik ateratzea da. Lehenik zuntz horiek findu eta homogeneizatu egiten dira mikrofibrilatutako zelulosa lortzeko. Horretatik aurrera, mikrofibrilatutako zelulosari prozesu kimiko eta mekanikoa ezartzen zaio isolatutako nanozuntzak lortzeko.

Aurretratamenduetarako garatutako teknika gehienak prozesu kimikoetan oinarritzen dira; prozesu erabilienak 2,2,6,6-Tetramethylpiperidine 1-oxyl (TEMPO) bidez katalizatutako oxidazioa, klorito-periodato bitarteko karboximetilazioa [75], sulfonazioa edo hidrolisi azidoa dira. Kontuan izan behar da aurretratamendu horiek sintesi-prozesuan produktu kimiko ez-jasangarriak eta kostu altuagoak dakarrela; beraz, beste teknika batzuk interesgarriagoak izan daitezke. Teknika horien artean hidrolisi entzimatikoa eta aurretratamendu mekanikoak daude; nahiz eta orain arte lortutako propietateak kaskarragoak izan, aukera jasankorragoak dira bai ekonomiaren ikus puntutik, bai ingurumenaren

aldetik. Beraz, zelulosa-nanozuntzen deskribapen eta ezaugarri nagusiak honako hauek dira [87,88]:

- Sintesi-metodoa: Presio handiko homogeneizazioaren eta ehoketaren ondoren, aurretratamendu kimikoa edo entzimatikoa erabiltzen da nanozuntzak isolatzeko, edo prozesu mekaniko erabil daiteke delaminazioa lortzeko eta zuntzetatik nanozuntzak lortzeko.
- Morfologia-egitura: Zelulosa-nanozuntz bakar edo agregatuak, luzeak eta malguak, alde kristalino eta amorfodunak.
- Partikula neurriak: 5 eta 50 nm inguruko diametroa eta 1-2 µm-ko luzera, izpitze prozesuaren eta aurretratamenduen arabera.
- Trakzio-erresistentzia eta malgutasun handia, 100 GPa inguruko Young Moduluarekin.
- Kristalinitatea: % 70 ingurukoa.
- Fisikoki korapilatutako sareak oso kontzentrazio baxuetan (<%1 pisuan).

Zelulosa-nanozuntzak eta haren deribatuak zabalki erabili izan dira partikula ezorganikoentzako txantiloi bezala, eta nanozuntzen malgutasun handiari eta neurri bereziei esker, zelulosa-nanozuntz/nanopartikula ezorganikodun konpositeak hainbat industria-aplikaziotarako erabiltzen dira: papergintza, mintzak, ehun-gaiak eta abar. Dena dela, zenbait aplikaziotarako, zuntzen luzerak mugak ezartzen ditu nanoeskalakoa ez bada.

### *2.3.1.3. Nanozelulosa bakterianoa (NZB)*

Nanozelulosa bakterianoa NZB, zelulosa mikrobianoa izenez ere ezaguna, zenbait bakteriok eragindako biosintesi bidez produzitzen da. Nanozelulosa

bakterianoaren ezaugarriak bakterio motaren eta hazkuntza-baldintzen arabera aldatuko dira, baina gehienetan kristalinitate altuko zelulosa-nanozuntzezko sare korapilatu baten forma hartzen du, hidrogeno-loturez batuta zuntzak gurutzatzen diren tokietan [67,89].

Adibidez, hazkuntza likido estatikoan eragiten denean, Gluconaceto-bacterxylinus, Gluconacetobacter medellinensis edo beste zelulosa mota bat produzitzeko espezie-kultibo garbien bitartez, gel uniforme bat sortzen da, haren % 1 zelulosa-zuntzei dagokie eta % 99 likidoa da, aire-inguru interfasean dagoena. Orokorrean, honako hauek dira nanozelulosa bakteria- noaren ezaugarriak:

- Sintesi-metodoak: bakterioek (Acerobacte xylinum) eragindako bio-sintesiaren bitartez; unitate txikietatik (Å) unitate txikiko (nm) nanozelulosa lortzen da; edo glukosa-kateak bakterio-gorputzaren barnean sortuz; behin lortuta, zelulosa bakterioaren zelulen bilgarriaren poro txikietatik kanporatzen da.
- Morfologia-egitura: glukosa-kateen konbinazioarekin mikrozuntzek lazo-itxurako agregatu bat osatzen dute, eta beste zelulosa-zuntzekin sare-itxurako egitura bat sortzen dute.
- Partikula neurriak: 5 nm eta 100 nm inguruko diametroa eta askotan 2 μm baino luzeagoak.
- Egonkortasun mekanikoa eta malgutasuna,% 1.5-2.00 elongazio balioekin
- Kristalinitatea (% 72-91).
- Porotasun oso handia.
- Gainazalaren modifikazio kimikorako erraztasuna.

Nanozelulosa bakterianoaren zuntzen egitura-ezaugarriak bitarteko direla, hidrogel-forman egonkortasun mekanikoa eta malgutasuna erakusten du. Hain zuzen ere, NZB gelak asko erabiltzen dira medikuntza, elektronika eta ehungintza moduko arloetan [90].

## 2.3.2. Nanozelulosan oinarritutako nanokompositeak

Nanozelulosaren funtzionalizazio-aukera ugariek eragin handia dute propietate berri eta pertsonalizatutako materialaren garapenean; bereziki, nanozelulosan oinarritutako nanokonpositeen garapenean. Nanozelulosaren gainazalak funtzionalizazio-aukera ugari eskaintzen ditu, nanoeskalako dimentsioak eragindako hainbat eta hainbat azaleko –OH talderen eta gainazal espezifiko handiaren ondorioz. Gainazal-funtzionalizaziorako prozesu esperimental gehienak kondizio epeletan egiten dira nanopartikulen integritatea eta eraldatutako gainazal- kateak *peeling* efektutik babesteko [49,56,76].

Funtzionalizatutako nanozelulosa polaritate baxuko likidoetan ere dispertsa daiteke, eta matrize soluzioekin nahasi. Horrek inguru ez-polarretan nanozelulosaren dispertsioaren hobetzea ahalbidetzen du eta nanozelulosaren azken aplikazioaren optimizazioa erraztu. Hala ere, horren ondorioz, hidrogeno-loturen bitartezko nanozelulosa partikulen interakzioak murrizten dira, eta murrizketa hori da nanozelulosaren dispertsio onaren arrazoia [91,92]. Beraz, nanozelulosaren propietate fisiko eta kimikoek baliagarri egiten dute hainbat konposite matrize hidrofiliko edo hidrofobikoetan erabiltzeko, eta bai material hibridoetan erabiltzeko ere. Gainera, nanozelulosaren gainazal espezifiko handiak barne interakzioak egiten ditu posible, baita beste polimero batzuekin, beste nanopartikulekin edo molekula txikiekin loturak sortzea ere.

Gaur egun materialak modu desberdinetan sailka daitezke, gehienetan aplikazioaren arabera edo jatorriaren arabera, baina sailkapen horiek ez dituzte material mota guztiak kontuan hartzen. Horregatik, eta aipatutako sailkapenak murriztuak direlako, askotan, aukera erabilgarria oinarrizko egituraren distribuzioaren arabera sailkatzea da edo, beste modu batera esanda, egituran duten bolumen aske kopuruaren arabera. Sailkapen horretan, *bottom-up* moduan fabrikatutako nanozelulosa egitura desberdinak aurkitu daitezke [93]. Hain zuzen ere, egituran bolumen aske handia edo txikia izateak, diferentzia nabarmenak eragiten ditu materialen ezaugarri fisikoetan eta portaeran.

Azaldutako sailkapenen arabera, hurrengo ataletan nanozelulosaren estruktura nabarmenenak aipatuko dira: filmak, gelak eta aerogelak.

#### *2.3.2.1 Filmak*

Nanozelulosa-filmek orri-antza daukate, eta lodiera aldakorra, nanozelulosa-kontzentrazioaren (% pisuan) kantitatearen eta lorpen-prosezuaren arabera (ikusi **9. irudia**). Nanozelulosa-filmek Young modulu handia dute, 14 GPa ingurukoa, eta dentsitate txikia, nahiz eta aerogelarenak (0,008-0,05 g/cm$^3$) baino askoz handiagoa (1-1,6 g/cm$^3$) [94].

**9. irudia** Nanozelulosa filma [65].

Filmak lortzeko teknika desberdinak daude (**10. irudia**) baina lan honetan lurruntzeak induzitutako automihiztatze metodoa (EISA, *Evaporation induced self-assembly* moduan ezagutua) erabili da. Filma lortzeko, ur-nanozelulosa dispertsioa, ondo nahasi ondoren, Petri plater batean isurtzen da, tenperatura egokian, ura lurrundu eta plateraren forma hartzen duen film lehorra lortu arte [65, 94].

Hala ere, zelulosa nanokristal filmak hot pressing edo beroko prentsatzeta bitartez ere lor daitezke, prentsa batean zelulosa solidoa sartu eta tenperatura egokian zapaldu eta luzarazi ondoren. Beste teknika batzuk *dip coating* edo *spin coating*-a dira, nahiz eta filma oso fin edo estaldurak lortzeko egokiagoak diren, edo extrusioa, baina azken teknika hau nanozelulosa errefortzu moduan gehitzen denean erabiltzen da [95,96,97]. Bestalde nanozelulosan oinarritutakoak bezalako filmak *nanopaper* moduan ere ezagutzen dira [98].

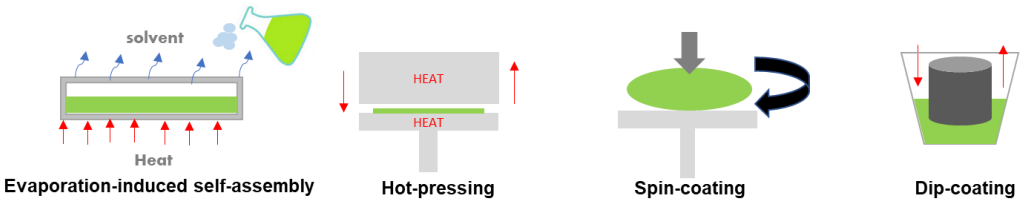


**10. irudia** film eta estaldurak fabrikatzeko teknika ezagunenak [95,96].

Nanozelulosaren erreaktibitate eta funtzionalizazioari esker, material honetan oinarritutako nanokonposite-aukera asko sintetiza daitezke talde kimiko desberdinak gehituz, aplikazio desberdinetarako. Aplikazio horien artean, enbalatzeko material moduko erabilera da ezagunenetarikoa, ohiko plastiko ez-biodegradagarriak ordezko gisa, baina medikuntzan eta beste arlo batzuetan ere ari dira nanozelulosa-filmen aplikazioa berriak agertzen [98].

### *2.3 2.2. Hidrogelak*

Gela material solido gelatinakara da eta haren propietateak itxura leun eta bigun batetik itxura gogor eta zurrunera alda daitezke (ikusi **11. irudia**) [99]. Egoera geldikorrean jariakortasun-eza duen material solido gelatinakar gisa ere defini daiteke. Bere sare tridimentsionalari esker, solido bezala portatzen da, nahiz eta barnean likidoa duen eta gel-estrukturak mugatzen duen solidoa izan. Beste era batera esanda, gela solido baten barneko molekula likidoen estalgarria da; non solidoa fase jarraitua dan, eta likidoa fase sakabanatua. Barneko likido hori ura denean, hidrogel deitzen zaio, eta gel bateko partikula solidoen diametroa 1 nm eta 1.000 nm bitartekoa izan daiteke.

Gel mota desberdinak aurki daitezke, gela osatzen duen konposatu organiko edo ez-organikoaren jatorriaren arabera, konposatuak zehazten baitu zein izango den erabileraren azken xedea Orain dela gutxi arte gel erabilienak eta ikertuenak silizezko gela eta aluminazkoa izan dira, baina azken urteetan nanozelulosa-gelak oso ezagunak egin dira.

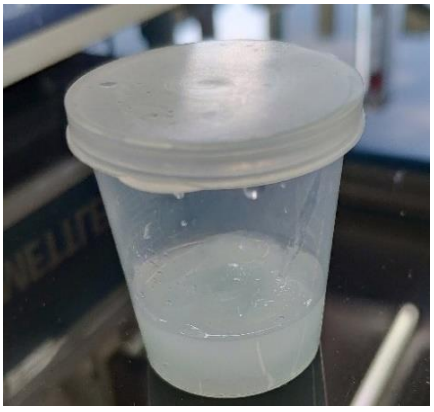

**11. irudia** Nanozelulosa hidrogela. [iturri propioa].

Gela lortzeko, nanozelulosaren suspentsio edo soluzioaren egoerak aldatu behar dira eta sol-gel oreka muga gainditu, gainazaleko taldeak estaliz (gatzak gehituz), gainazala eraldatuz (dela kationizazioz, dela silanizazioz), edo beste polimero

batekin gurutzatuz [100. 101]. Horrela, kateen arteko indar elektroestatikoak txikiagotzen dira, suspentsio koloidalaren egonkortasuna txikitzen da, eta, ondorioz, gela osatzeko aukera handitzen da. Kasu batzuetan, pisu molecular edo biskositate handiko polimeroetan, kontrentrazio handitzea nahikoa da gela lortzeko eta pHak eta temperaturak ere eragina dute gelifikazioa lortzeko orduan.

#### *2.3.2.3. Aerogelak*

Aerogelak material bereziak dira; oso arinak eta porotasun handikoak (% 90-99,8); dentsitate izugarri txikia dute, eta gainazal oso handia, 10 $cm^2/g$ eta 600 $cm^2/g$ artekoa. Aerogel ezagunenak eta lehenak, silize, ikatz edo polimero sintetikoetan daude oinarrituta, baina azkenaldian material berriztagarri eta jasankorretan oinarritutako aerogelak oso arrakastatsuak bilakatzen ari dira. Horien artean, nanozelulosa-aerogelek ezaugarri berriak agertzen dituzte: eroankortasun termiko txikia, malgutasuna, isolatzaile termiko moduko propietateak, bustitako erresilientzia nabarmena eta soinu-absortzioa. Zelulosa-aerogelak, normalki zenbait urratsetako sol-gel prozesuen bidez lortzen dira. Lehen pausoa zelulosaren dispertsioa da; ondoren, gela lortu eta azkenik, lehortze superkritikoaren edo liofilizazio-prozesuaren bitartez aerogelak eta kriogelak lortzen dira [101,102.]:

- ***Liofilizazioaren*** **kasuan,** gelak duen likidoa ura izaten da, eta presio eta temperatura baxuan ematen den deshidratazio prozesu bat da. Lehenik gela izoztu egin behar da (hotzgailu arruntean edo nitrogeno likido bitartez) eta baldintza egokietan, liofilizadorean **(12a. irudia)**, gelak duen ur izoztua sublimatu eta solido egoeratik gasera igaro eta galdu egiten da. Horrela, uzten duen tokia hutsik geratzen da, poroak sortuz baina egitura molekularra mantenduz [103,104].

- **Lehortze superkritikoa** temperatura altuetan egin daiteke (etanol moduko alkoholekin) edo temperatura baxuetan ($CO_2$ likidoa erabiliz) eta segurtasun handiagoarekin. Lehenik gelaren disobatzailea etanolarekin ordezkatzen da. Ondoren gela autoklabe moduko tresna batean kokatzen da **(12b. Irudia)** eta etanola $CO_2$ likidoarekin ordezkatzen da presioa igoz. Behin zirrikitu guztiak $CO_2$ likidoz beteta dauden, apurka apurka $CO_2$-aren punto kritikoa gainditu egiten da (temperaratura eta presio kritikoak 30,97ºC eta 73,77 bar gainditzuz) karbono dioxidoak fluido superkritiko egoera lortu eta modu zehatz eta kontrolatuan irtenarazteko eta gela aerogel bilakatzeko [105].


**12. irudia** (a) Laginak liofilizadorean eta (b) Lehortze superkritikorako ekipoa

Beraz prosezu bakoitzean, gelak dituen fluidoek (ura, etanola edo carbono dioxido likidoa) fase transizio desberdinak sufritzen dituzte, presio eta temperatura nabarmen desberdinen eraginez, **13. irudian** irudikatu den moduan [106]. Lehortze superkritikoak beste prozezuek baino kalte gutxiago eragiten dio egiturari eta gehienetan gainazal espezifiko handiagoak lortzen dira. Liofilizazioaren kasuan, izotz kristalak sortu eta egituran kalteak sortu daitezke eta lehorketa ez da hain kontrolatua. Bestalde geletik ez ezik suspentsio koloidal batetik ere aerogela zuzenean lortu daiteke, liofilizazioa teknika erabiliz, lan honen emaitza esperimentalean ikusiko dan bezala.

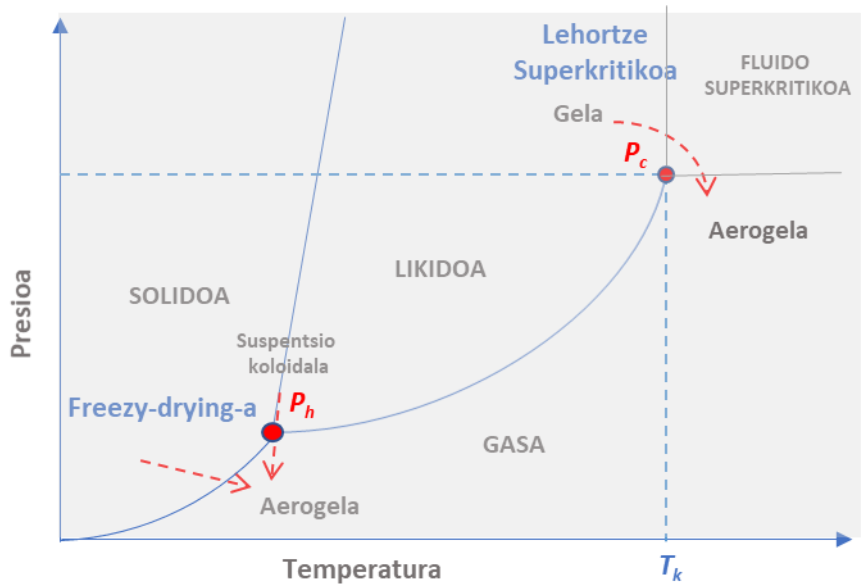


**13. irudia** Liofilizazioaren eta lehortze superkritikoan parte hartzen duten fase trantsizioak [106].

Behin gela lortuta, material porodunak lortzeko moduaren arabera, aerogelak, kriogelak edo baita xerogelak ere lor ditzakegu (**14. irudia).** Azken hauek lehortze arrunt bitartez lortzen dira, disolbatzailea berogailu batean temperatura aproposean lurrunduz. Xerogelek aerogelek baino porositate gutziago izaten dute

**14. irudia** ZNK-aerogela [iturri propioa].

Porodun materialak, poro neurriaren arabera, mikroporoso (>2 nm), mesoporoso (2 nm-50 nm) edo makroporoso (>50 nm) bezala sailkatzen dira. Hala ere, gehienetan material berean poro tamaina desberdinak agertzen dira.

### 2.3.3. Aplikazioak

Nanozelulosa funtzionalizatuak, material berriztagarri desberdin (likido, solido, gel) eta egonkorren inguruan, aukera zabalak ematen ditu aplikazio esparru handi baterako. Material horren propietate bereziak kontuan hartuta, nanozelulosan oinarritutako material konposatuak erabilera anitzetarako potentziala erakusten ari dira hainbat aplikazio-arlotan [107] (ikusi **15. irudia**). Hain zuzen ere, atal honetan, nanozelulosaren eta nanozelulosatik deribatutako materialen aplikazio-aukerak sailkatu eta deskribatuko dira sektore eta arlo desberdinen arabera.

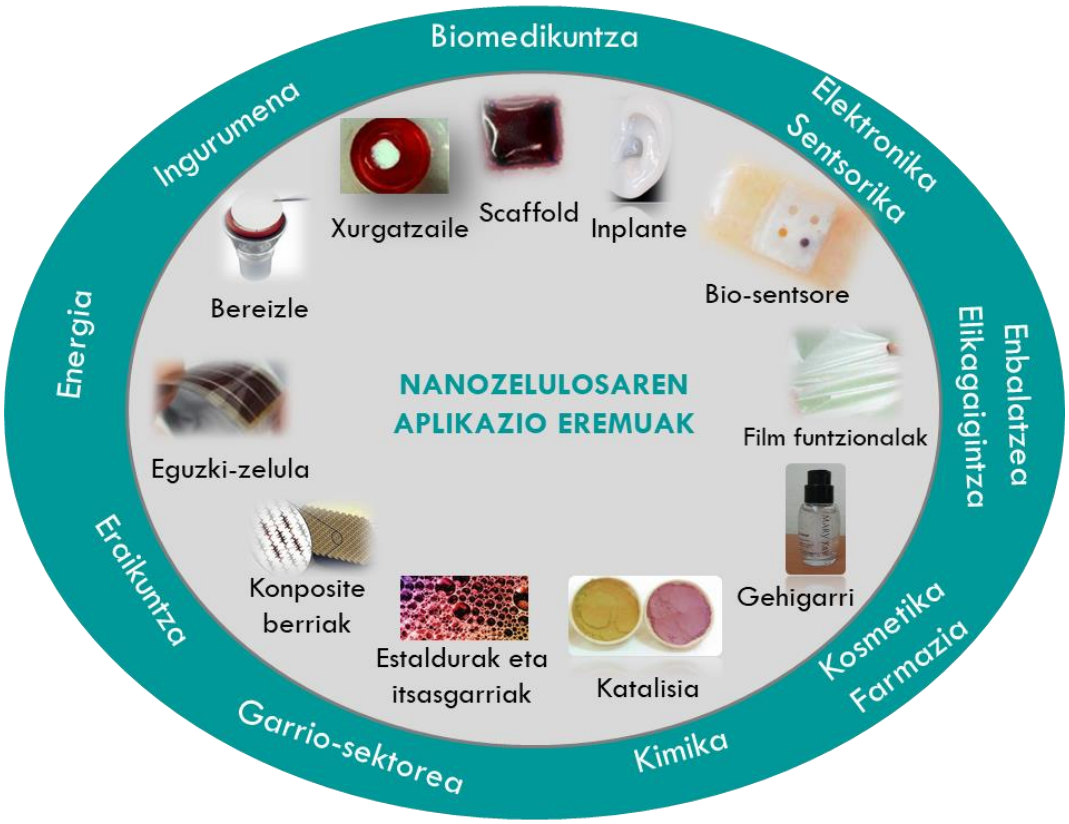


**15. irudia** Nanozelulosan oinarritutako konpositeen aplikazio eremuak [elaborazio propioa].

### *2.3.3.1. Enbalatze industria*

Nanozelulosa filmen lehenengo aplikazioetarikoa enbalatze-industria izan da, bereziki elikagaigintzan, non ohizko enbalatze-materialak ordezka baititzake [95]. Enbalatzearen helburu nagusia barnean duen produktua babestea eta haren biziraupena luzatzea da. Hasieran aipatu den bezala, gaur egun erabiltzen diren enbalaje sintetikoek ingurumenarekiko arazoak eragiten dituzte haien kopuru handiagatik eta biodegradagarritasun ezagatik. Honen ondorioz, enbalatze-industriaren joera ohiko material sintetikoak jatorri naturaleko material biodegradagarriekin ordezkatzea da. Material horien artean, nanozelulosa eta nanozelulosa-konpositezko filmak nabarmendu dira, erakusten duten propietate mekaniko eta hesi-propietate apartengatik [108]. Hala ere, oraindik hobekuntza eta ikerkuntza-eremu handia dago ohiko plastikoen zenbait propietate lortzeko eta plastiko funtzionalak lortzeko, hauen artean patogenoen aurkako edo suaren kontrako plastikoek interes handia dute. Paper eta kartoiaren kasuan ere, zelulosa nanofibren sarrerak hobekuntzak dakarkie berez zelulosa bidez fabrikatutako osagaiei.

### *2.3.3.2. Ingurumena eta Energia*

Ingurumenarekin eta energiarekin edo energia-efizientziarekin lotutako aktibitate askotan, nanozelulosak eta haren deribatuek aplikazio potentzialak dituzte. Aplikazio horietatik ezagunenak aipatuko dira.

- *Iragazkia ur-hondakinen tratamenduetan*

  Industria mota desberdinek eragindako ur-hondakinek, normalki, esekidura solidoak, partikula organiko edo inorganikoak, metalak eta beste ez-purutasun batzuk edukitzen dituzte. Partikula horien tamaina txikia eta gainazal-kargaren presentzia direla eta, erronka bihurtzen da partikula horiek masa handienetik gertu kokatzea eta iragaztea.

Partikula eta konposatu horiek erauzteko modu desberdinak daude: hauspeatze kimikoa, mintz bidezko separazioa, ioi-trukea, flokulazioa, elektrolisia eta baporizazioa. Zentzu horretan, nanozelulosa konposatuak ur industrialetan edo ur-hondarretatik kutsatzaile organiko edo ez-organikoak ezabatzeko erabil daiteke. Bere barne-egitura bereziari esker funtzionalizatutako nanozelulosaren zenbait taldek ioi metalikoak harrapatzeko ahalmena dute, gero uretatik ateratzeko [109].

Teknika batzuk amina eta karboxilato taldeetan oinarrituta daude gelazio eragile bezala edota nanozelulosaren –OH taldeen oxidazio katalitiko eta selektiboaren bitartez. Sukzinilazio-erreakzioa ere, beste funtzionalizazio aukera bat da. Ondorioz, funtzionalizatutako nanozelulosa berriki erabilia izan da, ur-hondakinen koagulazio-flokulazio tratamenduetan. Koagulazio-flokulazio tratamendu konbinatuak suspentsio egonkor baten uhertasun-hondarraren oxigeno-eskaera kimiko (OEK) txikiagoa eragiten du, eta, horrekin batera, kontsumo kimikoaren jaitsiera nabarmena.

- *Xurgatzailea eta bereizlea ur kaltetuetan*

Petrolioz edo olioz kutsatutako urek eragin tamalgarria dute uretako eta lurzoruetako izaki bizidunengan, eta baita gizakien osasun eta ekonomian ere. Besteak beste, turismoa mehatxupean jartzen dute, material horien geruza-propietate, zatarkeria eta usain nazkagarriarengatik. Horregatik, mundu mailan premiazko eskaria dago uretako petrolio-kutsadurak ezabatzeko teknologia eta modu desberdinak garatzearen inguruan.

Xurgatzaile bezala erabiltzen diren materialen inguruan ere kezka dago, eta jasangarritasuna, kostu efektiboa, berrerabilera eta ingurumenarekiko lagungarri izatea dira material horien ezaugarri interesgarriak. Zentzu horretan, nanozelulosan oinarritutako nanokonpositeek etorkizun handia

dute haren neurri nanometrikoari esker (2−100 nm). Bestalde, berriki garatutako nanozelulosa-aerogel berrienek konbinatu egin dituzte hiru dimentsioko aerogel materialen porotasuna, gainazal handia eta dentsitate baxua, eta material naturalen propietate mekaniko ikusgarria, oparotasuna, berritze-ahalmen naturala, biodegradagarritasuna eta azalera-aldaketarako ahalmen handia. Hori guztia kontuan hartuta, nanozelulosan oinarritutako aerogelak material jasangarri interesgarriak dira, olio-xurgatzaile bezala erabiltzeko duten xurgatzaile-ahalmen handiagaitik; aplikazio horretarako, lehenik aerogela funtzionalizatu egin behar da propietate hidrofobikoak ezartzeko [110-111-53].

Ezaugarri hori bereziki, aproposa da ingurumeneko kalteen zuzenketan; adibidez, itsasoetako edo beste inguru batzuetako olioak ezabatzeko. Xurgatzaile-aplikaziorako ez ezik, nanozelulosa-aerogeletan oinarritutako mintzen inguruko garapena nabarmen ari da hazten ingurumenerako aplikazioetarako ere; besteak beste, likido desberdinak bereizteko porositate izugarriko material horiek duten ahalmenagatik. Azkenaldian, mintz-teknologiak, beste ohiko adsortzio, destilatze edo erauzte-teknologia batzuen aurrean, gailendu egin dira etorkizuneko teknologia moduan, haien berezko abantaila eta nagusitasunarengatik. Mintzak erregai-zeluletan, gas-hesietan edo ur-purifikaziorako aplikazioetan erabil daitezke, besteak beste [112].

- *Energia-metaketa eta eguzki-zelulak*

Nanozelulosaren beste aplikazio arloa energia-metaketa da. Zentzu horretan, zelulosa-nanozuntzez osatutako foam edo aerogelek karbono dioxidoa harrapatu eta bakartu dezakete, gas- biltegi eta airea purifikatzeko iragazle gisa jarduten.

Bestalde, metaketa-sistemen (litio-baterien, superkondentsadoreen edo eguzki-zelulen) eskaria gero eta handiagoa da, eta, gainera, sistema horiek jasangarriak izatea eskatzen da; testuinguru horretan, nanozelulosaren garapenak eta erabilerak ere badituzte aukerak. Zehazki, nanozelulosan oinarritutako konposatuak elektrodo bezala erabil daiteke sistema elektrokimikoetan, material horren propietate fisiko onak direla eta, baina aplikazio horretarako beharrezkoa da aurretik nanozelulosan aldaketa fisiko-kimikoak eta konduktibitate elektrikoa eragitea [113].

Energia-metaketan ez ezik [114], nanozelulosa energia fotovoltaikoaren oinarri diren zenbait eguzki-zelulen osagai moduan ere erabil daiteke, hain zuzen ere *Dye sensitized solar cells* izenpean ezagututakoak. Azkenik, bateria eta superkondentsadoreetan, osagai bezala (elektrodo edo bereizgailu) era erabiltzen hasia da [115].

#### *2.3.3.3. Biomedikuntza*

Biomedikuntza arloan nanozelulosa gero eta osagai erabiliagoa da aplikazio desberdin eta berritzaileetan, kasu honetan aplikazio frogatuenetan nanozelulosa bakterianoa erabiltzen da honen purutasunagaitik. Aplikazio arlo interesgarrienak hurrengo hauek dira:

- *Substantzia kimikoen garraiobidea eta emailea*

Nanozelulosa funtzionalizatuaren aplikazio-arlo bat biomedikuntza da, eta arlo horren barruan, oso interesgarria da farmakoak dispentsatzeko izan dezakeen ahalmena. Hain zuzen ere, proteinak, entzimak edo peptidoak immobilizatzeko, garraiatzeko eta azkenik askatzeko ahalmena dauka nanozelulosaren gainazal porositate handiari esker [116, 117].

- *Soluzio antiseptikoak*

Nanozelulosak mintz edo gel bilakatzeko duen ahalmenari (lehenago azaldua) propietate antimikrobianoak gehitzen badizkiogu, zeinek zilarrarekin (Ag) funtzionalizatzeak ematen baitizkio, material aparta lor dezakegu tiritak eta beste soluzio antiseptiko malgu batzuk fabrikatzeko. Hain zuzen ere, zilarrak E. coli eta S. aureus bakterioen hazkuntza inhibitzen duela hantzeman da [118,119]. Beraz, zilar-partikula txikiekin funtzionalizatutako nanozelulosa erabilgarria da soluzio antiseptiko moduan edo tirita antiseptiko bezala erabiltzeko.

- *Inplante-protesi eta ehun ingenieritzarako scaffold biomedikoak*

Nanozelulosaren propietate bereziak direla eta, (horien artean propietate mekaniko onak) toxikotasun ezari eta biobateragarritasunari esker, nanozelulosa material egokia da gorputz barnean sartzen diren protesi, inplante eta ehunen osagai bezala erabiltzeko. Kasu batzuetan, nanozelulosa material estrukturala izan daiteke, eta beste batzuetan, zelulosa-nanokristalak eta nanozuntzak beste matrize batzuetan errefortzu-material bezala sakabanatzen dira. Aplikazio horren adibide dira hortz-birsorkuntzan erabiltzen diren inplante eta ehun sintetikoak, edo 3D inpresio bitartez fabrikatu daitezkeen nanozelulosa-protesiak, edo birsorkuntzan eta zelulen hazkuntzan erabiltzen diren *scaffold* edo hiru dimentsioko estrukturak [120,121,122] (ikusi **16. irudia**).

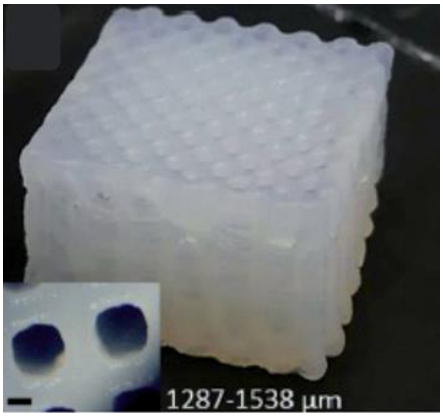


**16. irudia** 3D inprimagailu bitartez fabrikatutako zelulosa-nanokristalezko estruktura tridimentsional [120].

### *2.3.3.4. Sentsorika eta Elektronika*

Nanozelulosaren azaleko talde funtzionalak molekula biologiko mota desberdinekin uztar daitezke, eta nanozelulosak nanopartikula inorganikoak bere gainazalean kokatzeko ere balio dezake. Ezaugarri horiei esker nanozelulosa biosentsoreetan erabil daiteke [123]. Hain zuzen ere, biosentsoreek informazio analitikoa erakusten dute arlo desberdinetarako: medikuntza-diagnostikoak eta bioirudiak, ingurumenaren monitorizazioa, elikagaien kalitatearen kontrola eta sentsorika fisiko-kimikoa 4.0 industrian, besteak beste.

Adibidez, nanozelulosa funtzionalizatuarekin uztar daitezkeen biomolekulak azido nukleikoak dira. Horrek hibridazio itzulgarria ahalbidetzen du, eta nanozelulosak, azido nukleikoen molekulak detektatzeko duen gaitasuna bitarteko dela, tenperatura altuetan banantzen den duplex bat osa dezake. Bestalde, nanozelulosa bitartez funtzionalizatutako material inorganikoak azido nukleikoen hibridazioaren detekzio elektrikorako ere erabil daitezke. Nanozelulosa bitartez funtzionalizatutako titanio oxidoak ($TiO_2$) bide elektroi-eroale gisa erabil daitezke, hain zuzen ere metahemoglobina immobilizatzeko aproposa den nanozelulosa egitura zabaldu samartu bat erabilita. Aldiz, nanozelulosa zitosinaren bidez funtzionalizaten badugu, surfaktanteak detektatzeko sentsibilitate eta potentzial

nabarmena agertzen duen materiala lor daiteke. Azkenik, fotónika eta optika arloko sentsoreen inguruan aplikazioak agertzen ari dira zelulosa nanokristalek zenbait egoeratan hartzen duten egitura helikoidalak ematen dien berezitasunagaiatik.

Horrela nanozelulosa nanopartikula metaliko edo beste nanopartikula motekin hibridatuz, eragin elektriko, optiko, magnetiko edo kimikoetara erantzun dezake biosentsore moldakor aparta bilakatuz. Aurreikus daiteke plataforma gisa nanozelulosa duten biosentsore moldakorretara pasatuko direla laster gaur egun plastiko, beira edo paper-plataformetan oinarritutako sentsore eta inprimatutako tresna elektroniko asko, sentsorika konbentzionala guztiz aldatuz [124,125,126,127].

### *2.3.3.5. Material eta konposite berriak sektore desberdinetarako*

Gaur egun, nanozelulosadun materialak askotan aurkitu ditzakegu aplikazio eta sektore desberdinetan erabilita. Batzuetan, zelulosa bera da materialaren osagai estruktural eta nagusia, eta beste kasuetan, errefortzu gisa aritzen da material solido edo likidoen propietateak hobetzeko [128]. Hain zuzen ere, material konposatuetan, nanozelulosa kopuru txiki batekin, horien indarra eta zurruntasuna asko handitu daitezke; horregatik, nanozelulosa oso interesgarria da garraio-sektoreko eta bereziki automobilgintzarako konpositeen osagai moduan erabiltzeko, ez bakarrik propietate mekanikoengatik, baita haren pisu arinarengatik ere, beste material metaliko astunago batzuen ordez erabil baitaiteke. Konkretuki, arintasuna da gaur egun automobilgintzarako ezaugarri garrantzitsu bat, erregai-kontsumoarekin eta kutsadurarekin guztiz lotuta dagoena [129]. Baina, arintasuna ez ezik, nanozelulosaz indartutako plastikoek erresistentzia hobea ere erakusten dute: berotasunaren, uraren, oxigenoaren edo gasolina-isurien kalteen aurkako erresistentzia.

Nahiz eta aeronautikan eta energia-industrietan materialak ordezkatzea konplexuago den, nanozelulosak beira-zuntzak edo Kevlar bidez kargatutako plastikoak ordezka ditzake etorkizunean, eta badaude lan batzuk abian horren inguruan. Hain zuzen ere, ibilgailu-ekoizleak nanozelulosa bitartez indartutako plastikoak probatzen ari dira, emaitza onak lortuz, urte gutxitan erabiltzeko asmoarekin.[130]

Beste aplikazio-arlo bat eraikuntza da; nanozuntzak, material funtzional moduan, eraikin-blokeetan zabalki erabiltzen dira, biodegradagarri eta betegarri natural bezala, polimero konpositetan isolatzeko eta sugarra atzeratzeko ahalmenari eta jasangarritasunari esker. Hala ere, badago oraindik zer hobetu; zelulosaren polaritate eta hidrofilia direla eta, honek konpatibilitate eskasa ematen dio termoplastiko ez-polar eta hidrofobikoekin. Honen ondorioz, nanozelulosak dispertsio txarra eta interakzio ahulak ditu matrize eta betegarriekin baina badaude aurrerapenak zelulosa nanozuntz higrospikoen inguruan ere, material isolatzaile oinarri moduan, energetikoki efizienteak diren eraikinak garatzeko [131]

### *2.3.3.6. Fluido elektrorreologikoak robotikan*

Inguru elektriko edo magnetiko baten eraginez beren egoera aldatzen duten likidoak dira fluido elektrorreologikoak. Aplikatzen zaien eremuaren intentsitatearen arabera, material horiek milisegundo gutxitan uraren moduan jario, eztiaren moduan isuri edo gelatina moduan solidotu daitezke. Fluido horiek, berez, partikula mikroskopikoak esekita dauzkaten likido isolatzaileak dira. Erabiltzen diren partikulek propietate elektriko edo erdieroaleak dituzte, eta likidoak ez-polarrak izaten dira. Hain zuzen ere, nanozelulosaren eta funtzionalizatutako nanozelulosaren propietate erdieroaleak, besteak beste, material funtzional aparta bilakatzen du suspentsio elektroerantzule edo elektrorreologikoan erabiltzeko [132].

Fluido elektrorreologikoen aplikazio berrietakoa robotikara dago zuzendua, eta konkretuki robot bigunen sorrerara; robot berritzaile horiek, ohiko aginterako sistema elektrikoak erabili ezean, mikrofluidoz osatutako zirkuitu batzuen bidez kontrolatzen dira. Osagai-aldaketa horiek bitarteko direla, gizakien mugikortasuna imita dezakete; azkarragoak izan daitezke, seguruagoak eta merkeagoak, nahiz eta oraindik gaur egun aplikazio batzuetarako gogortasuna beharrezkoa den.

### *2.3.3.7. Estaldura , pintura eta itsasgarriak*

Nanozelulosa estaldura, pintura edo itsasgarri-material bezala ere erabiltzen da beste material batzuen azaleko propietate mekaniko edo fisikoak hobetzeko. Adibidez, nanozelulosa-zuntz monokapak deposizio fisiko edo *spraying* tekniken bitartez lor daitezke, eta kapa horiek estaldura solidoak sortzen dituzte [44].

Aplikazio honen adibide izan daitezke osagai desberdinetan motor-olioaren, butanol ez-polarren edo uraren akziotik libratzeko nanozelulosa-estaldurak. Autogarbiketa funtzio hau ZNKen egitura molekular bereziari esker lor daiteke, eta, hain zuzen ere, nanozelulosa-estaldurak efektibitate handiko babes bezala aritu daitezke, gas, hezatasun, ur, olio edo koipearen iragazia ekiditeko [133].

### *2.3.3.8. Industria Kimikoa eta katalisia*

Nanozelulosa funtzionalizatua, katalisi heterogeneo berrien sostengu- matrize bezala, gero eta gehiago erabiltzen da. Zentzu horretan, nanozelulosa paladio edo platinoa bezalako nanopartikulen dispertsio-matrize bezala erabil daiteke. Nanozelulosan partikula horien dispertsioa altua izaten da, eta beste abantaila bat da substratuen eta material ezorganikoaren arteko erreakzioak eragiten dituen kontaktua efizientea dela. Adibidez, nanozelulosan jasandako nanopartikula sistema hibridoen propietate katalitikoak fenolaren hidrogenazioan edo akoplamendu erreakzio desberdinetan erabiltzen dira, hasu hauetan

nanopartikula bezala paladioa erabiliz [134]. Prozesu honetan inguru-tenperaturan 24 orduz egon eta gero, konbertsio-graduak % 90ekoak izaten dira.

Azkenik, nanozelulosa elikagaigintzan ere erabiltzen da , kasu honetan gehigarri bezala eta elikagaiak egonkortzeko eta loditzeko [135,136], baita kosmetikan, farmazian,nekazaritzan edo ehungintzan, materiala osatzen duten nanozuntzen eta nanohagatxoen propietate aproposez baliatuta. Aipatu beharra dago, nanozelulosa eta zelulosa nanokristaletan oinarritutako nanokonpositeen inguruan ikerketa eta garapena etengabea eta oporoa izaten ari da eta aldi oro emaitza eta aplikazio berritzaileak agertzen ari dira honen inguruan. [137]

# 2.4. Polimero eta konpositeen entsegu eta karakterizazio teknikak

## 2.4.1. Mikroskopia elektronikoko teknikak

### *2.4.1. Ekorketako mikroskopia elektronikoa*

Ekorketako mikroskopia elektronikoa edo *scanning electron microscope* (SEM, ingelesez) luze-zabal erabiltzen den teknika bat da, hainbat materialen morfologia eta testura mikra eskalan aztertzeko. Ekorketa mikroskopia elektronikoa gai da lagin bateko gainazalaren bereizmen handiko irudiak sortzeko, elektroi-materia interakzioak baliatuz.

Ekorketako mikroskopia elektronikoak eremu-sakonera handia du, eta laginaren zati handi bat fokuratu dezake aldi berean. Halaber, bereizmen handiko irudiak sortzen ditu, eta, hala, laginaren zatirik txikienak ere anplifikazio-maila handiz azter daitezke. Laginak prestatzea nahiko samurra da. Izan ere, ekorketako mikroskopio elektroniko gehienek gauza bakarra eskatzen dute: laginak eroaleak izatea. Eskuarki, lagina karbono-geruza batez estaltzen da, edo urrezko edo tankerako metal batez eginiko geruza fin batez, lagina eroalea izan dadin [139].

Teknika honek, elektroi-sorta bat erabiltzen du, eremu elektriko baten bidez azeleraturik (ΔV) eta lente kondentsatzaile bidez kontzentraturik. Lente horrek laginaren gainean eragiten du sorta finaren forman, eta elektroiek ekortu egiten dute. Bobinei esker gainazala puntuz puntu ekortzen da, kanoitik barrena bidaiatzen duten elektroi azeleratuen bidez interakzio mota desberdinak emanez. Azkenik, elektroimanetan oinarrituriko lenteez osaturiko detektagailu batek laginak bueltaturiko elektroien kopurua eta intentsitatea neurtzen ditu, seinale konbertsioa egiten da eta hiru dimentsiotan irudi digitala lortzen da. Laginean irakurtzen den puntu bakoitza pixel bat da, eta, zenbat eta handiagoa izan dispositiboak

zenbaturiko elektroien kopurua, orduan eta handiagoa izango da pixelaren distira pantailan **(17. Irudia).**

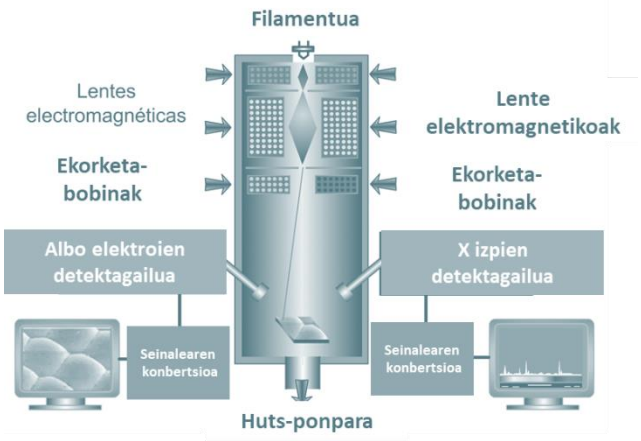


**17. irudia** Ekorketa mikroskopio elektronikoaren funtzionamendua.

Lan honetan, ekorketako bi mikroskopio elektroniko baliatu dira (**18. irudia**), premien arabera: batetik, bereizmen handiagoko ekipamendu bat (Hitachi S-4800N FEG-SEM), zeinaren bidez metalezko nanopartikulak behatu ahal izan baitira, eta, bestetik, X izpien energia dispertsiozko espektrometria-detektagailua edo *energy-dispersive X-ray spectroscopy* (EDS edo EDX, ingelesez) duen beste ekipamendu bat (Carl Zeiss STS EVO40 Ekorketa mikroskopio elektronikoa).

**18. irudia** Erabilitako SGIker-eko SEM ekipoak

Ohikoa da X izpien espektrometria-teknika horrekin konbinatzea, eta, hari esker, aldi berean erregistra daitezke elektroi-sortak zeharkatzen duen gainazaleko puntu bakoitzetik datozen X izpiak. X izpi bakoitzaren energia elementu bakoitzaren ezaugarria da; horrenbestez, gainazaleko nahi dugun neurriko eremuen mikroanalisiak egin daitezke eta informazio analitiko kualitatibo eta kuantitatiboa eskura daiteke, baita mapa elementalak ere.

Kasu guztietan, laginak prestatzeko prozedura honako hau izan da: aluminiozko egitura batean itsatzitako karbonozko zinta itsaskor baten gainean, lagin lehorraren zati txiki bat zuzenean finkatzen da, oso leunki manipulatuz. Horretaz gainera, laginei ihinztatze metalikoa egin zaie, urrezko estaldura-geruza finak sortzeko (<20 µm) eta beharrezko eroankortasuna lortzeko, Emitech K550X ihinztagailu baten bidez.

#### *2.4.1.2. Transmisiozko mikroskopia elektronikoa*

Transmisiozko mikroskopia elektronikoa edo *transmission electron microscopy* (TEM, ingelesez) materialen egitura eta morfologia eskala azpimikrometrikoan aztertzeko aukera eskaintzen duen teknika bat da, nanometrotan emaniko bereizmenarekin [140].

Transmisiozko mikroskopia elektronikoari esker, laginak ebaketa ultrafinetan behatzen dira. Horretarako, elektroi-sorta bat handitu nahi den objekturantz joaten da, elektroien parte batek errebotatu egiten du edo objektuak xurgatzen ditu, eta besteek, berriz, zeharkatu egiten dute objektua, laginaren irudi handitu bat osatuz. Handitutako irudia erregistratzeko, plaka fotografiko bat edo pantaila fluoreszente bat ipintzen da objektuaren atzean (**19. irudia**).

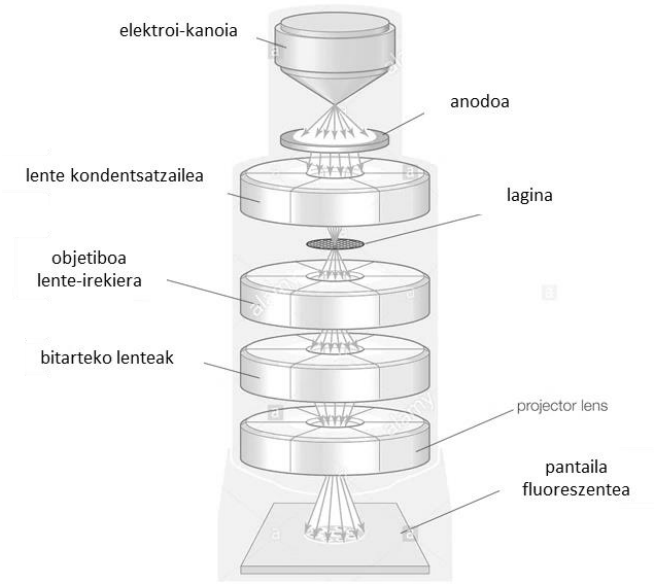


**19. irudia** Transmisiozko mikroskopio elektronikoaren osagaiak [140].

Horrenbestez, transmisiozko mikroskopia elektronikoak eskatzen du laginak geruza finetan ematea. Hori horrela, manipulatzeko adina sendotasun izan behar dute eta ez lurruntzeko adina egonkortasun ere.

Lan honetan, batez ere nanomaterialen neurriak behatzeko baliatu da teknika hori, hala nola nanozelulosazko kristalenak edo metalezko nanopartikulenak. Nanozelulosazko kristalen dispertsioen kasuan, uretan disolbatutako tanta bat ipini zen (0.1 %wt) ikatzez estaliriko sareta baten gainean, eta uranilo-azetatozko tindaketa negatibo bat aplikatu zen mikroskopioaren kontrastea hobetzeko. Ondoren, lagina urrearekin metalizatzen da, hutsean egindako metal-hautseztatzearen bidez, eroale egiteko eta, hala, behatu ahal izateko.

Lan honetarako, Philips CM120 Biofilter mikroskopioa baliatu da (**20. irudia**) 120 kV-ean jarduten duen STEM moduluarekin.

**20. irudia** Erabilitako TEM ekipoa (SGIker).

## 2.4.2 X izpien bidez ezaugarritzea

### *2.4.2.1 X izpien difrakzioa (XRD)*

X izpien difrakzio-teknikek edo *X-ray diffraction* (XRD, ingelesez) solido baten egitura kristalinoa X izpien iturri batekin elkarreraginean ipintzea dute oinarri. Egitura kristalino hori solido askotan agertzen da, eta solido hori osatzen duten atomoak edo molekulak aldiro errepikatzen ditu espazioko hiru norabideetan.

Hiru dimentsioko egitura horren gainean, infinitu plano paralelo trazatu daitezke, eta hainbat puntuk igaroko dute haietako bakoitza.Plano horietako bat hartzen baldin badugu, distantzia jakin batera beste plano bat egongo da, eta han ere berbera izango da ebakitzen duen puntuen banaketa. Bi plano horien arteko distantziari planoarteko d distantzia deitzen zaio, eta, hala, infinitu plano paralelo izango ditugu d distantziaren multiploetan.

X izpien sorta batek plano horietatik bitatik eragitean, fenomeno hau gertatzen da:

- Lehen planotik difraktatzen den uhin-frontea θ angeluan difraktatuz gero, bigarren planoko uhin-frontea ere θ angeluarekin difraktatuko da.

- Ibilbide berriko bi uhin-fronteak ez badaude fasean, interferentzia suntsitzaile bat gertatzen da, eta batak bestea baliogabetzen du. Aldiz, biak fasean irteten badira, interferentzia eraikitzailea gertatzen da: difraktatutako sorta ez da baliogabetzen eta detektagarria da.

- Interferentzia eraikitzailea izan dadin, atomoek emititutako erradiazioaren arteko fasearen aldeak 2π-ren proportzionala izan behar du. Braggen legeak (1.ekuazioa) ematen du baldintza hori:

$$n \lambda = 2 d \sin \theta \qquad (1)$$

non n zenbaki osoa den; λ, X izpien uhin-luzera; d, sare kristalinoaren planoen arteko distantzia, eta θ, berriz, izpi erasotzaileen eta dispertsio-planoen arteko angelua.

Plano-familia bakoitzak d distantzia duenez, plano horiek angelu desberdinetan detektatuko ditugu, eta emaitzak desberdinak izango dira, zer neurtzen ari garen arabera. Hori dela eta, lagina osatzen duten faseak ezaugarritu ahalko ditugu hautemate-pikoetan oinarriturik; hau da, fase bakoitzeko planoen erreflexioak. Bizkor identifikatzeko, faseen balioak fitxetan tabulaturik ageri dira, eta eskuraturiko emaitzekin alderatzen dira.

Atomoak inguratzen dituzten elektroiek X izpiak difraktatzen dituzte, haien uhin-luzera erradio atomikoaren magnitude berekoa baita. Interakzioaren ostean difraktatutako edo sakabanatutako X izpien sorta horrek informazioa gordetzen du bidean topaturiko atomoen posizioari eta motari buruz (**21. irudia**). Zehazki, detektagailuaren bidez, difraktaturiko X izpien intentsitatea eta posizioa behatzen eta neurtzen da, eta, bitarteko matematikoen bidezko osteko analisiaren bidez, aztertutako materialaren atomoen eta molekulen irudikapena lortzen da eskala atomikoan.

Kristalek, beren egitura periodikoari esker, elastikoki zabaltzen dituzte X izpien sortak hainbat norabidetan, eta anplifikatu egiten dituzte interferentzia eraikitzaile bidez, difrakzio-patroi edo difraktograma propioa sortuz [141].

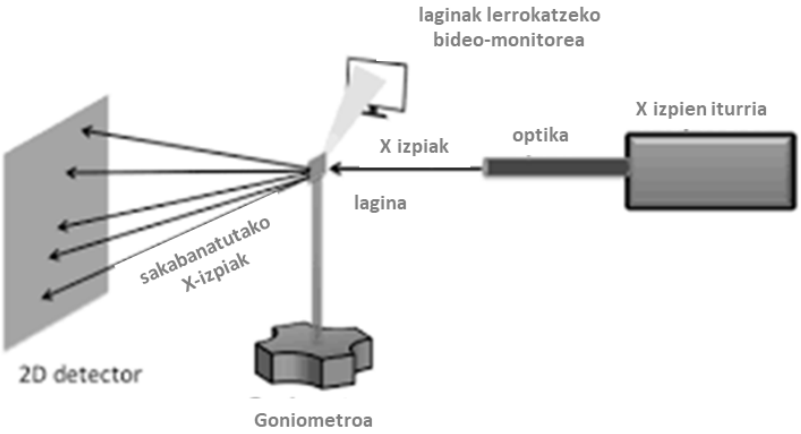


**21. irudia** X- izpi difrakzio teknikaren funtzionamendu eskema [141].

Lan honetan eskuraturiko laginen difraktogramak angelu zabaleko X izpien difrakzio-teknikaren bidez eginak dira, ingelesez *wide angel X-ray diffraction* (WAXD, ingelesez) moduan ezaguna. Erabilitako X izpien difrakzio-ekipamendu gisa, PHILIPS X'PERT PRO baliatu zen (**22. irudia**), theta-theta geometriakoa eta 40 kV eta 40 mA-ra operatzen duen difraktometro batekin. Sistemak zirriztu programagarri bat, kobre-erradiazio bati egokituriko grafitozko monokromatzaile sekundario bat (λ = 1,5418 Å), eta egoera solidoko PixCel detektagailu bizkor bat ditu, 3,347 º-ko 2θ-ko luzera aktibo bati egokiturik. Sistema automatizatu bat du, 45 posiziotarako lagin-aldagailuarekin. Horretaz gainera, ekipamenduak kalitatezko neurketak egiten ditu datuen osteko tratamendurako, profil osoko egokitzapen-mailan, eredu estrukturalarekin edo gabe. Laginak, hauts forman, euskarri generiko baten gainean muntatu ziren, zero hondoko siliziozko wafer batean. 2θ-ko datuak 5 eta 80º balioen artean jaso ziren, 600 segundoko igarotze-

denboran, eta guztizko eskaneatze-denbora, berriz, 2 ordu izan zen giro-tenperaturan.

Bestalde, egitura kristalinoa degradazio termikoaren aurrean aztertzeko, Bruker D8 Advance diffractometer ekipamendua baliatu zen, lagin polikristalinoduna, eta theta-theta geometria (30 kV eta 20 mA artean jarduten duena), kobrezko hodi batekin (λ = 1,5418 Å), Vantec-1 PSD detektagailu ultrabizkor batekin (6º-ko irekiera) eta tenperatura handiko Anton Parr HTK2000 labearekin horniturik. Tenperatura-ganberadun ekipamenduari esker, tenperatura handietan egin daitezke neurketak, giro-tenperaturarik 1600 ºC-ra arte; halaber, hainbat tenperaturatan egin litezke neurketak, atmosfera oxidatzaile estatikoan edo hutsean, isotermekin, edo 20 ºC/seg arteko hoztearekin edo berotzearekin.

Difraktogramak 0,0333º-ko 2θ-ko urratsetan hartu ziren, 8-38º tartean. Datuak 15 ºC eta 400 ºC artean gorde ziren 5 ºC-tik behin, 0,167 ºC/s-ko berotze-abiadurarekin.


**22. irudia** X-izpi difrakziorako erebilitako bi ekipoak (SGIker).

### *2.4.2.2. X izpien bidezko espektroskopia fotoelektronikoa (XPS)*

X izpien bidezko espektroskopia fotoelektronikoa edo *X-ray photoelectron spectroscopy* (XPS, ingelesez) sentikortasun handiko teknika analitiko bat da, eta, hari esker, materialen gainazaleko (10 nm) elementuen informazio espektrala eskuratzen da, nanometroa baino bereizmen txikiagoarekin [139,141].

Laginak X izpien bidez irradiatzen dira huts ultragaraiko baldintzetan, eta horrek eragiten du elektroiak isurtzea gainazaleko atomoen gaineko geruzatik. Isuritako elektroiak fotoelektroi deitzen dira (**23. irudia**), eta energia espezifikoa izaten dute (lotura-energia), zein atomo-kopuruaren eta sorrera-iturri diren geruza elektronikoaren mende egongo baita. Halaxe lortzen da lotura-energien espektroa.

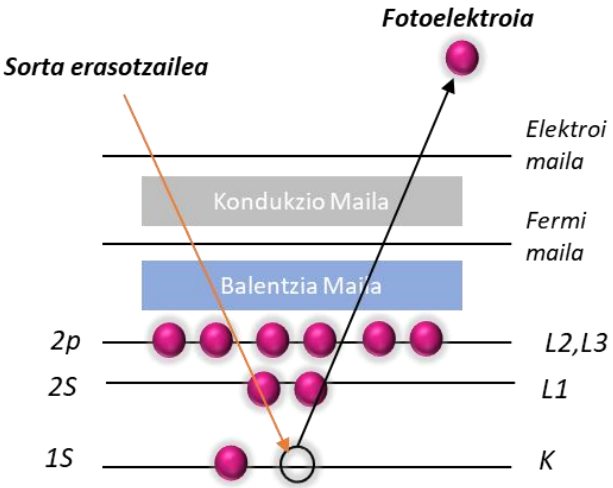


**23. irudia** Prozesu fotoelektronikoa [139].

XPS espektro-lerroak elektroia igortzen duen geruzaren arabera identifikatzen dira (1s, 2s, 3d eta abar). Emititutako fotoelektroiaren energia zinetikoa honako ekuazio honen bidez ematen da (2. ekuazioa):

$$BE = hv - EK \qquad (2)$$

non EK fotoelektroiaren irteerako energía da, hv sorta erasotzailearen energa eta BE atomoaren lotura-energia.

Elektroia kanporatu ostean, kitzikaturiko ioiak bi deskitzikapen-prozesuetako batean eskuratutako energia igorriko du: Auger elektroi baten igorpena edo X izpien igorpena fluoreszentzia bidez.

Pikoen posizioa eta seinalearen erdiko zabalera neurtuz (*full width at half maximun* FWMW, ingelesez), elementu kimikoaren informazioa eskura daiteke, baita haren oxidazio-egoera eta gainazaleko atomoen koordinazio-egoera ere. Beraz, teknika hau, batez ere laginen gainazalean ageri diren elementuak zeintzuk diren jakiteko erabiltzen da, baita haien oxidazio-egoera eta denboran izan dituzten aldaketak ezagutzeko ere.

X izpien bidezko espektroskopia fotoelektronikoari esker, hainbat motatako materialak azter daitezke, hala nola metalak, aleazioak, material zeramikoak, polimeroak, beirak, erdieroaleak, lagin geologikoak, lagin biologiko lehorrak eta, oro har, huts sistemarekin bateragarria den edozer azalera. Aplikazio-eremuak ere askotarikoak dira; esaterako, itsaspen-azterketak, katalisia, korrosioa, materialen gainazal-tratamenduak, elektronika, metalurgia, gainazal-segregazioa, geruzen deposizio-analisia eta abar.

XPS espektroak eskuratzeko, Phoibos 150 1D-DLD energia-analizatzailea baliatu da **(24. irudia),** zeinaren bidez laginen analisia egin baitaiteke behe-eremutik (mikrak) goi-eremura (milimetroak); halaber, Focus 500 erradiazio-iturri monokromatikoa du, Al/Ag(1486.7 eV) anodo dualarekin, zeinaren bidez 400 W arteko potentzietan lan egin baitaiteke aluminioaren (Al) kasuan, eta 600 W artekoetan zilarraren (Ag) kasuan, sentikortasuna eta analisi-denbora hobetzeko.

Sistemak MCU-8 zehaztapen handiko lagin-manipulatzaile bat dauka, eta, hari esker, mugimendu linealak egin ditzake x, y eta z norabideetan, baita errotazio azimutala eta polarra ere, bereizmen angeluarreko analisirako. 800 ºC arte berotzeko sistema ere badu, baita hoztekoa ere.

Lehenik, lehendabiziko analisi bat egin zen elementuak zehazteko, eta, ondoren, bigarren analisi bat detektaturiko elementuak aztertzeko, analizatzailearen eta gainazalaren artean 90º-ko angeluarekin (Electron Leave Angle). Espektrometroa zilarrez kalibratu zen aurrez (Ag 3d5/2, 368,26 eV) eta espektroak, berriz, CasaXPS 2.3.16 softwarearekin doitu ziren, zeinak Gauss-Lorentzian ekarpenak modelizatzen baititu. Kontzentrazioak kalkulatzeko, sentikortasun atomiko erlatiboko faktoreekin zuzendu ziren balioak.

**24. irudia** XPS ekipoa (SGIker)

## 2.4.3. Fourierren transformatu bidezko espektroskopia infragorria (FTIR)

Fourier transformatu bidezko espektroskopia infragorria edo *fourier transform infrared spectroscopy* (FTIR, ingelesez) espektro elektromagnetikoaren parte infragorriarekin loturiko espektroskopiaren adarra da, eta, infragorrian duen erradiazio-motaren arabera, gertukoa, ertaina eta urrunekoa izan liteke [139].

Energia uhin edo partikula (fotoi) gisa aurkez daiteke eta hainbat energia-maila aurkezten ditu, espektro elektromagnetikoa osatuz, zeina loturik baitago, halaber, uhin-maiztasun eta -luzerarekin.

Energia horrek uhin-maiztasuna eta luzera ditu oinarri, eta Planck-en ekuazioaren bidez (3a. ekuazioa) kalkula daiteke:

$$E = h \nu \qquad (3a)$$

non E fotoi baten erradiazio-energia baita, kaloriatan emana; h, berriz, Plancken konstantea, zeinaren balioa $1{,}58\times10^{-34}$ kaloria segundoko baita; eta ν, azkenik, erradiazio horren maiztasuna da, hertz edo $seg^{-1}$ gisa emana.

Mol batean xurgatzen duen energia kalkulatu nahi izanez gero, Avogadroren zenbakiarekin bidertu behar da; hau da, $6{,}023\times10^{23}$ molekula moleko, eta, horrenbestez:

$$E = h \nu \, Na \qquad (3b)$$

Molekula batek espektro infragorrian energia xurga dezan, sorturiko dardarek molekularen momentu dipolarra aldatu behar dute ($\mu > 0$). Alde horretatik, dardara batek simetrikoa denean ez du sortzen aldaketarik momentu dipolarrean ($\mu = 0$), eta inaktibotzat jotzen da espektro infragorrian. Horrenbestez, ez da erregistratzen xurgapen-bandarik. Aldiz, dardara asimetrikoak aktiboak dira, molekularen momentu

dipolarra aldatzen baitute ($\mu > 0$); hori horrela, xurgapen-bandak sortzen dituzte infragorrien eremuan.

Espektrometria infragorriaren oinarria zera da, materialen lotura kimikoek dardara-maiztasun espezifikoak dituztela, zeinak molekularen energia-maila desberdinetakoak baitira [142].

Substantzia batek eremu infragorriko erradiazio elektromagnetikoa xurgatzen duenean, xurgaturiko energiak bibrazioak eragiten ditu molekuletan atomoak elkartzen dituzten lotura kobalenteetan (molekula horiek tenkatu eta uzkurtu egiten dira erresorte gisa, edo guraizeen moduan flexionatzen).

Molekularen egituraren arabera, bi bibrazio molekular mota nagusi sor daitezke (**25. irudia**):

- Tentsio-bibrazioak (tenkatze simetrikoa eta asimetrikoa), mugimendu erritmiko bat egiten dute loturaren ardatzean zehar, eta, hala, atomoen arteko distantzia areagotu edo murriztu egiten da.
- Flexio-bribrazioak (planoan eta plano kanpotik), atomo arrunt bateko loturen arteko lotura-angeluetan izandako aldaketak, edo atomoen mugimendua molekularen gainerakoarekiko, taldean atomoen mugimendurik izan gabe bestearekiko.

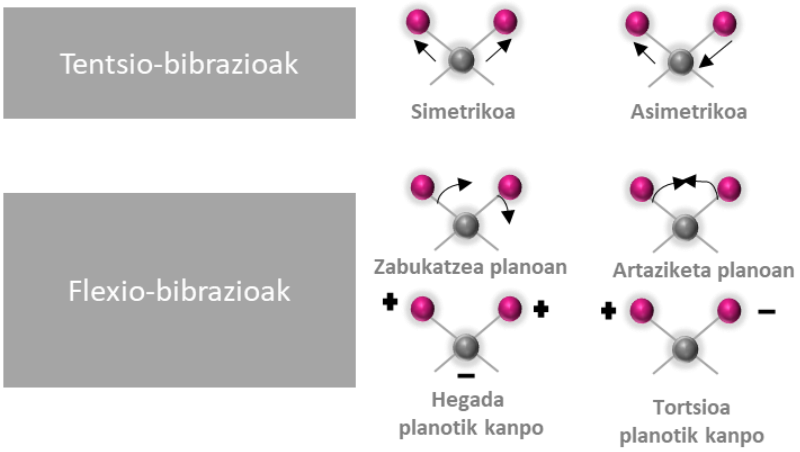


**25. irudia** Molekulen bibrazio mota desberdinak [142].

Hori dela eta, teknika honek informazioa ematen du aztertu beharreko materiala osatzen duten molekulen talde funtzionalen gainean.

Lagin baten neurketa honetan datza: lagina argi-izpi infragorri monokromatiko batekin irradiatzea laginean zehar, erradiazioaren maiztasuna aldatuz 4000 eta 400 $cm^{-1}$ artean eta xurgatutako edo transmititutako energia-kantitatea erregistratuz. Xurgaturiko energiaren aldakuntza (ordenatuen ardatza) maiztasunaren aldakuntzaren aurrean irudikatzen da (abzisen ardatza); hala, hainbat intentsitate eta zabaleratako xurgapen-bandak beha daitezke, zenbait maiztasunetan.

Grafikotik informazioa eskuratzeko, beharrezkoa da talde funtzionalen bereizgarri diren banden posizioa eta forma zein diren jakitea, eta espektroan intentsitate handiena duten bandak aztertzea.

Horrenbestez, xurgapen-bandak molekularen egituraren araberakoak izango dira, baina beste hainbat faktoreren mende ere egongo dira, hala nola geometria, dardara-akoplatze posibleak eta batez ere bandaren intentsitateari eragiten dion lagin-kantitatea.

Teknika honek oso ondo funtzionatzen du laginak lotura kobalenteak dituenean, eta, hori dela medio, kimika organikoan baliatzen da bereziki. Nolanahi ere, oso

erabilgarria da interakzio-erreakzioak identifikatzeko ere material polimerikoen edo material hibridoen nahasteak aztertzeko.

Lan honetan, Kimika Ezorganikoko Saileko Shimadzu FTIR-8400s ekipamendua baliatu da diamante-kristalezko sistema optiko batekin ekipaturik erreflektantzia oso arindurako, baita MIRacle ZnSe osagarri bat ere. Ekipamendu horri esker, erradiazio infragorria erreflektantzia oso arinduarekin (*atenued transmittance reflectance*-ATR, ingelesez) konbina daiteke, eta, era berean, neur daiteke zer aldaketa gertatzen diren barrutik islatutako infragorrien sorta batean, lagin batekin kontaktuan ipintzean. Infragorri-sortak kristal optikoki dentso baterantz jotzen du, zeinak errefrakzio-indize handia baitu angelu jakin batean. Barne-erreflektantzia horrek uhin desagerkor bat sortzen du, zeina kristalaren gainazaletik harago zabaltzen baita, kristalarekin kontaktuan dagoen lagineraino **(26. irudia).**

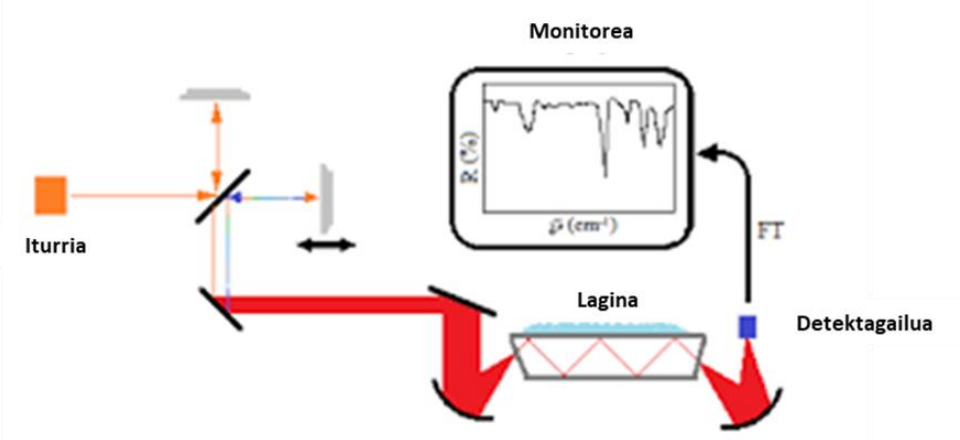


**26. irudia**. Infragorri espektrometria teknikaren funtzionamendua.

Laginak energia xurgatzen duen infragorrien espektroko eremuetan, uhin desagerkorra arindu egiten da. Sorta arindua kristalera itzultzen da, eta, ondoren, kristalaren kontrako muturretik irten eta detektagailurantz jotzen du infragorrien espektrometroan. Detektagailuak interferogramaren seinale gisa erregistratzen du

infragorri arinduen sorta. Interferograma hori infragorrien espektro bat sortzeko baliatzen da.

Teknika bizkor eta soil honen bidez ezaugarriturik, laginaren gainazala aztertu daiteke 0.5 eta 2 mikrako sakonerarekin, mahai gainean metalezko buru baten bidez doiturik **(27. irudia).**

**27. irudia** Infragorri espektrometria ekipoa (Kimika Ez-organikoa saila).

Hainbatetan, hauts-erako laginak KBr anhidrotan zabaldu izan dira, pastilla forman sendoturik, 10 tonako presiopean. Horretarako, FTIR NICOLET NEXUS ekipamendua baliatu da **(28. irudia).**

**28. irudia**. Pastilla moduan neurketan egiteko erabilitako ekipoa (Labquimac).

Infragorrien espektroak 4000 eta 500 $cm^{-1}$ artean erregistratu dira, 2 $cm^{-1}$ baino bereizmen txikiagoarekin.

## 2.4.4. Espektroskopia ultramore-ikusgarria (UV-Vis)

Espektroskopia ultramore-ikusgarriaren edo *ultraviolet-visible spectroscopy* (UV-Vis, ingelesez) teknikaren oinarria hau da: lagin batek xurgatu edo transmititu dezakeen erradiazio elektromagnetikoaren kantitatea (ultramorearen eta ikusgarriaren uhin-luzeraren tartean), ageri den substantzia-kantitatearen arabera izaten da.

Xurgatze-teknika guztiek suposatzen dutenez, erradiazio batek lagin baten gainean eragitean, erradiazio horren xurgapen partzial bat gertatzen da; horren ondorioz, trantsizio bat izaten da substantziaren maila energetikoen artean: atomoa, molekula edo ioia, $E_o$, azken hori kitzikapen-egoerara pasatuz, $E_f$; gainerako erradiazioa transmititu egiten da **(29.irudia).** Hala, bata edo bestea aztertuz, laginean ageri den espezie aktiboaren kantitatea zerrenda dezakegu.

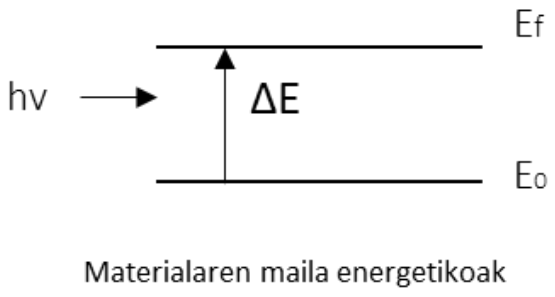


**29. irudia** Radiazioak eragindako energia trantsizioa.

Eragindako energia diferentziala hurrengo ekuazioaren (4. ekuazioa) arabera kalkulatu daiteke:

$$\Delta E = E_f - E_o = h\nu \qquad (4)$$

ΔE substantzia bakoitzaren bereizgarria da, eta horrek analito baten analisi kualitatiboa ematen digu lagin batean. Horretaz gainera, xurgatutako edo transmititutako E kantitatea proportzionala da X kontzentrazioarekin; beraz, analisi kuantitatiboa ere egin dezakegu.

Xurgatutako edo transmititutako argiaren intentsitatearen eta analito-kontzentrazioaren arteko aldea Lambert-Beer legearekin (5. ekuazioa) definitzen da.

$$I = I_o \, e^{-\varepsilon \, l \, c} \qquad (5)$$

non $I_o$ sorta monokromatiko erasotzailearen intentsitatea baita, L egindako bidearen lodiera, I transmititutako argiaren intentsitatea eta c, berriz, substantzia xurgatzailearen kontzentrazioa; azkenik, ε absortibitate molar deituriko proportzionaltasun-faktorea, eta loturik dago aztertzen den substantziaren erradiazio-xurgapenaren probabilitatearekin.

Bestalde, aurreko ekuazioaren logaritmoa erabiltzen badugu (6.ekuazioa), absorbantzia kalkula genezake:

$$\log \frac{I}{I_0} = \varepsilon \, L \, c \qquad (6)$$

non $\log I/I_o$ absorbantzia (A) den.

Edozer substantzia baldin badaukagu, X, tarte ultramore ikusgarrian xurgatzen duena, konfigurazio elektronikoa dela-eta ez du xurgatuko energia bakarrean, baizik eta energia-tarte batean xurgatu ahal izango du, haietako bakoitzean efizientzia desberdinez; horrek substantzia horren xurgapen-espektroa sorrarazten du **(30.irudia),** zeinak adierazten baitu uhin-luzera edo energia bakoitzeko xurgatutako argi-intentsitatea [143].

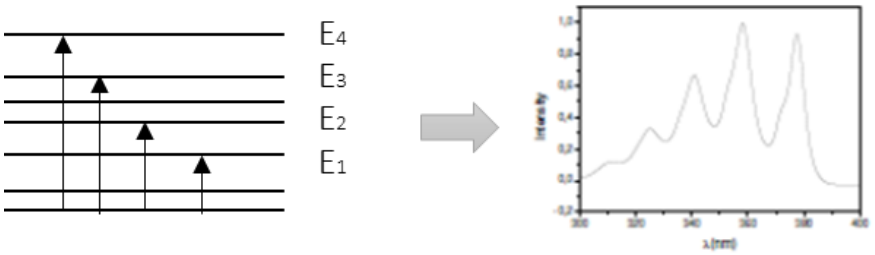


**30. irudia**. UV espektroaren sorrera.

Espektroskopia ultramore-ikusgarria teknika oso erabilgarria da, eta hainbat analito-motaren zehaztapen kuantitatibo edo/eta kualitatiboa egiteko baliatzen da. Espektroskopia ultramore-ikusgarriak, era berean, material baten argi ultramore-ikusgarriaren aurreko portaera-aldaketak frogatzeko ere balio du, material bat gaineratzen denean hala nola, energia xurga dezaketen metalak, eta ezaugarri optikoak eta barrera-ezaugarriak aldarazten dituzte material baten argiaren aurrean. Horretaz gainera, espektroskopia ultramore-ikusgarriaren bidez, erreakzio baten segimendua egin daiteke, zeinean argi ultramore ikusgarria xurgatzen duten materialak sortzen baitira, hala nola metalen erredukzioa. Lan honetan, espektroskopia ultramore-ikusgarria baliatu da azken bi aplikazio horietarako.

Nanokonpositeei egindako argi-xurgapenaren eta -transmisioaren espektroetarako, Shimadzu MultiSpec-1501 espektrometroa baliatu da **(31. irudia)**, zeinak 200-800 nm mailan jarduten baitu, 1 nm tartean eta 25 akumulaziorekin. Kasurik gehienetan, lagina bertikalean ipini da argi-sortarekiko, nahiz eta uretan disolbatutako laginen hainbat neurketa ere egin diren, kuartzozko edo beirazko kubetak baliatuz, egokitzailean txertaturik.

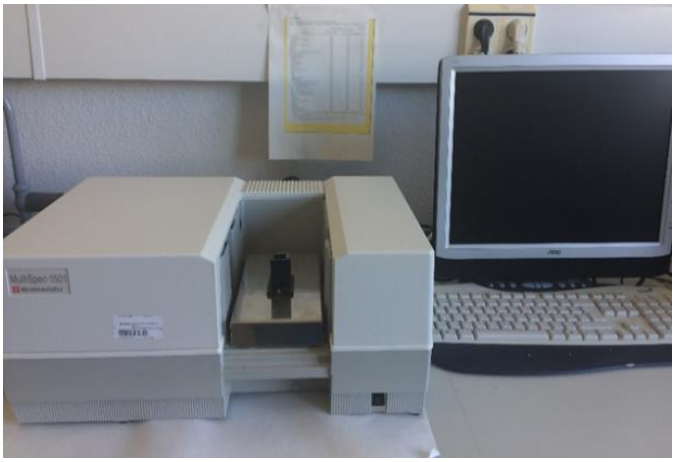

**31. irudia** Erabilitako Ultramore-ikusgarri espektroskopia ekipoa (Labquimac)

## *2.4.5. Analisi termikoa*

Analisi termikoaren metodoen barruan ditugu, batetik, material-lagin bat berotzea inplikatzen duten metodoak eta, bestetik, ezaugarri fisikoren bateko aldaketa neurtzea. Analisi termikoko tekniken artean ageri dira termograbimetria edo analisi termograbimetrikoa (*thermal gravimetric analysis TGA,* ingelesez), masa-aldakuntzan oinarritua, ekorketako kalorimetria diferentziala (*diferencial scanning calorimetry* DSC,*ingelesez*), bero-aldakuntzan oinarritua, eta analisi termomekanikoa (*dynamic mechanical analysis* DMA, ingelesez), ezaugarri mekaniko baten aldakuntzan oinarritua (hala nola tentsioa edo deformazioa) [144].

Analisi termograbimetrikoa horrenbestez, material baten portaera termikoa aztertzen duen teknika analitikoa da, atmosfera kontrolatu baten pean ($N_2$, $O_2$, airea, etab.), berotze- edo hozte-prozesu batean denborarekin gertatzen diren masa-aldakuntzak erregistratuz **(32.irudia).**

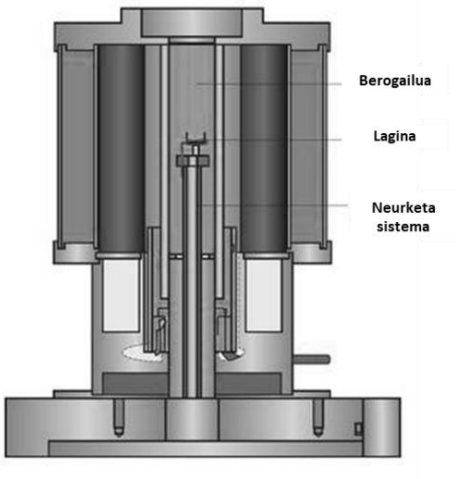


**32. irudia** Termobalantzaren eskema.

Termograbimetriari esker azter daitezke hainbat osagaitako sistemen konposizioa, egonkortasun edo deskonposizio termikoa, atmosfera erreaktibo edo korrosiboek materialetan duten efektua, hezetasunen edo hegazkorren edukia. Halaber, adsortzio- eta desortzio-azterketak ere egin daitezke. Teknika hori luze-zabal baliatzen da hainbat material-motatarako (polimeroak, metalak, zeramikak eta abar).

Lan honetako termogramak TGA METTLER TOLEDO 822e termobalantza **(33. irudia)** bat baliatuz eskuratu dira: lagina aldez aurretik kalibratutako aluminazko arragoa batean ipintzen da. Analisi-metodoak hainbat abiaduratan definitu dira (2, 5, 10 edo 20 ºC/min), laginak 25 ºC eta 600-800 ºC artean berotuz nitrogeno-atmosferan, nahiz eta analisi batzuetan amaierako isoterma bat txertatu den aire-atmosferan. Ondoren, datuak Origin Pro-8.5 softwarearekin esportatu, aztertu eta irudikatu dira parametro esanguratzuenak eta aktibazio energiak kalkulatzeko [145-146].

Ezaugarritze xehatuago bat egiteko, TGA sistemak linean akopla daitezke masa-espektrometro edo FTIR batera interfase baten bidez, askaturiko produktu gaseosoen ezaugarriak identifikatzeko.

Bestalde, ekorketako kalorimetria diferentzialak (*differential scanning calorimetry* DSC, ingelesez) lagin baten eta barne-erreferentzia baten arteko tenperatura-aldea neurtzen du, denboraren eta tenperaturaren arabera. Behatutako tenperaturaren aldeak bero-fluxu bat ematen du. Horri esker, trantsizio endotermikoak eta exotermikoak neur daitezke tenperatura horren arabera, eta hainbat fenomeno azter litezke, hala nola fusioa, beira-trantsizioa, kristalizazio-zinetikoak, eta solido-solido faseko bestelako trantsizioak.

Teknika horiek era askotako materialak eta produktuak ezaugarritzeko baliatzen dira (polimeroak eta itsasgarriak, produktu farmazeutikoak, elikadura-produktuak eta produktu biologikoak, zeramikak, erdieroaleak eta material organikoak, inorganikoak, metalikoak eta konposatuak).

Lan honetan, DSC METTLER TOLEDO 822e ekipamendu bat baliatu da, lagin porta automatikoa duena. Laginak aluminiozko kapsula zigilatu eta zulatuetan sartzen dira.

**33. irudia** Erabilitako TGA eta DSC ekipamendua (Labquimac).

## 2.4.6. Ezaugarri mekanikoen analisia

Material baten ezaugarri mekanikoak aztertzeko, material baten erantzuna aztertzen da, hainbat tentsio eta deformazio eragiten dizkion kanpo-indar baten pean ipintzen

denean. Saiakuntzarik ohikoena dimentsio bateko trakzioa da; hau da, materialaren probeta estandarizatu bat deformazio-abiadura konstante batean, eta, bien bitartean, deformazio bakoitzerako behar den indarra neurtzen da, harik eta materiala hautsi arte. Horretaz gainera, konpresioko deformazio-saiakuntza ere test interesgarria da aztertu beharreko materialerako aurreikusita dauden erabiltzeko edo aplikatzeko baldintzak eta eskakizunak aintzat harturik. Orokorrean, material baten konpresio-erresistentzia trakziokoa baino txikiagoa izan ohi da. Lan honetan azterturiko materialen kasuan, hainbat laginen erantzunak aztertu eta alderatu dira konpresioarekiko erresistentzia-testarekin.

Trakzioko edo konpresioko erresistentzia mekanikoko testen bidez, indarra, tentsioa eta konpresioa ordezkatzen dira deformazioaren aurrean **(35. irudia),** eta Youngen Modulua neurtzeko, berriz, tarte elastikoen puntu bakoitzeko kurbaren tangenteak irudikatzen dira.

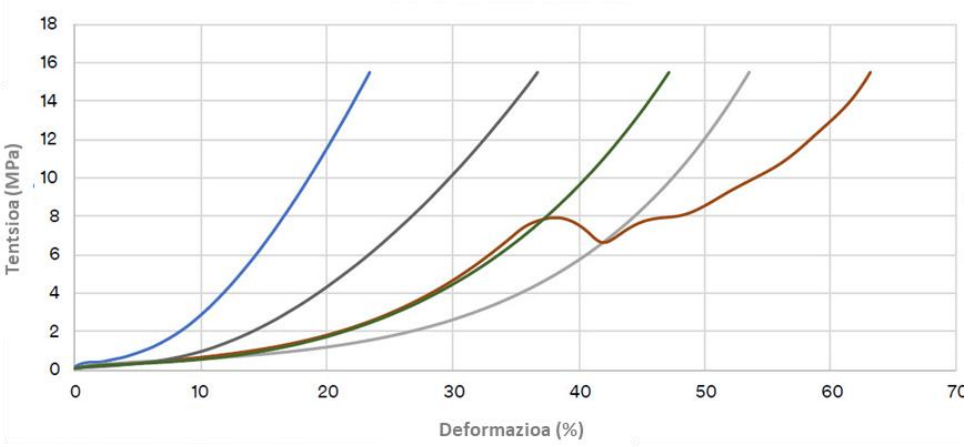


**34. irudia** Compresio Tentsio *vs* deformazio kurbak.

Hooken legearen araebera, deformazio saiakera baten badago tarte bat non eragindako indarra eta deformazia proportzionalak diren, tarte hori grafikatu ezkero lerro zuzena izan litzateke eta inguru horrretan kalkulatzen da Young Modulua. Beraz,

material lineal elastiko eta isotropiko baterako, E Youngen Modulua tentsioa deformazioarekin zatiturik lortzen da (E= σ/ε). Gainera, esfortzuaren konstantea independentea da, baldin eta muga elastiko izeneko balio maximoa gainditzen ez badu, eta beti izaten da zero baino handiagoa. Aldiz, material ez-linealetan, Youngen moduluaren balioa aldatu egin liteke kurbaren puntu bakoitzean; izan ere, tentsioa eta deformazioa ez dira proportzionalak edo ez dituzte tarte linealak. Kasu horietan, ageriko Youngen modulua tentsio-aldakuntza eta bi punturen arteko deformazio-aldakuntza zatituz eskuratzen da (7. ekuazioa) [81]:

$$E = \frac{\Delta\sigma}{\Delta\varepsilon} \qquad (7)$$

Lan honetan, konpresio-saiakuntzak Trapezium Shimadzu AGS-X testatze unibertsaleko ekipamendu batean egin dira **(36. irudia)**, zeina 10 N-an operaturiko karga-gelaxka batekin horniturik baitago, bai eta desplazamendua kontrolatzeko sistema batekin ere, 0,5 mm/min-ko konpresio-abiadura ahalbidetuz.


**35. irudia** Erresistentzia mekanikoa probatzeko ekipamendua (BCMaterials).

## 2.4.7. Bustikortasun-analisia (kontaktu-angeluaren neurketa)

Material baten ura xurgatzeko joera, bustikortasuna edo hidrofobizitatea parametro garrantzitsuak dira fase solido eta likidoaren arteko interakzio-mekanismoak aztertzeko. Horretaz gainera, material batek hainbat likidorekin interakzioan jardutean zer portaera duen ezaugarritzeko aukera ematen du, eta propietate garrantzitsua da hainbat aplikaziotan.

Aztertzeko materialaren eta likido baten arteko kontaktu-angelua parametro erabakigarria da solidoen gainazaleko propietateak aztertzeko eta haien bustikortasuna zenbatesteko. Horretaz gainera, kontaktu-angeluaren balioa oinarrizko parametroa da beste hainbat propietate kalkulatzeko garaian (hala nola gainazalaren tentsioa, materialaren gainazaleko energia askea edo haren propietate itsaskorrak).

Kontaktu-angelua zehazteko metodorik ohikoenetako bat *Sessile Drop* izenekoa da, eta goniometroa baliatzen da hura zehazteko. Metodo horretan, likido-tanta bat ipintzen da, gainazaleko energia ezagun batekin, aztertzeko materialaren lagin baten gainazal lau eta garbi baten gainean. Likido baten gainazaleko tentsioa bere azalera area-unitate bakoitzeko (J /$m^2$) handitzeko behar den energia-kantitateari lotuta dago, edo, modu baliokidean, luzera-unitate bakoitzeko eragiten duen indar normalari (N/m).

Aztertzeko material gainean tanta bat jaurti ezkero: interfaze likido/solido eta interfaze likido/aire arteko intersekzioak osaturiko angelua, θ kontaktu-angelua moduan definitzen da **(36. irudia).** Kontaktu-angelu altua izateak esan nahi du gainazal solidoko energia apala izango dela, eta bustikortasun-maila, berriz, txikia. Aldiz, kontaktu-angelu baxua izateak esan nahi du gainazal solidoko energia edo afinitate kimiko handia izango dela, eta bustikortasun-maila, ostera, handia. Kontaktu-angelua

zehazteko, Youngen ekuazioa hartzen da oinarri, Thomas Youngek 1805ean definitua (8. ekuazioa):

$$\gamma_{SV} = \gamma_{SL} + \gamma_{LV} \cos\theta \qquad (8)$$

non θ Youngen kontaktu-angelua baita; hau da, solido/likido eta likido/aire interfazeek osaturiko angelua, kontaktu hirukoitzeko lerroaren edozer puntutan [148, 149,150].

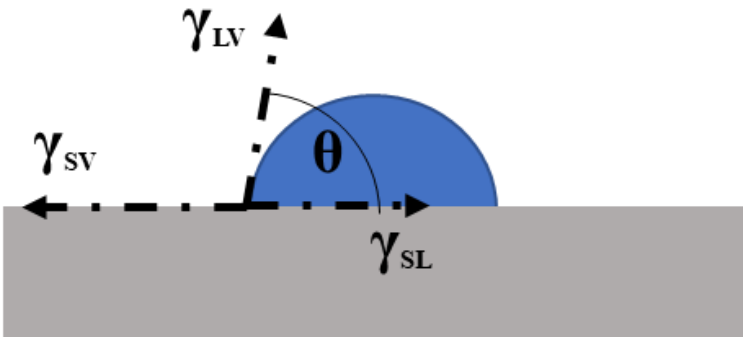


**36. irudia** Likido-tanta baten eskema, Youngen ekuazioko osagaiak erakutsiz [148].

Laginen bustikortasuna aztertzeko eta aerogeletan metalezko nanopartikulen eragina zehazteko, OCA 15 Dataphysics goniometroa baliatu da, zeinak mahai doigarri bat baitauka laginak kokatzeko **(37.irudia)**. Neurriak giro-tenperaturan hartuak dira, eta kontaktu-angeluak kalkulatzeko, berriz, gutxienez hiru neurketaren batezbestekoa egin da lagin bakoitzaren hiru eremu desberdinetan.

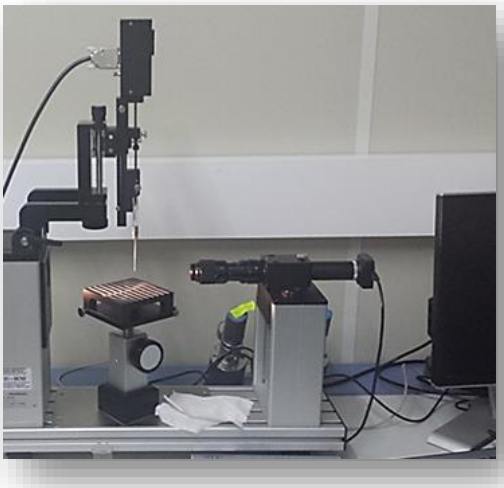

**37. irudia** Erabilitako OCA 15 Dataphysics goniometroa (Labquimac).

Kontaktu-angelua zero denboran zehazteaz gainera test likidoen eta laginen artean (kontaktu-angelu estatikoa), kontaktu-angeluak denborarekin duen bilakaera ere kalkulatu da (kontaktu-angelu dinamikoa), laginaren xurgapen-prozesua grabatuz eta denborarekin segimendua eginez.

Nahiz eta *Sessile Drop* metodoa luze-zabal baliatzen den kontaktu-angelurako, nabarmendu behar da laginaren ezaugarrien arabera badirela beste hainbat metodo ere parametro hori kalkulatzeko. Hona hemen metodo horietako batzuk [149]:

- Igoera kapilarraren metodoa (*Capillary Rise Method*, CRM) eta igoera kapilarraren metodo eraldatua (*Modified Capillary Rise Method*, MCRM).
- Wilhelmy plakaren testa (*Wilhelmy Plate Method*, WPM).
- Ur-tanta sartzeko denboraren testa (*Water Drop Penetration Time Test*, WDPTT).

Bestalde, gainazaleko energia, hidratazio gabeko energia eta tankerako gainazaleko parametroak zehazteko garaian, hainbat metodo eta teoria planteatu dira, gutxi-asko konplexuak, zein bere ekuazio kidetuekin [151].Teoria horien artean, hauek dira gehien erabiliak: Zisman-en teoria (gainazaleko energia kritikoa kalkulatzeko osagai bateko eredua), Owens-Wendt-en teoria (bi osagairen eredu unibertsala, geometrical mean izenez ere ezaguna), Fowkes-en teoria (bi osagaiko ereduak) eta Van Oss-en teoria (hiru osagaiko teoria, nahiko berria).

Aurretik aipatutako teoriez gain, badira beste hainbat ere, gainazalen inklinazioarekin edo gainazal ez-homogeneoetan sortutako efektuekin lotuak, hala nola Wenzel eta Cassie-ren legeak.

Ondoren, gainazaleko energia askea zehazteko oinarri teorikoa zehazten da, Owens-Wendt-en teoriaren arabera, baita hidratazio gabeko energia ere, Young-Dupre-ren ekuazioaren bitartez. Nabarmendu behar da gainazalen bustikortasun-teoriek dagoeneko aipaturiko Youngen ekuazioa dutela oinarri.

*Gainazal-energia askea eta hidratazio-energia askea*

Gainazal-energia askea materialen parametro bereizgarria da, eta interakzio ugari daude balio horrekin loturik, hala nola xurgapena, bustikortasuna edo itsaskortasuna. Gainazal-energia askea kalkulatzeko, hainbat likido baliatu ziren likido-test gisa **(1. taula)**, likido-tanten kontaktu-angelua zehazteko Neat CNC eta CNC/Pd laginak baliatuz, metal aitzindari kantitate desberdinekin. Kontaktu-angeluen balio horiek Owen-Wendt eredu matematikoan sartzen dira, CNC aerogel hibridoen gainazal-energia kalkulatzeko. Gainera, ur-bustikortasuna, kontaktu-angelu dinamikoa eta hidratazio-energia askea kalkulatzeko, ΔEw-ak definitu ziren hainbat laginetarako.

**1. taula** Kontaktu-angeluak zehazteko 25 ºC-ko tenperaturan baliatzen diren likido estandarren datuak.

| Likido-testak | $\gamma_L^d$ (mN/m) | $\gamma_L^p$ (mN/m) | $\gamma_L$ (mN/m) | Biskositatea (mPa·s) | Dentsitatea (g/cc) |
|---|---|---|---|---|---|
| **Ura (W)** | 21,8 | 51,0 | 72,8 | 1 | 1 |
| **Glizerola (G)** | 34 | 30 | 64 | 924,7 | 1,26 |
| **Etilenglikola (E)** | 29 | 19 | 48 | 17,3 | 1,12 |
| **Diiodometanoa (D)** | 50,1 | 0,7 | 50,8 | 2,8 | 3,4 |

Owens/Wendt teoria [86] gainazal likido eta solidoen arteko interakzioak kontuan hartzeko sortua da eta luze-zabal aplikatzen zaie ezaugarri polar samarrak dituzten gainazalei, hala nola poliuretanoa, heteroatomoak dituzten polimeroak, poliesterrak, poliakrilatoak edo polikarbonatoak. Owens eta Wendt-ek solido baten gainazalaren energia bi osagairen konbinaketa gisa irudikatu zuten: osagai dispertsibo bat eta osagai polar bat. Dispertsio-osagaiak, teorian, gainazal eta likido baten arteko Van der Waals eta beste interakzio espezifiko batzuk kontuan hartzen ditu. Osagai polarrak, teorian, dipolo-dipolo, dipoloak induzitutako-dipoloa, hidrogeno loturak eta gainazal baten likidoak aplikatu izan ditzakeen bestelako interakzio espezifikoak irudika ditzake. Ideia hori oinarri harturik, Owens eta Wendtek bi parametroko eredu bat garatu zuten gainazaleko interakzioak deskribatzeko (9. ekuazioa).

$$\gamma_S = \gamma_S^d + \gamma_S^p \qquad (9)$$

$$\gamma_{SL} = \gamma_S + \gamma_L - 2\sqrt{\gamma_S^d \gamma_L^d} + 2\sqrt{\gamma_S^p \gamma_L^p} \qquad (10)$$

non likidoak eta solidoak biek baitaukate osagai polar eta dispertsibo bat $\gamma$-rako ($\gamma_S$ eta $\gamma_L$) eta θ solidoaren eta likidoaren arteko kontaktu-angelua da. Hori horrela, kontaktu-angelua neurtzen denean eta probako likidoen osagaiak ezagutzen direnean

(1. taula), bi parametroko sistema bat eskuratuko dugu gainazal-energia aske solidoa zehazteko (11-12 ekuazioak).

$$\frac{\gamma_L(1+\cos\theta)}{2} = \sqrt{\gamma_S^d}\gamma_L^d + \sqrt{\gamma_S^p}\gamma_L^p \qquad (11)$$

$$\frac{\gamma_L(1+\cos\theta)}{2\sqrt{\gamma_L^d}} = \sqrt{\gamma_S^p}\left(\frac{\gamma_L^p}{\gamma_L^d}\right)^{1/2} + \sqrt{\gamma_S^d} \qquad (12)$$

12. ekuazioa linealki irudikatuz, gainazal-energia solidoaren osagai polarra (maldatik) eta dispertsio-osagaia (ordenatu-ardatza jatorrian) eskuratzen dira. Gainera, likidoen eta solidoen arteko oreka-interakzioak Young-en ekuazioaren bidez deskribatzen dira (13 ekuazioa):

$$\gamma_S = \gamma_{SL} + \gamma_L cos\theta \qquad (13)$$

non $\gamma_L \cos\theta$ itsaspen-tentsio deitzen baita. Erabateko bustitzea θ= 1 edo θ= 0 denean gertatuko da. Aldiz, solido eta likido bat kontaktuan ipintzean askatzen den energia, ΔE, Dupre-ren ekuazioaren bidez deskriba daiteke:

$$-\Delta \mathrm{E} = \gamma_S + \gamma_L - \gamma_{SL} \qquad (14)$$

13. eta 14. ekuazioak Young-Dupre-ren ekuazioan konbinatuz (15. ekuazioa), hidratazio-energia askea ΔEw kalkulatzen zen, eta interfaze solidoaren balantze hidrofobiko-hidrofilikoa aztertzen.

$$\Delta Ew = -\gamma_L\,(1+\cos\theta) \qquad (15)$$

## 2.4.8. Nitrogeno-adsortzioko isoterma (gainazal espezifikoa)

Poroak eta gainazal espezifikoa ezaugarritzea parametro erabakigarriak dira nanokonposite porotsuak aztertzeko; izan ere, eragin handia dute aplikatzen den materialaren prestazioetan hainbat fenomenorekin, hala nola absortzioa, adsortzioa, interakzioak eta abar.

Gainazal espezifikoa materialaren gainazalaren area gisa definitzen da masa-unitateko ($m^2/g$) eta gramo bat materia osatzen duten partikula guztien azaleraren baturaren baliokidea da.

Gainazal espezifikoa zehazteko, materiala nitrogeno-absortzioko eta desortzioko isotermen pean ipintzen da, eta, parametro hori kalkulatzeko, Brunauer, Emmet eta Teller Isoterma BET [153] da gehien baliatzen den teoria. Teoria horrek Langmuirren adsortzio fisikoko kurbaren tratamendu orokortua inplikatzen du; hala, gas bat (nitrogenoak, kasu) tenperatura baxuan adsorbatu egingo da gainazal solido garbien gainean, eta baliagarri dagoen gainazala osorik beteko du, hainbat geruza osatuz. Ondoren, BETen ekuazioaren bidez (16. ekuazioa), gainazalaren gaineko geruza kalkulatzen da.

$$\frac{P}{Va(Po-P)} = \frac{1}{VmC} + \frac{C-1}{VmC}\left(\frac{\mathrm{P}}{\mathrm{Po}}\right) \qquad (16)$$

non Va presioarekin xurgaturiko gas-kantitatea den; Vm xurgaturiko gas-kantitatea den, gainazal guztia gas molekularrezko geruza batez estalirik dagoenean; C, konstante bat; eta Po, lurrun presioa.

Nitrogenoaren adsortzio-prozesuak hainbat urrats biltzen ditu:

- Solidoa desgasifikatu egiten da (60 º-an, 24 orduz), hodi batean pisaturik eta 77 K-ra hozturik.

- Gas nitrogenoa P/Po erlazio progresiboen bidez txertatzen da, eta laginak adsorbatu egiten du.
- Presio-transduktoreek aldaketak neurtzen dituzte, eta gas-bolumenak neurtzea ahalbidetzen dute.
- Saiakuntza hainbat presiotan errepikatuz, adsorbaturiko gas-kantitateei buruzko datuak eskuratzen dira, tenperatura jakin batean orekan izandako presioarekiko.
- Adsorbaturiko gas-kantitateari buruzko eta orekan geratzen den gas-presioaren aurreko datu horiek –tenperatura berean harturikoak– izango dira adsortzio-isoterma.
- Teknika dinamikoa edo gas-fluxuarena baliatzen baldin bada, nitrogenoa laginaren gainean igaroko da He duen nahaste baten osagarri gisa, eta adsorbatutako nitrogeno-kantitatea TCD batekin zehaztuko da (gas inorganikoen eroankortasun termikoaren detektagailu bat).

Solido-adsortzioko isotermetan, X ardatzean orekako gasaren presioa (P) irudikatzen da; Y ardatzean, berriz, adsorbatutako kantitatea jasotzen da. Magnitude hori bi eratan adieraz daiteke: adsorbatutako mola/adsorbatzaile gramoak (n/m); edo adsorbatutako gas-bolumena/v adsorbatzaile gramoak ($cm^3/g$). Bolumena adierazteko, gas adsorbatuak baldintza arruntetan okupatuko lukeen bolumena ematen da T=273,15 ºK, P= 1 atm).

Eskuarki, isotermak 5 motaren inguruan sailkatzen dira, S. Brunauer-en arabera [154] **(38. irudia)**:

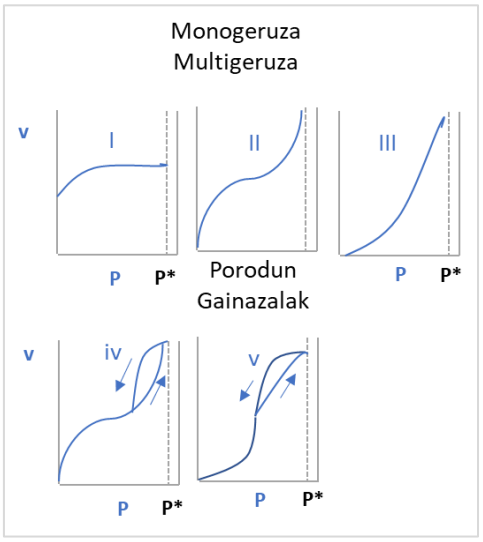


**38. irudia** Isoterma motak [154].

- I. mota edo Langmuirren isoterma; geruza bakarreko kimisortzio-prozesu baten isoterma bereizgarria da.
- II. mota hainbat geruzatako adsortzio fisikoari dagokio.
- III. mota hainbat geruzatako adsortzio fisikoari dagokio, baina lehen geruza eratzeko orekaren konstantea berdina da hurrengoekiko (ez da ikusten alderik lehen geruza eta gainerakoak betetzeari dagokionez).
- IV. eta V. motak hainbat geruzatako adsortzioari dagozkio, material porotsuen gainean. II. eta III. motakoen aldean duten desberdintasuna zera da, adar horizontal bat (saturazioa) eta histeresi-ziklo bat dutela (desberdinak dira adsortzio- eta desortzio-kurbak). Kondentsazioak eragiten du histeresi-zikloa, kapilarren forma irregularra dela eta.

Neurriak hartzeko, honako ekipamendu hau baliatu zen: Autosorb®-1-C/TCD (Quantachrome, USA) **(39. irudia).**

**39. irudia** Nitrogenoa adsorbatzeko baliatutako ekipamendua.

Gainazala area eskuratutako kurbetatik abiaturik kalkulatzen da, Brunauer-Emmet-Teller (BET) metodoa baliatuz (absortzio- eta desortzio-kurbetatik).

Horretaz gainera, poroen banaketa eta neurria ere zehatz daiteke isoterma beren bidez, Barrett-Jomer-Halenda teoria (BJH) baliatuz.

## 2.4.9. Z-potentzialeko neurriak

Z potentzialeko neurketek partikulen gainazaleko kargaren magnitudearen berri ematen dute. Zehazki, partikulen inguruan geruza elektriko bikoitza sortzen da eta bertan ioiak indartsu lotutako barnekalde bat eta kanpoalde difuso bat bereiztu daitezke. Kanpoaldetan muga batek bereizten du ioien mugikortasun edo mugikortasun-eza, muga honetan dagoen potentziala Zeta Potentzial bezala ezagutzen da (**40. irudia)** [155].

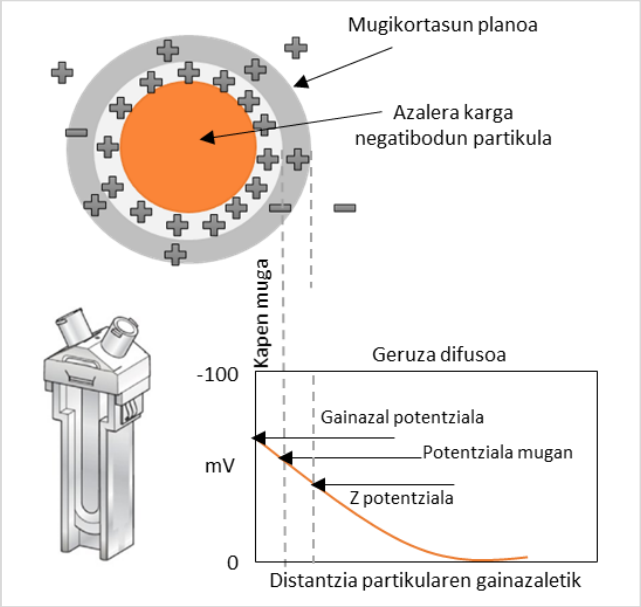


**40. irudia** Z potentzialaren irudikapena eta erabilitako zelda kapilarra (elaborazio propioa).

Parametro honekin hainbat materialen barnean edo material desberdinetan partikulen arteko aldaratzearen edo atrakzioaren buruzko informazioa lor daiteke. Neurri horrek partikulen arteko aldaratze-mekanismo nagusien gaineko informazioa eta koloidearen egonkortasunari buruzko informazioa ere eman dezake. Zeta potentzialean eragina duen faktorerik garrantsitsuena pH-a da.

Z potentzialeko neurriak eskuratzeko, Malvern Panalytical etxearen Zetatiser Nano tresna erabili da (**41. irudia**)., tresna honek Zeta Potentzialaz gain, partikula neurria, proteinen mugikortasuna eta pisu molekularra era automatikoan kalkulatu ditzake.

Lan honetan, CNCen neurketa egiteko, CNC-ur oso diluituta kubeta baten barneratzen da. Zeta potentzialaren kasuan, CNC suspentzioa $10^{-5}$ aldiz diluitu da.

**41. irudia** Zetasiser nano ekipamendua (Kimika Ez-organikoa saila)

Bertan, zeta potentziala kalkultatzeko, neurketa printzipioa Argi Dispertsio Elektroforetikoa da, eta 3.8 nm, eta 100 µm arteko diametroko partikulen mugikortasun elektroforetikoa neurtu daieke Henry-ren ekuazioa erabiliz (17. ekuazioa). Laginetan partikulen abiadura neurtzeko Laser Doppler Abiadura-neurgailua (LDA) erabiltzen da.

$$U_E = \frac{2\varepsilon z f(ka)}{3\eta} \qquad (17)$$

non z Zeta pontentziala da, $U_E$ mugikortasun elektroforetikoa, ε constante dielektrikoa, η biskositatea eta f(ka) 1.5 edo 1.0 baliodun Henry-ren funtzioa.

# Erreferentziak

[1] McKeen L.W. 2013. The Effect of UV Light and Weather on Plastics and Elastomers.Plastics Design Library1, chapter 1.Introduction to Plastics and Polymers Compositions, 1-16.

[2] Katime I., Katime O. 2010. Introducción a la ciencia de los materiales polímeros. Síntesis y caracterización. Publicaciones UPV-EHU.

[3] Baillie C. 2004. Green Composites, Polymer composites and environment. Woodhead publishing limited, Cambridge, England.

[4] Anastas P.T., Warner J.C.1998. Green chemistry: Theory and practice. Oxford University Press. New York.

[5] Hassanpour M., Unnisa S. 2017. Plastics; Applications, Materials, Processing and Techniques. Plastic Surgery Mod. Tech.: PSMT-109.

[6] North E.J., Halden R.U. 2013. Plastics and Environmental Health: The Road Ahead. Rev Environ Health; 28(1), 1-8.

[7] Dassanayake R.S., Acharya S., Abidi N. 2018. Biopolymer-Based Materials from Polysaccharides: Properties, Processing, Characterization and Sorption Applications. Sorption, 10.5772/intechopen.80898.

[8] Gandini A. 2011. The irruption of polymers from renewable resources on the scene of macromolecular science and technology. Green Chem., 13, 1061–1083.

[9] Thakur V.K., Kessler M.R. 2015. Green Biorenewable Biocomposites: From Knowledge to Industrial Applications; Apple Academic-CRC Press: Boca Raton, FL, USA, 1–568

[10] Garrison T.F., Murawski A., Quirino R.L. 2016. Bio-Based Polymers with Potential for Biodegradability. Polymers, 8, 262.

[11] Ebnesajjad S. 2013. Handbook of Biopolymers and Biodegradable Plastics: Properties, Processing and Applications.

[12] Zhong Y., Godwin P., Jin Y., Xiao H. 2020. Biodegradable Polymers and Green-based Antimicrobial Packaging Materials: A mini-review. Advanced Industrial and Engineering Polymer Research, 3 (1), 27-35.

[13] Rodriguez LJ., Orrego C. 2016. Applications of biopolymers and synthetic polymers blends: literature review. Revista Científica, 25, 252-264.

[14] Wu X., Luo Y., Liu Q., Jiang S., Mu G. 2019. Improved structure-stability and packing characters of crosslinked collagen fiber based film with casein, keratin and SPI. Journal of the Science of Food and Agriculture, 99(11), 4942-4951.

[15] Vilas Indubai,G., Das A., Mahanwar P., Gadekar P. 2018. Starch Based Bio-Plastics: The Future of Sustainable Packaging. Open Journal of Polymer Chemistry, 8(2), 21-33.

[16] Mesquita J.P., Donnici C.L., Teixeira I.F., Pereira F.V. 2012. Bio-based nanocomposites obtained through covalent linkage between chitosan and cellulose nanocrystals. Carbohydr. Polym., 90, 210–217.

[17] Rinaudo M. 2006. Chitin and chitosan: Properties and applications. Prog. Polym. Sci., 31, 603–632.

[18] Inoue A., Ojima T. 2019. Functional identifcation of alginate lyase from the brown alga Saccharina japonica. Scientific Reports, 9, 4937.

[19] Naima H., Cherif H., Fethi B., Benmansour K., Meghezzi A. 2019. Preparation of active antimicrobial and antifungal alginate-montmorillonite/lemon essential oil nanocomposite films. Materials Technology, 35(7), 383-394.

[20] Lagopati N., Pavlatou E.A. 2020. Advanced Applications of Biomaterials Based on Alginic Acid. Am J Biomed Sci & Res, 9(1).

[21] Lizundia E. 2013. Polimero biodegradagarrietan oinarrituriko material nanokonposatuak: Poli (L-laktida)/karbono nanotubu konpositearen kasua». Ekaia. EHUko Zientzia eta Teknologia aldizkaria ,26.

[22] Zhang C., Madbouly S.A., Kessler M.R. 2015. Biobased Polyurethanes Prepared from Different Vegetable Oils. ACS Applied Materials & Interfaces, 7 (2), 1226–1233.

[23] Younas T., Ali I., Jamil N. 2015. Polyhydroxyalkanoates production using canola oil by bacteria isolated from paper pulp industry. Kuwait J. Sci., 42(2), 236-249.

[24] Bugnicourt E., Cinelli P., Lazzeri A., Alvarez V. 2014. Polyhydroxyalkanoate (PHA): Review of synthesis, characteristics, processing and potential applications in packaging. Express Polym. Lett., 8, 791–808.

[25] Abol-Fotouh D., Hassan M.A., Shokry H., Roig A., Azab M.S., Kashyout A.E.B. 2020. Bacterial nanocellulose from agro-industrial wastes: low-cost and enhanced production by Komagataeibacter saccharivorans MD1. Scientific Reports, 10, 3491.

[26] Wendler F. et al. 2012. Cellulose Products from Solutions: Film, Fibres and Aerogels. The European Polysaccharide Network of Excellence (EPNOE), 153-185.

[27] Roco C.M., Mirkin C.A., Hersam M.C. 2011. Nanotechnology Research Directions for Societal Needs in 2020: Retrospective and Outlook. J. Nanopart. Res., 13, 897-919.

[28] Jeevanandam J., Stephanie Chan Y.S.,Dufresne A., Danquah M. 2018. Review on nanoparticles and nanostructured materials: History, sources, toxicity, and regulations. Beilstein Journal of Nanotechnology, 9, 1050-1074.

[29] Khan I., Saeed K., Khan I. 2019. Nanoparticles: Properties, applications and toxicities. Arabian Journal of Chemistry, 12(7), 908-931.

[30] Asim Ali Yaqoob A.A., Ahmad H., Parveen T., Ahmad A., Oves M., Ismail I.M.I., Qari H.A., Umar K., Ibrahim M.N.M. 2020. Recent Advances in Metal Decorated Nanomaterials and Their Various Biological Applications: A Review. Frontier in Chemistry, 8, 341.

[31] Lizundia E., Goikuria U. Vilas J.L, Cristofaro F., Bruni G., Fortunati E., Armentano I., Visai L., Torre L. 2018. Metal Nanoparticles Embedded in Cellulose Nanocrystal Based Films: Material Properties and Post-use Analysis. Biomacromolecules, 19, 2618−2628.

[32] Eitan A., Schadler L.S. 2014. Polymer Nanocomposites with Particle and Carbon Nanotube Fillers. Dekker Encyclopedia of Nanoscience and Nanotechnology, 2917-2930.

[33] Urrejola M.C., Soto L.V., Zumarán C.C., Peñaloza J.P., Álvarez B., Fuentevilla I., Haidar Z.S. 2018. Sistema de Nanopartículas Poliméricas II: Estructura, Métodos de Elaboración, Características, Propiedades, Biofuncionalización y Tecnologías de Autoensamblaje Capa por Capa. International Journal of Morphology, 36, 4.

[34] Althues H., Henle J., Kaskel S. 2007 Functional inorganic nanofillers for transparent polymers. Chemical Society Reviews, 36, 1454-1465.

[35] Bakirhan N.K., Ozkan S.A. 2018. Chapter 28 - Quantum Dots as a New Generation Nanomaterials and Their Electrochemical Applications in Pharmaceutical Industry, Handbook of Nanomaterials for Industrial Applications-Micro and Nano Technologies, 520-529.

[36] García-Pinel B., Porras-Alcalá C., Ortega-Rodríguez A.,Francisco Sarabia, Prados J., Melguizo C., López-Romero J.M. 2019. Lipid-Based Nanoparticles: Application and Recent Advances in Cancer Treatment. Nanomaterials ,9, 638.

[37] Jamkhande P., Ghule N., Bamer A., Kalaskar M. 2019. Metal nanoparticles synthesis: An overview on methods of preparation, advantages and disadvantages, and applications. Journal of Drug Delivery Science and Technology, 53,101174.

[38] Ealias M., Saravanakumar A. & M.P. 2017. A review on the classification, characterisation, synthesis of nanoparticles and their application. IOP Conference Series Materials Science and Engineering. 263. 032019. 10.1088/1757-899X/263/3/032019.

[39] Quintero-Quiroz C., Acevedo N., Zapata-Giraldo J., Botero L.E., Quintero J., Zárate-Triviño D., Saldarriaga J., Z. Pérez V. 2019. Optimization of silver nanoparticle synthesis by chemical reduction and evaluation of its antimicrobial and toxic activity. Biomaterials Research, 23(27).

[40] Parashar M., Shukla V., Singh R. 2020. Metal oxides nanoparticles via sol–gel method: a review on synthesis, characterization and applications. Journal of Materials Science: Materials in Electronics, 31(2).

[41] Li J., Wu Q., Wu Ji. 2016. Synthesis of Nanoparticles via Solvothermal and Hydrothermal Methods. Handbook of Nanoparticles, 295-328.

[42] Siddiqui M.T.H., Nizamuddin S., Baloch H.A. et al. 2018. Synthesis of magnetic carbon nanocomposites by hydrothermal carbonization and pyrolysis. Environ Chem Lett, 16, 821–844.

[43] Amiens C., Chaudret B., Ciuculescu-Pradines D., Collière V., Fajerwerg K., Fau P., Kahn M., Maisonnat A., Soulantica K., Philippot K. 2013. Organometallic approach for the synthesis of nanostructures. New J. Chem., 37, 3374-3401.

[44] Piszczek P., Radtke A. 2017. Silver Nanoparticles Fabricated Using Chemical Vapor Deposition and Atomic Layer Deposition Techniques: Properties, Applications and Perspectives: Review. Book .Noble and Precious Metals - Properties, Nanoscale Effects and Applications, 9.

[45] Herlin Boime N., Mayne-L'Hermitte M., Reynaud C. 2006. Advances in the laser pyrolysis synthesis of nanoparticles. European Journal of Control, 31, 295-315.

[46] Chikkanna M., Neelagund S., Rajashekarappa K. 2019. Green synthesis of Zinc oxide nanoparticles (ZnO NPs) and their biological activity. SN Applied Sciences, 1(117).

[47] Bárta J., Procházková L., Vaněček V., Kuzár M., Nikl M., Čuba V. 2019. Photochemical synthesis of nano- and micro-crystalline particles in aqueous solutions. Applied Surface Science, 479, 506-511.

[48] Xin H., Takada N., Machmudah S., Diono W., Kanda H., Goto M. 2020. Ultrasonic-Enhanced Fabrication of Metal Nanoparticles by Laser Ablation in Liquid. Ind. Eng. Chem. Res., 10.1021/acs.iecr.9b06384.

[49] Ha C.S. 2018 Polymer Based Hybrid Nanocomposites; A Progress Toward Enhancing Interfacial Interaction and Tailoring Advanced Applications. Chem Rec.,18(7-8), 759-775.

[50] Zheng W., Chen S., Zhao S., Zheng Y., Wang H. 2014. Zinc Sulfide Nanoparticles Template by Bacterial Cellulose and Their Optical Properties. Journal of Applied Polymer Science, 131(19): 40784.

[51] Oomen A.G., Bos P.M., Fernandes T.F., Hund-Rinke K., Boraschi D., Byrne H.J., Aschberger K., Gottardo S., von der Kammer F., Kühnel D., Hristozov D., Marcomini, A., Migliore L., Scott-Fordsmand J., Wick P., Landsiedel R. 2014. Concern-driven

integrated approaches to nanomaterial testing and assessment--report of the NanoSafety Cluster Working Group 10. Nanotoxicology, 8(3), 334–348.

[52] Drasler B.,Sayre P., Steinhäuser K.G., Petri-Fink A., Rothen-Rutishauser B. 2017. In vitro approaches to assess the hazard of nanomaterials. NanoImpact, 8, 99-116.

[53] SAbyNA Project. 2020. Simple, robust and cost-effective approaches to guide industry in the development of safer nanomaterials and nano-enabled product. Horizon 2020.

[54] Valery V., Vasiliev, Evgeny V. Morozov. 2018. Advanced Mechanics of Composite Materials and Structures (Fourth Edition).

[55] Park SJ., Seo MK. 2011. Types of composites. Interface Science and Technology, 18 (7), 501-629.

[56] Thakur V.K., Kumari M., Kessler M.R. 2017. Handbook of Composites from Renewable Materials, Nanocomposites: Science and Fundamentals, 7.

[57] Anadão P. 2012. Polymer/Clay Nanocomposites: Concepts, Researches, Applications and Trends for The Future. Nanocomposites: New Trends and Developments.

[58] Ray S.S., Okamoto M. 2003. Polymer/layered silicate nanocomposites: a review from preparation to processing. Progress in Polymer Science, 28, 1539-1641.

[59] Palza H. 2015. Antimicrobial Polymers with Metal Nanoparticles. Int. J. Mol. Sci. 2015, 16, 2099-2116.

[60] Wei H., Rodriguez K., Renneckar S., Vikesland P.J. 2014. Environmental science and engineering applications of nanocellulose-based nanocomposites. Environ. Sci.: Nano,1, 302-316.

[61] Meng Y., Young T.M., Liu P., Cristian I. Contescu C.I., Huang B., Wang S. 2015. Ultralight carbon aerogel from nanocellulose as a highly selective oil absorption material. Cellulose, 22, 435–447.

[62] Wegner T., Jones P. 2006. Advancing cellulose-based nanotechnology. Cellulose, 13, 115-118.

[63] Zhou C., Qinglin W. 2012. Recent Development in Applications of Cellulose Nanocrystals for Advanced Polymer-Based Nanocomposites by Novel Fabrication Strategies. Nanocrystals – Synthesis, Characterization and Applications (3).

[64] Dufresne, A. 2013. Nanocellulose: a new ageless bionanomaterial. Materials Today, 16, 6, 220-227.

[65] Goikuria U., Lizundia E., Larrañaga A., Vilas J.L. 2017. Thermal stability increase in metallic nanoparticles-loaded cellulose nanocrystal nanocomposites. Carbohydrate Polymers, 171,193-201.

[66] Sathishkumar P., Kamalakannan S., Cho M., Kim J., Hadibarata T., Salim M., Oh BT. 2014. Laccase immobilization on cellulose nanofiber: The catalytic efficiency and recyclic application for simulated dye effluent treatment. Journal of Molecular Catalysis B Enzymatic, 100, 111-120.

[67] Stanisławska A. 2016. Bacterial Nanocellulose as a Microbiological Derived Nanomaterial. Advances in Materials Science,16(4).

[69] Mishra R.K., Sabu A., Tiwari S.K. 2018. Materials chemistry and the futurist eco-friendly applications of nanocellulose: Status and prospect. Journal of Saudi Chemical Society.

[70] Joo-Hyung K., Shim B., Kim H. S., Lee YJ., Min SK., Jang D., Abas Z., Kim J. 2015. Review of Nanocellulose for Sustainable Future Materials. International Journal of Precision Engineering and Manufacturing-Green Technology, 2, 197-213.

[71] Coelho C., Michelin M., Cerqueira M., Gonçalves C., Tonon R., Pastrana L., Freitas-Silva O.l. Vicente A., Cabral L., Teixeira J. 2018. Cellulose nanocrystals from grape pomace: Production, properties and cytotoxicity assessment. Carbohydrate Polymers, 192, 327-336.

[72] Lizundia E.; Urruchi A., Vilas J., León L.M. 2016. Increased functional properties and thermal stability of flexible cellulose nanocrystal/ ZnO films. Carbohydrate Polymers, 136, 250-258.

[73] Nandi S., Guha P. 2018. A Review on Preparation and Properties of Cellulose Nanocrystal-Incorporated Natural Biopolymer. Journal of Packaging Technology and Research.

[74] Pereira B., Arantes V. 2020. Production of cellulose nanocrystals integrated into a biochemical sugar platform process via enzymatic hydrolysis at high solid loading. Industrial Crops and Products, 152 (15), 112377.

[75] Isogai A., Saito T., Fukuzumi H. 2010. TEMPO-oxidized cellulose nanofibers. Nanoscale, 3, 71-85.

[76] Thakur V.K. 2014. Nanocellulose Polymer Nanocomposites: Fundamentals and Applications, Scrivener Publishing, Hoboken, NJ, USA.

[77] Lizundia E., Meaurio E., Vilas J.L. 2016. Grafting of Cellulose Nanocrystals. Multifunctional Polymeric Nanocomposites Based on Cellulosic Reinforcements (3).

[78] Tavakolian M., Jafari S.M., van de Ven TGM. 2020. A Review on Surface-Functionalized Cellulosic Nanostructures as Biocompatible Antibacterial Material. Nano-Micro Lett.,12 (73).

[79] Siqueira G., Bras J., Dufresne A. 2010. New process of chemical grafting of cellulose nanoparticles with a long chain isocyanate. Langmuir, 26, 402–411.

[80] Zhao F., Repo E., Song Y., Yin D., Ben Hammouda S., Chen L., Kalliola S., Tang J., Tam K., Sillanpää M. 2017. Polyethylenimine-cross-linked cellulose nanocrystals for highly efficient recovery of rare earth elements from water and mechanism study. Green Chem.,19, 4816–4828.

[81] Wohlhauser S., Delepierre G., Labet M., Morandi G., Thielemans W., Weder C., Zoppe J. 2018. Grafting Polymers from Cellulose Nanocrystals: Synthesis, Properties, and Applications. Macromolecules, 51, 6157−6189.

[82] Goffin A. L., Raquez J. M., Duquesne E., Siqueira G., Habibi Y., Dufresne A., Dubois P. .2011. From interfacial ring-opening polymerization to melt processing of cellulose nanowhisker filled polylactide based nanocomposites. Biomacromolecules, 12(7), 2456–2465.

[83] Liqing W. 2016. McDonald, A. A review on grafting of biofibers for biocomposites. Materials, 9, 1–23.

[84] Miyashiro D., Hamano R., Umemura K. 2020. A Review of Applications Using Mixed Materials of Cellulose, Nanocellulose and Carbon Nanotubes. Nanomaterials,10(2),186.

[85] Lizundia E., Puglia D., Nguyen T., Armentano I. 2020. Cellulose nanocrystal based multifunctional nanohybrids. Progress in Materials Science, 112,100668.

[86] Trache D., Tarchoun A.F., Derradji M., Hamidon T.S., Masruchin N., Brosse N., Hussin M.H. 2020. Nanocellulose: From Fundamentals to Advanced Applications. Frontiers in Chemistry, 8, 392.

[87] Kim C.H., Youn H.J., Lee H.L. 2015. Preparation of cross-linked cellulose nanofibril aerogel with water absorbency and shape recovery. Cellulose, 22, 3715-3724.

[88] Siqueira G., Bras J., Dufresne A. 2008. Cellulose whiskers versus microfibrils: Influence of the nature of the nanoparticle and its surface functionalization on the thermal and mechanical properties of nanocomposites. Biomacromolecules, 10 (2), 425-432.

[89] Wang B., Yang D., Zhang H., Huang C., Xiong L., Luo J, Chen X. 2016. Preparation of Esterified Bacterial Cellulose for Improved Mechanical Properties and the Microstructure of Isotactic Polypropylene/Bacterial Cellulose Composites. Polymers,8 (4), 129-140.

[90] Wu Z.Y., Liang H.W., Chen L.F., Hu B.C., Yu S.H. 2016. Bacterial Cellulose: A Robust Platform for Design of Three Dimensional Carbon-Based Functional Nanomaterials. Acc. Chem. Res., 49, 96−105.

[91] Plugia D., Fortunati E., Kenny J.M. 2016. Multifunctional Polymeric Nanocomposites Based on Cellulosic Reinforcements. Elsevier. William Andrew Applied Science Publishers.

[92] Kassab Z., Abdellaoui Y., Salim M., Bouhfid R., Qaiss A., El Achaby M. 2020. Micro- and nano-celluloses derived from hemp stalks and their effect as polymer reinforcing materials. Carbohydrate Polymers, 245,116506.

[93] De France K., Zeng Z., Tingting W., Gustav N. 2020. Materials from Nanocellulose: Utilizing Structure–Property Relationships in Bottom-Up Fabrication. Advanced Materials, 2000657.

[94] Kontturi E., Spirk E. 2019. Ultrathin Films of Cellulose: A Materials Perspective. Frontiers in Chemistry, 7(488).

[95] Hubbe M.A., Ferrer A., Tiagy P., Yin Y., Salas C., Pal L., Rojas O.J. 2017. Nanocellulose in Thin Films, Coating and Plies for Packaging Applications: A review. BioResources, 12(1), 2143-2233.

[96] Sehaqui H., Liu A., Zhou Q., Berglund L.A. 2010. Fast Preparation Procedure for Large, Flat Cellulose and Cellulose/Inorganic Nanopaper Structures. Biomacromolecules, 11(9), 2195–2198.

[97] Gicquel E., Martin C., Garrido J., Bras J. 2016. Cellulose nanocrystals as new bio-based coating layer for improving fiber-based mechanical and barrier properties. J Mater. Sci.,52, 3048–3061.

[98] Huang W. 2018. Nanopapers-From Nanochemistry and Nanomanufacturing to Advanced Applications Micro and Nano Technologies, Chapter 3 - Clay Nanopapers, 59-86.

[99] Li P., Liu R. 2015. Cellulose Gels and Microgels: Synthesis, Service, and Supramolecular Interactions. Advances in Polymer Science, 268, 209-251.

[100] Filpponen I., Argyropoulos D.S. 2010. Regular linking of cellulose nanocrystals via click chemistry: Syntesis and formation of cellulose nanoplatelet gels. Biomacromolecules, 11,1060-1066.

[101] De France K.J., Hoare T., Cranston E.D. 2017. Review of Hydrogels and Aerogels Containing Nanocellulose. Chem. Mater., 29, 4609- 4631.

[102] Lavoine N., Bergström L. 2017. Nanocellulose-based foams and aerogels: processing, properties, and applications. J. Mater. Chem. A, 5, 16105-16117.

[103] Darpentigny C., Molina-Boisseau S., Nonglaton G. et al. 2019. Ice-templated freeze-dried cryogels from tunicate cellulose nanocrystals with high specific surface

area and anisotropic morphological and mechanical properties. Cellulose, 27(2), 233–247.

[104] Hu L., He R., Lu Z., Zhangab K., Baiab X. 2019. Step-freeze-drying method for carbon aerogels: a study of the effects on microstructure and mechanical property. RSC Adv., 9, 9931.

[105] Błaszczyńskia T., Ślosarczykb A., Morawskic M. 2013. Synthesis of Silica Aerogel by Supercritical Drying Method. Procedia Engineering, 57, 200- 206.

[106] Barrios E., Fox D., Li Sip Y.Y., Catarata R., Calderon J.E., Azim N., Afrin S., Zhang Z., Zhai L. 2019. Nanomaterials in Advanced, High-Performance Aerogel Composites: A Review. Polymers ,11, 726.

[107] Rezaie H.R., Bakhtiari l., Ochsner A. 2015. Biomaterials and their Applications. Springer International Publishing.

[108] Herrera M. A., Mathew A. P., Oksman K. 2014. Gas permeability and selectivity of cellulose nanocrystals films (layers) deposited by spin coating. Carbohydrate Polymers, 112, 494–501.

[109] Suman Kardam A., Gera M., Jain V. 2015. A novel reusable nanocomposite for complete removal of dyes, heavy metals and microbial load from water based on nanocellulose and silver nanoembedded pebbles. En- viron. Technol., 36(6), 706-714.

[110] Suopajärvi T., Liimatainen H., Karjalainen M., Upola H., Niinimäki, J. 2015. Lead adsorption with sulfonated wheat pulp nanocelluloses. J. Water Proc. Eng., 5, 136-142.

[111] Wang Y., Yadav S.; Heinlein T., Konjika V., Breitzkec H., Buntkowskyc G., Schneider J.J., ZhanG K. 2014. Ultra-light nanocomposite aerogels of bacterial cellulose and reduced graphene oxide for specific absorption and separation of organic liquids. RSC Adv., 4, 21553- 21558.

[112] Thakur V.K., Voicu S.I. 2016. Recent advances in cellulose and chitosan based membranes for water purification: A concise review. Carbohy- drate Polymers, 146,148-165.

[113] Lizundia E., Nguyen T., Vilas J.L., Hamad W.Y., MaclachLan M.J. 2017. Chiroptical, morphological and conducting properties of chiral nematic mesoporous cellulose/polypyrrole composite films. J. Mater. Chem. A, 5, 19184–19194.

[114] Kafy A., Sadasivuni K.K., Kim H.C., Akther A., Kim J. 2015. Designing flexible energy and memory storage materials using cellulose modified graphene oxide nanocomposites. Phys.Chem.Chem.Phys.,17, 5923.

[115] Jose J., Thomas V., Vinod V., Abraham R., Abraham S. 2019. NanoCellulose Based Functional Materials for SuperCapacitor Applications. Journal of Science: Advanced Materials and Devices, 4, 333-340.

[116] Alarcon C.D.L.H., Pennadam S., Alexander C. 2005. Stimuli responsive polymers for biomedical applications. Chem Soc Rev, 34(3), 276-285.

[117 Kolakovic R., Peltonen L., Laukkanen A., Hirvonen J., Laaksonen T. 2012. Nanofibrillar cellulose films for controlled drug delivery. European Journal of Pharmaceutics and Biopharmaceutics, 82(2), 308-315.

[118] Lizundia E., Goikuria U., Vilas J.L., Cristofaro F., Bruni G., Fortunati E., Armentano I., Visai L., Torre L. 2018. Metal nanoparticles embedded in cellulose nanocrystal based films: material properties and post-use analysis. Biomacromolecules, 19, 2618-2628.

[119] Tavakolian M., Jafari S.M., Van de Ven T.G. M. 2020. A Review on Surface-Functionalized Cellulosic Nanostructures as Biocompatible Antibacterial Materials. Nano-Micro Letters,12(73).

[120] Sahar Sultan S., Mathew A.P. 2018. 3D printed scaffolds with gradient porosity based on a cellulose nanocrystal hydrogel. Nanoscale, 10, 4421-4431.

[121] Bacakova L., Pajorova J., Bacakova M., Skogberg A., Kallio P., Kolarova, K., Svorcik V. 2019. Versatile Application of Nanocellulose: From Industry to Skin Tissue Engineering and Wound Healing. Nanomaterials, 9(2), 164.

[122] Sinha A., Martin EM., Lim K.T., Carrier D.J., Han H., Zharov V.P., Kim J.W. 2015. Cellulose Nanocrystals as Advanced “Green” Materials for Biological and Biomedical Engineering. J. of Biosystems Eng., 40(4), 373-393.

[123] Golmohammadi H., Morales-Narvaez E., Naghdi T., Merkoci A. 2017. Nanocellulose in Sensing and Biosensing. Chemistry of Materials,19(13), 5426-5446.

[124] Lizundia E., Delgado-Aguilar M., Mutje P., Fernández, E. Robles-Hernández B., De la Fuente M.R., Vilas J.L., Leon L.M. 2016. Cu-coated cellulose nanopaper for green and low-cost electronics. Cellulose, 23, 1997-2010.

[125] Han J. W., Kim B., Li J., Meyyappan M. 2012. Carbon Nanotube Based Humidity Sensor on Cellulose Paper. Journal of Physical Chemistry C, 116, 22094-22097.

[126] Schlesinger M., Hamad W.Y., MacLachlan M.J. 2015. Optically tunable chiralnematic mesoporous cellulose films. Soft Matter, 11, 4686-4694.

[127] Qi H., Chang C., Zhang L. 2009. Properties and Applications of Biodegradable Transparent and Photoluminescent Cellulose Films Prepared Via a Green Process. Green Chemistry, 11, 177-184.

[128] Ferreira F., Pinheiro, I., Souza S., Innocentini M.L., Lona L. 2019. Polymer Composites Reinforced with Natural Fibers and Nanocellulose in the Automotive Industry: A Short Review. Journal of Composites Science, 3(10).

[129] Kiziltas A., Kiziltas E.E., Sevda B.T., Gardner D.J. 2013. Micro-and nanocellulose composites for automotive applications, 1, 402-414.

[130] Agarwal J., Sahoo S., Mohanty S., Nayak S. 2019. Progress of novel techniques for lightweight automobile applications through innovative eco-friendly composite materials: A review. Journal of Thermoplastic Composite Materials, 1-36.

[131] Apostolopoulou-Kalkavoura V., Gordeyeva K., Lavoine N. Bergström L. 2018.Thermal conductivity of hygroscopic foams based on cellulose nanofibrils and a nonionic polyoxamer. Cellulose, 25, 1117-1126.

[132] Choi K., Gao G. Y., Nam J.D., Choi H.J. 2017. Cellulose-Based Smart Fluids under Applied Electric Fields Materials,10, 1060.

[133] Tyagi P., Hubbe M. Lucia L., Pal L. 2018. High performance nanocellulose-based composite coatings for oil and grease resistance. Cellulose, 25(10).

[134] Rezayat M., Blundell R.K., Camp J.E., Walsh D.A., Thielemans W. 2014. Green One-Step Synthesis of Catalytically Active Palladium Nanoparticles Supported on Cellulose Nanocrystals. ACS Sustainable Chem. Eng., 2(5),1241−1250.

[135] Wüstenberg T. 2014, Cellulose and Cellulose Derivatives in the Food Industry: Fundamentals and Applications, Wiley-VCH, Weinheim.

[136] Huang S., Liu X., Chang C., Wang Y. 2020. Recent developments and prospective food-related applications of cellulose nanocrystals: a review. Cellulose, 27, 2991-3011

[137] Sharma A., Thakur M., Bhattacharya M., Mandal T., Goswami S. 2019. Commercial Application of Cellulose Nano-composites - A review. Biotechnology Reports, 21: e0031.

[138] Crompton T. R. 1989. Analysis of Polymers: An Introduction, Pergamon, Oxford.

[139] Akbari B., Tavandashti M.P., Zandrahimi M. 2011. Particle size characterization of nanoparticles-a practical approach. IJMSE, 8(2), 48-56.

[140] Sperling LH. Introduction to Physical Polymer Science, 1992.

[141] Mitchell J. 1987. Applied Polymer Analysis and Characterisation: Recent Developments in Techniques, Instrumentation and Problem Solving, Hanser Publishers. ISBN 3-446-14710-1.

[142] Esposito L.,Koening J.L. 1978. In Applications of Fourier Transform Infrared to Synthetic Polymers and Biological Macromolecules- Eds.; Academic: New York, 1 (2).

[143] Begum R., Farooqi Z.H., Naseem K. 2018. Applications of UV/Vis Spectroscopy in Characterization and Catalytic Activity of Noble Metal Nanoparticles Fabricated in Responsive Polymer Microgels: A Review. Crit Rev Anal Chem.,48(6), 503-516.

[144] Ornaghi H.L., Zattera A.J., Amico S.C. 2015. Thermal behaviour and the compensation effect of vegetal fibers. Journal of Thermal Analysis and Calorimetry, 120, 1703-1714.

[145] Kissinger H.E. 1956. Variation of peak temperature with heating rate in differential thermal analysis .Journal of Research of the National Bureau of Standards, 57, 217-221.

[146] Ozawa T. 1965. A New Method of Analyzing Thermogravimetric Data. Bulletin of the Chemical Society of Japan, 38(11), 1881-1886.

[147] Aarstad O., Heggset E.B., Pedersen I.S., Bjørnøy S.H., Syverud K., Strand B.L. 2017. Mechanical Properties of Composite Hydrogels of Alginate and Cellulose Nanofibrils. Polymers, 9(8), 378.

[148] Adamson A.W. 1997. Physical Chemistry of Surfaces.

[149] Bachmann J., Woche S., Goebel M., Kirkham M., Horton, R. 2003. Extended methodology for determining wetting properties of porous media. Water Resources Research, 39(12).

[150] Kwok D.Y., Neumann A.W. 1999. Contact angle measurement and contact angle interpretation. Advances in Colloid and Interface Science, 81, 167-249.

[151] Firlik S., Molenda J. 2010. Comparison of methods for the surface free energy determination of polimeric layers aligning liquid crystals. Chemik, 64(4).

[152] Owens D.K., Wendt R.C. 1969. Estimation of the surface free energy of polymers. Journal of Applied Polymer Science, 13, 1741-1747.

[153] Barrett E.P., Joyner L.G., Halenda P.H. 1951. J. Am. Chem.Soc,.73, 373.

[154] Sing K. 2001. The use of nitrogen adsorption for the characterisation of porous materials. Colloids and Surfaces A: Physicochemical and Engineering Aspects 187-188,3-9.

[155] Chirayil C.J., Abraham J., Mishra R.K., George S.C., Thomas S. 2017. Thermal and Rheological Measurement Techniques for Nanomaterials Characterization. Micro and Nano Technologies. 1-36.

[156] Zhao J., He X., Wang Y., Zhang W., Zhang X., Zhang X., Deng Y., Lu C. 2014. Reinforcement of all-cellulose nanocomposite films using native cellulose nanofibrils. Carbohydrate Polymers, 104, 143–150.

[157] Beck-Candanedo S., Roman M., Gray D.G. 2005. Effect of reaction conditions on the properties and behavior of wood cellulose nanocrystal suspensions. Biomacromolecules, 6(2), 1048-1054.

[158] Cam D., Marucci M. 1997. Influence of residual monomers and metals on poly (l-lactide) thermal stability. Polymer, 38, 1879-1884.

# 3

# Experimental results and discussion

# 3.1. Thermal stability increase in metallic nanoparticles-loaded cellulose nanocrystal nanocomposites

## 3.1.1. Introduction

Recent environmental and political requirements encourage researchers from all over the world to find sustainable alternatives to replace the existing petro-based materials. These synthetic materials trend to be not compostable and biodegradable, representing serious environmental issues because of their complex recycling processes [1]. Due to the currently existing burnout of fossil resources, petroleum suffers from price volatility and scarce availability. In contrast, natural products like corn, wheat, soya bean, sugar cane or wood are renewable, and their market price is less volatile because they could be obtained in a more shared way across the biosphere [2]. All these above-mentioned characteristics make materials obtained from natural origin more attractive than petroleum transformation-based ones.

In this framework, materials synthesized from biological and natural resources emerge as suitable alternative to produce biodegradable and renewable materials with lower energy consumption [3]. Unfortunately, current biomaterial production techniques are not industrially competitive processes when comparing with petrochemical equivalent ones. In this sense, traditional papermaking approach is one of the few industries which can be able to successfully develop industrial-scale production of goods based on renewable resources [4]. Therefore, papermaking techniques represent a viable platform to develop novel biopolymer parts with relatively easy fabrication.

Several examples of biopolymers that could compete with commodity plastics are starch-based materials such as polylactides (PLAs, thermoplastic aliphatic polyesters) [5] and polyhydroxyalkanoates (PHAs), which are linear polyesters

naturally produced by bacterial fermentation as intracellular carbon and energy storage compounds [6-7].

Despite to the enormous industrial relevance of PLAs and PHAs, cellulose remains as the biopolymer which shows one of the brightest futures. Cellulose is a natural carbohydrate composed by β-D-glucose units that could be found as the most important structural component of the primary cell wall of plats [8]. It is the most abundant biopolymer on the earth and it has a renewable character [9]. Additionally, it has been showed that the unique mechanical strength and high-performance properties of plants arise from the hierarchical structure of natural cellulosic fibres, which is based on their elementary nanofibril components [10].

Therefore, it could be expected that the development of nanocomposites based on these nanoscale fibrils or crystals should present remarkable physic-mechanical properties. In this line, cellulose nanocrystals (CNCs), are rod-like nanostructures with high mechanical stiffness and low density which could be obtained through a controlled hydrolytic cleavage of cellulose [11-12]. CNC has been already used as reinforcing phases for different polymer nanocomposites [13-14] or even as free-standing and crack-free films for advanced optical and sensing applications [15].

Therefore, it is our hypothesis that CNC results a plausible alternative to conventional petroleum-based polymers like polypropylene (PP), polyethylene terephthalate (PET), polyethylene (PE) or polystyrene (PS). However, the poor thermal stability of CNCs remains as one of the main drawbacks which limits their use in the packaging and electronic industry [16] Indeed, as a result of the commonly used acid-induced destructuring process for CNC synthesis, typically sulphuric acid, anionic sulphate ester groups ($-OSO_3^-$) are grafted to CNC surfaces, resulting in relatively poor thermal stabilities [17]. Although it is widely accepted that the thermal stability of CNC could be upgraded by removing these surface $-OSO_3^-$ groups, this process finds difficulties

for its upscaling. Conversely, nanocomposite approach has been proven efficient to tackle several physico-mechanical properties of their hosting matrix due to the resulting synergetic effects [16]. Indeed, nanocomposites incorporating nanoparticles are a novel class of composite materials that are often multifunctional, providing unique optical, electrical, and mechanical properties of the nanofillers to the composite while maintaining, if not enhancing, the neat polymer properties. These nanocomposites are often characterized by low weight fractions of filler, which may then affect the entire matrix due to their large surface-area-to-volume ratio. For instance, photoluminescent CNC films have been obtained after the co-assembly of carbon dots with CNC at a concentration of 0.2 wt.% [18] while conductive photoswitchable structures based on cellulose was obtained by the incorporation of sol-gel synthesized vanadium nanoparticles [4]. Unfortunately, these nanocomposite materials are often obtained through expensive and tedious multi-step processes, limiting their use in industrially scalable applications.

Thanks to their high elastic modulus, wide availability, safety as denoted by Food and Drug Administration approval and antimicrobial resistance, it is our hypothesis that the introduction of different metallic nanoparticles would provide CNC-based materials with improved performance [19-20]. Accordingly, herein free-standing cellulose nanocrystal/metallic nanoparticle materials were synthesized after using solely water as dispersing agent. Our nanocomposite films were fabricated through an energetically efficient process which avoids waste generation. The thermal stability of CNC-based films having ZnO, $SiO_2$, $TiO_2$, $Al_2O_3$ and $Fe_2O_3$ nanoparticle concentrations between 1% wt and 10 % wt have been studied and the activation energies of thermodegradation process were determined in the light of Kissinger and Ozawa-Flynn-Wall methods. X-ray diffraction analysis confirms the improved thermal stability of cellulosic nanocomposites. Overall, obtained results reveal that the thermal

stability of CNC films could be increased up to 75 ºC after the proper selection of nanocomposite formulation, enabling the development of sustainable nanostructured functional cellulosic materials for high temperature applications. The findings here reported provide new solutions to the low thermal stability of CNCs avoiding their chemical modification and thus providing new strategies toward the improvement of the functional properties of biomaterials.

## 3.1.2. Materials and methods

### *3.1.2.1. Starting materials*

Microcrystalline cellulose with a particle size of 20 µm (310697-500G), sulfuric acid and sodium hydroxide have been supplied by Sigma Aldrich. Metallic oxide nanoparticles have been kindly purchased by L´Urederra technological centre (Spain).

### *3.1.2.2. Cellulose nanocrystals synthesis*

Synthesis method to obtain cellulose nanocrystals (CNC) was *via* sulphuric acid hydrolysis of microcrystalline cellulose [13]. The first step was the microcrystalline cellulose hydrolysis in 64 % (w/w) sulphuric acid solution at 45 ºC during 30 min, stopping the reaction by the addition of 20-fold distilled water. After that, hydrolysed cellulose was recovered by centrifugation (6000 rpm for 10 min), isolated at a reduced pressure using a Buchner flask and Buchner funnel and washed with distilled water. Obtained dispersion was neutralized by adding 1 % (v/v) 0.25 mol/L of sodium hydroxide (NaOH). Remaining dispersion was sonicated for 5 min at an output of 40 % using a Vibracell Sonicator.

*3.1.2.3. CNC-based nanocomposite film fabrication*

Metallic nanoparticles-loaded CNC nanocomposite films were fabricated by Evaporation-induced self-assembly (EISA) method. The required amounts of metallic nanoparticles (ZnO, $TiO_2$, $Fe_2O_3$, $Al_2O_3$ and $SiO_2$) were finely dispersed in distilled water via mild-sonication (20 % output for 5 minutes; Vibra-CellTM CV 334) and they were added to aqueous CNC dispersions to obtain 1 wt%, 5 wt% and 10 wt% metallic oxide concentration into CNCs respectively. Then, another sonication step has been applied to dispersions before casting them onto 70 mm diameter Petri-dishes. Finally, specimens were dried at 40 ºC during 24 h (**Figure 42**) followed by another 24 h at 60 ºC in a vacuum-oven. Neat CNC film was also prepared for comparison. Films with thicknesses of 50±5 µm were obtained.

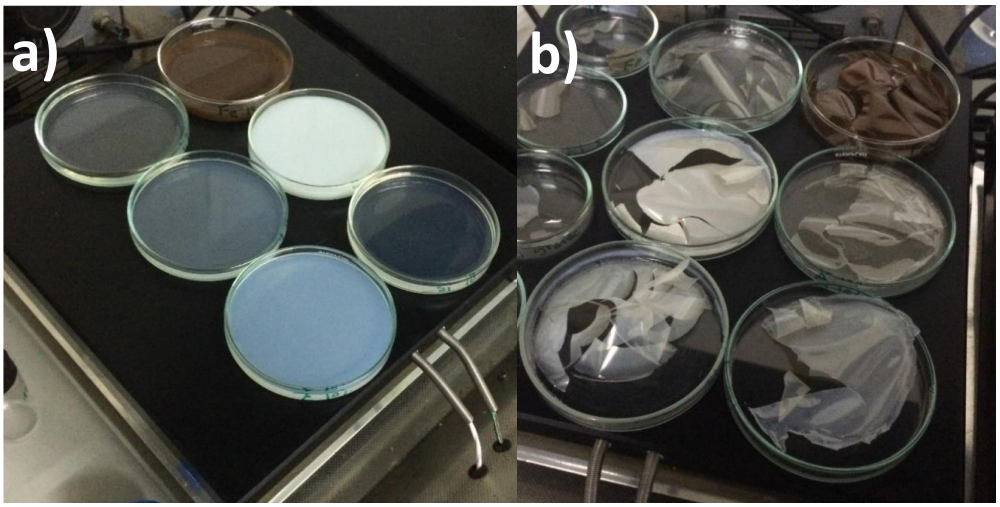


**Figure 42** Material dispersions drying and self-assembling in petri dishes over hot plate (a) and final samples of CNC with nanoparticles (10% wt) (b).

*3.1.2.4. Morphological characterization*

Employed metallic nanoparticles were examined by transmission electron microscopy (TEM) using a Philips CM120 Biofilter apparatus with STEM module at an acceleration voltage of 120 kV. A droplet of diluted suspension (0.1% (w/w)) in water was deposited on carbon-coated grids.

*3.1.2.5. Thermogravimetric analysis* (TGA)

Thermal degradation behaviour was studied by thermal gravimetric analysis (TGA METTLER TOLEDO 822e) in alumina pans under nitrogen atmosphere by heating the samples from room temperature to 600 ºC at 2, 5, 10 and 20º C/min. Before their characterization samples were thoroughly dried at 60 ºC under vacuum for 48 h.

*3.1.2.6. Wide angle X-Ray Diffraction (WAXD)*

Wide angle X-Ray Diffraction patterns (WAXD) were collected in a PHILIPS X'PERT PRO automatic diffractometer operating at 40 kV and 40 mA, theta-theta configuration, secondary monochromator with Cu-Kα radiation (λ = 1.5418 Å) and a PIXcel solid state detector (active length 3.347º). The samples were mounted on a zero-background silicon wafer fixed in a generic sample holder. Data were collected from 5 to 80° $2\theta$ (step size = 0.026) and time per step of 600 s (total scanning time 2 h) at RT. 1º fixed divergence and antiscattering slit with 2 s of revolution time for the spinner were used.

The crystalline structure of the starting metallic nanoparticles upon degradation was investigated on a Bruker D8 Advance diffractometer operating at 30 kV and 20 mA, equipped with a Cu tube ($\lambda$ = 1.5418 Å), a Vantec-1 PSD detector with 3º electronic window, and an Anton Parr HTK2000 high-temperature furnace. The powder patterns were recorded in $2\theta$ steps of 0.0333º in the $8 \leq 2\theta \leq 38$ range,

counting for 25 minutes per diagram (total experiment time 22 h). Data sets were recorded from 150 to 400 ºC each 5 ºC with a 0.167 ºC $s^{-1}$ heating rate.

## 3.1.3. Results and discussion

### *3.1.3.1. Nanoparticle morphological characterization*

Transmission electron microscopy (TEM) has been carried out to analyse the morphology of nanoscale nature of metallic particles. As displayed in **Figure 43**, the average length of synthesized CNCs is of about 190 nm, being their width of 9-17 nm. It is further observed that all nanoparticles except ZnO show a spherical morphology with diameters in the range of 10-30 nm for $SiO_2$, 20-30 nm for $TiO_2$, 10-50 nm for $Al_2O_3$ and 40-60 nm for $Fe_2O_3$. Conversely, ZnO nanoparticles present 25–85 nm long and 15-30 nm wide rod-shaped aspect [21]. The crystalline structure of nanoparticles was characterized by wide-angle x-ray diffraction (WAXD) analysis. Diffraction patterns in **Figure 44** show featured reflections of hexagonal wurtzite crystal structure from ZnO, a mixture of both anatase and rutile tetragonal crystal systems for $TiO_2$, gamma-alumina cubic structure for $Al_2O_3$, amorphous silica glass for $SiO_2$ and maghemite tetraoidal structure of $Fe_2O_3$ [22,23,24].

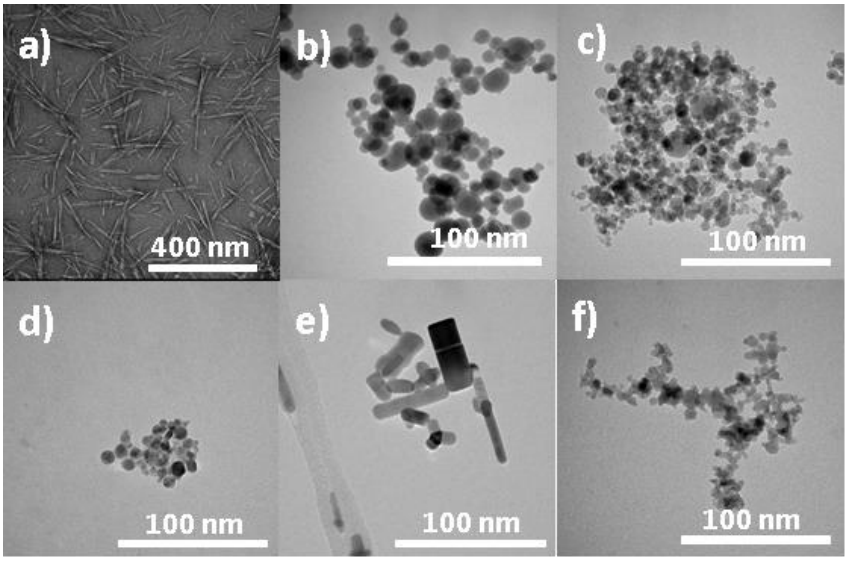


**Figure 43** Transmission electron microscopy (TEM) images showing synthesized CNCs (a), and commercial $Fe_2O_3$ (b), $Al_2O_3$ (c), $TiO_2$ (d), ZnO (e) and $SiO_2$ (f) metallic nanoparticles.

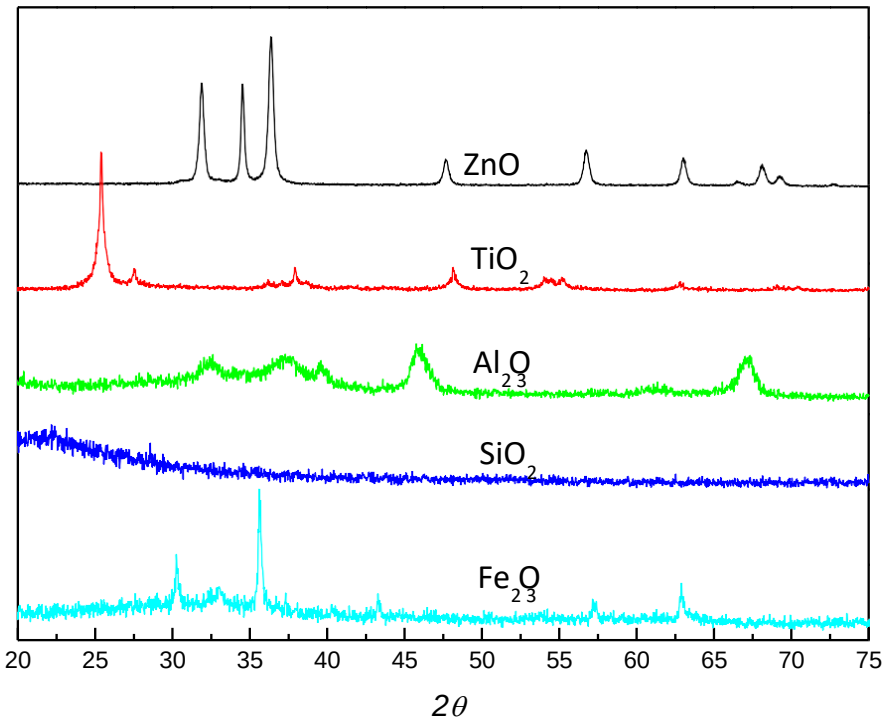


**Figure 44** WAXD patterns of ZnO, $TiO_2$, $Al_2O_3$, $SiO_2$ and $Fe_2O_3$ nanoparticles.

It is well known that when they are mixed together with cellulosic materials, metallic nanoparticles trend to form aggregates as a result of the high surface energy of nanoparticles [25]. Conversely, as highlighted in Figure 42, macroscopically homogeneous free-standing CNC-based films are obtained once water is fully dried. More precisely and as shown in the cross-section SEM micrographs in **Figure 45**, the characteristic layered structure formed by CNCs reported by Revol et al. is kept after nanoparticle incorporation (for the sake of clarity only CNC/ZnO nanocomposite is shown) [26]. Moreover, high magnification micrograph of CNC/ZnO film (b, right column) shows no sign of aggregated nanoparticles. The fact that the original long-range ordering of CNCs is not disturbed for the nanocomposites could be attributed to the achieved homogeneous dispersion of metallic nanoparticles within the CNC matrix. This is due to the employed fabrication method, evaporation induced self-assembly (EISA), where the electrostatic repulsion forces between adjacent CNCs when both CNCs and MNPs remain dispersed in water maintain incorporated MNPs homogeneously distributed at molecular level [15;18]. Therefore, we show that no complex grafting approaches or surfactant addition is needed for obtaining CNC-MNP composite films with well-dispersed nanoparticles. Note that the achieved optical colour differences are due to the nature of incorporated nanoparticles because of their strong light absorbing nature. For instance, CNC/$Fe_2O_3$ film shows a brownish appearance, while $Al_2O_3$ addition does not modify the optical transparency of the material and $TiO_2$-based film has a white aspect.

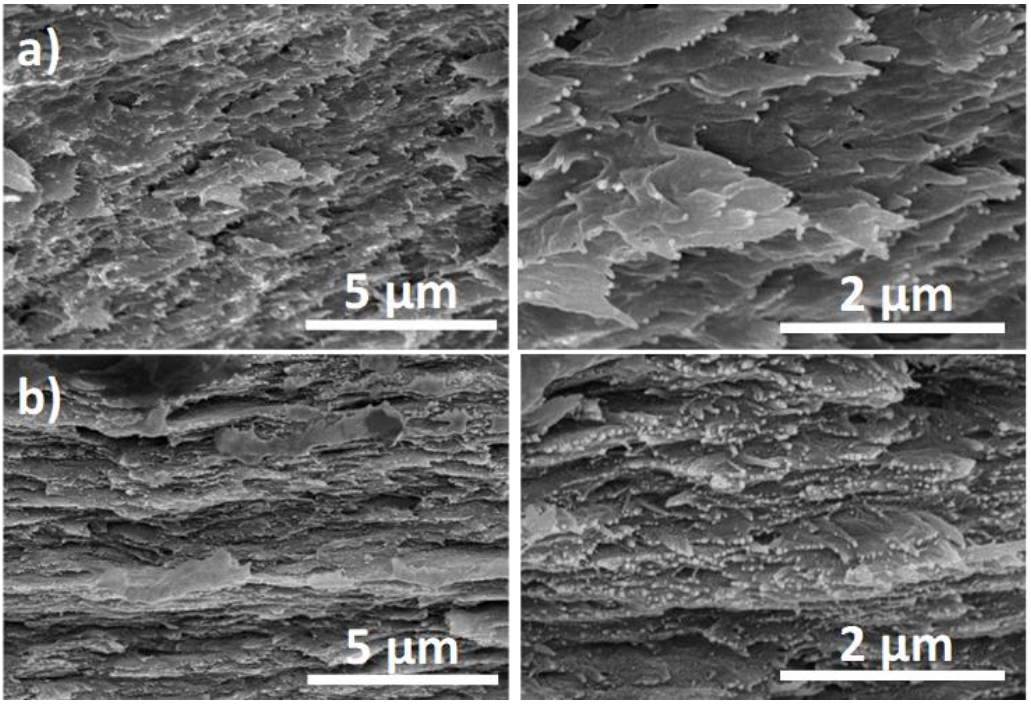


**Figure 45.** SEM cross-section images at two different magnifications of neat CNC(a) and CNC/ZnO 5 wt% nanocomposite film (b).

*3.1.3.2. Thermal stability of nanocomposites*

The thermal stability of neat CNC film has been determined by thermogravimetric analysis (TGA). As observed in **Figure 46**, the thermal decomposition of neat cellulose ($[C_6H_{10}O_5]_n$) involves a series of physical and chemical processes and occurs as follows. Initially, up to ~230 ºC, a desorption of physically bound water or dehydration that promotes the cross-linking of cellulose chains and anhydrocellulose formation occurs. Then, in the 230-270 ºC range, an unzipping of cellulose chain and the formation of levoglucosan from de monomer takes place [27]. Finally, dehydrated cellulose is decomposed to char and volatile products and levoglocusan can further decompose to smaller volatile products, including tars or eventually carbon monoxide. Char and volatile products generation and tar formation continue competing pathways even though with slow heating rates as in our experimental conditions, char formation

is promoted [28,29].Is also known that char formation is caused by dehydration and depends on the dehydration reaction temperature while the fragmentation occurs with scission of C-C bonds and that levoglocusan repolymerization opportunities increase at slower heating rates [30].

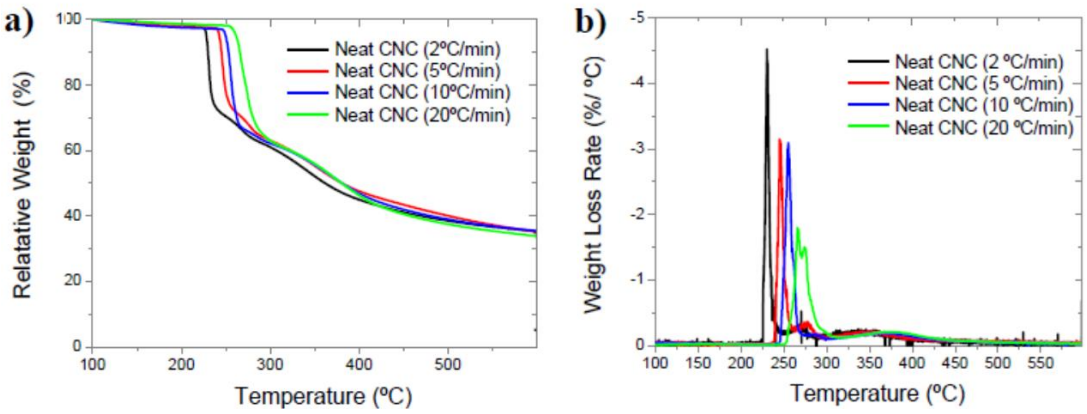


**Figure 46** Thermal degradation (a) and weight loss rates (b) of neat CNC film at different heating rates.

It is also observed that CNC film degradation occurs at higher temperatures as heating rate increases. This displacement towards high temperatures is caused because at low heating rates, heat has time enough to diffuse through the molten mass surface to internal polymer layers generating a slow layer splitting continued by the volatilization of the organic compounds. On the contrary, faster heating rates increase the degradation temperatures as Tpeak (temperature at degradation maximum) because temperature gradient between the heat source and the sample is bigger and there is not enough time for heat to diffuse and to reach the deeper polymer layers [31]. For this reason, when heating rate is increased degradation is produced at higher temperatures even though these temperatures are more equal when the process is ending. This phenomenon is observed in all analysed nanocomposite samples where temperature at thermal degradation maximum

(Tpeak) moves to higher values with the increase of the degradation rate (not shown).

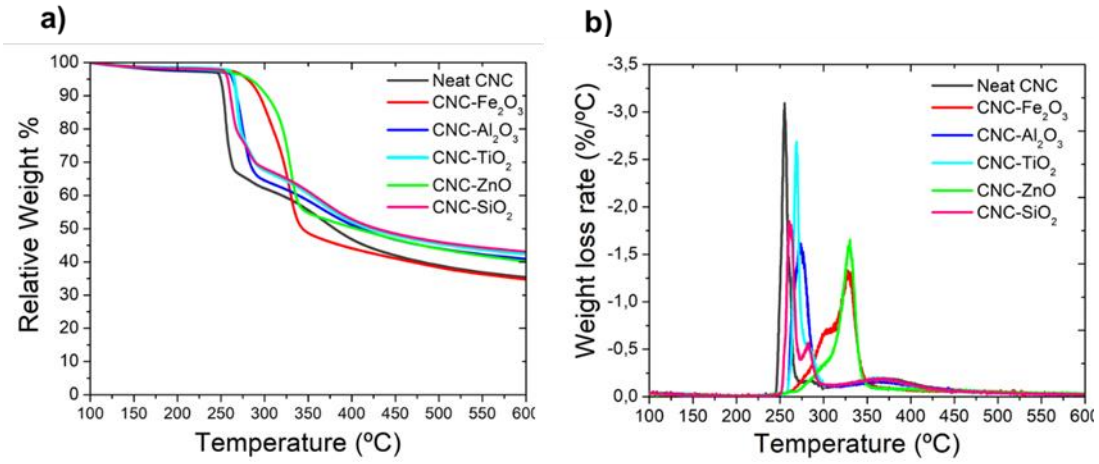


**Figure 47** Thermal degradation traces (a) and weight loss rates (b) of neat CNC, CNC/Fe2O3, CNC/Al2O3, CNC/TiO2, CNC/ZnO and CNC/SiO2 nanocomposites at 10wt.% particle concentration.

The influence of the different metallic nanoparticle incorporation into CNC films thermal stability is shown in **Figure 47**, while **Table 2** reports obtained main degradation parameters for all nanocomposite films. As graphically observed, neat CNC film thermal degradation begins at 249.6 ºC ($T_{onset}$) and its maximum degradation rate is reached at 255.1 ºC ($T_{peak}$) [32,33]. Overall, an increase in $T_{peak}$ is observed after the addition of MNPs, which is especially remarkable for the CNC/$Fe_2O_3$ and CNC/ZnO films, where the maximum thermodegradation rate takes place 72 and 75 ºC higher respectively. Indeed, with the addition of $Al_2O_3$, $TiO_2$ and $SiO_2$ nanoparticles the thermal stability is increased by 17, 14 and 5 ºC respectively.

Additionally, while neat CNC, CNC/$Al_2O_3$, CNC/$TiO_2$, and CNC/$SiO_2$ shows quite similar degradation profiles as illustrated in Figure 46b, when CNC is reinforced with $Fe_2O_3$ and ZnO double bell-shaped degradation traces are observed. Those results highlight that thermodegradation mechanism is modified by the presence

of these oxide nanoparticles as previously reported [15]. The full width half maximum (FWHM) value could be taken as an indicator of the degradation process length. It is observed in **Table 2** that FWHM values for CNC/$Fe_2O_3$, CNC/$Al_2O_3$ and CNC/ZnO are of 37.2, 19.1 and 17.8 ºC respectively, indicating longer and more complex degradation processes probably caused by a barrier effect of these nanoparticle to CNC combustion gas and decomposition products soaking through the material during the delaying the thermal degradation of the material [34].

**Table 2** Thermogravimetry analysis relevant parameters ($T_{5\%}$, $T_{10\%}$ and $T_{peak}$) obtained at 10 ºC/min degradation rate of Neat CNC, CNC/$Fe_2O_3$, CNC/$Al_2O_3$, CNC/$TiO_2$, CNC/ZnO and CNC/$SiO_2$ films at 10 wt.% concentration.

| **10% wt 10ªC/min** | **CNC** | **CNC/$Fe_2O_3$** | **CNC/$Al_2O_3$** | **CNC/$TiO_2$** | **CNC/ZnO** | **CNC/$SiO_2$** |
|---|---|---|---|---|---|---|
| **$T_{5\%}$ (ºC)** | 249.6 | 280.3 | 263.3 | 265.1 | 283.6 | 257.7 |
| **$T_{10\%}$ (ºC)** | 252.9 | 294.3 | 268.0 | 267.7 | 302.6 | 260.8 |
| **$T_{peak}$ (ºC)** | 255.1 | 327.6 | 272.1 | 268.9 | 330.1 | 260.6 |
| **$DTG_{max}$** | -3.1 | -1.3 | -1.6 | -2.7 | -1.6 | -1.8 |
| **FWHM (ºC)** | 7.9 | 37.2 | 19.1 | 6.7 | 17.8 | 9.8 |

*3.1.3.3. Activation energy determination*

*To provide deeper insights on the t*hermal degradation of fabricated nanocomposite films, Kissinger [35] and Ozawa-Flynn-Wall (OFW) methods[36,37] has been applied to quantitatively determinate the kinetics of thermal degradation. Kissinger model [38] is one of the most widely used iso-conversional methods to evaluate kinetics, which is based on the following equation (eq.18):

$$ln\frac{\beta}{T^2} = \left[ln\left(\frac{AE_a}{R(\alpha)}\right)\right] - \frac{E_a}{RT} \qquad (18)$$

The plot of ln ($\beta/T^2$) against *1/T* gives a straight line from which slope is obtained the activation energy ($E_a$) and the pre-exponential factor *A* is calculated from the intercept.

Also, OFW has been selected as a commonly used and integrated approach for the analysis of non-isothermal degradation kinetics. To simplify calculations, thermal degradation activation energy ($E_a$) has been determined according eq.19 and supposing that the conversion function *f(α)* does not change with the alteration of heating rates for all values of the conversion degree *α*. Thus, activation energy is easily determined from the weight loss versus temperature data obtained at different heating rates *β*:

$$\log \beta = [\log\left(\frac{AE_a}{R}\right) - \log f(\alpha) - 2.315] - 0.4567\frac{E_a}{RT} \qquad (19)$$

where *T* is the absolute temperature, $E_a$ is the activation energy, A is the pre-exponential factor and *R* is the universal gas constant (8.314 J/K mol) and $\alpha=(W_0-W_t/W_0-W_f)$ is the conversion degree.

For the purpose of required data obtention, TGA experiments at 3 different metal nanoparticle concentrations (1, 5 and 10 wt%) were conducted at 2, 5, 10 and 20 ºC/min under $N_2$ atmosphere for all the compositions

Thermodegradation activation energy ($E_a$) values have been calculated using both Kissinger and Ozawa-Flynn-Wall equations and are displayed in **Figure 48** as a function of metallic nanoparticle concentration. As shown, differences are observed in activation energy values comparing both theorical equations. Considering how experimental values fit to each theorical method, experimental data obtained by Kissinger show a good linear adjustment while the application of OFW method is only satisfactory to the nanocomposite films between the conversion fractions of 0.1-0.4, approximately phases I and II of the typical

degradation trace of CNC. This could be ascribed to the presence of complex and simultaneous degradation mechanisms so that the degradation kinetics is essentially governed by multiple reaction steps [31].

For this reason, experimental values obtained with Kissinger model are going to be deeply analysed than those obtained through Ozawa-Flynn-Wall equation. The activation energy for neat CNC film has been found to be 138 ± 4 kJ/mol with Kissinger method and 144 ± 19 kJ/mol using Ozawa-Flynn-Wall method, which fits well with data shown in literature [39].

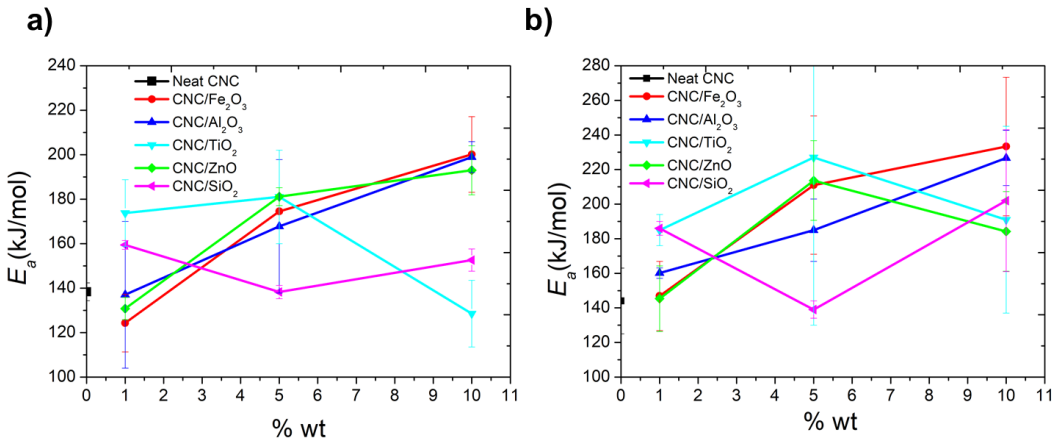


**Figure 48** Thermodegradation activation energy determined for all nanocomposites using Kissinger (a) and Ozawa-Flynn-Wall (b) equations.

Rather different trends could be observed depending on the nature of incorporated nanoparticles. On the one hand, nanocomposites loaded with $Fe_2O_3$, $Al_2O_3$ and ZnO metallic nanoparticles show a thermal stability and activation energy increase as nanoparticle concentration is increased achieving activation energy values of 200 ± 17, 199 ± 7 and 193 ± 11 kJ/mol respectively at a concentration of 10 wt.% [40]. Reasons generally credited for obtained experimental findings arise from the fact that these thermally stable nanoparticles could delay the thermal degradation by absorbing heat and quenching the generated radicals for CNC

acting like a networking barrier for chains splitting and also delaying the elimination of volatiles with more effectiveness at high concentration [41]. But also, these results reinforce the previously mentioned idea of the degradation mechanism modification due to the presence of these nanoparticles probably because of interactions between some metallic oxides and CNC chains that favour the location of nanoparticles closer to the cellulosic chains. The hypothesis is that these interactions could be electrostatic interactions between remaining sulphate groups result of an incomplete desulfonation during the initial cellulose nanocrystal obtaining processes by means of controlled acid-hydrolysis. These electrostatic attractive forces are supposed to be stronger than the cohesive forces between nanoparticles in the case of Zn, Fe and Al oxide nanoparticles and originate the positioning of better dispersed nanoparticles in some places near the polymer chain surface [42,43].

In this sense, the presence of sulphate groups onto CNC surfaces modifies their thermal stability [16]. Thus, in this case, this negatively charged CNC surfaces increase the effect of some metallic nanoparticle in the thermal stability, particularly at higher concentrations producing a double effect; favouring the disposition of nanoparticles at the polymer surface and promoting a better particle distribution along polymer matrix that generates more effectiveness of nanoparticles in the barrier effect and delaying of degradation process [44,45]**.** So, this remaining sulfonation degree in CNC surface, and the different interaction between some metallic nanoparticles and negatively charged CNC chains could explain the observed different behaviour between the lineal thermal stability activation energy increase in Fe, Zn and Al oxide loaded nanocomposites and those loaded with Ti and Si oxides, chemically more similar, and which exhibit more inconsistent conclusions [46,37].

In the case of CNC loaded with $TiO_2$ and $SiO_2$ nanoparticles, the increase of thermal stability is not so evident, nanoparticle concentration increase does not lead to an improvement in activation energies and it is observed that both systems show fluctuant behaviour with nanoparticle addition.

This is partially due to a non-homogeneous particle distribution of Ti and Si nanoparticles whith in composite matrix with some regions homogeneously distributed and some aggregated that causes a reduction of nanoparticle effect in thermal stability due to the reduction of the specific area and making the degradation process easier to happen [47,48,49,50]. Possibly, in these cases, the electrostatic interaction of this nanoparticle with similar electrostatic and chemical behaviour is not stronger than the cohesion force between nanoparticles. This explains a less marked effect of these nanoparticles in thermal stability of nanocomposite films.

*3.1.3.4. Wide angle X-ray diffraction (WAXD)*

XRD patterns of nanocomposite films were collected from room temperature to 400 ºC in order to observe the occurring changes of the CNC crystalline structure as the crystallinity changes are related to the thermally induced degradation of the fabricated materials. The broad WAXD peaks occurring in **Figure 49** at 15 and 22° are attributed to *(110)* and *(200)* planes of the cellulose structure [31], while the remaining smaller peaks achieved at higher $2\theta$ values correspond to incorporated metallic nanoparticles in concordance with previously showed nanoparticle patterns (**Figure 44**). The reflection peaks of (*110)* and *(200)* planes start to be less intense at a temperature of ~225 ºC for neat CNC and completely disappears at 275 ºC, indicating that no further cellulosic crystallites exist as a result of the decomposition of cellulose by a thermally activated process. Interestingly, it is seen that the crystalline structure of cellulose is keep up at higher

temperatures once metallic nanoparticles are incorporated into CNC film, indicating an increased thermal stability of metallic nanoparticle loaded films in regard with neat CNC film. To get further detail into how the crystalline structure of cellulose is modified upon heating, the normalized intensity area of cellulose crystalline reflections for different CNC nanocomposite films is displayed in **Figure 50a**. It is seen that $Fe_2O_3$ and ZnO are the most effective metallic nanoparticles for delaying the disruption of the cellulose crystalline structure upon heating.

In other words, the incorporation of these both metal oxides result the most successful strategy to overcome the relatively poor thermal stability of CNCs. Additionally, the crystalline structure could be kept up to higher temperatures as further nanoparticles are incorporated into CNCs (**Figure 50b**), which is in line with the Ea increase upon nanoparticle addition shown in Figure 47. Overall, these results further confirm the notably increased thermal stability of nanocomposites determined by thermogravimetry.

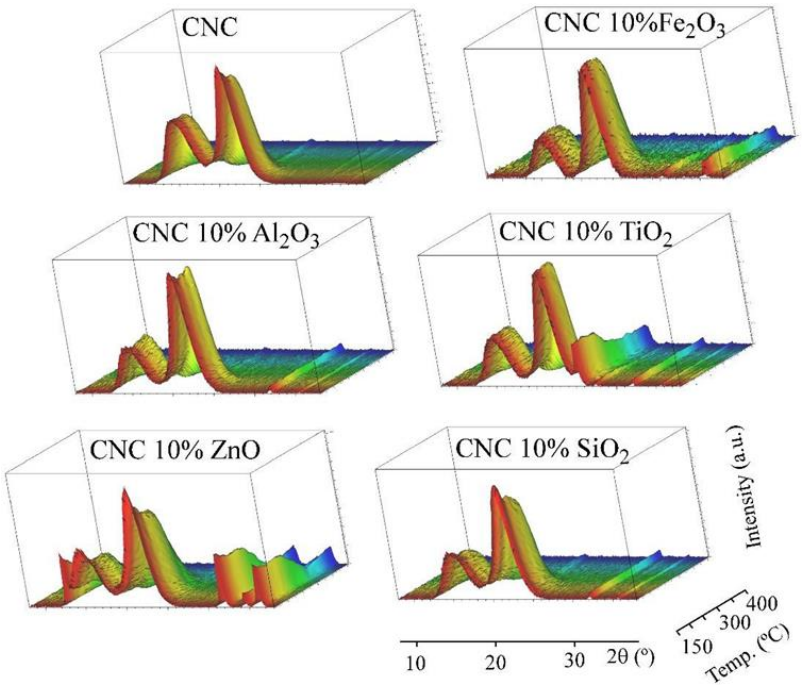


**Figure 49** WAXD diffractograms obtained for neat CNC and CNC loaded with MNPs at the highest concentration (10 wt. % particle concentration).

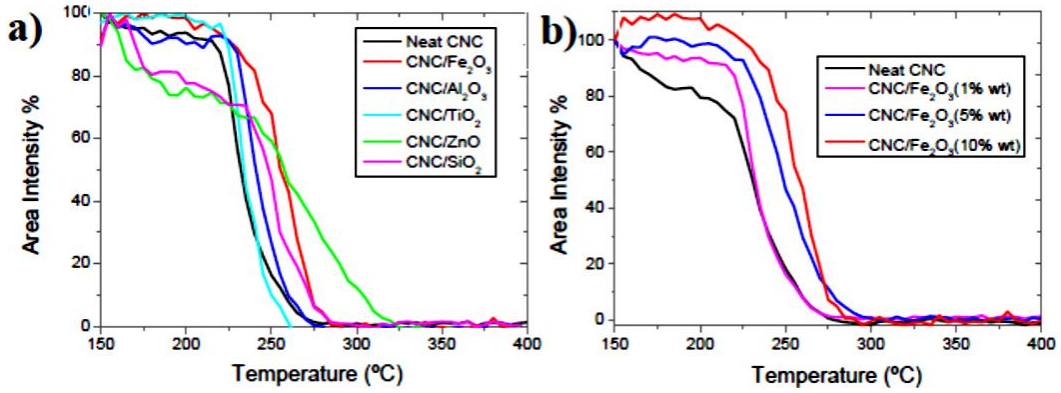


**Figure 50** Normalized intensity area of cellulose crystalline reflections for different CNC nanocomposite films at a concentration of 10 wt.% (a) and for CNC/$Fe_2O_3$ nanocomposite films (b).

## 3.1.4. Conclusions

This work aims to provide novel strategies for to the development of environmentally friendly materials with improved functional properties based on cellulose. Here we explore nanocomposite approach as an alternative method to increase the intrinsic poor thermal stability of CNCs obtained after sulphuric acid-assisted hydrolysis of cellulose instead of removing the remaining surface functional groups from CNC via complex, expensive and tedious chemical modification techniques. CNC-based nanocomposites having five different metallic nanoparticles (ZnO, $SiO_2$, $TiO_2$, $Al_2O_3$ and $Fe_2O_3$) have been fabricated by simple co-assembly method using water as dispersing agent. The thermal stability and activation energy of CNC nanocomposite films have been studied by TGA, while WAXD was carried out to determine the occurring crystalline modifications upon heating. Overall, a continuous enhancement on the thermal stability of cellulosic films is observed upon nanoparticle addition. A maximum increase of nearly 75 ºC was found for CNC/ZnO and CNC/$Fe_2O_3$ 10 wt% nanocomposite materials, while the thermodegradation activation energy is increased from 138.3 ± 3.9 kJ/mol for neat CNC to 200.1 ± 16.6 kJ/mol and 193.4 ± 10.6 kJ/mol for its CNC/ZnO and CNC/$Fe_2O_3$ 10 wt%, respectively. It is remarkable

the marked improvement on the thermal stability achieved by simply adding metallic nanoparticles. Overall, the results here reported provide further understanding towards the replacement of commonly used petrol-based polymers by cellulosic materials with increased thermal stability.

## References

[1] Pramila S., Fulekar M.H., Bhawana P. 2012. E-Waste-A challenge for tomorrow. Research Journal of Recent Sciences, 1(3), 86–93.

[2] Ross G., Ross S., Tighe B.J. 2017. Bioplastics: New Routes, New Products. Brydson's Plastics Materials, 8, 631-652.

[3] Raschka A., Carus M., Piotrowski S. 2014. Renewable Raw Materials and Feedstock for Bioplastics. Bio-Based Plastics: Materials and Applications, 1, 331-345.

[4] Gutierrez J., Fernandes S. C. M., Mondragon I., Tercjak, A. 2012. Conductive photoswitchable vanadium oxide nanopaper based on bacterial cellulose. ChemSusChem, 5, 2323-2327.

[5] Drumright R.E., Gruber P.R., Henton D.E. 2012. Polylactic acid technology, Advanced Materials, 12, 1841–1846.

[6] Lee S.Y. 1996. Bacterial polyhydroxyalkanoates. Biotechnology and Bioengineering. 49, 1-14.

[7] Lee S.Y. 1996. Plastic bacteria Progress and prospects for polyhydroxyalkanoate production in bacteria. Trends in Biotechnology,14, 431-438.

[8] Mark H. 1980. Fifty years of cellulose research. Cellulose Chemistry and Technology, 14, 569–581.

[9] Thakur M.K., Thakur V.K., Prasanth R. 2014. Nanocellulose-Based Polymer Nanocomposites: An Introduction. Nanocellulose Polymer Nanocomposites: Fundamentals and Applications, 1.

[10] Kettunen M. 2013. Cellulose Nanofibrils as a Functional Material. Aalto University publication series Doctoral Dissertations 114.

[11] Dufresne A. 2008. Polysaccharide nano crystal reinforced nanocomposites. Canadian Journal of Chemistry, 86(6), 484-494.

[12] Habibi Y., Lucia L. A., Rojas O. 2010. Cellulose nanocrystals: chemistry, self-assembly, and applications. Chemical Reviews, 110(6), 3479–3500.

[13] Lizundia E., Vilas J.L., León L.M. 2015. Crystallization, structural relaxation and thermal degradation kinetics in Poly(L-lactide)/cellulose nanocrystal renewable nanocomposites. Carbohydrate Polymers, 123C, 256-265.

[14] Lizundia E., Fortunati E., Dominici F., Vilas J.L., León L.M., Armentano I., Torre L., Kenny J.M. 2016b. PLLA-grafted cellulose nanocrystals: Role of the CNC content and grafting on the PLA bionanocomposite film properties. Carbohydrate Polymers, 142, 105-113.

[15] Schlesinger M., Giese M., Blusch L.K., Hamad W.Y., MacLachlan M.J. 2015a. Chiral nematic cellulose-gold nanoparticle composites from mesoporous photonic cellulose. Chemical Communications, 51, 530-533.

[16] Lizundia E., Urruchi A., Vilas J., León L.M. 2016. Increased functional properties and thermal stability of flexible cellulose nanocrystal/ZnO films. Carbohydrate Polymers, 136, 250-258.

[17] Lin N., Dufresne A. 2014b. Surface Chemistry, morphological analysis and properties of cellulose nanocrystals with gradiented sulfonation degrees. Nanoscale 6, 5384-5393.

[18] Lizundia E., Nguyen TD., Vilas J.L., Wadood Y. H.,MacLachlan M.J. 2016.Chiroptical luminescent nanostructured cellulose films. Materials Chemistry Frontiers, 1(5), 979-987.

[19] Kanmani P., Rhim J.W. 2014. Properties and characterization of bionanocomposite films prepared with various biopolymers and ZnO nanoparticles. Carbohydrate Polymers, 106, 190-199.

[20] Sambandan D. R., Ratner D. 2011. Sunscreens: An overview and update. Journal of the American Academy of Dermatology, 64(4), 748–758.

[21] Lizundia E., Ruiz-Rubio L., Vilas J.L., León L.M. 2016. Towards the development of eco-friendly disposable polymers: ZnO-initiated thermal and hydrolytic degradation in poly(L-lactide)/ZnO nanocomposites. RSC Advances, 6, 15660-15669.

[22] Mesquita-Guimaräes J., Leite M.A., Souza J.C.M., Henriques B., Silva F.S., Hotza D., Boccaccini A.R., Fredel M.C. 2016. Processing and strengthening of 58S

bioactive glass-infiltrated titania scaffolds. Journal of Biomedical Materials Research Part A, 105, 590-600.

[23] Matori K.A., Wah L.C., Hashim M., Ismail I., Zaid M.H.M. 2012. Phase Transformations of α-Alumina Made from Waste Aluminum via a Precipitation Technique. International Journal of Molecular Sciences,13(12), 16812-16821.

[24] Wu W., Xiao X.H., Zhang S.F., Peng T.C., Zhou J., Ren F., Jiang C.Z. 2010. Synthesis and Magnetic Properties of Maghemite (γ-Fe2O3) Short-Nanotubes. Nanoscale Research Letters, 2010, 5(9), 1474–1479.

[25] Ifuku S., Tsuji M., Morimoto M., Saimoto H., Yano H. 2009. Synthesis of Silver Nanoparticles Templated by TEMPO-Mediated Oxidized Bacterial Cellulose Nanofibers. Biomacromolecules, 10 (9), 2714–2717.

[26] Revol J.F., Bradford H., Giasson J., Marchessault R. H., Gray, D. G. 1992. Helicoidal self-ordering of cellulose microfibrils in aqueous suspension. International Journal of Biological Macromolecules, 14, 170–172.

[27] Beyler C.L., Hirschler M.M. 2001. Thermal Decomposition for Polymers. SFPE 3, Section 1, chapter 7.

[28] Pisupati S.V., Tchapda A.H. 2015. Thermomechanical processing of Biogas. Advances on Bioprocess Technology, 2, 275-295.

[29] Shen D., Xiao R., Gub S., Luob K. 2011. The pyrolytic behavior of cellulose in lignocellulosic biomass: a review. RSC Advances, 1, 1641-1660.

[30] Lin T., Goos E., Riede U. 2013. A sectional approach for biomass: Modelling the pyrolysis of cellulose. Fuel Processing Technology 115, 246-253.

[31] Silva R.P., Oliveira, R.V.B. 2016. Non-isothermal degradation kinetics and morphology of PP/$TiO_2$ nanocomposites using titanium n-butoxide precursor. International Journal of Plastics Technology, 20(2), 364–377.

[32] Morán J.I., Vazquez A., Cyras V.P. 2008. Extraction of cellulose and preparation of nanocellulose from sisal fibers. Cellulose, 15(1), 149–159.

[33] Marshall, J.S. 2015. Comparative kinetic study of the thermal decomposition of nanocellulose produced by $H_2SO_4$ hydrolysis, Tempo, and AVAP processes. ETD

Collection for AUC Robert W. Woodruff Library, Atlanta University Center, Paper 3114.

[34] Liu A., Walther A., Ikkala O., Belova L., Berglund L.A. 2011. Clay nanopaper with tough cellulose nanofiber matrix for fire retardancy and gas barrier functions. Biomacromolecules, 12(3), 633-641.

[35] Kissinger H.E. 1956. Variation of peak temperature with heating rate in differential thermal analysis. Journal of research of the National Bureau of Standards, 57(4), 217-221.

[36] Ozawa T. 1970. Kinetic analysis of derivative curves in thermal analysis. Journal of Thermal Analysis and Calorimetry, 2, 301.

[37] Flynn J. H., Wall L.A. 1966. A quick, direct method for the determination of activation energy from thermogravimetric data. Journal of polymer Science Part B: Polymer Physics, 4(5), 323-328.

[38] Kissinger H.E. 1957. Reaction Kinetics in Differential Thermal Analysis. Analytical Chemistry, 29(11), 1702-1706.

[39] Pasquini D., Alves M., Flauzino W.P., Alves H., Ferreira D., Alves L.V., de Morais L.C. 2015. Kinetic study of the thermal decomposition of cellulose nanocrystals with different polymorphs, cellulose I and II, extracted from different sources and using different types of acids. Industrial Corps and products, 76, 128-140.

[40] Ul-Islam, M., Khattak, W.A., Ullah M.W., Khan S., Park, J. K. 2014. Synthesis of regenerated bacterial cellulose-zinc oxide nanocomposite films for biomedical applications. Cellulose, 21, 433-447.

[41] Kashiwagi T. 2007. Progress in Flammability Studies of Nanocomposites with New Types of Nanoparticles. Flame Retardant Polymer Nanocomposites 10, 285-324.

[42] Kim J., Montero G., Habibi Y., Hinestroza J.P., Genzer J., Argyropoulos D.S., Rojas O.J. 2009. Dispersion of cellulose crystallites by nonionic surfactants in a hydrophobic polymer matrix. Polymer Engineering and Science, 49(10), 2054-2061.

[43] Polte J. 2015. Fundamental growth principles of colloidal metal nanoparticles, a new perspective. CrystEngComm, 17, 6809-6830.

[44] Roman M.,Winter W.T. 2004. Effect of sulfate groups from sulfuric acidhydrolysis on the thermal degradation behaviour of bacterial cellulose. Biomacromolecules, 5, 1671-1677.

[45] Lin M., Li B., Li Q., Li S., Zhang S. 2011. Synergistic effect of metal oxides on the flame retardancy and thermal degradation of novel intumescent flame-retardant thermoplastic polyurethanes. Journal of Applied Polymer Science. 121(4), 1951–1960.

[46] Belucci F., Fabiani D., Montanari G.C., Tesla L. 2010. The processing of nanocomposites. Dielectric Polymer Nanocomposites, 2, 31-54.

[47] Mina F., Seema S., Matin R., Rahaman M.J., Sarker R.B., Gafur Md.A., Bhuiyan Md. A.H. 2009. Improved performance of isostactic polypropylene/titanium dioxide composites: Effect of processing conditions and filler contents. Polymer Degradation and Stability, 94, 183-188.

[48] Silva, C. G., Pastrana-Martinez L. M., Morales-Torres S. 2016. When carbon meets light: synergistic effect between carbon nanomaterials and metal oxide semiconductors for photocatalytic applications. Boletín GEC, 40(6).

[49] Klapiszewski L., Pawlak F., Tomaszewska J., Jesionowski T. 2015. Preparation and Characterization of Novel PVC/Silica–Lignin Composites. Polymers, 7, 1767-1788.

[50] Ahmad M.B., Gharayebi Y., Salit M.S., Hussein M.Z., Ebrahimiasl S., Dehzangi A. 2012. Preparation, Characterization and Thermal Degradation of Polyimide (4-APS/BTDA)/$SiO_2$ Composite Films. Molecular Sciences,13, 4860-4872.

[51] Roig F., Dantras E., Dandurand J., Lacabanne C. 2011. Influence of Hydrogen Bonds on Glass Transition and Dielectric Relaxations of Cellulose. Journal of Physiscs D: Applied Physics, 44, 045403.

[52] Sun Q.F., Lu Y., Xia Y.Z., Yang D. J., Li J., Liu Y.X. 2012. Flame retardancy of wood treated by $TiO_2$/ZnO coating. Surface Engineering, 28, 555-559.

[53] Toivonen M.S., Kurki-Suonio S., Schacher F.H., Hietala S., Rojas O.J., Ikkala O. 2015. Water-Resistant, Transparent Hybrid Nanopaper by Physical CrossLinking with Chitosan. Biomacromolecules, 16, 1062-1071.

[54] Utsel S., Malmström E.E., Carlmark A., Wågberg L. 2010. Thermoresponsive nanocomposites from multilayers of nanofibrillated cellulose and specially designed N-isopropylacrylamide based polymers. Soft Matter, 6, 342-352.

[55] Wei B., Zou C., Li X. 2017. Experimental Investigation on Stability and Thermal Conductivity of diathermic oil based $TiO_2$ nanofluids. International Journal of Heat and Mass Transfer, 104, 537-543.

[56] Yu J. H., Duan J.K., Peng W.Y., Wang L.C., Peng P, Jiang P.K. 2011. Influence of nano-AlN particles on thermal conductivity, thermal stability and cure behaviour of cycloaliphatic epoxy/trimethacrylate system. eXPRESS Polymer Letters, 5(2), 132-141.

[57] Balasubramanian G., Dionysios D., Suidan M.T. 2014. Titanium Dioxide Coatings on Stainless Steel. Dekker Encyclopedia of Nanoscience and Nanotechnology, 3917-3926.

[58] Fan H., Li G., Yang F., Yang L., Zhang, S. 2011. Photodegradation of cellulose under UV lightcatalysed by $TiO_2$. Journal of Chemical Technology and Biotechnology, 86(8), 1107-1112.

[59] Lizundia E, Oleaga A. Salazar A., Sarasua J.R. 2012. Nano- and microstructural effects on thermal properties of poly (L-lactide)/multi-wall carbon nanotube composites. Polymer, 53, 2412-2421.

[60] Lizundia E., Ruiz-Rubio L., Vilas J.L., León L.M. 2015. Poly(l-lactide)/ZnO nanocomposites as efficient UV- shielding coatings for packaging applications. Journal of Applied Polymer Science, 132, 42426.

# 3.2. Metal Nanoparticles Embedded in Cellulose Nanocrystal Based Films: Material Properties and Post-use Analysis

## 3.2.1. Introduction

In recent years, the threat of potentially harmful bacteria stresses is increasing the importance in the scientific research of developing new antimicrobial biomaterials to combat human pandemics. Furthermore, to combine the antimicrobial properties with biobased and degradable materials is an important challenge. Biomaterials with antibacterial properties have ideally to respond to a wide spectrum of infections, with a primary scope to prevent the treatment or the reduction of the infections [1]. In this regard, high antibacterial performance with bactericidal or adhesion-resistant properties has been achieved and nanostructured materials with antibacterial properties are under exploration [2.3].

Cellulose is an excellent natural material with wide promising applications thanks to its good biodegradability, biocompatibility, and nontoxicity [4-6]. It could be considered as the major natural and inexhaustible source of raw materials meeting the increasing appeal for green and biocompatible products [7]. During the past decade, cellulose-based materials have been proven to be suitable for the development of environmentally friendly films with potential applications in different field because of their biocompatibility, low cost, and wide availability [8], mainly in combination with other biobased or biodegradable polymer to develop bionanocomposite materials. Cellulosic nanostructures are recognized as innovative nanomaterials that enable the development of new materials with improved performance. In this sense, cellulose nanocrystals (CNC) emerge as one of the most promising form of cellulosic materials for novel applications due to their inherent characteristics. CNC are extracted via

controlled disintegration of cellulose, being acid-hydrolysis the most common method [7−9].

As a result of the controlled disintegration of the amorphous and disordered regions of cellulose, well-defined nanosized crystals having a modulus of elasticity of 150 GPa and low density of 1.57 g/cm$^3$ are achieved [10].

Cellulose has been explored as material for nanocomposite development due to the presence of various functional groups that may be employed in different activation processes. The development of nanocomposites is a common strategy to upgrade the functional properties of the hosting matrix [8,9,11−13]. For example, the addition of nanofillers into several biopolymers has already leaded to improvements in the physicomechanical performance of their hosting matrices [8,14]. In this framework, the incorporation of metal nanoparticles such as silver, titanium, and zinc into a hosting matrix has been proven to efficiently provide antibacterial properties to the whole system at the same time that they provide ultraviolet (UV) screening properties [15−17]. Silver nanoparticles were extensively studied due to their potential antibacterial properties [8,15-17]; nanosized silver particles show both Gram-positive and Gram-negative antimicrobial properties [18]. However, the biomedical applications of silver nanoparticles are potentially limited due to their genotoxicity toward mammalian cell and their nonspecific biological toxicity [19,20]. Alternatively, zinc oxide (ZnO), an interesting transition metal oxide, is used as an effective entity for devastating the microbial growth. ZnO possesses good catalytic, electrical, photochemical, and optical properties, it is used in the area of bioscience as a biomimetic membrane; furthermore, it can immobilize and modify proteins because of the fast electron transfer between the enzyme's active sites and the electrode [21]. In addition, ZnO has a lot of advantages: it is nontoxic and chemically stable under exposure to both high temperatures and UV light [22]. The assembly of nanometer-

scale building blocks with distinct sizes, shapes, and compositions is a promising approach to the design and fabrication of functional nanocomposite materials with new structures and properties [23]. Fine dispersion of nanoparticles in a polymer matrix that can permit the functional presence, without the direct contact of the nanoparticles with biological entities, is an important challenge. Additionally, from an environmental point of view, it is desirable to speed-up the film disintegration in compost conditions once the films have been used. This modulation of the biodegradation profile could be attempted as well by the introduction of proper nanoparticles into the hosting polymer matrix. Unfortunately, obtaining a homogeneous dispersion of these nanoparticles is not a trivial issue due to their tendency to aggregate thanks to their high surface energy [24]. Several approaches known as grafting from, grafting to, and grafting through have been carried out to overcome this issue, although they usually require long and complex chemical processes, which are not easily scalable [25]. Moreover, the introduced surfactants when preparing nanocomposites with well-dispersed particles are toxic and not suitable for biomedical applications [26]. Conversely, evaporation induced self-assembly (EISA) arises as an efficient approach to fabricate CNC-based nanohybrids with randomly distributed nanoparticles because the electrostatic repulsion forces between adjacent CNC (when dispersed in water) keep the composite constituents well distributed in solution at the nanoscale [27]. This simple approach is scalable through the existing papermaking technologies, enabling the fabrication of simple formulations for the industry via a cost-effective process.

The aim of this work is to design, synthesize, and characterize innovative antibacterial biomaterials based on cellulose nanocrystals and metal nanoparticles and to explore the effect of dimensions, shape, and chemistry on final nanocomposite properties

including the disintegration of these materials in composting conditions and their suitability as antimicrobial systems.

## 3.2.2. Materials and methods

### *3.2.2.1. Starting Materials*

Microcrystalline cellulose with a particle size of 20 μm (310697−500G), sulfuric acid, and sodium hydroxide (NaOH) have been supplied by Sigma-Aldrich. The acetone (HPLC grade, assay >99.8%) was purchased from LabScan, while methanol (reagent ≥99.5%) was purchased by Panreac. ZnO and $TiO_2$ nanoparticles have been kindly purchased by ĹUrederra technological center (Spain). $Ag_2O$ was provided by Cima NanoTech (Corporate Headquarters, Saint Paul, MN, USA).

### *3.2.2.2. Cellulose Nanocrystals (CNC) Synthesis*

CNC were synthesized via sulfuric acid hydrolysis of microcrystalline cellulose [28]. Briefly, microcrystalline cellulose was hydrolyzed in a 64% (w/w) sulfuric acid solution at 45 °C for 30 min. The reaction was quenched by adding 20-fold distilled water. Remaining cellulose was recovered by centrifugation (6000 rpm for 10 min) and it was further isolated at a reduced pressure using a Buchner flask and Buchner funnel and washed with distilled water. Resulting dispersion was then neutralized by adding 0.25 mol/L of sodium hydroxide (NaOH). Finally, remaining dispersion was sonicated at an output of 40% for 5 min with a Vibracell Sonicator. CNC having a zeta potential of −0.6 mV (Malvern Zetasizer Nano instrument) have been obtained.

*3.2.2.3. CNC Based Film Fabrication*

Mechanically flexible CNC/ZnO, CNC/$TiO_2$, and CNC/$Ag_2O$ films have been prepared by evaporation-induced self-assembly (EISA) [9]. Nanoparticles were dispersed in distilled water via mild-sonication (20% output for 5 min in a Vibra-CellTM CV 334) and they were added to 2.2 wt % aqueous CNC dispersions to yield composite materials with 1 wt % (CNC to metal nanoparticles). Another sonication step at 20% output for further 5 min has been applied to aqueous CNC/metal oxide dispersions before casting them in 6 × 4 $cm^2$ silicone molds. Samples were dried at 30 °C on a hot plate (RH of 52%) for 48 h followed by 24 h at 60 °C in a vacuum oven. Neat CNC film was also prepared for comparison, and 300 ± 20 μm thick films were obtained.

*3.2.2.4. Morphological Characterization*

Cellulose nanocrystals were analyzed by transmission electron microscopy (TEM) by using a Philips CM120 Biofilter apparatus with STEM module (120 kV). CNC-based films have been analyzed using a Hitachi S-4800 field emission scanning electron microscope (FE-SEM) at an acceleration voltage of 15 kV. Before analysis, samples were copper-coated in a Quorum Q150T ES turbo-pumped sputter coater (5 nm thick).

*3.2.2.5. Thermogravimetric Analysis*

Thermogravimetric analysis (TGA) was performed on 10 mg samples by a Seiko Exstar 6000 TGA quartz rod microbalance. The tests were done under nitrogen atmosphere from 25 to 900 °C at 10 °C/min.

*3.2.2.6. UV−VIS Spectroscopy*

UV−VIS absorption spectra were recorded by a Shimadzu MultiSpec-1501 spectrophotometer. Total transmittance experiments have been analyzed in the range of 200 to 800 nm with a sampling interval of 1 nm and 25 accumulations.

*3.2.2.7. Contact Angle Measurements.*

Milli-Q water was used as probe liquids for the determination of film surface hydrophobicity. Measurements were done by sessile drop method (2 µL per drop at a rate of 2 µL/s) using a Neurtek Instruments OCA 15 EC at 25 °C. The average values were calculated using six measurements.

*3.2.2.8. Antibacterial Assays*

As previously reported [29], Escherichia coli RB (E. coli RB) and Staphylococcus aureus (S. aureus 8325−4) were used in this study. Both bacterial strains were routinely grown overnight in their culture medium (E. coli RB in Luria−Bertani Broth (LB) (Difco, Detroit, MI, USA) and S. aureus 8325−4 in Brian Heart Infusion (BHI) (Difco)) under aerobic conditions at 37 °C using a shaker incubator (New Brunswick Scientific Co., Edison, NJ, USA). These cultures were diluted in fresh culture medium and statically incubated at 37 °C under aerobic conditions. Cell density of the bacterial suspension was determined by optical density (OD600) and compared to a standard curve relating OD600 to cell number.

All types of CNC-based films were previously sterilized (70% ethanol for 10 min, followed by washings with sterile distilled water) and directly incubated with 200 µL $5 \times 10^4$ S. aureus or E. coli cell suspensions for 3 and 24 h at 37 °C, respectively. At the indicated time points, an MTT test was performed both on the planktonic cell cultures after being in contact with the different CNC-based films and on the cells adherent to the surface of materials to determine the number of live cells. The

same aliquot of bacteria was cultured and treated in a tissue culture plate (TCP). Results were normalized to TCP and expressed as the ratio between bacterial surviving fraction on CNC-based films and neat CNC films. The experiments were performed in duplicate and repeated three times.

*3.2.2.9. Scanning Electron Microscopy*

Adherent cells were evaluated morphologically for bacteria observation [30]: both bacterial suspensions were seeded on either thermanox coverslip (internal control) (NuncTM) positioned at the bottom of a 24-well culture plates, on CNC and on all types of CNC films containing metallic nanoparticles. The incubation was performed for both 3 and 24 h at 37 °C. Samples were washed carefully with sterile water and fixed with 2.5% (v/v) glutaraldehyde in 0.1 M Na-cacodylate buffer, pH 7.2 for 1 h at +4 °C. The samples were then dehydrated using increasing concentrations of ethanol and dried to the critical point using an Emitech K-850 apparatus (Emitech, Ashford, Kent, UK) placed on a mounting base and sputter coated with gold. Once prepared, the samples were observed using a Zeiss EVO-MA10 scanning electron microscope (Carl Zeiss, Oberkochen, Germany). SEM observations were performed at two magnifications: 3.000× and 10.000×.

*3.2.2.10. Disintegrability in Composting Conditions*

Disintegration test under composting conditions was carried applying the European standard ISO 20200 (ISO20200 - Determination of the degree of disintegration of plastic materials under simulated composting conditions in a laboratory-scale test). The test was performed at laboratory-scale and determines the degree of disintegration of plastic materials under simulated intensive aerobic composting conditions at 58 °C and 50 % of humidity. The degree of disintegration D was calculated in percent by normalizing the sample weight at different days of incubation to the initial weight by using eq 20:

$$D = \frac{m_i - m_r}{m_i} \text{ x } 100 \qquad (20)$$

where $m_i$ is the initial sample mass; $m_r$ is the dry sample mass after the test.

CNC-based films of dimension 15 mm × 15 mm × 0.03 mm were weighed and buried into the organic substrate at 4−6 cm depth in the perforated boxes guaranteeing the aerobic conditions. The films were considered disintegrable according to the European standard when 90% of the plastic sample weight is lost within 90 days of analysis. A solid synthetic waste was prepared, mixing sawdust, rabbit food, compost inoculum supplied by Genesu S.p.a., starch, sugar, oil, and urea, for simulating the real disintegrability in compost conditions The CNC and CNC based nanohybrid films tested were taken out at different times (3, 7, 21, 35, 49, and 90 days), washed with distilled water, and dried in an oven at 37 °C for 24 h. Fourier infrared (FT-IR) spectra of the samples in the 400−4000 $cm^{-1}$ wavelenght range, operating in attenuated total reflection (ATR) mode, were recorded by using a Jasco FT-IR 615 spectrometer, at selected times. Thermogravimetric analysis (TGA) was performed on 10 mg samples by a Seiko Exstar 6000 TGA quartz rod microbalance. The tests were done under nitrogen atmosphere from 25 to 900 at 10 °C/min, and the maximum degradation temperatures were considered for the different studied formulations.

*3.2.2.11. Statistical Analysis*

The length-distribution of CNCs, ZnO, $TiO_2$ and $Ag_2O$ nanoparticles have been obtained based on a count of 50 particles from different transmission electron microscopy images using ImageJ software. Statistical analysis was performed against neat CNC film (∗ for Planktonic cells, # for adherent cells) (∗,# $p < 0,05$; ∗∗, ## $p < 0,01$; ∗∗∗, ### $p < 0,001$) using one-way analysis of variance (ANOVA).

Statistical significance was established at two-tailed $p \leq 0.05$. All calculations were generated using GraphPad Prism 5.0 (GraphPad Inc., San Diego, CA).

## 3.2.3. Results and Discussion

### *3.2.3.1. Material Characterization*

Transmission electron microscopy (TEM) was performed to determine the morphological features of starting raw materials. Synthesized cellulose nanocrystals shown in **Figure 51a** were obtained after sulfuric acid hydrolysis of commercial microcrystalline cellulose and are 172 ± 25 nm long and ~10 nm wide. Moreover, ZnO nanoparticles were (43 ± 24) nm long and 20 nm wide (**Figure 51b**), while $TiO_2$ and $Ag_2O$ nanoparticles show a spherical morphology with a diameter of 12 ± 4 nm and 270 ± 50 nm, respectively (**Figure 51c,d**) (statistics based on count of 50 particles).

**Figure 51e−h** shows the physical appearance of synthesized CNC, CNC/$Ag_2O$, CNC/ZnO, and CNC/$TiO_2$ films. It was observed that all fabricated materials present crack-free and free-standing characteristics; optical color depends on the nature of reinforcing metal nanoparticle.

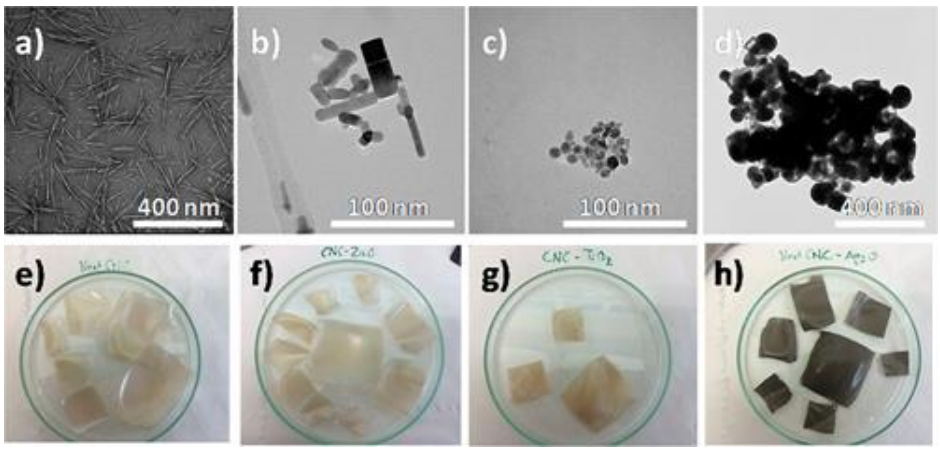

**Figure 51** First row shows the representative transmission electron microscopy (TEM) images of (a) cellulose nanocrystals, (b) ZnO, (c) $TiO_2$, and (d) $Ag_2O$ nanoparticles. Second row displays the macroscopic appearance of synthesized films composed of (e) CNC (f) CNC/ZnO, (g) CNC/$TiO_2$, and (h) CNC/$Ag_2O$.

Regarding the brittleness/mechanical properties of the films, it is worthy to note that these films could be easily handled (included twisting and bending) without breaking. According to a work published by our group dealing with the same materials, the Young's modulus of these films is found in the range of 6−6.5 GPa [9]. While $Ag_2O$ changes the transparent-like appearance of raw CNC film as a result of the strong absorbing nature of silver oxide, after ZnO and $TiO_2$ addition no remarkable changes in the film coloration are observed.

*3.2.3.2. TGA Characterization*

Thermogravimetric analysis (TGA) of the CNC and CNC based nanocomposites under nitrogen atmosphere was conducted to evaluate the effect of different metal nanoparticles on the thermal stability properties of CNC based films and the results are summarized in **Figure 52**, showing the weight loss and derivative curves of weight loss, for different produced formulations. The curves underline that all the produced films show a multistep degradation behavior. The degradation step of raw CNC film begins at about 240−250 °C and reaches its maximum rate at around 260 °C, which corresponds to depolymerization, dehydration, and decomposition reactions of cellulose gyclosyl units [32].

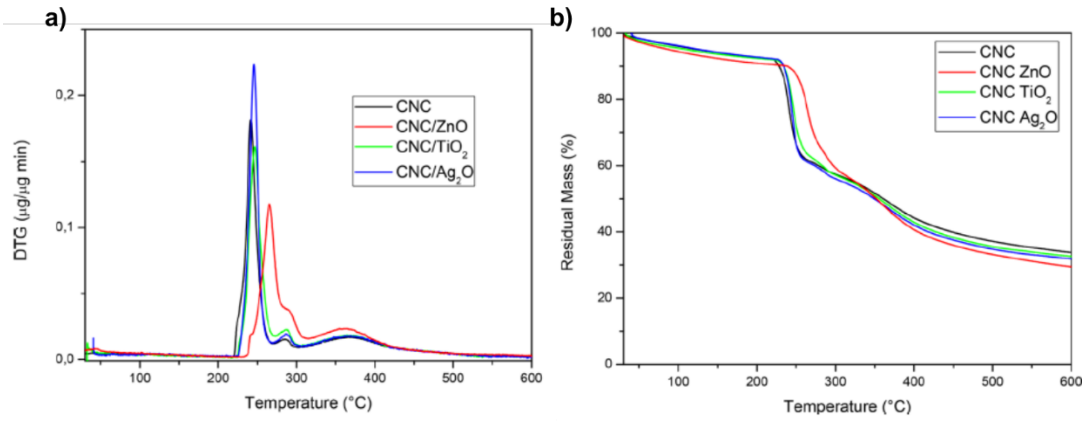


**Figure 52** (a) TGA and (b) weight loss curves of CNC and CNC nanocomposites.

As with many inorganic materials, all the used metal particles are highly stable upon increasing temperature and they do not display any weight loss in the 25-600 °C range. In this specific case, $TiO_2$ and $Ag_2O$ nanoparticles maintain the thermal stability of CNC whereas ZnO nanoparticles are able to increase the main degradation peak of respect to raw CNC film as previously reported [33]. The residual mass of the samples is higher than 30 % at 600 °C. All CNC nanohybrids samples show similar value of the residual mass.

*3.2.3.3. Microstructure and Transparency*

Cross-section SEM micrographs shown in **Figure 53** reveal that for all the studied systems, spindle-like CNC form a closely packed network, which is arranged in a layered structure, indicating that the incorporation of ZnO, $TiO_2$, and $Ag_2O$, does not substantially modify the original long-range structure of CNC [29,34]. A layered structure of physically entangled cellulose nanocrystals was first reported in the 1990s by Revol and co-workers, who showed that the evaporation-induced self-assembly (EISA) of CNC yields a stable chiral nematic structure [35].

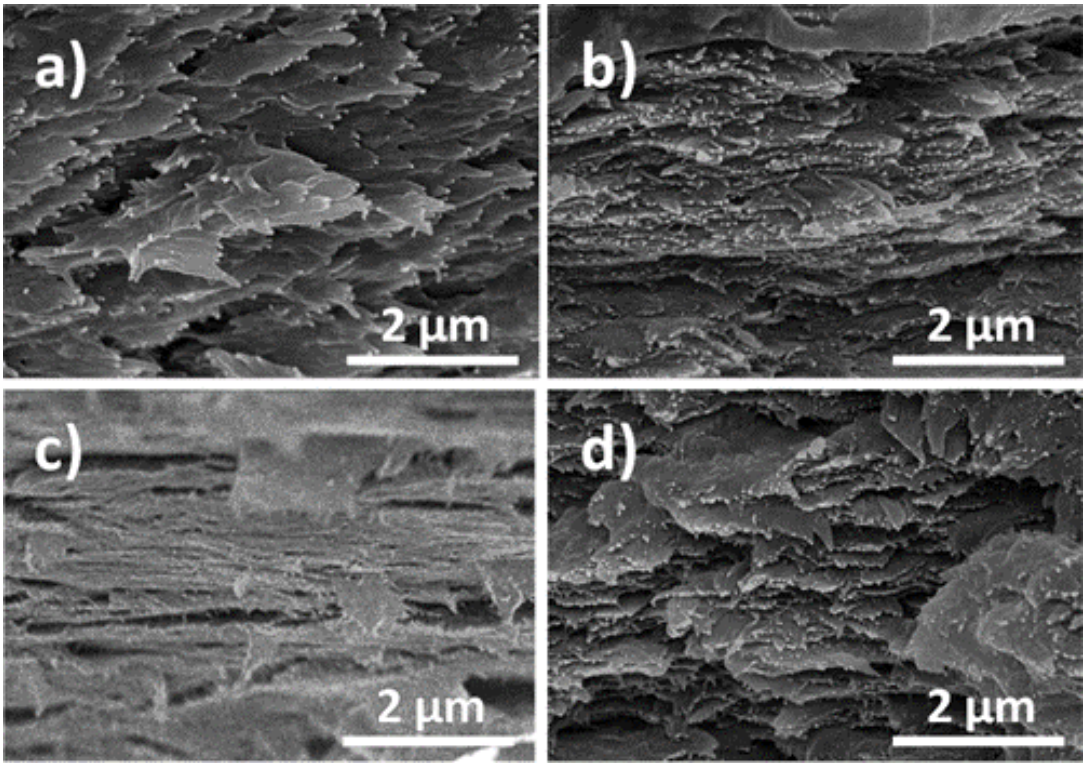


**Figure 53** SEM cross-section images of (a) CNC, (b) CNC/ZnO, (c) CNC/$TiO_2$, and (d) CNC/$Ag_2O$ films.

According to Bragg's law, when the helical pitch of these layered materials is on the order of the wavelength of visible light, the obtained films show brilliant iridescent colors [36]. Conversely, if the helical pitch (measured as the periodic distance between adjacent layers) falls out of the 400−800 nm range, the resulting film may reflect light in the ultraviolet (UV) or infrared region, yielding optically transparent films. Since the nanocomposite films here fabricated showed a helical pitch of about 200−230 nm as indicated by the maximum of the UV−vis reflectance peak for neat CNC film and high-magnification SEM images, synthesized CNC based films should present high optical transmittances in the visible region, yielding therefore transparent films. Additionally, no sign of aggregated ZnO, $TiO_2$, and $Ag_2O$ nanoparticles could be observed, suggesting that they remain uniformly distributed through the nanocomposite films thanks to the electrostatic repulsion

forces of CNC when dispersed in water. These forces allow obtaining more homogeneous nanocomposites than those obtained through hard-templating methods, for example, because during the coassembly of CNC with nanoparticles, the latter remain well-distributed in solution at the molecular level [36]. These interactions allow obtaining homogeneous cellulose based nanocomposites without using complex functionalization steps which involve the use of surfactants (phosphate esters, nonylphenol, sorbitan monostearate) [31,37].

According to UV−vis spectroscopy shown in **Figure 54**, the optical properties of the nanocomposite films are markedly modified after the addition of metallic nanoparticles. The presence of 1 wt % of nanoparticles drastically decreases transmitted UV light (measured at 300 nm) from 19% for neat CNC to roughly 0% for nanocomposites [9].The strong UV absorption of nanocomposite films is produced by the structure of reinforcing nanoparticles which present a filled valence band and an empty conduction band [38]. Moreover, while raw CNC film presents an optical transparency (determined according to the ASTM D1746−03 standard) of ~41%, the transmittance in the 540−560 nm regions falls to 22 and 20 % for CNC/ZnO and CNC/$TiO_2$ films, respectively, while CNC/$Ag_2O$ film does not allow light to pass through in the whole UV and visible region (from 200 to 800 nm). A small reflectance peak located at 208 nm is noticed for neat CNC film. According to SEM investigations, this peak arises from the chiral structure of the films and it is not observed for reinforced films because the strong absorption of NPs in the UV region overlaps this peak [27]. The small helical pitch of few nanometers yields this reflectance peak within the UV-region in contrast to the iridescent CNC films developed by MacLachlan group, which showed an intense absorption peak in the visible region [39−42].

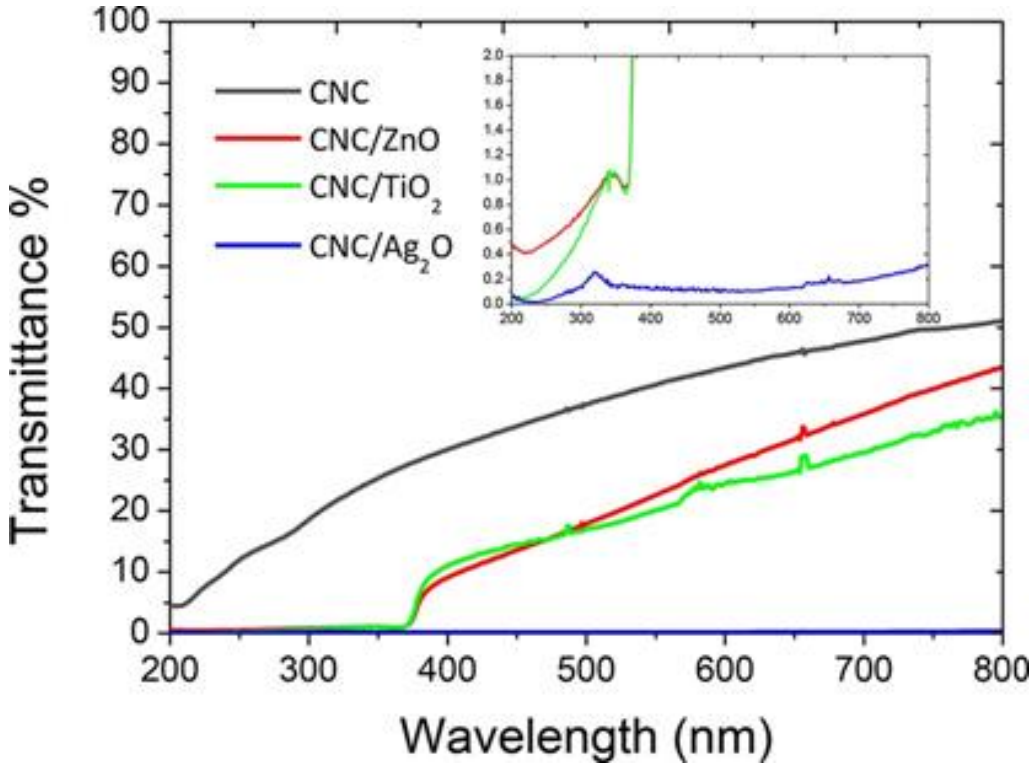


**Figure 54** UV−vis transmittance spectra of CNC-based films. The insert displays an enlarged view in the 0−2% transmittance region of the CNC-based films.

*3.2.3.4. Wettability*

Surface hydrophobicity is an important parameter to take into account when exploring the material biomedical applications; furthermore, the composting behavior of materials can be also affected by the wettability properties because it may be expected that highly hydrophobic materials should present enhanced resistance against the diffusion of water through the film, which in turn may delay the degradation of CNC films during the composting process. This is of special interest in the case of cellulosic materials because of the hydrophilic nature of cellulose thanks to the presence of −OH groups in the basic cellulose unit (C6H10O5) [43]. In this regard, **Figure 55** shows the dynamics of water contact angle (WCA) after droplet deposition. Contact angle values were determined by analysing consecutively recorded photos over a period of 450 s. For the sake of

clarity, representative images of a water drop at the surface of each film are as well provided. Overall, WCA is continuously decreased due to water absorption by the CNC [44]. The WCA of neat CNC at time 0 is measured to be 94°, while this value is slightly decreased to 83° and 87° for CNC/$TiO_2$ and CNC/$Ag_2O$ nanocomposites. On the contrary, surface hydrophobicity of the films is markedly increased to yield a WCA of 114° after the addition of 1 wt % of ZnO as previously reported values for PLLA-based materials [13]. A careful analysis of the WCA dynamics reveals a single stage of water spreading as indicated by the linear decrease of WCA values over the studied time frame. Once water is deposited onto the cellulosic film, it is adsorbed by the CNC network [45]. Besides of the initial WCA value which depends on the surface hydrophobicity of nanocomposite films, the adsorption dynamics are also affected by the presence of nanoparticles. The slope of WCA change has been calculated to be −0.12° $s^{-1}$ for neat CNC film, while it is decreased up to −0.08° $s^{-1}$ for CNC/$TiO_2$ film, indicating that the water adsorption of CNC films is reduced upon nanoparticle addition. We expect that these hydrophobicity differences may yield CNC films with distinctive sensitivities to compost degradation.

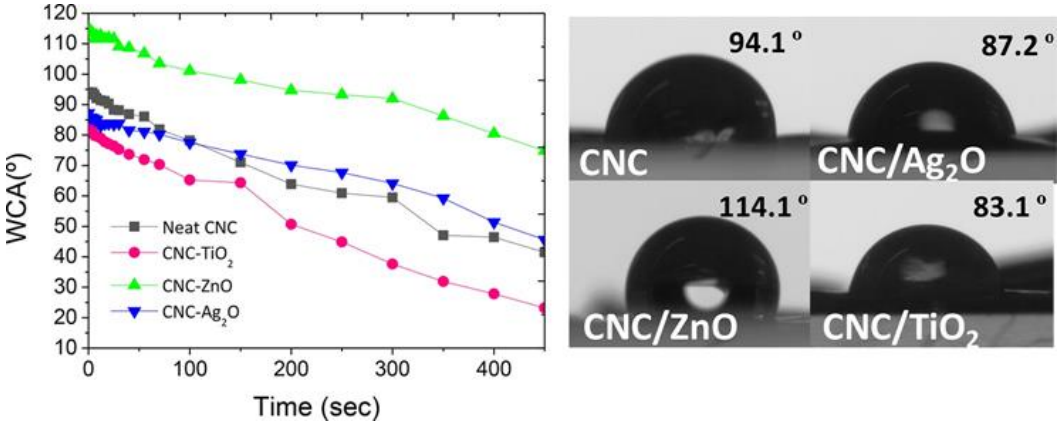


**Figure 55**. WCA dynamics for CNC-based films. Representative images of a water drop at the surface of each film are provided.

*3.2.3.5. Antibacterial Property of CNC-Based Films.*

To investigate if the incorporation of oxide metal nanoparticles in CNC samples could exert antimicrobial activity, CNC-based films were tested against E. coli RB and S. aureus 8325−4 at both 3 h and 24 h, respectively (**Figure 56**). In particular, the antibacterial activity was evaluated both on the planktonic bacteria after being in contact with the CNC-based films or on the bacterial cells adherent to the surfaces. Differences in surviving fractions were observed based on the bacterial strains, the planktonic or adherent cells, and the incubation times.

At short incubation time (3 h), the surviving fraction of E. coli cells adherent to the surfaces showed a significant reduction on CNC/$Ag_2O$ ($p < 0,0001$) followed by CNC/ZnO ($p < 0,0001$) and, at a lesser extent, on CNC/$TiO_2$ (**Figure 56A**). A similar trend was observed for the planktonic cells after being in contact with CNC-based films. Interestingly, at longer incubation time (24 h), the bacterial reduction for both planktonic and adherent cells showed the trend previously observed at 3 h and, in comparison to CNC, it was more noteworthy but for all the CNC-based films (**Figure 56B**).

After 3 h of incubation, the surviving fraction of S. aureus cells adherent to CNC-based films was significantly diminished on CNC/$Ag_2O$ ($p < 0,0001$), followed by CNC/$TiO_2$ ($p < 0,0001$) and CNC/ZnO ($p < 0,0001$) (**Figure 56C**). The trend was completely different for the staphylococcal cells after being in contact with CNC-based films: no significant reduction following incubation with CNC/$TiO_2$ was observed, whereas an important decrement in cell survivability ($p < 0,0001$) for both CNC/$Ag_2O$ and CNC/ZnO was detected, even if it was less noteworthy for the ZnO nanoparticles embedded in CNC film. At 24 h, the surviving fraction of the adherent cells was significantly reduced for all types of CNC- based films ($p <$

0,0001) but for the planktonic cells the results were different, being important only for CNC/$Ag_2O$ ($p < 0,05$) and CNC/$TiO_2$ ($p < 0,005$) (**Figure 56D**).

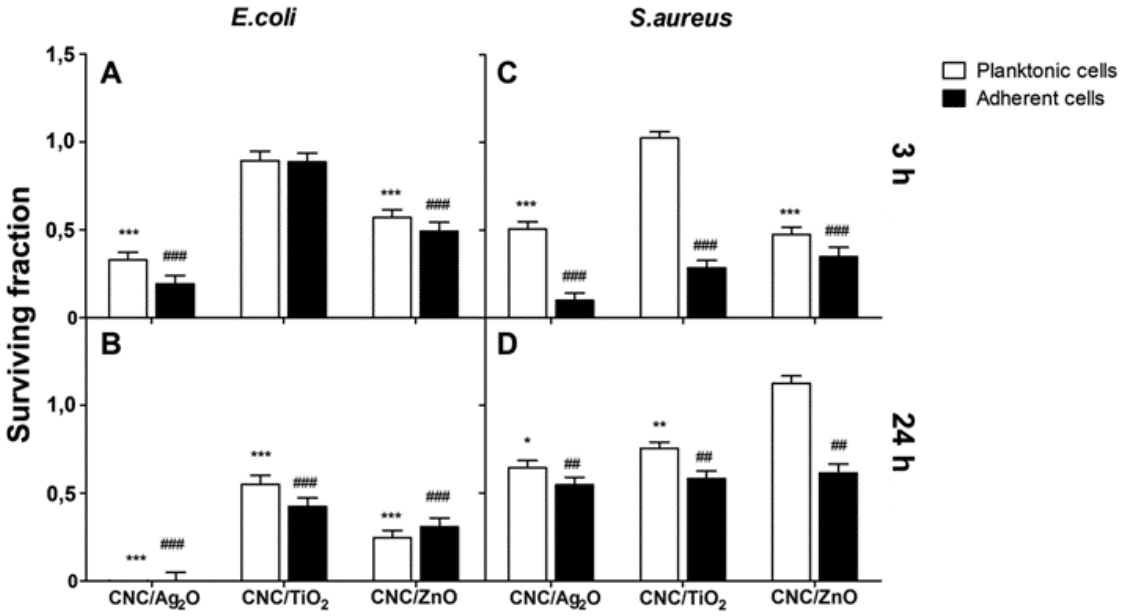


**Figure 56.** Antimicrobial activity was performed on neat CNC and CNC-based films incubated with (A, B) E. coli and (C, D) S. aureus cells at 37 °C for (A, C) 3 h and (B, D) 24 h, respectively. At the indicated time points, MTT test was performed on both bacteria having being in contact with each surfaces (planktonic) or on those adherents to the CNC-based films to determine the surviving fraction. Results were normalized with TCP and expressed as ratio between bacteria either planktonic or adherent on CNC-based films and those on neat CNC. Bars indicate mean and SEM of three different experiments. Statistical analysis was performed against neat CNC film (∗ for Planktonic cells, # for adherent cells) (∗, # $p < 0,05$; ∗∗, ## $p < 0,01$; ∗∗∗, ### $p < 0,001$).

The antimicrobial efficacy of $Ag_2O$ nanoparticles against E. coli [46] and methicillin resistant S. aureus was already demonstrated [47]. Similarly, ZnO nanoparticles showed an antibacterial activity against both Gram-positive and Gram-negative bacteria [48−50] In our experimental conditions, the direct exposition of E. coli cells to CNC-based films containing $Ag_2O$ or ZnO nanoparticles seems to be effective either at shorter and longer incubation times on both adherent and planktonic cells (with the trend $Ag_2O$ > ZnO). The antimicrobial effect exerted by both CNC/$Ag_2O$

and CNC/ZnO is still visible on S. aureus cells even if it is more significant on adherent cells at 3 h in comparison to 24 h. The effect of both types of CNC-based films resulted less important for planktonic staphylococcal cells at either 3 or 24 h.

The effect is different when treating bacterial cells with CNC/$TiO_2$: the antibacterial effect is more evident at longer incubation times for adherent E. coli cells and viceversa for S. aureus cells. Numerous bacteria were shown to be successfully killed by $TiO_2$ nanoparticles [51]. Interestingly, both types of cells after being in contact with CNC/$TiO_2$ showed higher survivability suggesting the importance of the direct contact for antibacterial activity. So far, metal nanoparticles and oxide metal nanoparticles have been demonstrated to show antibacterial effects, but the exact mechanism of their action is still being under investigation.

In this regard, the mechanisms of nanomaterials against bacteria depend on different parameters: surface charge, shape, and type of the metal nanomaterial, its concentration, dispersion and contact to the bacterial cell, presence of active oxygen (ROS), liberation of antimicrobial ions, medium components and pH, physicochemical properties, specific surface-area-to-volume ratios, size, role of growth rate/biofilm formation, bacterial cell wall properties, and effect of UV illumination [49,51].

Beside all of this, our results undoubtedly seem to confirm that the incorporation of the tested types of nanoparticles in CNC films provide an effective antibacterial activity.

Furthermore, to visualize the morphology of bacterial cells adherent to CNC-based films, SEM studies were carried out (**Figure 57**). In general, the morphology of both type of bacterial cells was not modified following the direct contact with CNC-based films as documented by SEM observation at higher magnification (all the insets of **Figure 57)** and comparative analysis with the control. As expected, at 24

h the surfaces of the control and CNC films appeared completely covered by both types of bacterial cells, whereas at 3 h the number of adherent cells was less important (**Figure 57A,B**). Again, the CNC/$Ag_2O$ film showed the lower number of adherent cells for both type of bacterial cells at both 3 h and 24 h, followed by CNC/ZnO and CNC/$TiO_2$.

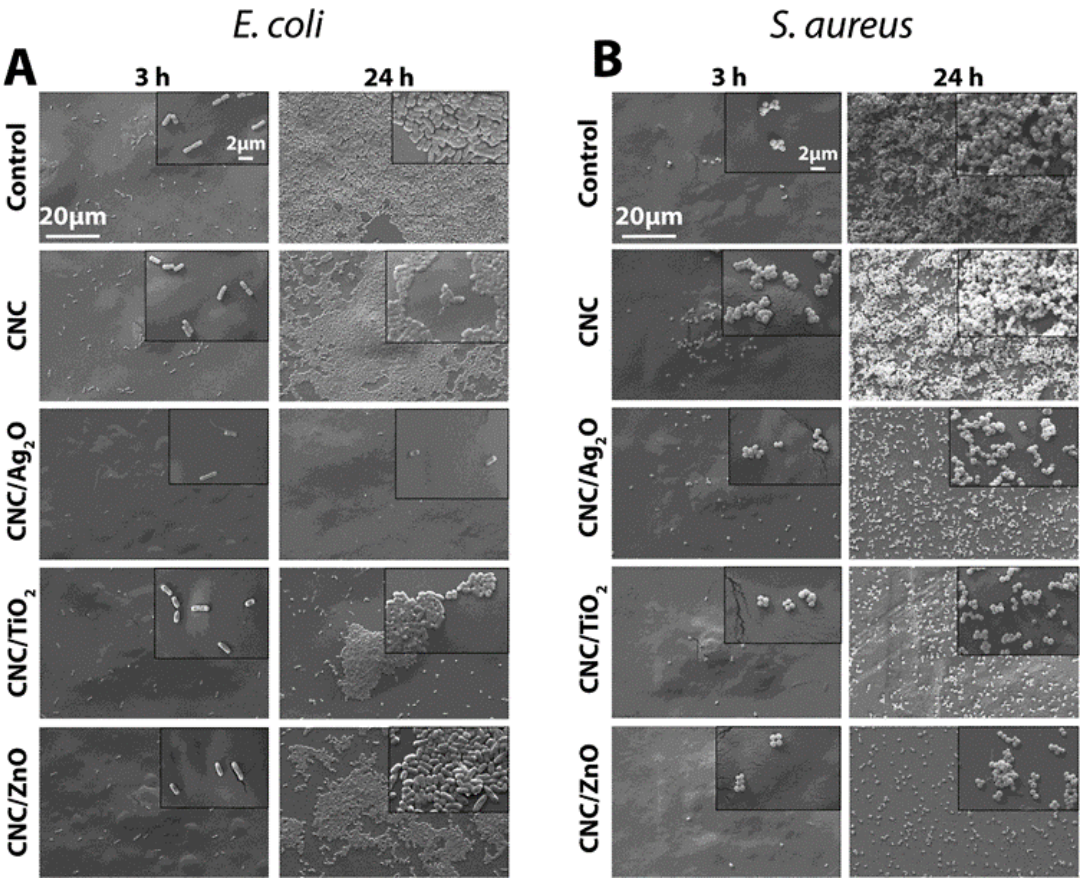


**Figure 57**. Representative SEM images of adherent (A) E. coli and (B) S. aureus cells on thermanox (Ctrl), CNC, and CNC-based films incubated at 37 °C for 3 h and 24 h, respectively. Samples for SEM observations were prepared as indicated in Materials and Methods section. Magnifications: 3000× (panel) and 10 000× (insert). Scale bar: 20 µm in all panels and 2 µm in all inserts.

According to these results and the strong need to mitigate bacterial colonization by equipping the surfaces of biomedical devices and implants with features such as surface chemistry and surface roughness that are unfavourable for bacterial

attachment, we suggest the developed materials for biomedical applications, where antibacterial performance is required, as wound healing. The problem of infections related to biomedical devices and implants continues even if considerable research and development efforts have been performed. The surfaces of synthetic materials, such as those used for the fabrication of catheters, hip and knee implants, and many other devices are unfortunately readably colonized by bacteria.

*3.2.3.6. Disintegrability in Composting Conditions*

**Figure 58** shows the visual observation (**Figure 58a**) and the disintegrability values (**Figure 58b**) of CNC, CNC/ZnO, CNC/$TiO_2$, and CNC/$Ag_2O$ samples taken out at different times of composting (obtained for comparison of initial weights at time 0 and final weights of the sample at the different composting times).

a)

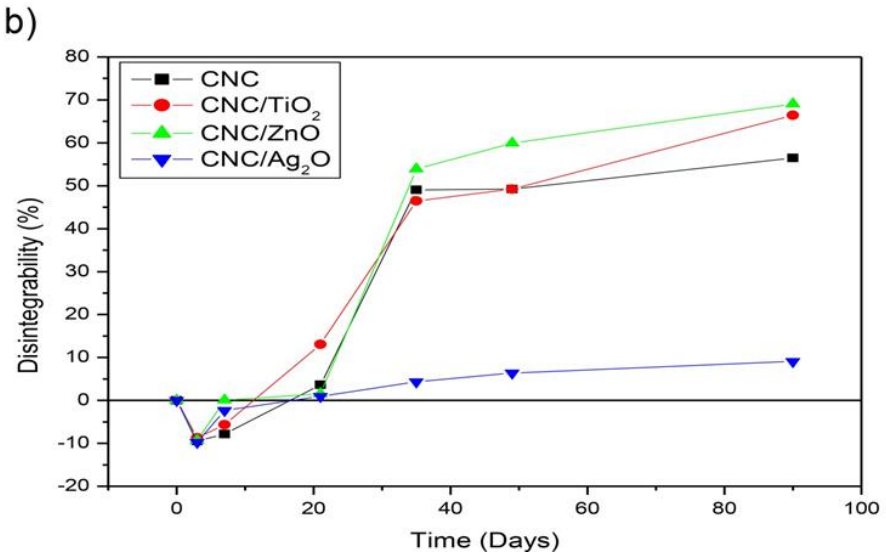


**Figure 58**. (a) Visual observation and (b) disintegrability values of CNC, CNC/$TiO_2$, CNC/$Ag_2O$, and CNC/ZnO samples before and after different days in composting conditions.

Observing the different formulation during the first day of incubation and until 7 days (Figure 8a), no particular alterations were detected with the exception of neat CNC film that was characterized by a browning and a deformation of the surface more evident after the seventh day in composting conditions. Moreover, the dynamics of weight loss for all CNC based films were similar to the neat CNC sample in the first part of the degradation process. Initially (after 3 days), for all the materials studied, there is an increment of the mass that is visible in Figure 8b as a negative weight loss, that continued, for all formulations, until 3 weeks. This effect is due to the swelling behavior of the CNC based material in humid conditions. However, opacity properties, that indicated changes of the refractive index and due to water absorption and hydrolytic degradation phenomena, started after 21 days in composting conditions [52,53]. for all the studied formulations. Moreover, at the 21st day, fragmentation phenomena started especially for CNC/ZnO films, whereas more evident fragmentation processes characterized all the studied film after 35 days in composting conditions. The results were also confirmed by the

weight loss behavior since all the formulations, with the exception of CNC/$Ag_2O$ film, reached about 50% of disintegration in 35 days. The lower disintegration rate obtained for CNC/$Ag_2O$ that reached at least a 10% of disintegration after 90 days of incubation (90 days represents the time-limit imposed by the ISO 20200 during which the samples need to reach 90 % of disintegration to be considered compostable in a degradation soil) was attributed to the presence of silver nanoparticles that could be able to slow and inhibit the microorganism attack due to the well know antimicrobial properties of silver. After 90 days in composting, the degradation proceeded reaching a 70% for CNC/$TiO_2$ and CNC/ZnO and a 60% for CNC neat film. However, although quite high levels of disintegration were reached for these three formulations, not one of the produced film reached the 90% of the disintegration representing the limit imposed by the ISO 20200. This may be due to the high crystalline structure that usually characterized CNC and so, as consequence, CNC based film, able to inhibit the diffusion phenomena and to slow the disintegration process [54].

The behavior of the main degradation peaks of the different formulations obtained by the TGA thermograms are reported in **Table 3**.

**Table 3** Main Degradation Temperatures for CNC, CNC/ $TiO_2$, CNC/$Ag_2O$, and CNC/ZnO Samples before and after different days in composting conditions

| Samples | $T_{dmax}$ (°C) | | | | | | |
|---|---|---|---|---|---|---|---|
| | **0 days** | **3 days** | **7 days** | **21 days** | **35 days** | **49 days** | **90 days** |
| **CNC** | 242 | 261 | 293 | 228 | 298 | 293 | 280 |
| **CNC/$TiO_2$** | 246 | 290 | 289 | 278 | 300 | 317 | 331 |
| **CNC/ZnO** | 264 | 302 | 244 | 229 | 314 | 324 | 323 |
| **CNC/$Ag_2O$** | 246 | 282 | 276 | 225 | 281 | 278 | 269 |

An increase of the maximum degradation temperatures with the incubation times was registered for all the studied formulations until 7 days confirming previous results and due to the absorption phenomena. On the contrary, a reduction of the Td max was registered at 21 days of incubation in composting soil that represents the kinetic inversion for the studied films and that corresponds also to the beginning of the compost maturation [55]. At this time, in fact, the samples started to change their appearance as previously discussed and some fragmentation phenomena occurred justified by this reduction in thermal stability. However, with the increase of the incubation times, all the tested samples showed an increase in the main degradation temperatures due to probably the formation a strong interaction between the OH group (probably induced by the absorption phenomena) that requires more energy to start the thermal degradation process [56].

The changes in the chemical composition of the CNC based films during disintegration in compositing conditions were explored also by using FTIR. **Figure 59a** and **59b** show the infrared spectra of CNC and CNC/Ag films at different incubation times, whereas Figure 9c shows the comparison of all the studied materials after 90 days in contact with the incubation soil, in the 4000−600 $cm^{-1}$ wavenumber range. The decreasing of signal for the band, between 1000 and 1200 $cm^{-1}$, was evident in the CNC infrared spectra acquired during degradation in composting conditions due to the decomposition processes of organic components and that can be used to evaluate the composting processes. Meanwhile, the formation of two peaks at 1540 and 1640 $cm^{-1}$ after 7 days of incubation was observed, due to the amide I and II, respectively.

Furthermore, the increase in the intensity of these amide bands is evident and it is followed to a consequently decrease in the main cellulose band in the 1000−1200 $cm^{-1}$ wavenumber region.

The FTIR results do not show any significant spectra differences between the four materials tested after 90 days of incubation. **Figure 59c** shows a comparison of all samples at the end of disintegration experiments.

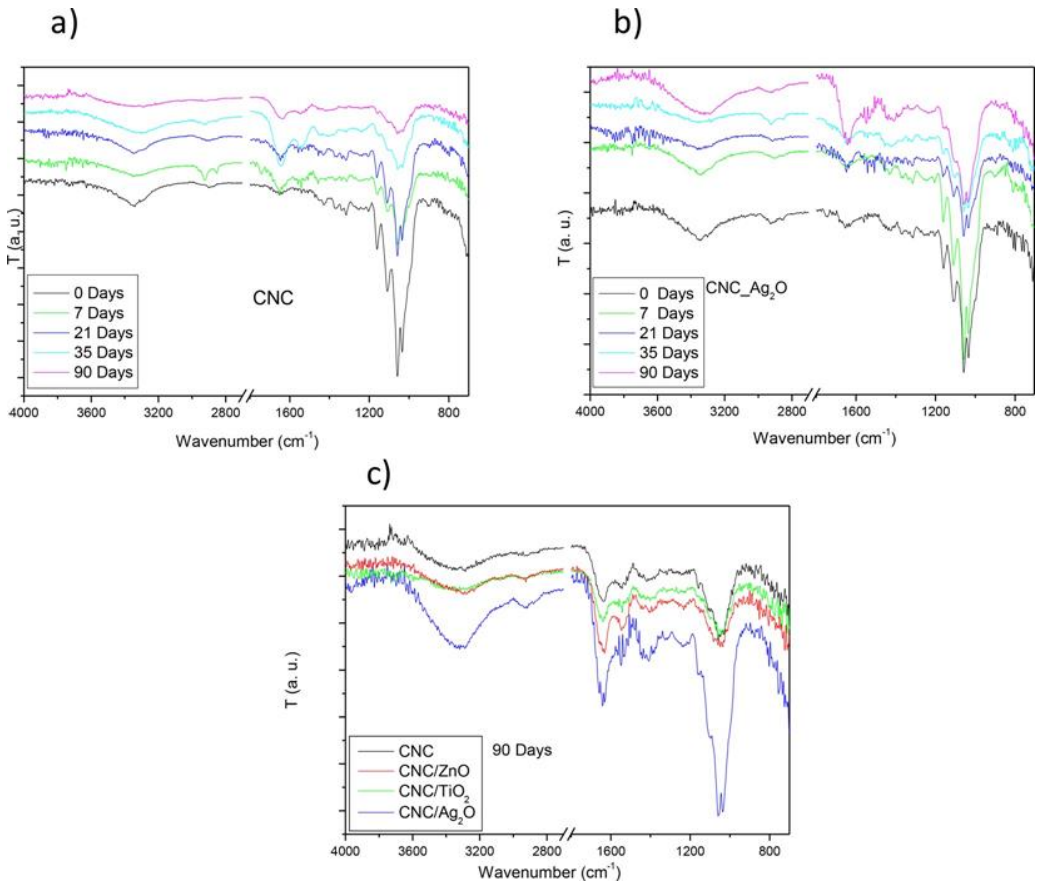


**Figure 59** Infrared spectra of (a) CNC and (b) CNC/Ag films at different incubation time and CNC nanocomposites compared to (c) CNC films after 90 days of incubation in composting conditions, in the 4000−600 cm−1 wavenumber range.

After 90 days of incubation, the intensity of the band of cellulose shows similar level than the new peak in the amide region due to decomposition process. By the analysis of the peaks, it is evident that the nanocomposites with silver nanoparticles show the most stable behavior since the peak in the C−O due to CNC is the most intense. This can be due to the antibacterial effect of the silver ions that can also affect the kinetic process of the disintegration in composting

conditions, as previously said. The chemistry of the nanoparticles strongly affects disintegration performance, but other environmental and nanostructural factors must be considered: the dimension, the shape, the geometry of the nanoparticles will impact the dispersion in the CNC film, which affect the rate of water penetration, as well the disintegration process in composting conditions. We think that the obtained remarkable disintegration window of 10−70 % after 90 days for nanocomposites having only 1 wt % of nanoparticle opens new possibilities for the easy-tuning of cellulose disintegration. Furthermore, parallel approaches can be followed to decrease the time to reach the required disintegration performance, working both on cellulose nanocrystals than nanoparticles. Some studies in fact have been shown that the inoculation of specific microorganisms, at different phases of composting, such as bacteria and fungi, improved cellulase activities, accelerated the biodegradation of cellulose during composting process [57].

## 3.2.4. Conclusions

In the present study, we have demonstrated that CNC can be used to finely disperse functional nanoparticles to successfully develop nanocomposite films with antibacterial performance with ZnO, $TiO_2$, or $Ag_2O$ nanoparticles by a simple and cost-effective approach. The results of the present work show that the chemistry, composition, the shape, and the dimension of the nanoparticles introduced in CNC films at a fixed concentration affect the film appearance, microstructure, and optical properties, including thermal stability, with the nanocomposite films that exhibit the properties of both components.

This study shows the different efficacy of the tested metal oxide nanoparticles incorporated in CNC-based films against both E. coli and S. aureus strains, performed on adherent or planktonic cells after being in contact with the materials surfaces. In

general, the effect was more evident on adherent E. coli at both 3 h and 24 h in comparison to S. aureus cells. CNC/ $Ag_2O$ films showed the best antibacterial activity in comparison to CNC/ZnO and CNC/$TiO_2$ films either at shorter and longer incubation time on E. coli cells.

## References

[1] Campoccia D., Montanaro, L., Arciola C.R.A. 2013. Review of the biomaterials technologies for infection-resistant surfaces. Biomaterials, 34, 8533-8554.

[2] Anselme K., Davidson P., Popa A.M., Giazzon M., Liley M., Ploux L. 2010. The interaction of cells and bacteria with surfaces structured at the nanometer scale. Acta Biomater., 6, 3824-3846.

[3] Fortunati E., Mattioli S., Visai L., Imbriani M., Fierro J.L.F., Kenny J. M., Armentano I. 2013. Combined Effects of Ag Nanoparticles and Oxygen Plasma Treatment on PLGA Morphological, Chemical, and Antibacterial Properties. Biomacromolecules, 14, 626−636.

[4] Domingues R.M.A., Gomes M.E., Reis R.L. 2014. The Potential of Cellulose Nanocrystals in Tissue Engineering Strategies. Biomacromolecules, 15, 2327−2346.

[5] Grishkewich N., Mohammed N., Tang J., Tam K.C. 2017. Recent advances in the application of cellulose nanocrystals. Curr. Opin. Colloid Interface Sci., 29, 32−45.

[6] Foresti M.L., Vaźquez A., Boury B. 2017. Applications of bacterial cellulose as precursor of carbon and composites with metal oxide, metal sulfide and metal nanoparticles: A review of recent advances. Carbohydr. Polym., 157, 447−467.

[7] Dufresne A. 2013 Nanocellulose: A new ageless bionanomaterial. Mater. Today, 16, 220−227.

[8] Fortunati E., Armentano I., Zhou Q., Iannoni A., Saino E., Visai L., Kenny J.M., Berglund L. A. 2012. Multifunctional bionano- composite films of poly(lactic acid), cellulose nanocrystals and silver nanoparticles. Carbohydr. Polym., 87, 1596−1605.

[9] Lizundia E., Urruchi A., Vilas J.L., Leoń L.M. 2016. Increased functional properties and thermal stability of flexible cellulose nanocrystal/ZnO films. Carbohydr. Polym., 136, 250−258.

[10] Habibi Y., Lucia L A., Rojas O. J. 2010. Cellulose nanocrystals: Chemistry, self-assembly, and applications. Chem. Rev.,110, 3479-3500.

[11] Larranaga A., Ramos D., Amestoy H., Zuza E., Sarasua J. R. 2015. Coating of bioactive glass particles with mussel-inspired polydopamine as a strategy to improve the thermal stability of poly(l-lactide)/ bioactive glass composites. RSC Adv., 5, 65618−65626.

[12] Larrañaga A., Diamanti E., Rubio E., Palomares T., Alonso-Varona A., Aldazabal P., Martin F.J., Sarasua J.R. 2014. A study of the mechanical properties and cytocompatibility of lactide and caprolac- tone based scaffolds filled with inorganic bioactive particles. Mater. Sci. Eng., C , 42, 451−460.

[13] Lizundia E., Ruiz-Rubio L., Vilas J.L., Leoń L.M. 2016. Towards the development of eco-friendly disposable polymers: ZnO-initiated thermal and hydrolytic degradation in Poly (L- lactide)/ZnO nanocomposites. RSC Adv., 6, 15660−15669.

[14] Arrieta M.P., Fortunati E., Dominici F., Lopez J., Kenny J.M. 2015. Bionanocomposite films based on plasticized PLA-PHB/cellulose nanocrystal blends. Carbohydr. Polym., 121, 265−275.

[15] Rinaldi S., Fortunati E., Taddei M., Kenny J.M., Armentano I., Latterini L. 2013. Integrated PLGA-Ag nanocomposite systems to control the degradation rate and antibacterial properties. J. Appl. Polym. Sci., 130, 1185-1193.

[16] Tang Y., Hu X., Zhang X., Guo D., Zhang J., Kong F. 2016. Chitosan/titanium dioxide nanocomposite coatings: Rheological behavior and surface application to cellulosic paper. Carbohydr. Polym., 151, 752−759.

[17] Varaprasad K., Raghavendra G.M., Jayaramudu T., Seo J. 2016. Nano zinc oxide-sodium alginate antibacterial cellulose fibres. Carbohydr. Polym.,135, 349−355.

[18] Dallas P., Sharma V. K., Zboril R. 2011. Silver polymeric nanocomposites as advanced antimicrobial agents: Classification, synthetic paths, applications, and perspectives. Adv. Colloid Interface Sci., 166, 119−135.

[19] Panyala N.R., Pena-Mendez E.M., Havel J. 2009. Gold and nano- gold in medicine: Overview, toxicology and perspectives. J. Appl. Biomed., 7, 75−91.

[20] Gardner D.J., Oporto G.S., Mills R., Azizi Samir M.A.S. 2008. Adhesion and surface issues in cellulose and nanocellulose. J. Adhes. Sci. Technol., 22, 545−567.

[21] Gunalan S., Sivaraj R., Rajendran V. 2012. Green synthesized ZnO nanoparticles against bacterial and fungal pathogens. Prog. Nat. Sci., 22, 693−700.

[22] Ambika S., Sundrarajan M. 2015. Antibacterial behaviour of Vitex negundo extract assisted ZnO nanoparticles against pathogenic bacteria. J. Photochem. Photobiol., B, 146, 52−57.

[23] Lukach A., Theŕien-Aubin H., Querejeta-Fernańdez A., Pitch N. Chauve G., Meťhot M., Bouchard J., Kumacheva E. 2015. Coassembly of Gold Nanoparticles and Cellulose Nanocrystals in Composite Films. Langmuir, 31, 5033−5041.

[24] Ifuku S., Tsuji M., Morimoto M., Saimoto H., Yano H. 2009. Synthesis of silver nanoparticles templated by TEMPO-mediated oxidized bacterial cellulose nanofibers. Biomacromolecules, 10, 2714−2717.

[25] Lizundia E., Meaurio E., Vilas J.L. 2016. Grafting of Cellulose Nanocrystals. Multifunctional Polymeric Nanocomposites Based on Cellulosic Reinforcements, 61-113.

[26] Zhang W., Liang Y., Luo, W., Fang Y. 2003. Effects of clay-modifying agents on the morphology and properties of poly(methyl methacrylate)/clay nanocomposites synthesized via X-ray irradiation polymerization. J. Polym. Sci., Part A: Polym. Chem., 41, 3218−3226.

[27] Lizundia E., Nguyen T.D., Vilas J.L., Hamad W.Y., MacLachlan M.J. 2017. Chiroptical luminescent nanostructured cellulose films. Mater. Chem. Front.,1, 979−987.

[28] Lizundia E., Vilas J.L., Leoń L.M. 2015. Crystallization, structural relaxation and thermal degradation in Poly(l-lactide)/cellulose nano- crystal renewable nanocomposites. Carbohydr. Polym., 123, 256−265.

[29] Yalcinkaya E.E., Puglia D., Fortunati E., Bertoglio F., Bruni G., Visai L., Kenny J. M. 2017. Cellulose nanocrystals as templates for cetyltrimethylammonium bromide mediated synthesis of Ag nano- particles and their novel use in PLA films. Carbohydr. Polym., 157, 1557−1567.

[30] Bari A., Bloise N., Fiorilli S., Novajra G., Vallet-Regí M., Bruni G., Torres-Pardo A., Gonzaĺez-Calbet J. M., Visai L., Vitale- Brovarone C. 2017. Copper-containing mesoporous bioactive glass nano- particles as multifunctional agent for bone regeneration. Acta Biomater., 55, 493−504.

[31] Fortunati E., Mattioli S., Armentano I., Kenny J.M. 2014. Spin coated cellulose nanocrystal/silver nanoparticle films. Carbohydr. Polym., 113, 394−402.

[32] Roman M., Winter W. T. 2004. Effect of sulfate groups from sulfuric acidhydrolysis on the thermal degradation behaviour of bacterial cellulose. Biomacromolecules, 5, 1671-1677.

[33] Goikuria U., Larrañaga A., Vilas, J.L., Lizundia E. 2017. Thermal stability increase in metallic nanoparticles-loaded cellulose nanocrystal nanocomposites. Carbohydr. Polym., 171, 193−201.

[34] Revol J.F., Bradford H., Giasson J., Marchessault R.H., Gray, D. G. 1992. Helicoidal self-ordering of cellulose microfibrils in aqueous suspension. Int. J. Biol. Macromol., 14, 170−172.

[35] Kelly J. A., Giese M., Shopsowitz K.E., Hamad W.Y., MacLachlan M.J. 2014. The development of chiral nematic mesoporous materials. Acc. Chem. Res., 47, 1088−1096.

[36] Xu J., Nguyen T.D., Xie K., Hamad W.Y., MacLachlan M.J. 2015. Chiral nematic porous germania and germanium/carbon films. Nanoscale, 7, 13215−13223.

[37] Kim J., Montero G., Habibi Y., Hinestroza J.P., Genzer J., Argyropoulos D.S., Rojas O. J. 2009. Dispersion of cellulose crystallites by nonionic surfactants in a hydrophobic polymer matrix. Polym. Eng. Sci., 49, 2054−2061.

[38] Kubacka A., Fernańdez-García M., Coloń G. 2012. Advanced nanoarchitectures for solar photocatalytic applications. Chem. Rev., 112, 1555−1614.

[39] Giese M., Blusch L.K., Khan M.K., MacLachlan M.J. 2015. Functional materials from cellulose-derived liquid-crystal templates. Angew. Chem., Int. Ed., 54, 2888−910.

[40] Schlesinger M., Hamad W.Y., Maclachlan M. J. 2015. Optically tunable chiral nematic mesoporous cellulose films. Soft Matter, 11, 4686−4694.

[41] Shopsowitz K. E., Qi H., Hamad W.Y., Maclachlan M.J. 2010. Free-standing mesoporous silica films with tunable chiral nematic structures. Nature, 468, 422−425.

[42] Silvestre C., Duraccio D., Cimmino S. 2011. Food packaging based on polymer nanomaterials. Prog. Polym. Sci., 36, 1766−1782.

[43] Khwaldia K., Arab-Tehrany E., Desobry S. 2010. Biopolymer Coatings on Paper Packaging Materials. Compr. Rev. Food Sci. Food Saf., 9, 82−91.

[44] Gao Z., Zhai X., Liu F., Zhang M., Zang D., Wang C. 2015. Fabrication of $TiO_2$/EP super-hydrophobic thin film on filter paper surface. Carbohydr. Polym., 128, 24−31.

[45] Tammelin T., Abburi R., Gestranius M., Laine C., SetaÏa¨H., Österberg M. 2015. Correlation between cellulose thin film supramolecular structures and interactions with water. Soft Matter, 11, 4273− 4282.

[46] Sondi I., Salopek-Sondi B. 2004. Silver nanoparticles as antimicrobial agent: a case study on E. coli as Amodel for Gram-negative bacteria. J. Colloid Interface Sci., 275, 177−182.

[47] Thiagarajan P., Sangappa M. 2015. Combating drug resistant pathogenic bacteria isolated from clinical infections, with silver oxide nanoparticles. Indian J. Pharm. Sci., 77, 151−155.

[48] Azam A., Ahmed A.S., Oves M., Khan M.S., Habib S.S., Memic A. 2012. Antimicrobial activity of metal oxide nanoparticles against Gram-positive and Gram-negative bacteria: a comparative study. Int. J. Nanomed., 7, 6003−6009.

[49] Dizaj S.M., Lotfipour F., Barzegar-Jalali M., Zarrintan M.H., Adibkia K. 2014. Antimicrobial activity of the metals and metal oxide nanoparticles. Mater. Sci. Eng., C, 44, 278−84.

[50] Emami-Karvani Z., Chehrazi P. 2012. Antibacterial activity of ZnO nanoparticle on Gram positive and gram-negative bacteria. Afr. J. Microbiol. Res., 5(12), 1368−1373.

[51] Hoseinzadeh E., Makhdoumi P., Taha P., Stelling J., Hossini H., Kamal M.A., Ashraf G. M. 2017. A review on nano-antimicrobials: metal nanoparticles, methods, and mechanisms. Curr. Drug Metab., 18, 120−128.

[52] Bitinis N., Fortunati E., Verdejo R., Bras J., Kenny J.M., Torre L., Loṕez-Manchado M.A. 2013. Poly(lactic acid)/natural rubber/cellulose nanocrystal bionanocomposites Part II. Properties evaluation. Carbohydr. Polym. 2013, 96(2), 611−620.

[53] Fukushima K., Tabuani D., Abbate C., Arena M., Ferreri L. 2010. Effect of sepiolite on the biodegradation of poly(lactic acid) and polycaprolactone. Polym. Degrad. Stab., 95, 2049−56.

[54] Fortunati E., Peltzer M., Armentano I., Torre L., Jimenez A., Kenny J.M. 2012. Effects of modified cellulose nanocrystals on the barrier and migration properties of PLA nano-biocomposites. Carbohydr. Polym., 90, 948−56.

[55] Luzi F., Fortunati E., Jimenez A., Puglia D., Pezzolla D., Gigliotti G., Kenny J. M., Chiralt A., Torre L. 2016. Production and characterization of PLA_PBS biodegradable blends reinforced with cellulose nanocrystals extracted from hemp fibres. Ind. Crops Prod., 93, 276−289.

[56] Luzi F., Fortunati E., Giovanale G., Mazzaglia A., Torre L.; Balestra G. M. 2017. Cellulose nanocrystals from Actinidia deliciosa pruning residues combined with carvacrol in PVA_CH films with antioxidant/antimicrobial properties for packaging applications. Int. J. Biol. Macromol., 104 (Part A), 43−55.

[57] Zhao Y., Zhao Y., Zhang Z., Wei Y., Wang H., Lu Q., Li Y., Wei Z. 2017. Effect of thermo-tolerant actinomycetes inoculation on cellulose degradation and the formation of humic substances during composting. Waste Manage., 68, 64−73.

# 3.3. Effect of metal-oxide nanoparticle presence and alginate cross-linking on cellulose nanocrystal-based aerogels

## 3.3.1. Introduction

Nowadays, the production of biodegradable materials based on natural resources is a growing area of interest, among other reasons due to the serious problem of waste accumulation and plastic contamination in oceans and seas [1]. Therefore, research around more sustainable materials, using more accessible resources or even recovered waste is significantly increasing.

Within biodegradable materials, natural origin polymers have special relevance and are being widely studied and used to develop new composites [2]. But apart from the relevancy of renewable polymers regarding to sustainability aspects, some materials are showing even more interesting properties in their nanometric size and highlighting an extraordinary potential forming new bionanocomposite structures for innovative applications [3-5].

In this sense, naturally available polymer-based materials such as nanocellulose have attracted great interest during the last years, owing to their low density, high specific surface, biodegradability, abundance, high functionalization possibilities and their vast applicability [6]. Nanostructured cellulose can be found as nanofibrillated cellulose (NFC) bacterial cellulose (BC) and cellulose nanocrystal (CNC) [7]. Among the cellulosic materials, rod-like CNC present interesting properties, including high mechanical stiffness, low density, good biocompatibility, low cost and large possibilities for chemical modification [8-9].

Even if CNC have been used like reinforcement material for a while [10-12] they are also showing promising attributes as matrix for new nanocomposites [13].

Nevertheless, the improvement of relevant functional properties of CNC like mechanical resistance, stability against moisture or thermal stability are required to successfully replace conventional polymer, biopolymers or even other nanocellulose derivates in several industrial applications. Fortunately, the high functionalization possibilities of CNCs [14] allow numerous alternatives to obtain CNC-based functional templates. The high-capacity of CNC to be superficially tuned or even combined with other materials like polymers, inorganic nanoparticles or carbon allotropes opens a wide range of fields of study and to achieve new advanced applications for these nanocomposites [15-16].

In addition to the functionalization possibilities, CNC could be synthesized according to different structures and forms. In this sense, considering the internal structure distribution, CNC could be transformed into films, hydrogels, foams or aerogels [17]. Particularly, nanocellulose based aerogels are opening novel possibilities for innovative applications and providing interesting results owing to the low weight and density, high porosity and versatility, among other unusual properties [18].

Incorporation of metal and metal oxide nanoparticles (MOx) has been proven as an efficient approach to obtain multifunctional materials based on cellulose [19-20]. The functionality can be tailored by simply controlling the concentration and characteristics (size, morphology, chemical character) of the inorganic phase. Interestingly, CNC aerogels have been successfully used as a platform material for the immobilization of diverse metal and metal oxide nanoparticles, facilitating their applicability in areas such as catalysis / sensing and their subsequent separation [15]. To that end, diverse approaches such as hydrothermal reduction assisted by the hydroxyl groups of cellulose [21], electroless plating have been used [22] through electrostatic interactions between sulfate ester groups and metal cations [23] or by chemical cross-linking [24]

In this framework, the hypothesis of this study is to develop and demonstrate different customization possibilities of CNC-based aerogels by combination with transition metals to afford novel properties to cellulosic aerogels. In this sense, the aim is to analyse the effect of in situ produced copper oxide nanoparticles (CuOx) and palladium oxide nanoparticles (PdOx) over final CNC/MNP hybrid aerogels properties. Among the large available transition metal possibilities, copper (Cu) and palladium (Pd) have been selected due to their potential scientific and industrial applications. Copper displays a remarkable electrical conductivity, high thermal conductivity, pseudocapacitive characteristics, good corrosion resistance, no toxicity and cost effectiveness [25] while palladium has a high selectivity and reactivity in many catalytic reactions and enables unique transformations that cannot be readily achieved using other materials [26-28]. It is our hypothesis thus that the in situ created copper and palladium oxide nanoparticles into highly porous cellulosic aerogels may provide functional materials with application potentials in the fields of catalysis, gas capture/sensing, electronics or thermal management.

Besides, and looking for mechanical resistance improvement for applicability optimization, a second biopolymer, in this case, sodium alginate, has been introduced to obtain a new kind of hybrid aerogel [29]. The intention is to take advantage of the well-known alginate bivalent cation promoted crosslinking capacity and gel formation and to proof this behaviour with palladium and copper cations in the presence of CNCs to obtain more consistent nanocomposotes [30-31].

In overall, this work highlights CNC-based aerogel functionalization possibilities through the incorporation of different metal nanoparticles. Additionally, sodium alginate is incorporated to improve the mechanical integrity of the aerogels, which is a recognized drawback of neat CNC structures, preserving the natural origin feature of the aerogel matrix.

## 3.3.2. Materials and methods

### *3.3.2.1. Starting materials*

Microcrystalline cellulose with a particle size of 20 µm (310697-500G), sulphuric acid and sodium hydroxide were supplied by Sigma Aldrich. Copper (II) nitrate trihydrate ($Cu(NO_3)_2.3H_2O$), palladium (II) nitrate hydrate ($Pd(NO_3)_2.XH_2O$), with a purity of 99 % used as precursor materials and sodium alginate (SA powder Mw = 396.000 Da and M/G ratio= 1,49, determined by viscosity and NMR measurements) were also supplied by Sigma Aldrich.

### *3.3.2.2. Cellulose nanocrystal synthesis*

Cellulose nanocrystals (CNC) were obtained by sulphuric acid hydrolysis of microcrystalline cellulose as described previously [32]. Firstly, microcrystalline cellulose was hydrolyzed in a 64 wt.% sulphuric acid solution at 45 ºC during 45 min. Hydrolytic reaction was stopped by adding 20-fold distilled water and hydrolyzed cellulose was recovered after several centrifugations (1500 rpm for 15 min) and it was subsequently washed using a Buchner flask and Buchner funnel Resulting dispersion was further neutralized by adding several drops of 0.5 M sodium hydroxide (NaOH). Finally, remaining dispersion was for 5 min with a 500 watt Vibracell Sonicator. Water-dispersed CNCs (1 wt%) with a zeta potential of -11.6mV (as measured using a Malvern Zetasizer Nano instrument) have been obtained.

### *3.3.2.3. Preparation of CNC-based aerogels*

CNC dispersion (3 mL) was mixed with 0.02 and 0.06 mmol (low and high starting concentrations respectively) of metallic precursors, palladium (II) and copper (II) nitrates, dissolved in an equal volume of MilliQ water and vigorously stirred for 30 minutes. Obtained dispersions were degassed under vacuum, frozen at -20 ºC

during 24 h and deposited in the lyophilizer at -50 ºC and 0.123 atm for 24 hours. Neat CNC aerogels were obtained in a similar way.

Concurrently, some CNC and CNC/MOx samples were subjected to carbon dioxide supercritical drying. For that, water contained in samples was replace for ethanol and 5 ml of dispersion where introduced in an open recipient with a filter on the bottom. The purpose of the recipient was to hold de solution and to allow liquid and supercritical fluid exchange. The recipient was fixed in the center of the $CO_2$ supercritical drying home-made device. Unfortunately, the experiment was not completed adequately due to a bad fluid exchange. While freeze drying is produced starting with a liquid sample instead of a gel like sample, for supercritical drying, in the absence of a suitable sample holder a gelled sample is required.

Besides, a second generation of hybrid aerogels with improved properties were fabricated by crosslinking CNCs with sodium alginate (ALG), where copper and palladium ions act as crosslinking agents. In this case, obtained hydrogels were kept at room temperature for equilibration during 30 minutes before freezing.

Finally, aerogels were cured at 100 ºC under vacuum for 30 minutes and part of the samples were exposed to UV irradiation between 250-600 nm with a 100W lamp (Sylvania R100W MERCURY SPOT U.S.A H44GS-100MDSKSP) for 8 hours. Aerogels with diameters of 29 mm ± 3 mm and heights of 6 ± 2 mm were obtained.

***Characterization***

*3.3.2.4. Density and porosity*

Aerogel apparent density was calculated by measuring the weight and volume of obtained samples.The weight was measured by an analytical balance (Sartorious 224I 1S std deviation= +/- 0.0001) and the diameter and height were determined

by a digital calliper (TESA-TWIN-CAL IP67). Aerogel porosity (P) was calculated using the Eq. 21.

$$P\ (\%) = (1-\rho^*/\rho_{cel})\ x\ 100 \qquad (21)$$

where ρ* is aerogel apparent density and ρcel is cellulose bulk density (1.6 g/cm$^3$) for neat CNC and the value calculated according CNC and metal nanoparticles (MNP) average concentrations in the case of hybrid aerogel

*3.3.2.5. Morphological characterization and elemental analysis*

Scanning electron microscopy (SEM) images of aerogel samples structure were performed using an EVO40 scanning electron microscope (Carl Zeiss STS, Germany) coupled to an X-Max Energy-Dispersive X-Ray Spectrometer (Oxford Instruments, UK).

Energy-dispersive-X-ray (EDX) analyses were carried out to obtain semi-quantitative elemental results using a working distance of 8–10 mm, and I Probe of 200 pA, a 35º take-off angle, an acceleration potential of 20 kV, an integration time of 100 s and a number of scans between 6 and 10. The INCA Microanalysis Suite 4.3 (Oxford Instruments, UK) software was used to collect and manage the data.

Besides, higher resolution SEM images were performed to visualise metal oxide nanoparticles and their disposition in CNC matrix using a high a resolution Scanning Electron Microscopy (FEG-SEM) Hitachi S-4800N.

Material preparation for SEM-EDX and SEM analysis was performed by a precise and clean cut of 3 parts of each sample and fixing them in a specific aluminium sample holder using adhesive carbon types. Samples were placed in order to

observe and measure top, cross/inner section and bottom parts in the same measurement, so further manipulation was not needed.

Finally, with the aim of improving the quality of SEM images collected from samples, a thin gold coating (~ 10 nm) was applied on their surface using an Emitech K550X sputter coater vacuum chamber (Quorum Technologies, UK).

Metal particle sizes were estimated using ImageJ 1.52v image processing software, measuring 50 nanoparticles at 2560x1920 pixel resolution images from SEM analysis. During the manual counting procedure (automatic option also is disponible), a threshold was applied to better distinguish metal nanoparticles from CNC matrix. Obtained diameters were visualized in a histogram showing particle distribution and a scatter curve was generated and fitted (generally using Gaussian Model) to calculate median diameters and standard deviation using OriginPro8.5 software.

*3.3.2.6. Surface Area determination*

Surface area and pore characteristics of the samples were evaluated from the $N_2$ adsorption desorption isotherms obtained at 77 ºK over the whole range of relative pressures. Measurements were made using an Autosorb®-1-C/TCD (Quantachrome, USA). Previously, the outgassing step was conducted upon vacuum application to remove the remaining water from the aerogels at 60 ºC for 24h.The surface area was determined via the Brunauer-Emmet-Teller (BET) method from the obtained absorption and desorption curves. Pore distribution (using Barrett-Jomer-Halenda BJH theory) was calculated from obtained isotherms.

*3.3.2.7. X-ray Diffraction*

Powder X-Ray diffraction (XRD) patterns were collected in a PHILIPS X'PERT PRO automatic diffractometer operating at 40 kV and 40 mA, theta-theta configuration, secondary monochromator with Cu-Kα radiation (λ = 1.5418 Å) and a PIXcel solid state detector (active length 3.347º). The samples were mounted on a zero-background silicon wafer fixed in a generic sample holder. Data were collected from 5 to 80° 2θ (step size = 0.026) and time per step of 600 s (total scanning time 2 h) at RT. 1º fixed divergence and antiscattering slit with 2 s of revolution time for the spinner were used.

*3.3.2.8. X-ray photoelectron spectroscopy*

Non-destructive X-ray photoelectron spectroscopy (XPS) was used to analyse the elements present on the surface and their oxidation state and / or environmental situations (coordination) using an Energy-analyser Phoibos 150 1D-DLD with a focus monochromatic radiation source 500 with dual anode Al/Ag Kα (1486.7 eV), which allows working with powers of 400 W and 600 W to improve the sensitivity and analysis time. A first analysis was realized to determine present elements (wide scan: step energy 1 eV, dwell time 0.1 s, pass energy 80 eV) before a more detailed one to (detail scan: step energy 0.08 eV, dwell time 0.1 s, pass energy 30 eV), both with an electron leave angle of 90º. The spectrometer was previously calibrated with Ag (Ag 3d5/2, 368.26 eV) and the spectrums were adjusted by software CasaXPS 2.3.16 which models Gauss-Lorentzian contributions, after background subtraction (Shirley). Concentrations were calculated correcting the values with relative atomic sensibility factors (Scofield).

*3.3.2.9. Surface free energy and hydration free energy*

Surface free energy (SFE) and hydration free energy (ΔEw) were calculated using Owens-Wendt and Young-Dupre equations [33-34]. Contact angles measurements of different test liquid [35] were carried out by sessile drop technique using an OCA 15 Dataphysic measuring device at room temperature.

*3.3.2.10. Fourier transform infrared spectroscopy (FTIR)*

Attenuated total reflectance Fourier transform infrared spectroscopy (ATR-FTIR) measurements were performed on a Shimadzu FTIR-8400s Fourier transform infrared spectrometer equipped with diamond ATR optics and a MIRacle ZnSe ATR accessory. Each spectrum has been collected in the range of 500-4000/cm with a resolution of 2/cm. Reported spectra consist of average values over three repetitions.

*3.3.2.11.Thermogravimetric analysis (TGA)*

Thermal degradation behaviour was studied by thermal gravimetric analysis (TGA) on a METTLER TOLEDO 851e machine in alumina pans under nitrogen atmosphere by heating the samples from room temperature to 800 ºC at 20 ºC/min.

*3.3.2.12. Mechanical performance*

Mechanical response of 7 ± 1 mm thick neat CNC, CNC/ALG and CNC/ALG/MOx aerogels was studied in compression mode on a universal testing machine (Trapezium Shimadzu AGS-X) equipped with a 10 N load cell in displacement control mode at a rate of 0.5 $mm \cdot min^{-1}$.

## 3.3.3. Results and discussion

### *3.3.3.1. CNC based hybrid aerogels*

Different aerogels were synthesized from cotton linters origin cellulose powder, after an acid hydrolysis and by means of metal precursors and/or sodium alginate addition in a surfactantless and scalable process (**Figure 60a**).

Obtained aerogels (**Figure 60b-c**) showed low density and high porosity (**Table 4**). Neat CNC aerogels were lightest, and density was higher as added metal concentration increased. Aerogels which include alginate showed an excellent weight/ volume rate and small volume shrinkage.

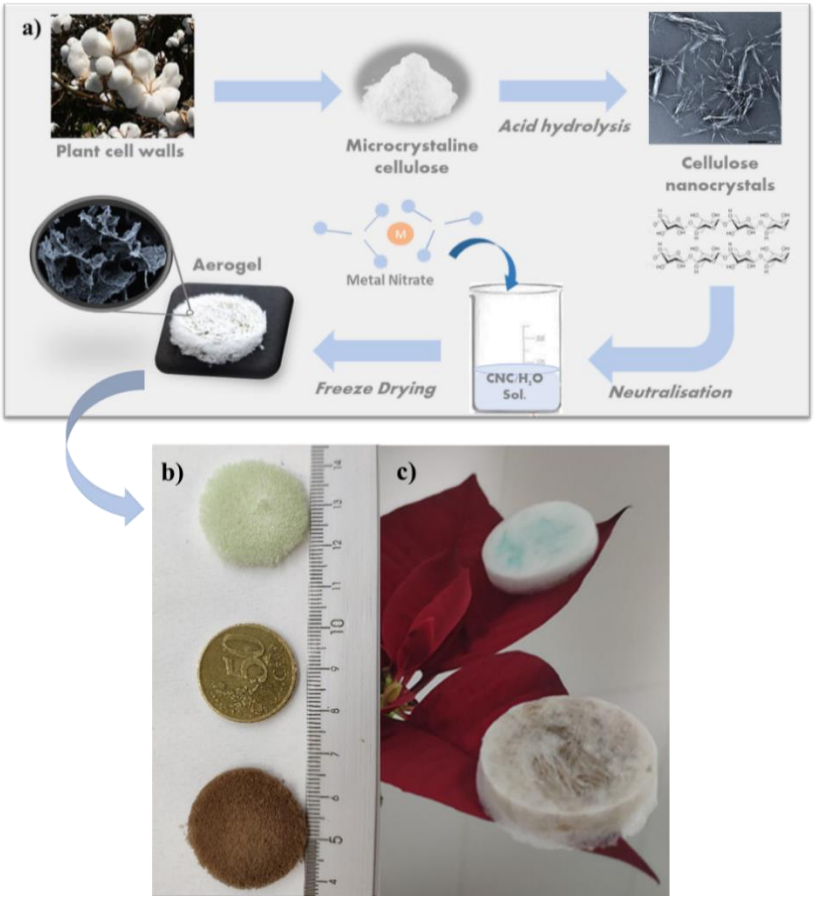


**Figure 60** Illustration of the preparation of CNC/MOx hybrid aerogels (a) images of CNC/CuOx, and CNC/PdOx low aerogels (b) and CNC-ALG/CuOx, CNC-ALG/PdOx aerogels (c)

**Table 4** Apparent density, porosity and volume shrinkage values for each aerogel. Samples are classified into pure CNC, hybrid CNC and metal oxide nanoparticles CNC/MOx (with higher and lower metal oxide concentration) and hybrid CNC, algiante and metal oxide CNC-ALG/MOx.

| Sample ID | Starting materials | CNC[a] (wt %) | Metal precursor[b] (wt %) | Apparent Density (mg/cm$^3$) | Porosity (%) | Volume Shrinkage (%) |
|---|---|---|---|---|---|---|
| **CNC** | CNC | 1 | _ | 15±5 | 98±0.5 | _ |
| **CNC/CuOx low** | CNC, $Cu(NO_3)_2$ | 1 | 0,083 | 23±2 | 98±0.5 | _ |
| **CNC/PdOx low** | CNC, $Pd(NO_3)_2$ | 1 | 0.083 | 22±2 | 98±0.5 | _ |
| **CNC/CuOx high** | CNC, $Cu(NO_3)_2$ | 1 | 0.25 | 27±2 | 98±0.5 | _ |
| **CNC/PdOx high** | CNC, $Pd(NO_3)_2$ | 1 | 0.25 | 26±2 | 98±0.3 | _ |
| **CNC/ALG** | CNC NaAlginate | 0.9 (1: 1 with ALG) | _ | 23±3 | 98±0.4 | 16 |
| **CNC-ALG/PdOx** | CNC NaAlginate $Pd(NO_3)_2$ | 0.85 (1:1 with ALG) | 0.21 | 21±2 | 98±0.6 | 12 |
| **CNC-ALG/CuOx** | CNC NaAlginate $Cu(NO_3)_2$ | 0.85 (1:1 with ALG) | 0.21 | 23±3 | 98±0.4 | 18 |

[a-b]Values for Starting concentrations in $H_2O$ dispersion

*3.3.3.2. Morphological and compositional analysis*

**Figure 61** shows SEM micrographs of the porous structures of the different aerogels. It was observed that sheet like structures were homogeneous in all sections (top, bottom and cross-section) even though small differences are observed between aerogel type in pores size and shape.

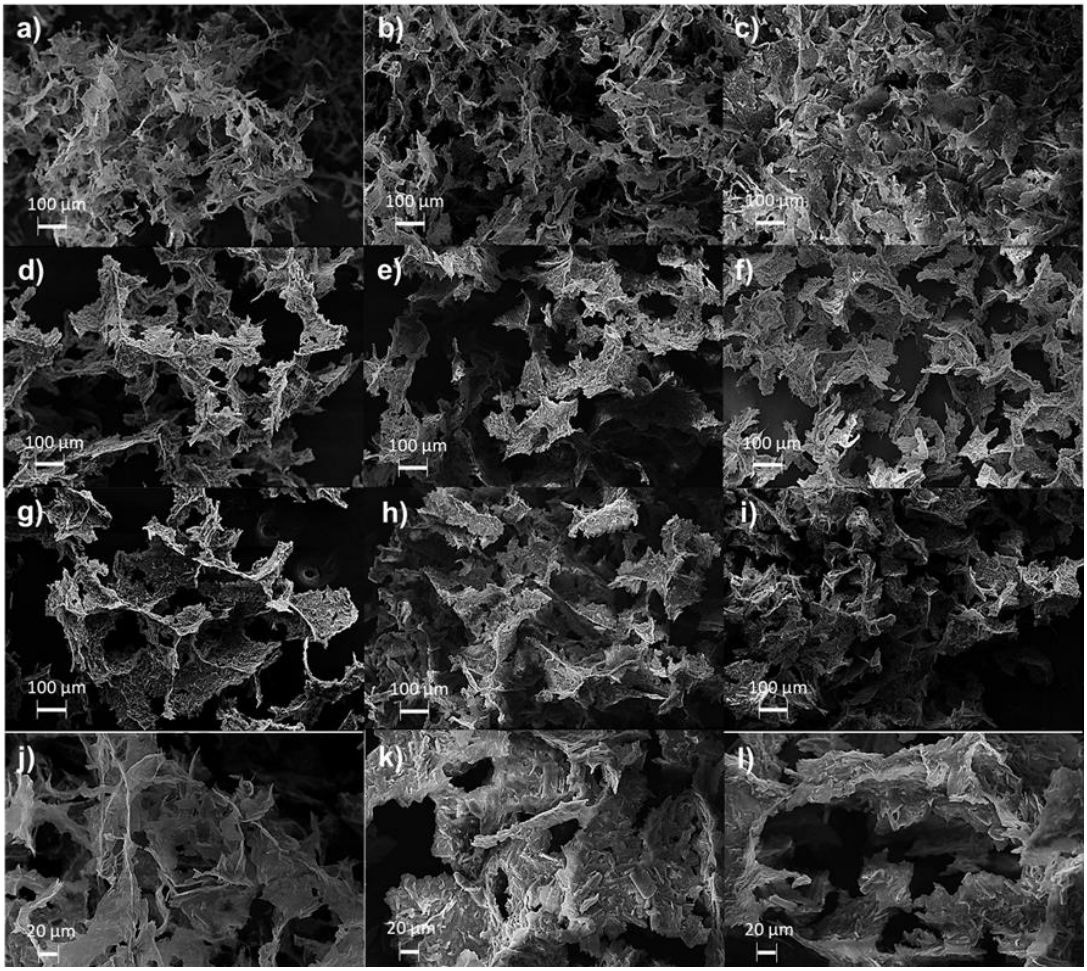


**Figure 61** Scanning electron microscopy (SEM) images showing porous structure for CNC aerogel (a) top (b) cross and (c) bottom sections, CNC/CuOx low aerogel (d) top (e) cross and (f) bottom sections , CNC/PdOx low aerogel (g) top (h) cross and (i) bottom sections and CNC (j) CNC/CuOx low (k) and CNC/PdOx low (l) cross sections at higher magnification.

Meanwhile, analysing the corresponding EDX spectra, apart from the main elements, C and O, Cu and Pd peaks were also detected for the hybrid aerogels, estimating the presence of 2-3 % MNPs in the final low concentration (0.02 mmol metal precursor) aerogels (**Figure 62**). Besides, residual Na and S concentrations were observed, these elements corresponded to remaining sulfate half ester anions and sodium cations from initial acid hydrolysis to obtain CNCs [36]. Furthermore, it is expected that negatively charged sulfate half ester groups (-

$OSO_3H$) may afford a better dispersion of CNCs in water due to the repulsive interactions between negatively charged nanocellulose rod-like structures [37].

Besides, EDX confirmed (**Table 5**) that the initial nitrate from the metal precursor agent was eliminated during the degas operation via nitrate reduction and nitrogen evaporation [38].

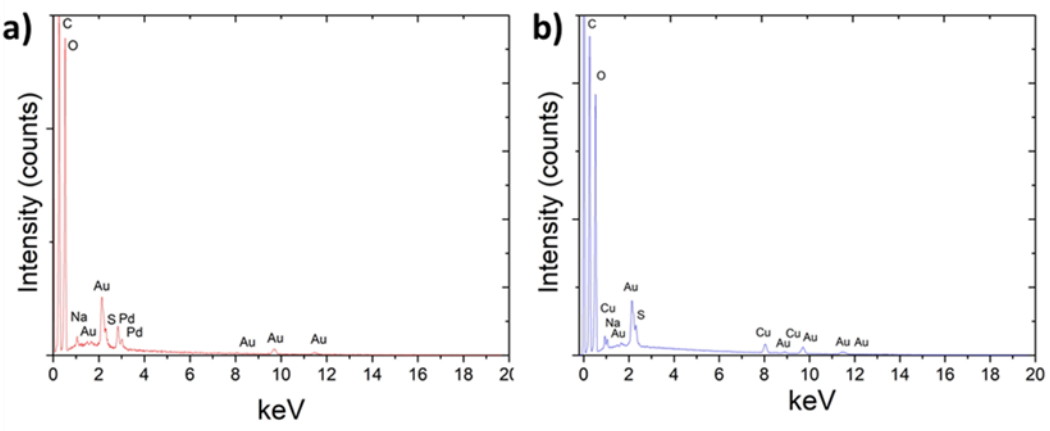


**Figure 62** EDX spectra for CNC/Pd low (a) and CNC/Cu low (b) aerogels.

**Table 5** Average element concentration in aerogels according EDX analysis.

| Sample | %C | %O | %Na | %S | %Metal |
|---|---|---|---|---|---|
| **Neat CNC** | 44.2 | 54.3 | 0.9 | 0.6 | _-_ |
| **CNC/CuOx low** | 43.1 | 53.1 | 0.8 | 0.4 | 2,7 |
| **CNC/PdOx low** | 48.3 | 47.0 | 0.6 | 0.5 | 3.6 |

Furthermore, to observe the metal presence and distribution over the CNC support, higher resolution SEM analysis were done and repeated on a weekly basis to observe the evolution and the effect of UV irradiation over the material.

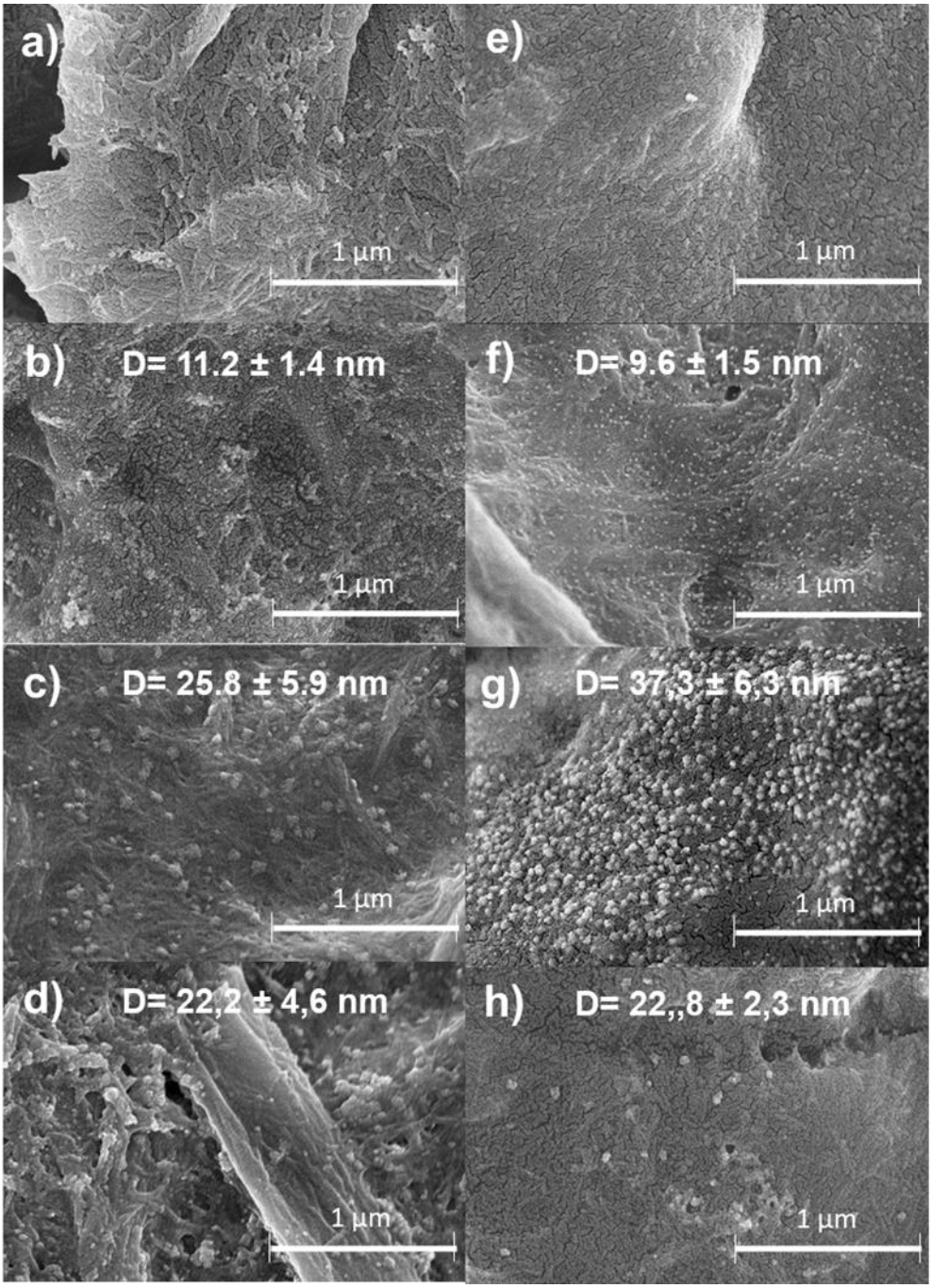


**Figure 63** High resolution SEM images for CNC/PdOx high aerogel 1 week after synthesis (a) and monitoring of the same sample after UV irradiation and (b) 2 weeks (c) 4 weeks and (d) 6 weeks after the synthesis. SEM images for (e) CNC/CuOx high aerogel (f) CNC/PdOx low aerogel and (g) CNC/PdOx high aerogel samples several months after synthesis and (h) CNC/PdOx high monitored no UV irradiated sample after 6 weeks.

In **Figure 63**, SEM images show palladium oxide nanoparticles monitoring on the entire CNC substrate for different time periods for a UV irradiated CNC/Pd high sample (**Figure 63b-d**). Analysing sample surface evolution, it was observed that palladium oxide nanoparticles migrated and emerged to aerogel surface upon time in all cases [39]. Thus, once aerogels were irradiated with UV, nanoparticle deposition and attachment on sample surface was enhanced and particle growing and/or aggregation was observed (**Figure 63b-d**) with the time [40]. If analysing a similar CNC/PdOx high sample (**Figure 63a**) but when UV irradiation is not applied (**Figure 63h**), a lower nanoparticle concentration with a similar size was observed after the same period. Moreover, CNC/PdOx low and CNC/PdOx high samples surfaces were analysed and compared several months after the synthesis (**Figure 63f,g**) observing clear differences related to nanoparticles size and amount.

Metal nanoparticle estimated mean diameters were calculated and indicated on each image in **Figure 63** [41-43]. Thus, mean diameters of surface nanoparticles for CNC/PdOx high and UV irradiated samples achieved values of 37.3 ± 6.3 nm months after synthesis (**Figure 63g**) while CNC/PdOx samples with lower concentration (**Figure 63f**) after the same period showed clearly smaller diameters of 9.6 ± 1.5 nm.

In the case of CNC/CuOx samples this migration was not observed for copper oxide containing samples with plane and inalterable surfaces (**Figure 63e**) so probably nanoparticle remain inside and between CNC structure, making difficult the measurement. This different behaviour could be explained considering the higher reactivity of palladium and the weaker interactions of this metal with the hydroxyl (-OH) groups onto CNC surfaces. This weaker interaction was observed at gel formations for CNC-ALG samples, when copper cation mediated promoted gel was formed clearly faster than palladium cation promoted one.

*3.3.3.3 Nitrogen adsorption and Surface area, XRD and XPS analysis*

Specific surface area (SSA) for different samples was determined by Brunauer-Emmet-Teller (BET) method using the data obtained of the $N_2$ adsorption and desorption curves (**Figure 64**). Different drying methods are available for the development of nanocellulose aerogels, where freeze-drying and supercritical-$CO_2$ drying are the most common procedures. Usually, freeze-drying affords lower SSA values (15-100 $m^2 \cdot g^{-1}$) in comparison supercritical-$CO_2$ drying (216-605 $m^2 \cdot g^{-1}$) due to a larger collapse of the three-dimensional cellulosic structure in the gel state [44-46]. Moreover, aerogels obtained from freeze-drying tend to be anisotropic as a result of the ice crystal growth during the freezing process, resulting in different architecture depending on whether the longitudinal section or the cross-section is considered [47]. In this sense, supercritical-$CO_2$ drying was tried but obtained results were not satisfactory because this technique is more suitable when the previous state is gel instead of a dispersion as in our case.

As showed in **Figure 64**, all samples display the same isotherm (type IV-V) with a hysteresis cycle similar to other porous cellulosic structures. Despite of the obtained SSA low values, some differences were observed, and palladium functionalised aerogel showed a higher surface area that almost triplicate the value of copper functionalised aerogel. The increased SSA for the aerogel containing Pd could be explained in terms of a higher intrinsic SSA of Pd nanoparticle and due to weaker interaction and a better distribution along the CNC matrix. [48].

Besides, average pore diameters were determined by Barret-Joyner-Halenda (BJH) method and the results indicate mesoporous (<50 nm) structures with pore sizes of 2.4, 10.5 and 24.2 nm for neat CNC, CNC/PdOx and CNC/CuOx samples respectively [6]. The results reveal that metal incorporation considerably increases the pore size of neat CNC aerogels, being more marked in the case of copper. The

porous architecture, as mentioned before, is influenced by the processing method and by the particle size, shape and interactions. For this reason, different obtained values for palladium and copper-containing aerogels were originated due to different metallic particle size and/or different interactions between CNC and metals.

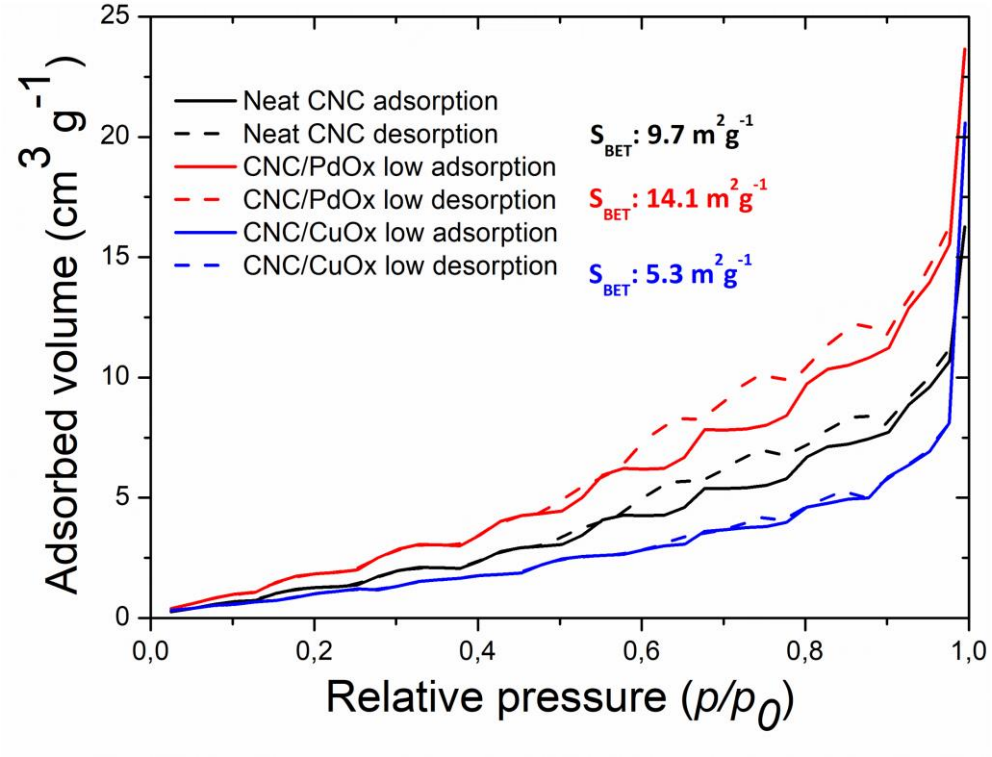


**Figure 64** Nitrogen absorption and surface area results.

*3.3.3.3. XRD and XPS analysis*

X-ray diffraction (XRD) measurements for different samples (**Figure 65**) showed typical CNC peaks occurring at 15.1º, 16.9º, 23° and 3.7º attributed to (1-10) (101), (002) and (040) characteristic planes of the cellulose I [49-50]. It could be concluded that cellulose structure did not suffer any substantial structural change with the incorporation of metals and/or alginate.

Metallic nanoparticle patterns were not observed in a first and standard analysis, but when a more accurate analysis was don, in the 2θ region ranging from 35 to 70 º (insert in Figure 6), palladium characteristic peaks were observed at 40.2º, 46.6º and 68.3º, assigned to the (110), (200) and (220) planes of palladium. These peaks were measured to calculate crystal size.

In the case of copper, crystal peaks were not detected, probably due to finely and atomically dispersed particles with diameters below 2 nm, in the limit of the technique resolution [51-52]. Furthermore, copper atom has a smaller electron density than palladium that results on weaker signal. As expected, when alginate was incorporated no changes were observed in the pattern due to the amorphous nature of the polymer and a small change around palladium characteristic peak was observed even if signal is not so clear as in CNC/Pd due to the smaller palladium concentration.

The crystallite size τ (nm), perpendicular to the lattice plane (002) of CNC signal was calculated by the Scherrer equation (Eq. 22), where K is the Scherrer constant (0.94), l is the wavelength of the X-ray radiation (0.154 nm), and β is the full width at half maximum of the diffraction peak (in radians) and θ is the diffraction angle of the peak.

$$\beta = \frac{K\,\lambda}{L\cos\theta} \qquad (22)$$

Besides, the Segal crystallinity index was calculated according to Eq. 23, where I002 is the total intensity of the (002) peak for cellulose, and Iam is the amorphous intensity [53].

$$CI = \frac{I_{002} - I_{am}}{I_{002}} x100 \qquad (23)$$

Calculated crystallite size and crystallinity index for CNC were 3.9 nm and 88.4 % respectively. According to the same equation, the crystallite size τ (nm), perpendicular to the lattice plane (111) of detected palladium was calculated and a value of 35.2 nm was obtained.

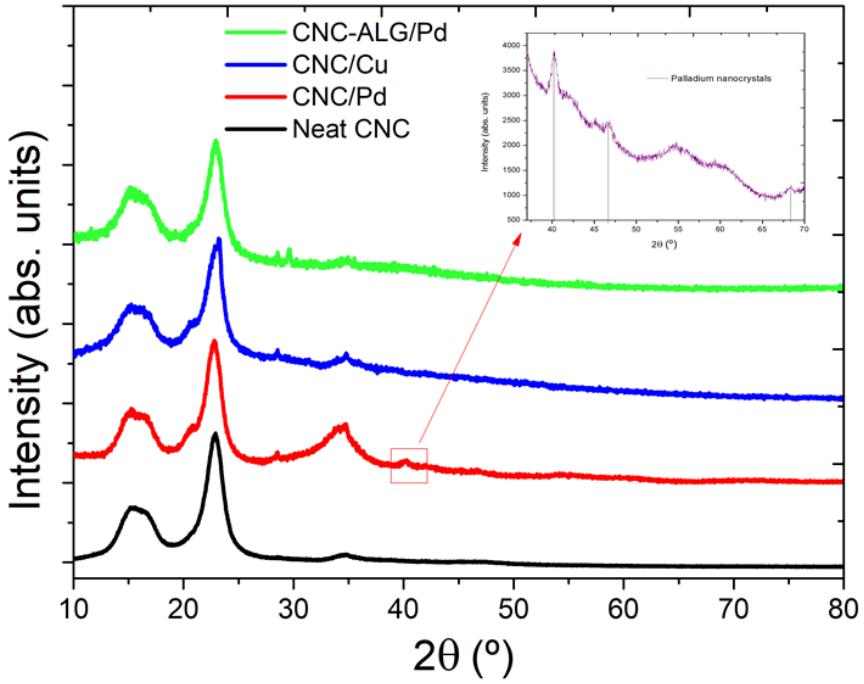


**Figure 65** X-ray diffraction diffractograms for different samples.

**Table 6** Main parameters of palladium XRD characteristic peaks (insert in **Figure 65**)

| Pos. (°2Th.) | Height (cts) | FWHM (°2Th.) | d-spacing (Å) | Rel. Int. (%) | Tip width (°2Th.) |
|---|---|---|---|---|---|
| 40.2109 | 815.89 | 0.3070 | 2.24366 | 100.00 | 0.3120 |
| 46.6237 | 233.58 | 0.6140 | 1.94892 | 28.63 | 0.6240 |
| 68.3635 | 104.05 | 0.7488 | 1.37108 | 12.75 | 0.6240 |

X-ray photoelectron spectroscopy (XPS) analysis was performed onto aerogel samples to determine the metal state on palladium and copper containing samples. Obtained results were represented in **Figure 66** where the overall spectrum for a CNC/Pd high sample shows main elements signal: carbon, oxygen and palladium (**Figure 66a**). Analysing individual signals (**Figure 66b-e**), carbon and oxygen showed characteristic signals at 286.4 and 533.7 eV. As for the metallic elements, palladium signal showed 3d 5/2 and Pd 3d 3/2 peaks at 337.3-337.8 and 342.7-343.3 respectively (**Figure 66d**), corresponding to palladium oxide, probably palladium (II) oxide [55-56] but the presence of $PdO_2$ and $PdO_3$ oxides was not discarded.

In the case of copper containing samples (**Figure 66e**), characteristic signals corresponding to Cu II oxide with a main 2p 3/2 peak at 935.4 eV and two satellite peaks at 941.2 and 945.0 eV were observed [57]. The superficial analysis offered semi quantitative information about metal oxidation states, signal positions, full width at half maximum values (FWHM) and surface elements atomic concentrations (**Table 7**). Observed metal oxidation states and element concentrations were in coherence with samples brownish and blue colours and element presence on surface was in accordance with elements observed by EDX analysis.

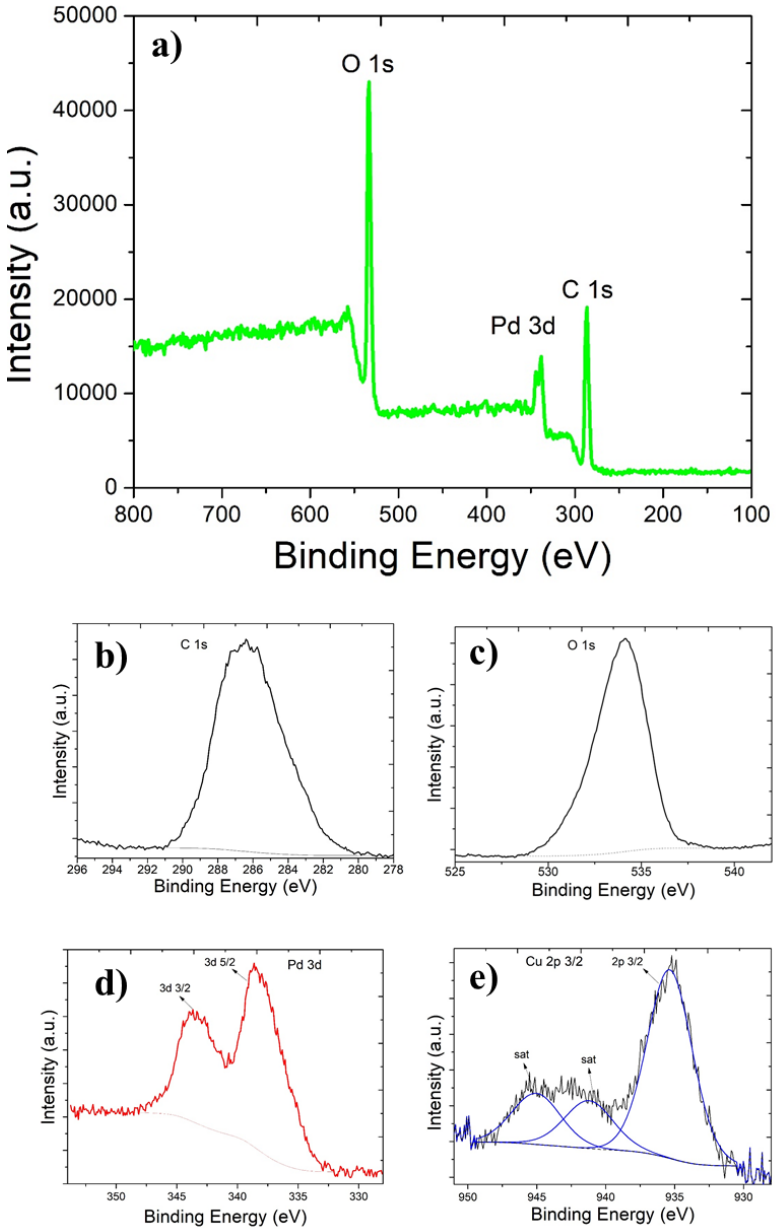


**Figure 66** XPS full spectra for (a) CNC/PdOx high sample and elements individual spectrum for (b) carbon (c) oxygen (d) palladium (f) and copper (e).

**Table 7** CNC/PdOx sample spectrum and element atomic concentration a) and CNC/CuOx sample spectrum and element atomic concentration (b).

| a) Element | Peak | Position | FWHM | % Conc. | % Atom. rel. |
|---|---|---|---|---|---|
| **C** | C 1s | 286.4 | 3.464 | 62.33 | 62.33 |
| **O** | O 1s | 533.3 | 2.645 | 34.75 | 34.75 |
| **Pd** | Pd (3d 5/2) | 337.3 | 3.355 | 1.72 | 2.9 |
| | Pd (3d 3/2) | 342.7 | 3.505 | 1.16 | |

| b) Element | Peak | Position | FWHM | % Conc. | % Atom. rel. |
|---|---|---|---|---|---|
| **C** | C 1s | 286.4 | 3.481 | 61.6 | 62.6 |
| **O** | O 1s | 534.1 | 3.212 | 33.6 | 36.4 |
| **Cu** | Cu 2p 3/2 | 935.4 | 3.848 | 0.82 | 1.3 |
| | Cu 2p 3/2, sh | 941.2 | 4-154 | 0.22 | |
| | Cu 2p 3/2, sh | 945.0 | 4.154 | 0.24 | |

Finally, copper surface concentration values was estimaded around 1.3 % while palladium oxide concentration weakly measurement offered surface concentration fluctuations with a final stabilization (Table 7b) in concordance with SEM results.

*3.3.3.4. Surface free energy and hydration free energy*

Surface free energy (SFE) was quantified and compared for neat CNC, CNC/PdOx low and CNC/PdOx high samples with Owens-Wendt equation using previously obtained contact angle values by means of sessile drop technique [58-59]. Owens-Wendt method is widely used to observe and measure the changes in the surface behaviour and to quantify the hydrophobicity of a solid surface [60].

Neat CNC and CNC/CuOx hydrophilic samples suffered a rapid penetration of the test liquids (0º contact angles) into the porous structures getting them wet immediately. Thus, it was observed that native nanocellulose and copper containing aerogel structures were rapidly disintegrated due to strong polar interactions with nanocellulose surface -OH groups.

By contrast, this hydrophilic behaviour was clearly altered at CNC/PdOx samples, but this effect was not immediate and reached the maximum approximately 25-30 days after the synthesis. Furthermore, this hydrophobicity was more evident when samples were exposed to UV light as a post-treatment 4 hours for each side (**Figure 67**).

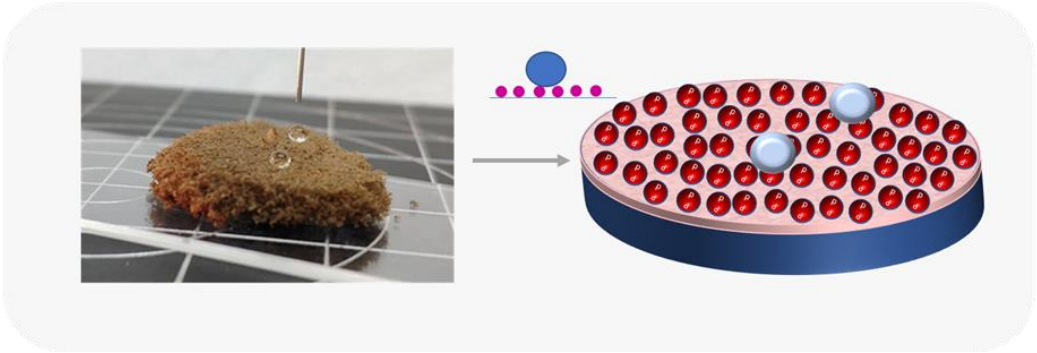

**Figure 67** Optical photograph of a water drop over a CNC-PdOx high sample and a scheme showing the possible surface structure.

As previously explained and in coherence with SEM measurements and surface evolution monitoring, the reason of this hydrophobicity is the presence of well dispersed palladium oxide nanoparticles onto CNC surfaces. Consequently, roughness increased, and wettability behaviour modification matched with Wenzel and Cassie and Baxter theories [61]. Nanoparticles act like nanopines where drops can repose avoiding absorption during a long time and blocking -OH interaction with polar liquids (**Figure 67**). For not irradiated samples, surface nanoparticles also promote contact angle improvement but they are not able to stop liquid absorption so long because the lower amount of particles acting as nanopines on the surface, at least during the first 2 weeks since the synthesis (**Figure 63h**). Thus, can be assumed that nanoparticle come out process was enhanced by UV radiation.

The analysis also concluded that surface modification was not always homogeneous along the sample and sometimes particle aggregation was observed. Therefore, it is important to achieve a homogeneous and continuous particle distribution over the entire surface to get a good hydrophobic effect (**Figure 63g**).

To quantify the hydrophilicity alteration, water contact angles were measured and the contact angle for CNC/PdOx high sample reached almost super-hydrophobicity values (**Figure 68a**). Besides, dynamic water contact measurements were done to follow and quantify this effect (**Figure 68c**) and it was concluded that palladium oxide at lower concentrations does not ensure enough nanoparticle concentration over the surface to cover the necessary space to avoid liquid absorption. Previously mentioned high resolution SEM images, reinforced this hypothesis showing more spaced particles disposition and smaller nanoparticles for lower concentration samples CNC/PdOx low (**Figure 63f**).

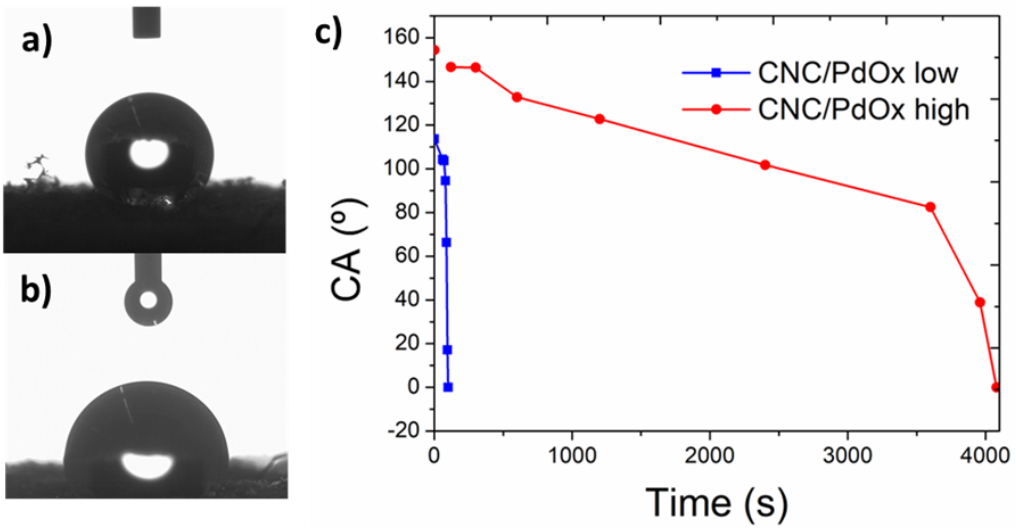


**Figure 68** Representative images of a water drop (at time 0) on the surface of (a) CNC/PdOx high and (b) CNC/PdOx low and (c) dynamic WCA values of CNC/PdOx aerogels with different metal concentrations.

To deeply analyse this surface modification, different samples surface free energy (SFE) and hydration free energies $\Delta E_W$ were determined by Owens-Wendt and Young-Dupre equations [62] respectively (**Table 8**).

**Table 8** Average contact angles, surface free energy, and hydration free energy comparison for neat CNC and palladium oxide-containing samples at different concentrations.

| Sample | Contact angle (degree) at 0 seconds | Surface free energy ($mJ/m^2$) | Hydration free energy ($mJ/m^2$) |
|---|---|---|---|
| **Neat CNC** | 0 º | 70.58±1.8 | -145.60 |
| **CNC/PdOx low** | 116.9 º | 22.26±0.2 | -39.86 |
| **CNC/PdOx high** | 141.6 | 15.34±0.7 | -15.75 |

Obtained values (**Table 8**) confirmed experimentally observed behaviour for palladium oxide containing samples with the lowest values for higher concentration samples. For this sample (CNC/PdOx high) water-drops formed a round droplet over the entire aerogel surface and remained static, besides drop was easily removed and rolled down when the surface was inclined.

SFE of a porous solid depends upon the chemical composition, the surface tension of the liquid, the used freezing and drying method [63-64] and is influenced by the porosity and surface roughness. This surface roughness in a very fine scale is a requirement to get super-hydrophobic properties and it is specifically boosted by overhang forms like fibres, pores or mushroom like structures [65].

In this sense, the hypothesis to explain the obtained hydrophobic effect when palladium oxide nanoparticles were combined with CNCs is the modification of the surface roughness at a nanoscale level. Cellulose surface has a high density of hydroxyl groups which make cellulose hydrophilic and quick water absorbing. These hydroxyl groups need to be removed or blocked to achieve hydrophobicity and in this case palladium oxide nanoparticles situated onto cellulose surfaces block the polar interactions, forming a nanopine structure which modifies surface morphology. For lower palladium oxide concentration, the surface presented gaps between smaller nanoparticles and the surface was less granulated (hydroxyl

group blocking was not as efficient). Therefore, water contact angle increased from complete wettability 0º to 116.9º and 141.6º as the palladium concentration increased and consequently surface free energy values decreased from 70.58 to 22.26 and 15.34 mJ/m$^2$ respectively. The same trend was observed for ΔEw values, decreasing from 145.60 mJ/m$^2$, hydrophilic value of neat CNC, to 39.86 and 15.76 mJ/m$^2$, hydrophobic values for palladium oxide containing samples [62,66].

*3.3.3.5. Infrared spectroscopy*

Fourier transform infrared spectroscopy (FTIR) analysis has been carried out because it provides a mean to study the occurring interactions between aerogel partners (CNCs, metal oxide nanoparticles and alginate). As shown in **Figure 69**, CNC and CNC/PdOx spectra presented the characteristic broad band at 3500-3200 cm$^{-1}$ arising from free O-H stretching vibration of the OH groups and another low intensity band located at 2900 cm$^{-1}$ corresponding to characteristic C-H stretching vibration of asymmetric/symmetric methyl and methylene groups and the band at 1650 cm$^{-1}$ is associated to O-H bending of adsorbed water in cellulose. In addition, the vibration peaks observed at 1450 and 1420 cm$^{-1}$ correspond to bending vibration of C-H and C-O bonds in the aromatic ring, the vibration peak at 1150 cm$^{-1}$ is related to C-O-C bending, absorption peak at 1060 cm$^{-1}$ indicated C-O-C pyranose ring stretching vibration, and the band located at 900 cm$^{-1}$ is associated with glycosidic 1-4 linkages between glucose units in cellulose [32,67]. All absorption signals are the typical nanocellulose bands and no appreciable modifications are observed due to the presence of metallic nanoparticles in samples.

This absence of modification is probably due to the fact that metal oxide nanoparticles remain entrapped between CNCs by means of ionic and/or Van der Waals interactions, which are not strong enough to be detected by FTIR. But when alginate and alginate+metal were incorporated, obtained FTIR spectra suffered modifications related to peak displacement (**Figure 69b-c**) and intensity and shape variations. The modifications were mainly a consequence of the formation of strong -OH interactions between CNC and alginate and the simultaneous ionic interactions between -OH and carboxyl groups present in alginate chains and the bivalent metal [73,81]. In this regard, the clearest displacement was observed for characteristic peak related to stretching vibration of -OH bonds (3500-3200 $cm^{-1}$) and the displacement of the arising peaks corresponding to carboxylic ions asymmetric and symmetric stretching vibrations (around 1600 and 1400 $cm^{-1}$). Besides, characteristic band intensity decreases for CNC-ALG and CNC-ALG/MOx samples comparing neat alginate is probably because stronger interactions promoted by metal cations limited the involved group vibration [68].

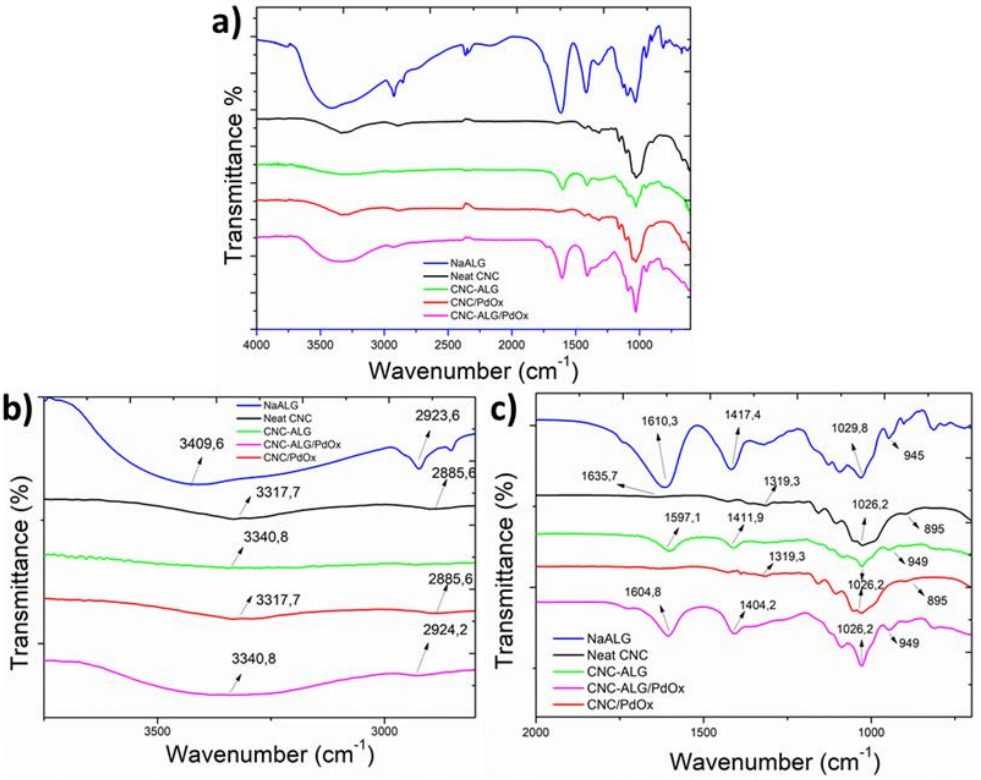


**Figure 69** FTIR curves of prepared aerogels in the 4000-700 $cm^{-1}$ (a) and enlarged views (b), (c).

### *3.3.3.6. Thermal stability of aerogels*

Thermo gravimetric analysis (TGA) is a commonly conducted experiment to determine the thermal stability of materials and maximum operating temperatures. As the aerogels here synthesized may be potentially applicable in catalytic applications (typically carried out at intermediate-high temperatures), studying their thermal stability is of prime relevance.Furthermore, with the aim of understanding the effects of palladium and copper oxides presence and alginate crosslinking on the stability of neat CNC aerogel, thermogravimetric analysis (TGA) tests were carried out at a heating rate of 20 ºC/min. **Figure 70** shows TG and DTG profiles of neat CNC and hybrid CNC/MOx samples for different metal oxide concentrations and metal precursors (**Figure 70a-b**) and TG and DTG profile comparison between

neat CNC, sodium alginate, CNC/MNP high, CNC-ALG and CNC-ALG/MNP aerogels (**Figure 70c-d**).

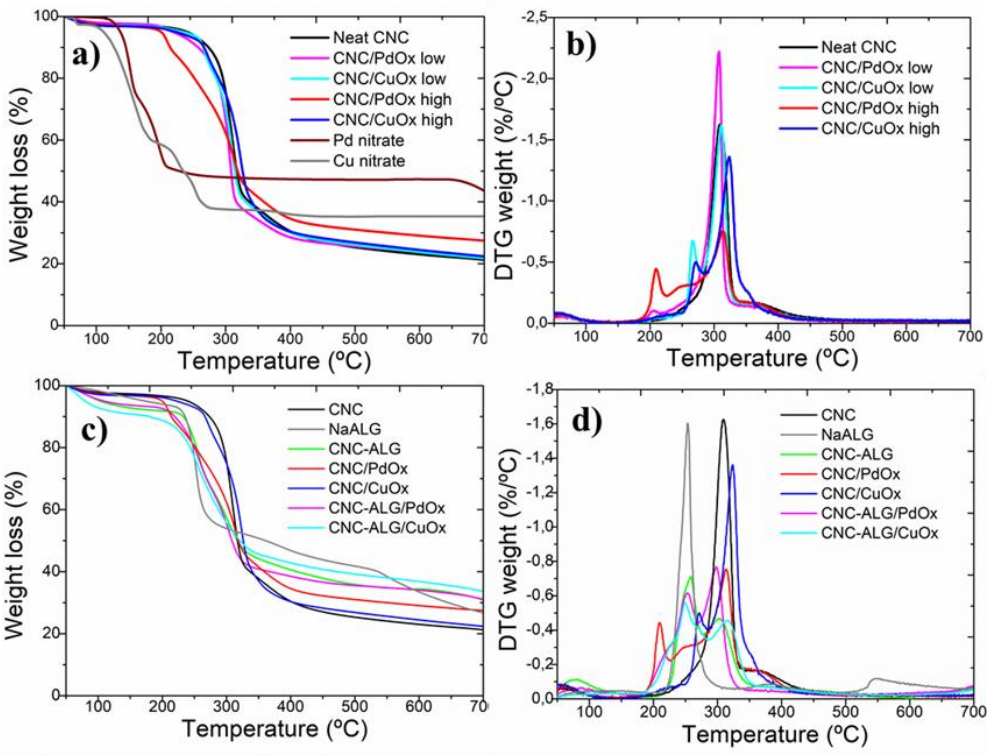


**Figure 70** TG (a) and DTG (b) curves of CNC and CNC/MOx hybrids aerogel with different metal concentrations and TG (c) and DTG (d) including CNC-ALG/MOx hybrid aerogels.

Neat CNC samples presented a similar curve as reported in previous studies [69] but characteristic $T_{peak}$ moved to higher values, from 265 ºC to 310 ºC, when CNC takes aerogel structure instead of film structure. The reason of this improvement was the high porosity of aerogels and the degradation retardancy caused when flame finds air in his way instead of material. This step had been previously ascribed to evaporation, depolymerization, dehydration and decomposition of cellulose glycosyl units [70]. In the case of neat sodium alginate (**Figure 70d**), a high hygroscopic polymer, characteristic degradation curve was obtained, showing a sharp $T_{peak}$ at 253 ºC  a small degradation peak at 530 ºC [71].

If hybrid CNC/MOx behaviour was analysed (**Figure 70a-b**), nanoparticles addition promoted a double degradation peak mechanism and the emergence of the first degradation peak at lower values, 210 ºC and 267 ºC for palladium and copper higher concentration samples, respectively. This thermal degradation modification was more evident for CNC/PdOx high sample where degradation process first small peak started at lower temperature (210 ºC), but final sample amount (at 700 ºC) was also lower with a 27 % of remaining mass instead of 22 and 21 % of CNC/Cu and neat CNC, respectively. These results highlighted that thermal degradation mechanism of neat CNC was altered by the present of palladium in sufficient concentration (> 3%), promoting an earlier degradation initiation due to the catalytic effect of palladium and CNC glycosidic bond fracture at lower temperatures. Despite of this initial thermal acceleration, final higher amount could arise from the fact that metals, in this stage, were acting as flame retardants by absorbing heat. The fact that the sample CNC/CuOx high shows a comparable remaining mass to neat CNC at 700 ºC does not arise from a low CuOx loading, but occurs due to a formation of smaller char residue quantities originating from the decomposition of anhydrocellulose in the presence of CuOx (in comparison with PdOx, which is more efficient in char formation) [72].

When thermal degradation curves of CNC-ALG and CNC-ALG/MOx samples were compared with neat polymer (CNC and sodium alginate) curves (**Figure 70c-d),** the first conclusion was that again hybrid (biopolymer or biopolymer-metal) samples DTA curves showed two degradation peaks. While, as mentioned before, pure polymers showed different behaviours but only one sharp degradation peak. Furthermore, in this case degradation maximum was reached in the first peak for CNC-ALG and CNC-ALG/CuOx samples at 259 ºC and 249 ºC, respectively. In the case of CNC-ALG/PdOx sample two degradation peaks showed very similar

degradation rate. Next table (**Table 9**) shows the characteristic values of the thermogravimetric analysis for all the studied samples.

**Table 9** Representative thermogravimetric parameters for prepared materials extracted from TGA results.

| Sample | $T_{onset}$ (ºC) | $T_{peak}$ (ºC) | DTG $_{max}$ | FWHM (ºC) |
|---|---|---|---|---|
| **CNC** | 240 | 310 | 1.62 | 26.3 |
| **CNC/PdOx low** | 218 | 308 | 2.25 | 17.3 |
| **CNC/CuOx low** | 233 | 311 | 1.62 | 25.3 |
| **CNC/PdOx high** | 200 | 314 | 0.75 | 43.3 |
| **CNC/CuOx high** | 223 | 324 | 1.35 | 25.3 |
| **NaALG** | 174 | 253 | 1,60 | 19.62 |
| **CNC-ALG** | 104 | 259 | 0.70 | 41.93 |
| **CNC-ALG/PdOx** | 110 | 298 | 0.76 | 37.45 |
| **CNC-ALG/CuOx** | 80 | 249 | 0.55 | 64.22 |

It was observed that TG curves obtained for these biopolymer systems were a combination of cross-linked CNC and sodium alginate curves. These curves showed two stages, before 200 ºC and between 310 and 520 ºC, very similar to alginate degradation behaviour and other two stages, between 200 ºC and 310 ºC and from 520 ºC to 700 ºC, similar to neat CNC degradation curve profile. The first stage, before 100-200 ºC, was ascribed to very hygroscopic alginate dehydration while second stage coinciding with hybrid samples first degradation peaks was attributed to alginate decarboxylation, fracture of glycosidic bonds and decarbonylation of the alginate chains [73]. While third stage coinciding with second degradation peak was attributed to cellulose chains depolymerization, previously described, and finally residual substances decomposition was produced.

As observed before for neat CNC, metal addition promoted the degradation acceleration but a decrease of final degradation rate, particularly in the case of CNC-ALG/CuOx sample with remaining weights of 21.2 %, 30.6 % and 33.7 % for neat CNC, CNC-ALG and CNC-ALG/CuOx, respectively. Small variations between different metals behaviour were probably due to slight concentrations differences in analysed samples due to less homogeneous metal distribution and different material losses from initial precursor during synthesis process steps.

In overall, neat CNC aerogel thermal degradation could be modified by the addition of sodium alginate combined with metal particles in an adequate concentration. Besides, at the studied cases showed, polymer chain decomposition phase [74] for hybrid polymer-metal, biopolymer and biopolymer-metal samples occurred in two different stages when for neat polymer occurred in a unique and more intense stage with a lower final thermal stability.

*3.3.3.7. Mechanical performance*

Tighter aerogels obtained by -OH crosslinking and cation mediated crosslinking were analysed through compression test and compared with neat CNC. The mechanical properties of aerogels with similar densities (**Table 4**) were determined by their compressive strength. **Figure 12** shows the plots of compressive stress (σ) versus strain (ε).

The stress–strain curves of CNC-ALG aerogels showed two distinct deformation stages, during the first stage (ε< 20 %) strain increases lineary and very fast practically without pressure reflecting porous deformation. Meanwhile at second stage (20 % < ε < 90 %) curves showed an exponential growth due to the suffered densification [75]. In this stage, the achieved densification is maximum at the end of the curve (80 % < ε < 90 %) where for small strain percentages the required

pressure markedly increased. With respect to neat CNC, stress-strain curve showed a linear and flat behaviour almost until ε < 80 % where high densification offered a small resistance to the compression.

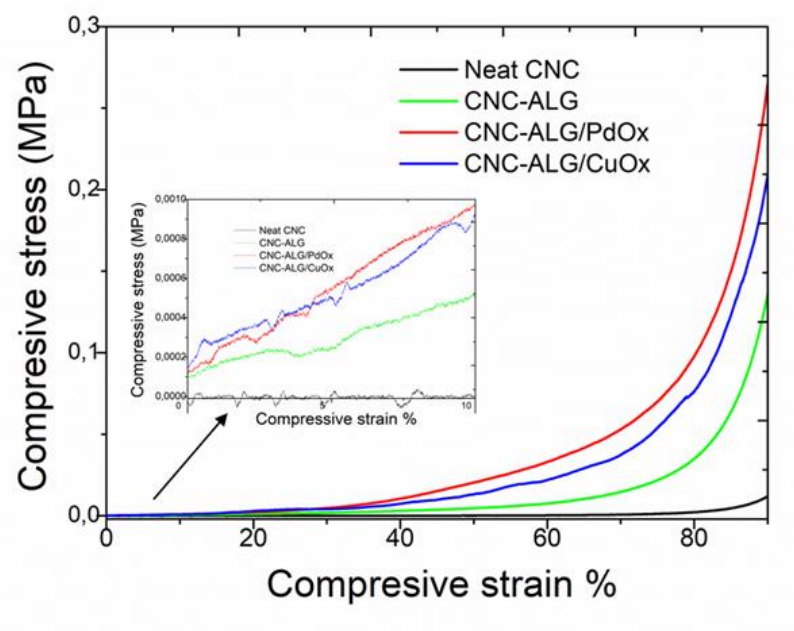


**Figure 71** Mechanical behaviour of fabricated samples under compression stress.

Young modulus (E) calculated at Hook´s region (ε < 10 %) of compressive strain (insert **in Figure 71**), confirmed the observed improved performance of samples reinforced with sodium alginate (**Table 10**). Meanwhile, neat CNC could not support any pressure and did not oppose resistance (ECNC=1.7 Pa), alginate containing samples showed a soft but more mechanically resistant performance even when 95 % compressive strain was achieved (ECNC-ALG=38.7 Pa). As it was expected, metal containing samples offered an improved mechanical resistance due to the contribution to the hardness of the metal itself and because stronger crosslinking promoted by metal cations. Besides, palladium oxide containing samples are slightly more resistant (ECNC-ALG/PdOx= 101.2 Pa vs. ECNC-ALG/CuOx= 91,5 Pa) probably due to a better and more homogeneous

distribution of the metal over the CNC and alginate matrix and small concentration variations [76]. Besides, Poisson´s ratios (ν) were calculated from lateral and axial strain values for the different aerogels and maximum strengths were graphically obtained. Obtained near zero poisson values with were in coherence with reported values for high strains in rigid plastic foams [77-78] and the observed low cross-section variation after compression in all samples. The mechanical response and the obtained parameters are dependent on the material density and the characteristics of the formed aerogel network [79].

**Table 10** Representative parameters of compression test.

| Sample | E (Pa) | Poisson´s Ratio (v) | Maximum Strength (MPa) |
|---|---|---|---|
| **CNC** | 1.7 | 0.052 | 0.06 |
| **CNC-ALG** | 38.7 | 0,084 | 0.4 |
| **CNC-ALG/CuOx** | 91.5 | 0.089 | 0.5 |
| **CNC-ALG/PdOx** | 101.2 | 0.095 | 0.6 |

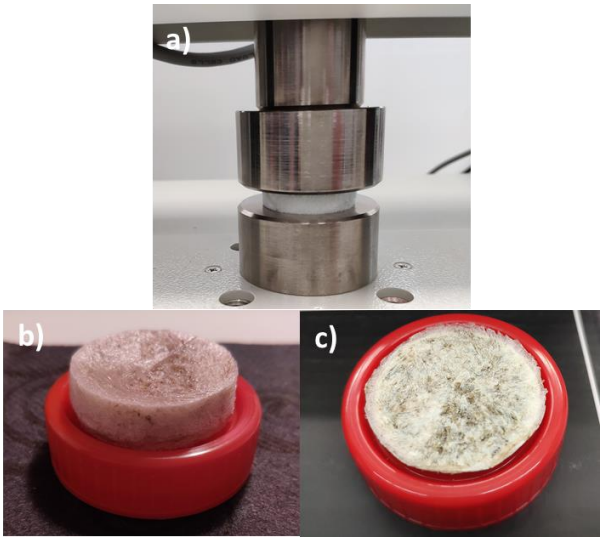


**Figure 72** Images of (a) the trial and the aerogel (b) before and (c) after the compressive strain.

Compression trials confirmed that the inclusion of sodium alginate biopolymer was a sustainable and effective choice to improve CNC based aerogels integrity to be used in applications where certain compression strength is required.

## 3.3.4. Conclusions

This work analyses a simple and surfactantless way to obtain metal nanoparticle loaded cellulose nanocrystal-based aerogels. Experimental results reveal that copper and palladium oxide containing hybrid aerogels improve their thermal stability. Regarding other properties such as specific surface area and surface energy, only palladium oxide nanoparticle containing aerogels show a clear surface modification. Interestingly, palladium-oxide nanoparticle containing aerogels present a strong hydrophobic behaviour with a water contact angle > 140º, while neat CNC aerogels suffered immediate wetting. Furthermore, developed hybrid aerogels display improved thermal and compressive resistance upon the incorporation of alginate crosslinking, which is promoted by palladium and copper cations. As transition metal oxides and nanoparticles supported on sustainable biopolymer structures are achieving great interest in the form of different catalyst and biosensor systems, these materials may emerge interesting candidates for novel environmental safety, energy or biomedical application.

# References

[1] Debbie J. Winton D.J., Anderson L.G., Rocliffe S., Loiselle S. 2020. Macroplastic pollution in freshwater environments: Focusing public and policy action. Science of The Total Environment, 704, 135242.

[2] Yu L., Dean K., Li L. 2006. Polymer blends and composites from renewable resources. Progress in Polymer Science , 31(6), 576-602.

[3] Thomas S., Pothan L.A., Mavelil-Sam R. 2018. Biobased Aerogels: Polysaccharide and Protein-based Materials. The Royal Society of Chemistry. Green Chemistry Series, 58.

[4] Barrios E., Fox D., Li Sip Y.Y., Catarata R., Calderon J.E., Azim N., Afrin S., Zhang Z., Zhai L. 2019. Nanomaterials in Advanced, High-Performance Aerogel Composites: A Review. Polymers ,11, 726.

[5] Shchipunov Y. 2012. Bionanocomposites: Green sustainable materials for the near future. Pure Appl. Chem., 84, 2579–2607.

[6] Lavoine N., Bergström L. 2017. Nanocellulose-based foams and aerogels: processing, properties, and applications. J. Mater. Chem. A., 5, 16105.

[7] Filpponen I., Argyropoulos D.S. 2010. Regular linking of cellulose nanocrystals via click chemistry: Synthesis and formation of cellulose nanoplatelet gels. Biomacromolecules, 11(4), 1060-1066.

[8] Habibi Y., Lucia L.A., Rojas, O.J. 2010. Cellulose nanocrystals: chemistry, self-assembly, and applications. Chemical Reviews, 110(6), 3479-3500.

[9] Oksman K., Aitomäki Y., Mathew A.P., Siqueira G., Zhou Q., Butylina S., Tanpichai S., Zhou X., Hooshmand S .2016. Review of the recent developments in cellulose nanocomposite processing. Composites Part A: Applied Science and Manufacturing, 83, 2-18.

[10] Kim J., Montero G., Habibi Y., Hinestroza J.P., Genzer J., Argyropoulos D.S., Rojas O.J. 2009. Dispersion of cellulose crystallites by nonionic surfactants in a hydrophobic polymer matrix. Polymer Engineering and Science, 49(10), 2054-2061.

[11] Lee K.Y., Aitomäki Y., Berglund L.A., Oksman K., Bismarck A. 2014. On the use of nanocellulose as reinforcement in polymer matrix composites. Composites Science and Technology, 105,15-27.

[12] Azizi Samir M.A.S., Alloin F., Dufresne A. 2005. Review of Recent Research into Cellulosic Whiskers, Their Properties and Their Application in Nanocomposite Field. Biomacromolecules, 6 (2), 612-626.

[13] Eichhorn S.J., Dufresne A., Aranguren M., Marcovich N.E., Capadona J.R., Rowan S.J., Weder C., Thielemans W., Roman M., Renneckar S., Gindl W., Veigel S., Keckes J., Yano H., Abe K., Nogi M., Nakagaito A.N., Mangalam A., Simonsen J., Benight A.S. , Bismarck A., Berglund L.A., Peij T.2010. Review: current international research into cellulose nanofibers and nanocomposites. Journal of Materials Science, 45(1),1-33.

[14] Dufresne A. 2013. Nanocellulose: a new ageless bionanomaterial. Materials Today, 16(6), 220-227.

[15] Lizundia E., Puglia D., Nguyen T.D., Armentano I. 2020. Cellulose nanocrystal based multifunctional nanohybrids. Prog. Mater. Sci.,112, 100668.

[16] Tang T., Sisler J., Grishkewich N., Tam K.C. 2017. Functionalization of cellulose nanocrystals for advanced applications. Journal of Colloid and Interface Science, 494, 397-409.

[17] De France K.J., Hoare T., Cranston E.D. 2017. Review of Hydrogels and Aerogels Containing Nanocellulose. Chem. Mater, 29(11), 4609-4631.

[18] Budtova T. 2019. Cellulose II aerogels: a review. Cellulose 26, 81-121.

[19] Lizundia E., Goikuria U., Vilas J.L., Cristofaro F., Bruni G., Fortunati E., Armentano I., Visai L., Torre L .2018. Metal nanoparticles embedded in cellulose nanocrystal based films: material properties and post-use analysis. Biomacromolecules, 19, 2618-2628.

[20] Rezayat M., Blundell R.K., Camp J.E., Walsh D.A., Thielemans W. 2014. Green One-Step Synthesis of Catalytically Active Palladium Nanoparticles Supported on Cellulose Nanocrystals. ACS Sustainable Chem. Eng., 2(5), 1241-1250.

[21] Cai J., Kimura S., Wada M., Kuga S. 2010. Nanoporous cellulose as metal nanoparticles support. Biomacromolecules,10, 87-94.

[22] Schestakow M., Muench F., Reimuth C., Ratke L., Ensinger W. 2016. Electroless synthesis of cellulose-metal aerogel composites. Appl. Phys. Lett. 108, 213108.

[23] Van Rie J., Thielemans W. 2017. Cellulose–gold nanoparticle hybrid materials. Nanoscale, 9, 8525-8554.

[24] Yang X., Shi K., Zhitomirsky I., Cranston E.D. 2015. Cellulose Nanocrystal Aerogels as Universal 3D Lightweight Substrates for Supercapacitor Materials, 27 (40), 6104-6109.

[25] Tran T.H., Nguyen V.T. 2014. Copper Oxide Nanomaterials Prepared by Solution Methods, Some Properties, and Potential Applications: A Brief Review. International Scholarly Research Notices, ID 856592.

[26] Han X., Wang M., Le M.L., Bedford N.M., Woehl T.J., Thoi V.S. 2019. Effects of substrate porosity in carbon aerogel supported copper for electrocatalytic carbon dioxide reduction. Electrochimica Acta, 297, 545-552.

[27] Kaushik M., Moores A. 2016. Review: nanocelluloses as versatile supports for metal nanoparticles and their applications in catalysis. Green Chem, 18, 622–637.

[28] Fan J., Xu H., Lv M., Wang J., Teng W., Ran X. 2017. Mesoporous carbon confined palladium–copper alloy composites for high performance nitrogen selective nitrate reduction electrocatalysis. New J. Chem., 41, 2349-2357.

[29] Shan Y., Li C., Wu Y., Li Q., Liao J. 2019. Hybrid cellulose nanocrystal/alginate/gelatin scaffold with improved mechanical properties and guided wound healing. RSC Adv., 9, 22966.

[30] Balavandy S.K., Shameli K., Abidin Z.Z. 2015. Rapid and Green Synthesis of Silver Nanoparticles via Sodium Alginate Media. Int. J. Electrochemical. Sci., 10, 486-497.

[31] Larraza I., Ugarte L., Fayana A., Gabilondo N., Arbelaiz A., Corcuera M.A., Eceiza A. 2020. Influence of Process Parameters in Graphene Oxide Obtention on the Properties of Mechanically Strong Alginate Nanocomposites.Materials, 13, 1081.

[32] Lizundia E., Vilas J.L., León L.M. 2015. Crystallization, structural relaxation and thermal degradation in Poly(L-lactide)/cellulose nanocrystal renewable nanocomposites. Carbohydrate Polymers,123, 256-65.

[33] Owens D.K., Wendt R.C. 1969. Estimation of the surface fee energy of polymers. Journal of Applied Polymer Science, 13, 1741-1747.

[34] Ebnesajjad S. 2011. Surface Tension and Its Measurement. Handbook of Adhesives and Surface Preparation Technology, Applications and Manufacturing Plastics Design Library, 21-30.

[35] Kozbial A., Li Z., Conaway C., McGinley R., Dhingra S., Vahdat V., Zhou F., D'Urso B., Liu H., Li L. 2014. Study on the Surface Energy of Graphene by Contact Angle Measurements. Langmuir, 30, 8598-8606.

[36] Lin N., Dufresne A. 2014. Nanocellulose in Medicine: Current status and future prospect. European Polymer Journal, 59, 302-325.

[37] Börjesson M., Sahlin K., Bernin D., Westman G. 2018. Increased thermal stability of nanocellulose composites by functionalization of the sulfate groups of cellulose nanocrystals with azetidinium ions. J. Appl. Polym. Sci. ,135, 45963.

[38] Deganello F., Liotta L.F., Macaluso A., Venezia A.M., Deganello G. 2000. Catalytic reduction of nitrates in water solution on pumice-supported Pd-Cu catalysts. Applied Catalysis B: Environmental, 24, 265-273.

[39] Jin Z., Nackashi D., Lu W., Kittrell C., Tour J.M. 2010. Decoration, Migration, and Aggregation of Palladium Nanoparticles on Graphene Sheets. Chem. Mater.,22, 5695–5699.

[40] Kumar R., Awasthi K. 2018. Effect of UV irradiation on PC membrane and use of Pd nanoparticles with/without PVP for $H_2$ selectivity enhancement over $CO_2$ and $N_2$ gases. International Journal of Hydrogen Energy, 43(47), 21690-21698.

[41] Vippola M., Valkonen M., Sarlin E., Honkanen M,Huttuken H. 2016. Insight to Nanoparticle Size Analysis-Novel and Convenient Image Analysis Method Versus Conventional Tecniques. Nanoscale Research Letters, 11,169.

[42] Barreto J.C.G., Tita D.L. 2019. Development o and automated method to perform a quantitative study of particle size distribution and the effect of a conductive layer in scanning electron microscopy. Química Nova, 42(4).

[43] Akbari B., Tavandashti M.P., Zandrahimi M. 2011. Particle size characterization of nanoparticles-a practical approach. Iranian Journal of Materials Science and Engineering, 8(2).

[44] Li Y., Xu L., Xu B., Mao Z., Xu H., Zhong Y., Zhang L., Wang B., Sui X. 2017. Cellulose Sponge Supported Palladium Nanoparticles as Recyclable Cross-Coupling Catalysts. ACS Appl. Mater. Interfaces, 9, 17155−17162.

[45] Dong H., Snyder J.F., Tran D.T., Leadore J.L. 2013. Hydrogel, aerogel and film of cellulose nanofibrils functionalized with silver nanoparticles. Carbohydrate Polymers, 95, 760-767.

[46] Heath L., Thielemans W. 2010. Cellulose nanowhisker aerogels. Green Chem. 12, 1448-1453.

[47] Darpentigny C., Molina-Boisseau S., Nonglaton G., Bras J., Jean B. 2020. Ice-templated freeze-dried cryogels from tunicate cellulose nanocrystals with high specific surface area and anisotropic morphological and mechanical properties. Cellulose, 27, 233-247.

[48] Lucchini M.A., Lizundia E., Moser S., Niederberger M., Nyström G. 2018. Titania-Cellulose Hybrid Monolith for In-Flow Purification of Water under Solar Illumination. ACS Appl. Mater. Interfaces, 10, 29599−29607.

[49] Xu X., Liu F., Jiang L., Zhu J.Y., Haagenson D., Wiesenborn D.P. 2013. Cellulose Nanocrystals vs. Cellulose Nanofibrils: A Comparative Study on Their Microstructures and Effects as Polymer Reinforcing Agents. ACS Appl. Mater. Interfaces, 5, 2999−3009.

[50] Aguayo M.G., Perez A.F., Reyes G., Oviedo C., Gacitúa W., Gonzalez R., Uyarte O. 2018. Isolation and Characterization of Cellulose Nanocrystals from Rejected Fibers Originated in the Kraft Pulping Process. Polymers ,10, 1145.

[51] Isaeva V.I., Eliseev O.L., Chernyshev V.V., Bondarenko T.N., Vergun V.V., Kapustin G.I., Lapidus A.L, Kustov L.M. 2019. Palladium nanoparticles embedded in

MOF matrices: Catalytic activity and structural stability in iodobenzene methoxycarbonylation. Polyhedron, 158, 55–64.

[52] Petek U., Ruiz-Zepeda F., Bele M., Gaberscek M. 2019. Nanoparticles and single atoms in commercial Carbon-Supported Platinum Group Metal Catalysts. Catalysts, 9, 134.

[53] Sofla M.R.K., Brown R.J., Tsukuki T., Rainey T.J. 2016. A comparison of cellulose nanocrystals and cellulose nanofibres extracted from bagasse using acid and ball milling methods. Adv. Nat. Sci.: Nanosci. Nanotechnol., 7, 035004.

[54] Holder C.F., Schaak R.E. 2019. Tutorial on Powder X-ray Diffraction for Characterizing Nanoscale Materials. ACS Nano, 13(7), 7359–7365.

[55] Stasinska B., Machocki A., Antoniak K., Rotko M., Figueiredo J.L., Goncalves F. 2008. Importance of palladium dispersion in Pd/Al2O3 catalysts for complete oxidation of humid low-methane–air mixtures. Catalysis Today, 137, 329-334.

[56] Reddy G.K., Ling C., Peck T.C., Jia H. 2017. Understanding the chemical state of palladium during the direct NO decomposition – influence of pretreatment environment and reaction temperature. RSC Adv, 7, 19645-19655.

[57] Aria A.I., Kidambi P.R., Weatherup R.S., Long Xiao L., Williams J.A., Hofmann S. 2016. Time Evolution of the Wettability of Supported Graphene under Ambient Air Exposure. J. Phys. Chem. C ,120, 2215-2224.

[58] Kwok D.Y., Neumann A.W. 1999. Contact angle measurement and contact angle interpretation. Advances in Colloid and Interface Science, 81, 167-249.

[59] Gindl M., Sinn G., Gindl W., Reiterer A., Tschegg S. 2001. A comparison of different methods to calculate the surface free energy of wood using contact angle measurements. Colloids and Surfaces A: Physicochemical and Engineering Aspects, 181, 279-287.

[60] Rudawska A., Jacniacka E. 2009. Analysis for determining surface free energy uncertainty by the Owen–Wendt method. International Journal of Adhesion and Adhesives, 29, 451-457.

[61] Roach P., Shirtcliffe N.J., Newton M.I. 2008. Progress in superhydrophobic surface development. Soft Matter, 4, 224-240.

[62] Gardner D.J., Oporto G.S., Mills R., Samir M.A.S.A. 2008. Adhesion and Surface Issues in Cellulose and Nanocellulose. Journal of Adhesion Science and Technology, 22, 545-567.

[63] Peng Y., Gardner D.J., Han Y., Cai Z., Tshabalala M.A. 2013. Influence of drying method on the surface energy of cellulose nanofibrils determined by inverse gas chromatography. Journal of Colloid and Interface Science, 405, 85-95.

[64] Hubbe M.A., Gardner D.J., Shen W.2015. Wettability of cellulosics. Bioresources, 10(4), 8657-8749.

[65] Huang X., Wang A., Xu X., Liu H., Shang S. 2017. Enhancement of Hydrophobic Properties of Cellulose Fibers via Grafting with Polymeric Epoxidized Soybean Oil. ACS Sustainable Chem. Eng., 5, 1619-1627.

[66] He Y., Zhu J., Wang W., Ni H. 2018. Surface modification of cellulose nanocrystals with different acid anhydrides for improved dispersion in poly (butylene succinate). RSC Adv, 8, 38305-38314.

[67] Wu Z.Y., Liang H.W., Chen L.F., Hu B.C., Yu S.H. 2016. Bacterial Cellulose: A Robust Platform for Design of Three Dimensional Carbon-Based Functional Nanomaterials. Acc. Chem. Res., 49, 96-105.

[68] Abulateefeh S.R., Khanfar M.A., Al Bakain R.Z., Taha M.O. 2013. Synthesis and characterization of new derivatives of alginic acid and evaluation of their iron (III)-crosslinked beads as potential controlled release matrices. Pharm Dev Technol, Early Online, 1-12.

[69] Goikuria U., Larrañaga A., Vilas J.L., Lizundia E. 2017. Thermal stability increase in metallic nanoparticles-loaded cellulose nanocrystal nanocomposites. Carbohydrate Polymers, 171,193-201.

[70] Beyler C.L., Hirschler M.M. 2001. Thermal Decomposition for Polymers. SFPE Handbook 3, Section 1, chapter 7.

[71] Morani L.M., Ribeiro A.A., de Oliveira M.V., Dantas F.M.L., Leão M.H.M.R. 2010. Physical and chemical characterization of titanium-alginate samples for biomedical applications. 19º Congresso Brasileiro de Engenharia e Ciência dos Materiais-CBECiMat.

[72] Shen D., Xiao R., Gu S., Zhang H. 2013. The overview of thermal decomposition of cellulose in lignocellulosic biomass. DOI: 10.5772/51883.

[73] Liu Y., Zhao J.C., Zhang C.J., Guo Y., Cui L., Zhu P., Wang D.Y. 2015. Bio-based nickel alginate and copper alginate films with excellent flame retardancy: preparation, flammability and thermal degradation behaviour. RSC Adv., 5, 64125.

[74] Xu Z., Zhou H., Tan S., Jiang X., Wu W., Shi J., Chen P. 2018. Ultralight super-hydrophobic carbon aerogels based on cellulose nanofibers/poly(vinyl alcohol)/graphene oxide (CNFs/PVA/GO) for highly effective oil–water separation. Beilstein J. Nanotechnol. ,9, 508-519.

[75] Zhou S., Apostolopoulou-Kalkavoura V., Tamares da Costa M.V., Bergström L., Strømme M., Xu C. 2020. Elastic Aerogels of Cellulose Nanofibers@Metal–Organic Frameworks for Thermal Insulation and Fire Retardancy. Nano-Micro Lett ,12 (9).

[76] Ganesan K., Barowski A., Ratke L., Milow B. 2019. Influence of hierarchical porous structures on the mechanical properties of cellulose aerogels. Journal of Sol-Gel Science and Technology, 89,156-165.

[77] Rinde J.A. 1970. Poisson´s ratio of rigid plastic foams. Journal of Applied Polymer Science, 14(8).

[78] Roberts R.J., Rowe R.C., York P .1994 The Poisson´s ratio of microcrystalline cellulose. International Journal of Pharmaceutics, 105(2), 177-180.

[79] Sescousse R., Gavillon R., Budtova T. 2011. Aerocellulose from cellulose–ionic liquid solutions: Preparation, properties andcomparison with cellulose–NaOH and cellulose–NMMO route. Carbohydrate Polymers, 83, 1766-1774.

[80] Mourdikoudis S, Pallares R.M, Thanh N.T.K. 2018. Characterization techniques for nanoparticles: comparison and complementary upon studying nanoparticle properties. Nanoscale, 10, 12871-12934.

[82] Dalmoro A., Barba A.A., Lamberti G., Grassi M., D´Amore M. 2012. Pharmaceutical Applications of Biocompatible Polymer Blends Containing Sodium Alginate. Advances in Polymer Technology, 31(3), 219-230.

[83] Kas L.M., Ribeiro A.A., de Oliveira M.V., Dantas F.M.L., Leão M.H.M.R. 2010. Physical and chemical characterization of titanium-alginate samples for biomedical applications. 19º Congresso Brasileiro de Engenharia e Ciência dos Materiais-CBECiMat.

[84] Van Oss C.J., Chaudhury M.K., Good R.J. 1988. Interfacial Lifshitz-van der Waals and polar interactions in macroscopic systems. Chemical Reviews, 88(6), 927-941.

[85] Van Oss C.J. 2006. Interfacial Forces in Aqueous Media. CRC Press, 9-28.

[86] Schuster J.M., Schvezov C.E., Rosenberger M. 2015. Analysis of the results of surface free energy measurement of Ti6Al4V by different methods. Procedia Materials Science, 8, 732-741.

[87] Zisman W.A. 1963. Influence of constitution on adhesion. Industrial and Engineering Chemistry, 55,18-38.

[88] Wu S.1971. Calculation of interfacial tension in polymer systems. Journal of Polymer Science Part C: Polymer Symposia, 34,19-30.

[89] Zhao Q., Liu Y., Abel E.W. 2004. Effect of temperature on the surface free energy of amorphous carbon films. Journal of Colloid and Interface Science ,280,174-183.

[90] Zhou S., Wang M., Chen X., Xu F. 2015. Facile Template Synthesis of Microfibrillated Cellulose/Polypyrrole/Silver Nanoparticles Hybrid Aerogels with Electrical Conductive and Pressure Responsive Properties. ACS Sustainable Chem. Eng., 3 (12), 3346-3354.

[91] Roy R.K., Choi H.W., Park S.J., Lee K.R. 2007. Surface energy of the plasma treated Si incorporated diamond-like carbon films. Diamond and Related Materials, 16,1732-1738.

# 3.4. Metal supporting bio-based porous systems, preliminary requirements analysis for environmental and energy applications in gaseous medium

## 3.4.1. Introduction

Metal supporting bio-based mesoporous materials offer relevant properties for being used as a versatile green platform for several application fields. Among these applications areas, biomass based porous systems containing transitions metal are being successfully studied in different environmental remediation applications (water pollutants and heavy metal removal, gas adsorption) and as novel material for future energy alternatives (hydrogen storage).[1,2].

Even if nanocellulose-based composites are widely used as sorption materials, especially in liquid medium, other promising and innovative uses of this kind of systems are still arising in gaseous medium [3,4]. As for liquid medium applications, nanocellulose complex chemical functionalization by the introduction of functional groups (silanization, carbonization, fluoridisation) or polymer grafting are the most common pathways [5]. While, in the case of the mentioned gaseous medium applications, metal supporting biobased porous systems as those developed in this study could be considered as versatile materials with high customization possibilities based on final application and its specific requirements [6].

In this sense, the variety of available transition metals supported on biopolymers offer multiple options, combinations and advantages related to interactions with gases and gaseous fluids [7]. Some metals like palladium and platinum are known and used as catalyst for numerous reactions due to their reactivity, stability, high selectivity and hydrogen adsorption and stabilization capacity [8-10]. Besides, other metals like nickel, copper, titanium or iron offer other interesting properties like magnetic,

electrical or photoswitchable properties, among others, including new possibilities arising from combining different metals. [11-15].

Looking for the final applicability of the developed hybrid porous systems, firstly target should be selected and defined, and several requirements need to be analysed concerning both the biopolymer structure and supported metals parameters as concentration, size, shape, oxidation state, selectivity or distribution and the operation conditions [16]

In this work, hybrid biopolymer-metal systems like cellulose nanocrystal-alginate-palladium (CNC-ALG/PdOx), cellulose nanocrystals-alginate/copper oxide (CNC/ALG-CuOx) and cellulose nanocrystals-alginate/palladium-copper oxides (CNC-ALG/PdOx-CuOx) have been preliminary analysed considering their potential application and customization possibilities as environment remediation and energy solutions in gaseous media.

## 3.4.2. Materials and methods

*Starting materials and cellulose nanocrystals*

Microcrystalline cellulose with a particle size of 20 µm (310697-500G), sulphuric acid and sodium hydroxide and hydrazine hydrate were supplied by Sigma Aldrich. Copper (II) nitrate trihydrate ($Cu(NO_3)_2.3H_20$), palladium (II) nitrate hydrate ($Pd(NO_3)_2.xH_20$), with a purity of 99 % used as precursor materials and sodium alginate (ALG) (SA powder Mw = 396.000 Da and $M/G_{ratio}$= 1.49, determined by viscosity and NMR measurements) were also supplied by Sigma Aldrich.

Used cellulose nanocrystals (CNC) obtention process has been previously described (3.3 section, page. 187).

*Preparation of biopolymer-metal aerogels*

CNC dispersion (3 mL 1 wt.%) was mixed with the equivalent weight of sodium alginate (1:1 with CNC), previously dissolved in 2 ml of MilliQ water by vigorous stirring, and the mixture was also magnetically stirred for 30 minutes. Concurrently, 0.015 g of metallic precursor, palladium (II) nitrate or copper (II) nitrate, were dissolved in 2 ml of MilliQ water and intensely stirred in a Vortex for a few seconds. Water well dissolved metal precursor was added drop by drop to cellulose nanocrystals-alginate dispersion with stirring until gel formation was observed.

Besides, bipolymer-bimetal aerogel was synthesized adding a palladium and copper nitrate mixture (containing 0.015 g of each precursor) over the vigorously stirred CNC-alginate dispersion. Metal solution was drop by drop after and a strong gel was rapidly obtained. Moreover, the same aerogel with reduced palladium (CNC-ALG/Pd-CuO) was obtained by adding only one drop of hydrazine hydrate (50-60 %) to the previously well stirred CNC-water dissolved palladium (II) nitrate solution. Solution turned black few seconds after and sodium alginate was added and well mixed during 30 minutes before the crosslinking using copper nitrate and the final gelification.

Obtained gels were degassed under vacuum for nitrate transformation and evaporation and deposited in the lyophilizer at -50 ºC and 0.123 at for 24 hours. Freeze-drying method was used to obtain a slightly coloured perfect round aerogels

Finally, aerogels were cured at 100 ºC under vacuum for 30 minutes. Aerogels with diameters of 30 mm ± 0,3 mm and heights of 7 ± 1 mm were obtained.

### *Characterisation*

*Density and porosity*

Aerogel apparent density was calculated by measuring the weight and volume of obtained samples The weight was measured by an analytical balance (Sartorius 224I 1S std deviation= +/- 0.0001) and the diameter and height were determined by a digital calliper (TESA-TWIN-CAL IP67). Aerogel porosity (P) was calculated using the Eq. 24.

$$P\ (\%) = (1-\rho^*/\rho) \times 100 \qquad (24)$$

where ρ* is aerogel apparent density and ρ is bulk density for neat CNC and the value calculated according CNC, alginate and metal nanoparticles (MNP) average concentrations in the hybrid aerogel.

*Morphological and microstructural characterization*

Electronic images of aerogel samples were performed using an EVO40 scanning electron microscope (Carl Zeiss STS, Germany) coupled to an X-Max Energy-Dispersive X-Ray Spectrometer (Oxford Instruments, UK). Before the Scanning Electron Microscopy-Energy Dispersive X-Ray Spectroscopy (SEM-EDX) analyses, the selected samples were fixed in specific aluminium sample holders (pins) with carbon type.

Besides, electronic images to visualise CNC , alginate and metal nanoparticles and their disposition in CNC matrix were performed using a high a resolution Scanning Electron Microscopy (FEG-SEM) Hitachi S-4800N. Material preparation has been previously explained in section 3.3 (page 163).

## 3.4.3. Applicability preliminary study

As some of the properties of cellulose nanocrystals-alginate-metal-oxide (CNC-ALG/MOx) aerogels have been already analysed in previous section, the aim of this section is to offer some extra results and to give an overview around these hybrid porous systems focusing into the minimal requirement fulfilment and the potential for gas adsorption, capture or separation applications.

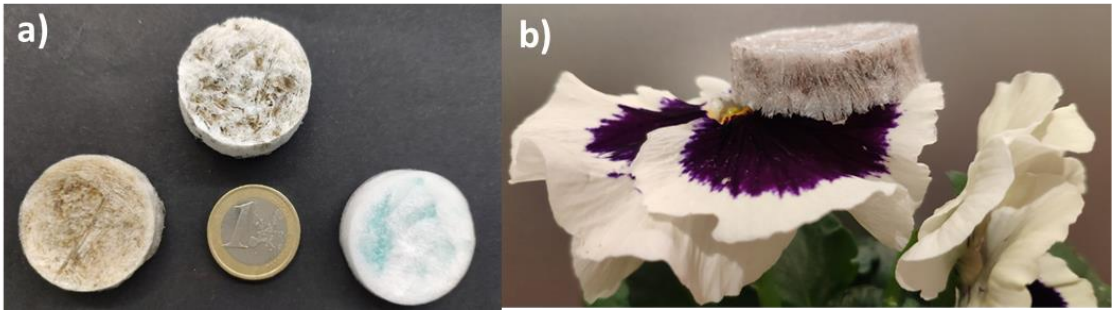


**Figure 73** Images of a) CNC-ALG/PdOx , CNC-ALG/PdxOx-CuOx and CNC-ALG/CuOx samples and b) other perspective of CNC-ALG/Pd sample.

Obtained light, porous and homogeneously round and coloured samples (**Figure 73**) showed a good repeatability. In the case of CNC-ALG sample, CNC and alginate linked by hydrogen bonds while in metal oxide containing samples (CNC-ALG/MOx), added metal precursor cations ($Pd^{+2}$/$Cu^{+2}$) promoted strong ionic interactions and cross-linking, with polymer chain functional groups, according to the alginate *Egg-Box* mode [17]. Then, rapidly formed stable gels were transformed into aerogels by freeze-drying while metal oxide nanoparticle were produced (**Figure 74).**

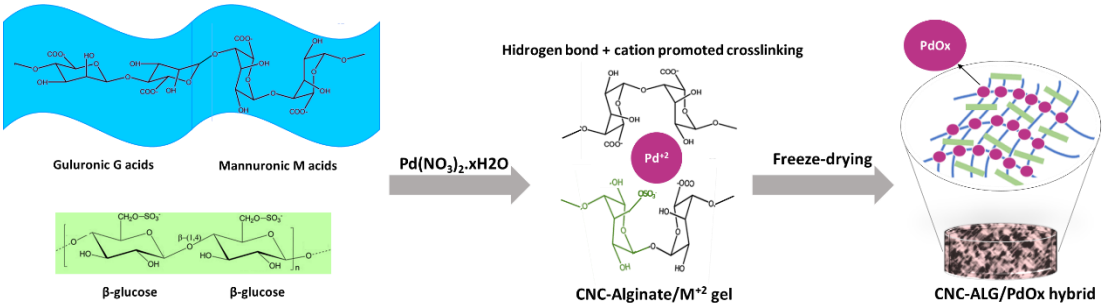


**Figure 74.** Schematic of the synthesis process of CNC-ALG/PdOx hybrid. [25].

Parameters as initial concentrations, apparent density, porosity and volume shrinkage for three different samples were indicated in **Table 11.**

**Table 11** Apparent density, porosity and volume shrinkage values for each aerogel

| Sample ID | Initial Materials | wt % CNC[a] | wt % metal precursor[b] | Apparent Density (mg/cm$^3$) | Porosity (%) | Volume Shrinkage (%) |
|---|---|---|---|---|---|---|
| **CNC-ALG/PdOx** | CNC NaAlginate $Pd(NO_3)_2$ | 0.85 (1:1 with ALG) | 0.21 | 21±2 | 98±0.6 | 12 |
| **CNC-ALG/CuOx** | CNC NaAlginate $Cu(NO_3)_2$ | 0.85 (1:1 with ALG) | 0.21 | 23±3 | 98±0.4 | 18 |
| **CNC-ALG/PdOx-CuOx** | CNC NaAlginate $Cu(NO_3)_2$ $Pd(NO_3)_2$ | 0.66 (1:1 with ALG) | 0,16 (each metal) | 25±2 | 98±0.6 | 22 |

[a-b]Starting concentrations in $H_2O$ dispersions

Samples mantained a low density, dependant on the added metal quantity, high porosity and acceptable volumetric shrinkages.

*Morphological characterization*

Scanning Electronic Microscopy analysis of samples at medium resolution (**Figure 75**) showed morphology variations due to CNC-ALG crosslinking if comparing with only CNC based samples. More fibrillar or apparently elastic structures were observed with not significant differences considering different sections, even for metal containing samples

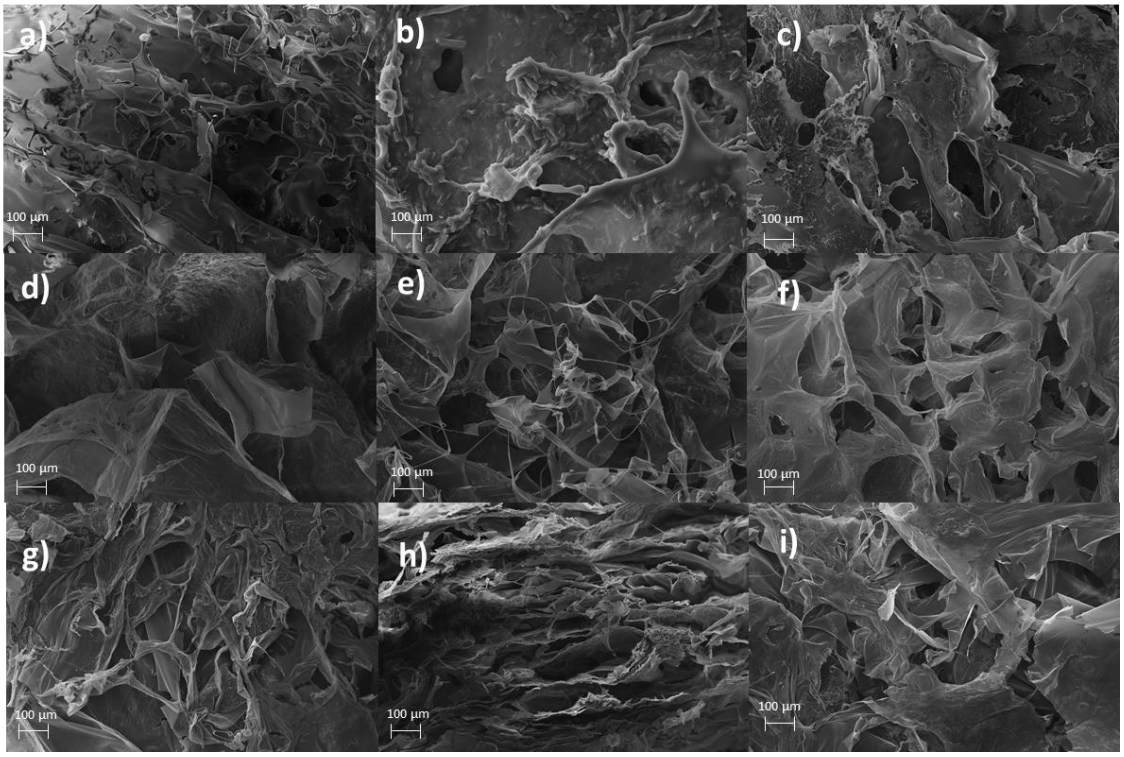


**Figure 75** Top (a) cross-section (b) and bottom (c) images of CNC-ALG; Top (d) cross-section (e) and bottom (f) images of CNC-ALG/CuOx; Top (g) cross-section (h) and bottom (i) images of CNC-ALG/PdOx.

When samples were analysed at higher resolution (**Figure 76**), differences were more evident. In the case of CNC-ALG sample, top and bottom sections morphology showed more elastic or gum like aspect while cross section structure is more similar to neat CNC morphology (**Figure 76 a-d**).The new microstructure is a consequence of the generated crosslinked cellulose-alginate network and probably alginate chains

are enclosing the structure while CNC chains are more internally positioned [17]. If analysing metal containing samples, different morphology and apparently less porous structures were observed including some variations between sections. Metal oxide presence was not observed on sample surfaces (top and bottom sections) due to the strong ionic interactions between metal cations ($Pd^{+2}$ and $Cu^{+2}$) and alginate chains [17] that blocked the metal oxide movement because metal nanoparticle were fixed into CNC-alginate network. Nevertheless, CNC-ALG/Pd cross-section micrograph showed palladium oxide particle aggregation presence and also the hydrophobic effect, previously studied at section 3.3 for CNC/PdOx samples (**Figure 76e**). However, copper oxide particles were not observed by SEM analysis (**Figure 76 c-f**) even though they were detected by XPS and EDX techniques. Even if further analysis are needed, first EDX results indicate an average metal concentration of 2 % for analysed CNC-ALG/PdOx and CNC-ALG/CuOx samples.

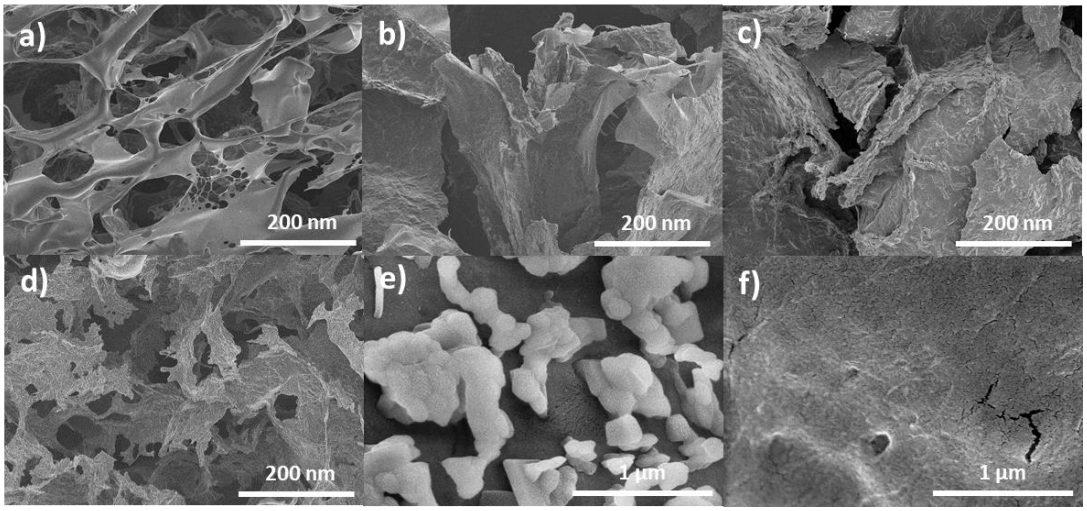


**Figure 76** Comparative images of top (a) and cross-section (d) for CNC-ALG sample, cross sections at different magnification for CNC-ALG/PdOx (b)-(e) and CNC-ALG/CuOx (c)-(f).

*Permeability analysis and integrity*

Even if obtained samples were porous systems, according to porosity calculation, permeability of the material, conditioned by porous size, shape and disposition [18], is a determinant parameter to allow gases to permeate through the material in a specific time. In this sense, a test was done to analyse samples permeability in gas medium and to confirm that pressure falls were not produced when a gas goes through the sample.

**Figure 77** Assembly for permeability tests.

Thus, a home-made but effective trial was performed to test gas permeability and sample´s integrity using Helium inert gas as test-fluid (**Figure 77).** Helium flow was measured once fluid left the material and it was observed that flow speed hardly decreased in studied samples (**Table 12).** Furthermore, with low flow speed (60 ml/min) the observed delay was the higher than with high flow speeds.

**Table 12** Permeability test results.

| Flow Speed/Sample | ΔV (ml/min) CNC-ALG/Pd | ΔV (ml/min CNC-ALG/Pd-Cu |
|---|---|---|
| Vi = 60 ml/min | 12 | 10.5 |
| Vi = 400 ml/min | 3 | 4 |

This different flow variations were attributed to the pressure increment due to flow increases and probably because system opening was produced, while at lower flows the systems was shrinked. Anyway, test revealed the excellent permeability of samples and even an adequate initial mechanical performance.

*Requirements analysis and customization potential*

As mentioned before, the aim of this last section is to identify and check some preliminar aspects for a proper operation of the developed hybrid porous aerogels in gaseous medium where gas adsorption, sensing or capture applications are targeted.

Thus, looking for the application of the developed materials, different requirements and modification alternatives have been analysed and summarised in next table (**Table 13**.)

**Table 13** Preliminary requirements analysis of the developed hybrid porous systems as solutions for gas capture/adsorption applications [19].

| Requirement | Fulfilment | Alternatives/ Comments |
|---|---|---|
| **Material weight (minimum 150 mg) and dimensions** | Yes, weight and size could be adapted | Limited by liophilizer dimensions and equipment power ( ϕ500 mm approx.) |
| **Metal concentration (>1 % metal)** | Yes, adjustable but without precision | Better dispersion is possible with longer and best mixing processes |
| **High porous structure** | Yes | Approximately 98% porosity |
| **Surface Area/Active Surface and adsorption capacity mg/g))** | Partially, not high enough | Determined for CNC/Pd sample (14 $m^2$/g), further tests are needed |
| **Open Pore Structure** | Yes, according to permeability test | – |
| **Metal type (customization according to application and demanded properties)** | Yes | Numerous alternatives for one metal or metal oxide loading (PdOx, CuOx, Pt, FeOx, MgOx) [20,21, 25] and for metal combinations (Pd-CuO, Ag-CoO) (**Figure 78**) |
| **Metal size** | Yes, variable parameter depending on application [23] | Nanoparticles around 35 nm could be in situ synthesized (further study needed for CNC/ALG based systems) |
| **Metal oxidation state** | Yes | Metal oxide are more easily obtained, but the introduction of reducer allows metallic particle obtention (**Figure 78**) |
| **Metal reactivity and selectivity** | Yes, in the case of palladium | Depending on application and the adsorbed/captured gas |
| **Metal accessibility** | Not determined | Generally, gas immobilization without activity blocking is required |
| **Mechanical performance at working conditions (variable pressures)** | Yes, according to preliminary test but cyclic resistance study is needed | Mechanical strength could be improved by components concentration modification |
| **Thermal stability (host material)** | Preferable maximun operation temperature below 100- 150 ºC | There are different pathways for thermal stability improvement |
| **Gas corrosion resistance (host material)** | Yes, in theory ,but not tested [24] | – |

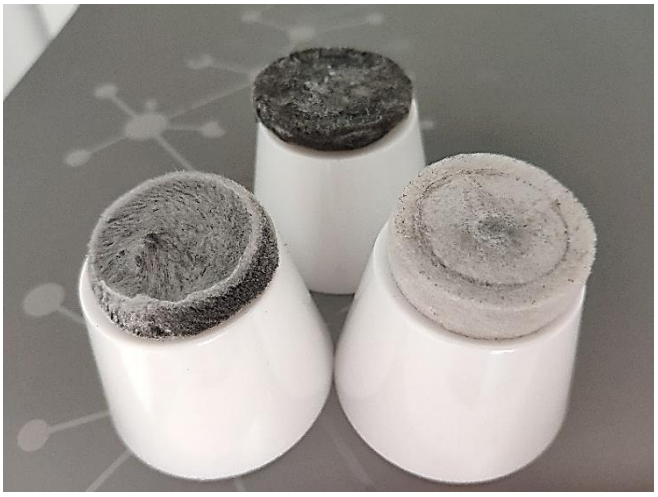

**Figure 78** CNC-ALG aerogels loaded with (a) Pd-ZnO (b) Pd-CuO and (c) Ag-CoO metal oxide and metal nanoparticles.

According to the preliminary analysis, even if a deeper research and tests are necessary, it could be affirmed that developed hybrid aerogels fulfil some initial requirements to be considered and tested as versatile platforms for gas ($CO_2$,$H_2$,$NO_x$) capture, adsorption or sensing applications [6, 20, 26]. Besides, depending on the specifications of the target application, there are different alternatives to design the adequate hybrid porous system, loaded with the suitable metal nanoparticles, metal concentrations and oxidation state, among other possible adaptations. In this sense, **Figure 78** show alternative developed hybrid aerogels, based on biopolymers and loaded with different metal nanoparticle and metal oxide nanoparticle combinations

## 3.4.4. Conclusions

We have developed different hybrid porous systems with cellulose nanocrystal/alginate matrix and loaded with metal oxide nanoparticles (Pd, Cu and Pd-Cu oxides).Different aspects of the hybrid porous systems have been analysed in order to check their applicability as solutions for gas adsorption, capture or sensing

applications related to energy or environment fields and to give an overview of requerement fullfilment and adaptation alternatives. The potential of the developed materials is given by host materials biodegradability and non-reactivity, nanocellulose capacity for nanoparticle growth and support, retaining its special morphology, the wide variety of metal oxide nanoparticle and metal nanoparticle combination loading possibilities, the mechanical enhancement and metal fixation offered by alginate and the permeability and high porosity of the materials. The reported preliminary study offers orientations for new research lines and new steps to achieve an effective application of hybrid porous systems based on cellulose nanocrystal in relevant and high added value applications concerning to global challenges.

## References

[1] Shak K.P.Y., Pang Y.L., Mah S.K. 2018. Nanocellulose: Recent advances and its prospects in environmental remediation. Beilstein J. Nanotechnol., 9, 2479-2498.

[2] Hirscher M., Yartys V.A., Baricco M., Bellosta von Colbe J., Blanchard D., Bowman R.C., Broom D.P., Buckley C.E., Chang F., Chen P., Whan Cho Y., Crivello J.C., Cuevas F., David W.I.F., Petra de Jongh P.E., Denys R.V., Dornheim M., Felderhoff M., Filinchuk Y., Froudakis G.E. 2020. Materials for hydrogen-based energy storage past, recent progress and future outlook. Journal of Alloys and Compounds, 827, 153548.

[3] Zhu H., Yang x., Cranston E.D., Zhu S. 2016. Flexible and Porous Nanocellulose Aerogels with High Loadings of Metal–Organic-Framework Particles for Separations Applications. Adv. Mater., 28, 7652-7657.

[4] Valencia L., Aguilar Sánchez A., Rosas W., Mathew A, Palmqvist A. 2019. Biobased Micro/Meso/Macro-Porous Hybrid Foams with Ultra-high Zeolite Loadings for Selective Capture of Carbon Dioxide. ACS Applied Materials & Interfaces.,10.1021/acsami.9b11399.

[5] Jin H., Kettunen M., Laiho A., Pynnönen H., Paltakari J., Marmur A., Ikkala O., Ras R.H.A. 2011. Superhydrophobic and Superoleophobic Nanocellulose Aerogel Membranes as Bioinspired Cargo Carriers on Water and Oil. Langmuir, 27(5), 1930-1934.

[6] Thomas B., Raj M.C., Athira B., Rubiyah H., Jithin J., Moores A., Drisko G., Sanchez C. 2018. Nanocellulose, a Versatile Green Platform: From Biosources to Materials and Their Applications. Chemical Reviews, 118 (24), 11575-11625.

[7] Rouquerol F.; Rouquerol J.; Sing K. 1999. Adsorption by Powders and Porous Solids; Academic Press: London,166-174.

[8] Kozlov S.M., Aleksandrov H.A., Neyman K.M. 2015. Energetic Stability of Absorbed H in Pd and Pt Nanoparticles in a More Realistic Environment. J. Phys. Chem. C, 119, 5180-5186.

[9] Zalineeva A., Baranton S., Coutanceau C., Jerkiewicz G. 2017. Octahedral palladium nanoparticles as excellent hosts for electrochemically adsorbed and absorbed hydrogen. Science Advances, 3. e1600542.

[10] Ning G., Zhuangzhuang M., Jin L. 2019. Palladium nanoparticles doped polymer microfiber functioned as a hydrogen probe. International Journal of Hydrogen Energy, 40(10).

[11] Gielens F.C., Knibbeler R.J.J., Duysinx P.F.J., Tong H.D., Vorstman M.A.G., Keurentjes J.T.F. 2006. Influence of steam and carbon dioxide on the hydrogen flux through thin Pd/Ag and Pd membranes. Journal of Membrane Science, 279(1–2),176185.

[12] Nayebossadri S., Book D. 2019. Development of a high-pressure Ti-Mn based hydrogen storage alloy for hydrogen compression, Renew. Energy, 143,1010-1021.

[13] Kulprathipanja A., Alptekin G.O., Falconer J.L., Way J.D. 2005. Pd and Pd–Cu membranes: inhibition of $H_2$ permeation by $H_2S$. Journal of Membrane Science, 254(1–2), 49-62.

[14] Deganello F., Liotta L.F., Macaluso A., Venezia A.M., Deganello G. 2000. Catalytic reduction of nitrates in water solution on pumice-supported Pd-Cu catalysts. Applied Catalysis B: Environmental, 24, 265-273.

[15] Liu C.Y., Chen C.F., Leu, J.J. 2009. Fabrication of Mesostructured Cobalt Oxide Sensor and Its Application for CO Detector. Electrochemical and Solid-State Letters. 12 (4), J40-J43.

[16] Gibson A., Mangano E., Shiko E., Greenaway A., Gromov A., Lozinska M., Friedrich D., Campbell E., Wright P., Brandani S. 2016. Adsorption Materials and Processes for Carbon Capture from Gas-Fired Power Plants- AMPGas. Industrial and Engineering Chemistry Research, 55(13), 3840-3851.

[17] Shan Y., Li C., Wu Y., Li Q., Liao J. Hybrid cellulose nanocrystal/alginate/gelatin scaffold with improved mechanical properties and guided wound healing. 2019. RSC Adv.,9, 22966-22979.

[18] Hu Y., Tong X., Zhuo H., Zhong L., Peng X., Wanga S., Sunab R. 2016. 3D hierarchical porous N-doped carbon aerogel from renewable cellulose: an attractive carbon for high-performance supercapacitor electrodes and CO2 adsorption. RSC Adv.,6, 15788.

[19] Ansón A., Jagiello J., Parra J.B. Sanjuán M.L., Benito A.M., Maser W.K., Martínez M.T. 2004. Porosity, Surface Area, Surface Energy, and Hydrogen Adsorption in Nanostructured Carbons. J. Phys. Chem. B, 108, 15820-15826.

[20] Samoylov A.M., Ryabtsev S.V., Popov V.N., Badica P. 2018. Palladium (II) Oxide Nanostructures as Promising Materials for Gas Sensors. Novel Nanomaterials - Synthesis and Applications,12, 212-229.

[21] Musa A., Ahmad M.B., Hussein M.Z., Izham S.M., Shameli K., Sani H.A. 2016. Synthesis of Nanocrystalline Cellulose Stabilized Copper Nanoparticles. Journal of Nanomaterials, ID 2490906.

[22] Pomerantz N., Ma Y.H., Novel method for producing high $H_2$ permeability Pd membranes with a thin layer of the sulfur tolerant Pd/Cu fcc phase. 2011. Journal of Membrane Science,370(1–2), 97-108.

[23] Joo S.H., Park J.Y., Renzas J.R., Butcher D.R., Huang W., Somorjai G.A. 2010. Size Effect of Ruthenium Nanoparticles in Catalytic Carbon Monoxide Oxidation. Nano Lett.,10, 2709-2713.

[24] Tyagi P., Lucia L.A., Hubbe M.A., Pal L. 2019. Nanocellulose-based multilayer barrier coatings for gas, oil, and grease resistance, Carbohydrate Polymers,206, 281-288.

[25] Wang N., Liu Q., Li Y., Chen J., Gu J., Zhanga W., Zhanga D. 2017. Self-crosslink assisted synthesis of 3D porous branch-like Fe3O4/C hybrids for high-performance lithium/sodium-ion batteries. RSC Adv.,7, 50307.

[26] Islam S., Chen L., Sisler J., Tam K. 2018. Cellulose Nanocrystal (CNC) – Inorganic Hybrid Systems: Synthesis, Properties and Applications. Journal of Materials Chemistry B.,6(6), 864-883.

[27] Figueroa S.J., Miranda-Hernández M. 2012. Carbon Film Electrodes as Support of Metallic Particles. Int. J. Electrochem. Sci.,7, 150-166.

# 4

# Conclusions and prospective analysis on the trends

## 4.1. Conclusions

This work demonstrates the tailoring potential of cellulose nanocrystal-based nanocomposites by the combination with different metal and metal oxide nanoparticles concentrations, using simple, surfactantless and scalable processes.

CNC-based free-standing nanocomposite films have been fabricated by Evaporation induced self-assembly-EISA method and it has been demonstrated that metal oxide nanoparticle loaded CNC films properties can be altered depending on the incorporated metal and concentration. In this sense, Ti oxide addition promotes a good disintegrable behaviour, Ag oxide changes optical properties and provides antibacterial behaviour and Zn, Al and Fe oxides promote thermal stability improvement. Thus, a low-cost and green strategy to overcome some properties is showed.

Regarding to aerogels, light and highly porous CNC-based hybrid aerogels have been obtained by a surfactantless and scalable process with the in situ and concurrent generation of entrapped palladium and copper oxide nanoparticles. Results reveal the obtention of hydrophobic surfaces in the case of palladium containing samples with thermal stability modifications. Besides, when CNC is combined with alginate via metallic cation (Cu or Pd cations) promoted crosslinking, mechanical performance is enhanced. Obtained biopolymer-metal hybrid porous systems offer wide customization possibilities according to final application requirements and potential interest for different application fields.

Even if CNCs are especially attractive looking to sustainability challenges or biocompatibility aspects, as well as raw material ubiquity, low cost and their potential as a versatile platform for several applications, most of the tests for novel applications are still being developed at laboratory level. Even though nanocellulose is being considered as a promising material in the area of green chemistry, some challenges

need still to be overcome to achieve large scale incorporation in advanced and innovative applications, as it is detailed in next section.

## 4.2. Prospective analysis on the trends

In this moment and motivated for the climate crisis and other issues, governments and organizations strategies and plans are being actualized and adapted to give response to different environmental challenges.

At global level, United Nations Organization has identify 17 goals for sustainable development [1]. The 2030 agenda for Sustainable Development was adopted by all United Nations Member States in 2015 and stablished an action plan to be accomplished for 2030. The goals are oriented to people equality (no poverty and hunger, education, good health, gender equality), planet protection (clean water, responsible production, climate actions) and prosperity (decent work and economic growth, industry, innovation and infrastructures).

Concerning European Strategies, a new industrial model is being defined [2] where the objective is to get a competitive and sustainable industry and key aspects as climate neutrality, circular economy, clean technologies, digital economy, SME (small and medium-sized enterprises) approach and industrial innovation, professional training, autonomy and partnerships can be highlighted.

Regarding to climate neutrality and environmental degradation and as a pillar for european recovery (35% EU R&D oriented to climate issues) , European Commission is defining The European Green Deal strategy and roadmap. Sustainability (sustainable-by-design) is the target and safety, circularity and functionality are key challenges to obtain sustainable products focusing on resource intense sectors such as textiles, construction, electronics and plastics and considering materials life cycle assessment [3]. In this sense, the strategy has identified sustainable by design plastics development (**Figure 79**) as a relevant issue which will also requires

industrial relevance (cost-efficiency and faster arrival to market), regulatory preparedness and societal enpowerment for a succesful implementation [4].

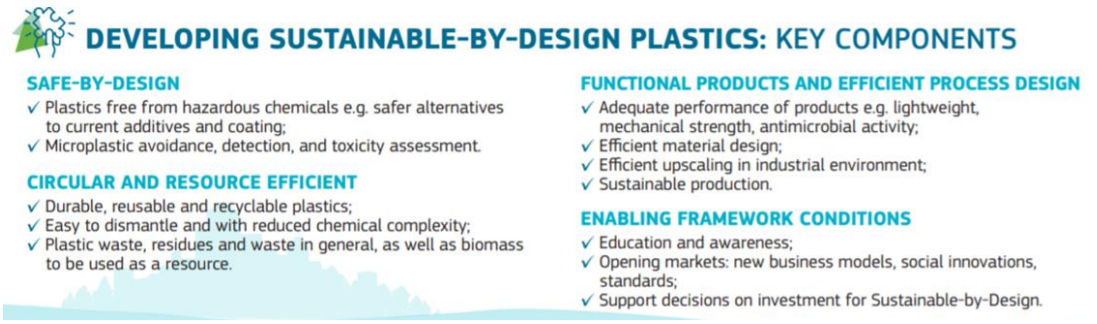


**Figure 79** Key components of Green Deal Strategy concerning to plastics [4]

Looking to local strategies, Basque Government´s new Science Technology and Innovation Plan (PCTI Euskadi 2030) has identified a triple transition to be faced: technological-digital, environmental-energetic, and social transitions and has identified circular economy, cleaner energies, and sustainable mobility as challenges and priorities. Concerning to Key Technologies to solve theses challenges, Advanced Functional Materials and Nanotechnology are included in the Map of Base Technologies [5].

In this context, with sustainability and circularity in the centre of all strategies, development of new materials and specifically biobased or sustainable materials with high functionalization possibilities is a work area that can contributed to produce more sustainable products and even to solve problems in relevant fields.

Regarding bio-based nanocomposites and metal supporting porous nanocomposites like those developed in this work, in this moment they are being studied and tested for different environmental and clean energy applications like water purification, $CO_2$ and NOx capture, biogas separation membrane, hydrogen storage , battery components or as catalyst for different reactions.

Besides, these porous nanocomposites are also considered as sustainable products or functional components for the mentioned resource intensive sectors: textiles

(tailored biofibres), construction (isolation components), electronics (sensors for industry 4.0) and plastics (biopolymers or biocomposites to replace conventional polymers in multifunctional applications).

Furthermore, biopolymer based functional composites offer interesting characteristics for biomedical applications such as drug delivery, implants, scaffolds, biosensor or antipathogen surfaces .

Even if these are the most novel applications, there are still development needs in other more conventional applications like envelope industry, food or cosmetic industry.

If analysing investment plans and strategies in advanced materials, European calls and specific initiatives (H2020-NMBP, EUMAT, Materplat or EIT Raw Materials) related to nanomaterials and nano-structured materials for multifunctional applications and the relevant researcher groups studying in this field, surely new and promising applications will arise. Finally, is necessary to emphasize that nowadays, in a context of global pandemic due to COVID-19, innovations oriented to solve bio-health challenges are becoming even more relevant and it is foreseen an increment of investment in this field. In this sense, also functional nanomaterials with antipathogen behaviour and different bionanosensors could be relevant fields of study [5]. Moreover, technological sovereignty ,including raw materials supply, is a increasing concern in Europe to be considered for new material and products researchers and developers.

Next table **(Table 14**), resumes the most relevant applications and future trends for metal supporting biopolymer-based materials (where CNC-based materials have interesting opportunities) and demonstrates the transversely of the materials with a variety of potential applicability in different sectors [7-11].

**Table 14** Trends and opportunities for metal supporting biopolymer-based nanocomposites in different application fields.

| Field | Environment | Energy | Bio-health | Construction | Industry-Transport |
|---|---|---|---|---|---|
| Trends and application opportunities | Hybrid materials for $CO_2$ and NOx capture and transformation | Component in advanced flexible energy storage devices and batteries | Biocompatible and functional implants, prosthetics and tissue healing | Light and resistant antipathogen materials and surfaces | Reinforcement agent for lighten and property improvement |
| | Selective chemically resistant membranes and catalyst support for different reactions | Hydrogen fuel cell: polymers and composite for hydrogen storage | Biosensors por health diagnosis (flexible electronics, optical imaging) | Acoustic and thermal isolation materials | Multifunctional and multiresponsive composites (autoreparable, insulations, barrier, electrical conductivity, fire retardant) |
| | Adsorbent in water purification (heavy metals, oil and other pollutant removal) | Dye Sensitized Solar Cells: Recyclable encapsulation polymeric materials with high optical transmittance and low cost | Functionalization of scaffolds as reabsorbable material and cell growth orientation | Self-healing composites and coatings | Components with less materials and lower carbon footprint |
| | Gas sensor (CO) and surface active materials | Photovoltaic: coating for maximise sun light entrance | Development of nanostructures for diagnosis and treatments (drug delivery) | Sensitive paints and adhesives with improved properties | Biosensor for Industry 4.0 with optical, electrical or chemical response (nanoelectronics) |
| | Filter for biogas separation toxics or virus ultrafiltration | Ion Conductor Polymeric membranes for improvement of operation temperature | New coatings and materials with antibacterial/ virus and autoreparable properties | | |

Besides, 2 different concepts combined in this work like renewable plastics and smart nanomaterials are prioritized areas in Smart Materials Framework, one of the 5 technological frameworks (**Figure 80**) that have been identified in European Commission Future Technology for Prosperity report [12].

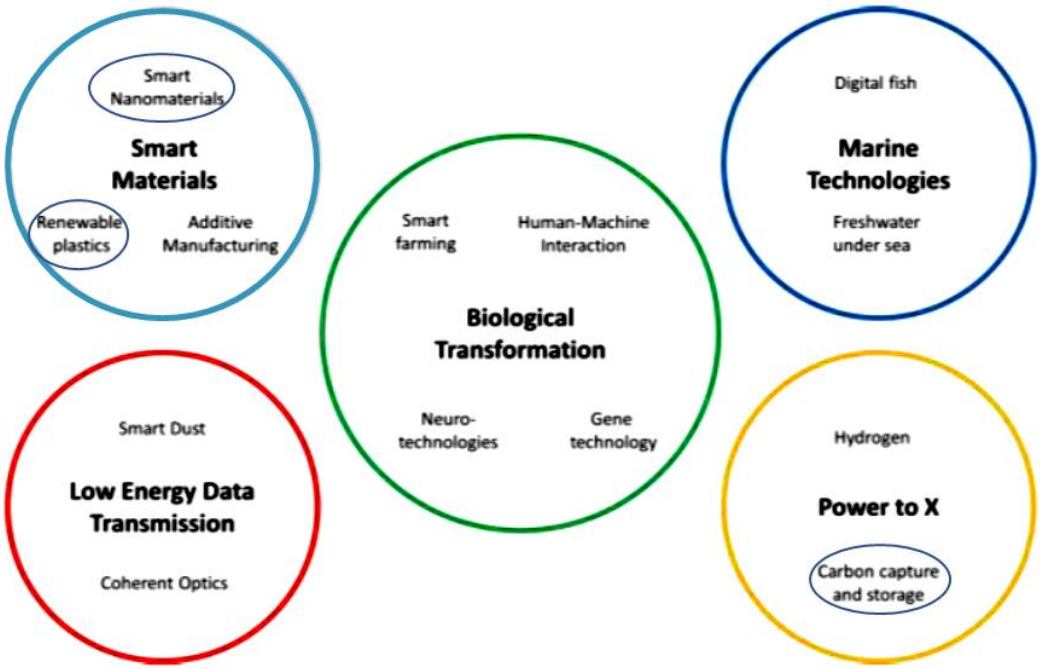


**Figure 80** Overview of technology frameworks and technologies in Future Technology and Prosperity report [11].

In this report, renewable plastics description includes the replacement of fossil-based materials for plastic production and the recycling technologies, research and investment to produce different grades or raw materials for further production. Furthermore, a regulatory framework is proposed to create incentives for the recycling of plastics (focusing on packaging plastics) and to reduce $CO_2$.

Additionally, smart nanomaterials scope is focusing on moving materials on small-scale (nano or quantum), for instance by lasers, that enables new materials creation and that can be found throughout all industries but highlighting the multiple medical applications [13].

Furthermore, research is needed on embedding data or information in materials and smart materials technologies by adding capabilities and materials properties on a nano level are considered. Finally, complex new products or a second-generation of commodities are highlighted and can have a significant impact on more sustainable products and processes, enabling new ways of materials properties, recycling, repair and self-healing or sensing.

If considering Power to X technology framework, the long-term vision is to turn natural sources of energy, for instance sunlight, directly into heat, fuels, or further chemical products. In this framework, developed biopolymer-based nanocomposite also can contribute to defined objectives as $CO_2$ and hydrogen capture and storage. In fact, this work has made a preliminary approach to the gas capture application.

As complementary data to reflect research and development evolution around nanocellulose a study published this year provides some conclusions [14]:

- Within 2010–2017 4500 nanocellulose-related patents were published worldwide and nearly 70 % of those were published within 2015–2017.
- Approximately 50 % of CNC and BNC patents include profit companies among their assignees and this value arises to 80% in the case of CNF.
- Highest nanocellulose innovation protection was identified in China, US and Japan with 3150 patents worldwide, and China as the country with highest innovation protection.
- An outstanding rise in the annual number of publications has been produced during this decade, and especially during 2015–2017 and is expected that innovation on nanocellulose will continue arising and accelerating during the following years.
- The analysis highlights some specific roles of nanocelluloses in innovations related to:
    - polymeric composite materials

- the relevance of oxidative methods referring to plant nanocelluloses
- the interest for innovative filtration devices including CNC
- papermaking compositions based on CNF
- and medical devices involving BCN

***Challenges and barriers for polymer nanocomposites***

Even if, as showed before, nanomaterials and advanced material as bio-based nanocomposites are considered as key enabling technologies and transversal technologies with potential for different sector improvement and new industries creation, there are already several barriers and challenges to solve.

In this sense, to achieve most of the mentioned applications and to fulfil the requirements and replace current solutions, CNC and nanocellulose-based nanocomposites ought to face up some of the next challenges [7,8,16,22]:

1. *More sustainable* CNC *knowledge generation* and disponibility:
    - CNC autonomy and supply may be ensured
    - New treatment routes to produce nanocellulose (less energy consuming and sustainable process with wastes recycle and reuse)
    - CNC and other raw materials may be conveniently characterised*
    - CNC and CNC-based materials life cycle and reuse of products and subproducts may be analysed (valorisation and lifetime management and waste use promotion)
2. *Property improvement and adaptation to final applications.* In the case of bio-based materials:
    - dimensional stability and mechanical resistance improvement by physical or chemical processes is needed*
    - biomimetic: research the possibilities where material shows in final product the same behaviour as in nature

- Research the behaviour of natural material-based products in external environments (lifetime)*

3. *Functionality implementations:* Some relevant demanded functionalities oriented to previously mentioned applications are mentioned below:
    - Additive integration for electronic properties in polymers (Plastronic)
    - Electrical conductivity
    - Sensibility to magnetic fields
    - Antiphatogen properties
    - Autoreparable properties
    - Surface treatment properties*
    - Optical performance*
    - Nanomaterial semielaborate encapsulated in composites for several sectors
    - Diversification of nanomaterial applications by means of physical of chemical modifications. Morphological knowledge of nanomaterials and application of different techniques to vary reactivity (UV, plasma, microwave) *
4. *New synthesis techniques, design methodologies and simulation* in order to extend application fields and looking to sustainability and industrial implementation of new technologies for nanocellulose synthesis, drying, freezing, functionalization, purification and filtration.
5. *Obtention of reproducible and reliable nanomaterial/nanocomposite.* To achieve this challenge parameters control and testing infrastructures are required*
6. *Assembly or integration of nanocomposite in final application,* union with dissimilar materials

7. *Scaling Up: efficient and one step processes.* Production capacity improvement is required for a competitive prize
8. *Comparative cost analysis of process and raw materials to assure final viability*
9. *Optimization of biomass supply logistic systems* to boost the industrial use of nanocellulose materials:
    - Industrial production of nanocellulose (cellulose nanocrystals)
    - Transport, recollect and other processes to supply industrial plants
    - Promote the investment on pilot plants, where biomaterials can be produced at the same time as bioenergy or biofuel
10. *Nanosafety in nanomaterials processes.* Deeper studies and standard around nanomaterial risks are need as well as regulations relating to nanomaterial quality control and rules and guidelines about uses and toxicological risks. In this sense, toxicology of CNC and other nanoparticles, like metal nanoparticles is unclear at laboratory level and even more at industrial level, Safe by Design tools, control of risk in processes and monitoring and training are required [19].

As previously exposed, the fields of research, development and innovation towards the effective use of biopolymer-based nanocomposites in novel applications and even in more conventional applications are numerous, in order to fulfil all the identify challenges and trends. Some of this fields or topics, indicated with *, have been studied in this work.

Apart from the main challenges, main barriers looking to definitive validation and final industrialization of the studied materials are summarized below:

- Scarcity of suppliers and raw materials sovereignty
- Raw materials cost (in the case of metals and nanocelulose isolation process )

- Manual and multi-step production processes and long times for characterization and testing (automatization is required, self-driving laboratories as a fast up-scaling alternative) [21].
- No availability and low robustness of demonstration equipment
- Difficult integration in final applications
- Low technology transfer
- few patents and complex and expensive certification and validation processes
- Lack of standardization and
- Regulatory barriers and difficulties for industrial acceptance

In overall, even if biopolymer-based nanocomposites and particularly those derived from nanocellulose are promising materials, further investigation is needed at material science level to make progress and to improve material properties and functionalities, develop new synthesis routes, as well as make advances in material characterization ,recycling and valorisation analysis.

Meanwhile, other challenges and limitations concercing other fields need to be solved to incorporate these advances materials as scalable, cost-effective and sustainable end-products for future applications [16]. These challenges include, the production automatization, the new biobased nanocomposites lifecycle analysis (from biomass to final product and including each production step energy consumption), different issues related to the production process implementation and costs, and safety aspects of nanomaterials related to health and environmental risks [17,18,19]. For this last purpose, recently a European project has been launched with the aim to develop a simple, robust and cost-effective approaches to guide industry in the development of safer nanomaterials and nano-enabled products [20].

Regarding to the materials developed in this study, next steps at laboratory level should be to select and deeply analyse a target application specifications in order to identify the requirements and to adequate CNC based hybrid materials. In this sense, CNC-based nanocomposites can be customised according variable concentrations, shapes, dimensions and the most suitable nanoparticle incorporation. Finally, properties and behaviour should be tested and/or modified in near final conditions where sample validation depends on the necessary equipment and the complementary knowledge related to the final application field.

# References

[1] United Nations. 2019. Transforming our world: the 2030 agenda for sustainable development.

[2] European Commission. 2020. A new Industrial Strategy for a globally competitive, green and digital Europe.

[3] European Commission. 2019. The European Green Deal- ANNEX to the Communication from the commission to the European Parliament, the European council, the council, the European Economic and social committee and the committee of the Regions.COM/2019/640 final.

[4] European Commission. 2020. European Commission. 2019. Plastics Sustainable by design. European Union, 2020.

[5] Consejo Vasco de Ciencia y Tecnología. 2019. Bases Estratégicas y Económicas del Plan de Ciencia, Tecnología e Innovación 2030.

[6] Hamed Golmohammadi H., Morales-Narváez E., Tina Naghdi‖ T., Merkoçi A. 2017. Nanocellulose in Sensing and Biosensing. Chem. Mater.,29, 5426-5446.

[7] Materplat-Plataforma Tecnológica Española de Materiales Avanzados y Nanomateriales. 2020. Roadmap de Innovación tecnológicas en materiales avanzados y nanomateriales.

[8] European Institute of Innovation and Technology- Raw Materials. 2018. Strategic Agenda 2018-22 of EIT RawMaterials.

[9] Shchipunov Y. 2012. Bionanocomposites: Green sustainable materials for the near future. Pure Appl. Chem., 84, 2579-2607.

[10] Yee Shak K.P., Pang Y.L., Mah S.K. 2018. Nanocellulose: Recent advances and its prospects in environmental remediation. Beilstein J. Nanotechnol., 9, 2479-2498.

[11] Ummartyotin S., Manuspiya H. 2015. A critical review oncellulose: From fundamental to an approach on sensor technology. Renewable and Sustainable Energy Reviews, 41, 402-412.

[12] European Commission. 2019 Future technology for prosperity-Horizon scanning by Europe's technology leaders. Publications Office of the European Union.

[13] Zhang L.J., Webster T.J. 2009. Nanotechnology and nanomaterials: Promises for improved tissue regeneration. Nano Today, 4 (1), 66-80.

[14] Charreau H. Cavallo E., Foresti M.L. 2020. Patents involving nanocellulose: Analysis of their evolution since 2010, Carbohydrate Polymers, 237,116039.

[15] Sweileh W.M., Al-Jabi S.W., Sawalha A.F., AbuTaha A.S., Zyoud S.H. 2016. Bibliometric analysis of medicine-related publications on poverty (2005-2015). Sweileh et al. SpringerPlus, 5,1888.

[16] Reid M.S., Villalobos M., Cranston E.D. 2017. Benchmarking Cellulose Nanocrystals: From the Laboratory to Industrial Production. Langmuir ,33(7), 1583-1598.

[17] Groso A., Petri-Fink A., Magrez A., Riediker M., Meyer T. 2010. Management of nanomaterials safety in research environment. Part. Fibre Toxicol.,7,40.

[18] Savolainen K., Backman U., Brouwer D., Fadeel B., Fernandes T., Kuhlbusch T., Landsiedel R., Lynch I., Pylkkänen P. 2013. Nanosafety in Europe 2015-2025: Towards Safe and Sustainable Nanomaterials and Nanotechnology Innovations. Nanosafety Cluster.

[19] Clark K.A., White R.H., Silbergeld E.K. 2011. Predictive models for nanotoxicology: Current challenges and future opportunities, Regulatory Toxicology and Pharmacology,59 (3), 361-363.

[20] SAbyNA Project. 2020. Simple, robust and cost-effective approaches to guide industry in the development of safer nanomaterials and nano-enabled product. Horizon 2020.

[21] Häse F., Roch LM., Aspuru-Guzik A. 2019. Next-Generation Experimentación with Self-Driving Laboratories. Trends in Chemistry, 1(3), 281-291.

[22] Klemm D., Cranston E., Fischer D., Gama M., Kedzior S., Kralisch D., Kramer F., Kondo T., Lindström T., Nietzsche S., Petzold-Welcke K., Rauchfuss F. 2018 Nanocellulose as a natural source for groundbreaking applications in materials science: Today's state. Materials Today, 21(7).

# 5

# Anexoa/
# Annex

# Anexoa/Annex

Doktoretza lan honek erantsi egiten diren hurrengo emaitzak eman ditu:

*PhD list of contributions::*

1. U. Goikuria, A. Larrañaga, J.L. Vilas , E. Lizundia .2017. Thermal stability increase in metallic nanoparticles-loaded cellulose nanocrystal nanocomposites. *Carbohydrate polymers, 171,193-201.*

2. E. Lizundia, U. Goikuria, J.L. Vilas, F. Cristofaro, G. Bruni, E. Fortunati, I. Armentano, L. Visai , L. Torre .2018. Metal Nanoparticles Embedded in Cellulose Nanocrystal Based Films: Material Properties and Post-use Analysis. *Biomacromolecules, 19, 2618−2628.*

3. U. Goikuria , E. Lizundia. 2019. Zelulosa-nanokristaletan oinarritutako material nanokonposatuak. *Ekaia, 35, 121-144.*

4. U. Goikuria, J.L. Vilas , E. Lizundia. 2020. Effect of metal-oxide nanoparticle presence and alginate cross-linking on cellulose nanocrystal-based aerogels. Under review for publication in *Journal of Applied Polymer Science.*

5. U. Goikuria, J.L. Vilas , E. Lizundia. 2020. Cellulose nanocrystal based nanocomposites. LatinXChem Twitter Conference, September 7th.

6. U. Goikuria, J.L. Vilas , E. Lizundia. 2020. Cellulose nanocrystal based nanomaterials: development and characterization. IMAGENANO 2020-*Nanospain Conference*, september 29-october 01 (on line).

eman ta zabal zazu
Universidad del País Vasco
Euskal Herriko Unibertsitatea
ZIENTZIA ETA TEKNOLOGIA FAKULTATEA
FACULTAD DE CIENCIA Y TECNOLOGÍA
Labquimac

**Zientzia eta Teknologia Fakultatea. Kimika-Fisikoa Saila**
**Kimika Makromolekularreko Laborategia**
**Sarriena auzoa S/N 48940, Leioa/ Bizkaia**